

---

# 3D-Printed Capillaric Circuits for Autonomous Liquid Delivery

---

*Author:*

Ayokunle Oluwafemi OLANREWAJU

Biological and Biomedical Engineering Program

McGill University, Montreal

June 2017

*A thesis submitted in fulfillment of the requirements  
for the degree of Doctor of Philosophy*

©Ayokunle Olanrewaju 2017

# Contents

<b>Abstract</b>	<b>ix</b>
<b>Résumé</b>	<b>xi</b>
<b>Acknowledgements</b>	<b>xiii</b>
<b>Preface and Contribution of Authors</b>	<b>xv</b>
<b>1 Introduction</b>	<b>1</b>
1.1 Scope of the thesis . . . . .	3
<b>2 Background on Microfluidic Liquid Handling</b>	<b>9</b>
2.1 Preface . . . . .	9
2.2 Introduction to Microfluidic Liquid Handling . . . . .	10
2.3 Actively-Powered Microfluidics . . . . .	10
2.4 Self-Powered Microfluidics . . . . .	13
2.5 Capillary Microfluidics . . . . .	14
2.5.1 Fibrous capillary microfluidics . . . . .	15
2.5.2 Microchannel-based capillary microfluidics . . . . .	17
Positive pressure capillary microfluidics . . . . .	17
Negative pressure capillary microfluidics . . . . .	19
Fibrous vs. microchannel-based capillary microfluidics . . . . .	19
2.6 Summary . . . . .	22
<b>3 Capillary microfluidics in microchannels: from microfluidic networks to capillary circuits</b>	<b>31</b>

3.1	Introduction . . . . .	32
3.2	Brief Historical Perspective . . . . .	35
3.2.1	1st wave capillary microfluidics: Mechanical Micromachining and Lamination . . . . .	37
3.2.2	2nd wave capillary microfluidics: Cleanroom Fabrication . . . . .	39
3.2.3	3rd wave capillary microfluidics: Rapid prototyping . . . . .	40
3.3	Fundamentals Parameters and Equations . . . . .	41
3.3.1	Capillary Pressure . . . . .	41
3.3.2	Flow Resistance . . . . .	42
3.4	Capillarie Microfluidic Elements . . . . .	44
3.4.1	Flow Resistors . . . . .	44
3.4.2	Capillary pumps . . . . .	46
3.4.3	Stop valves . . . . .	49
3.4.4	Trigger valves . . . . .	51
3.4.5	Retention valves . . . . .	52
3.4.6	Delay valves . . . . .	52
3.4.7	Capillary soft valves . . . . .	55
3.4.8	Retention burst valves . . . . .	55
3.5	Capillarie Circuits for Preprogrammed Liquid Delivery . . . . .	57
3.5.1	Capillarie Circuits for Immunoassays . . . . .	57
3.5.2	Capillarie Circuits for DNA analysis . . . . .	62
3.5.3	Preprogrammed Multi-Step Liquid Delivery . . . . .	64
	Air vents connected to inlets . . . . .	65
	Combining Retention Burst Valves and Trigger Valves . . . . .	66
	Dissolvable barriers . . . . .	69
3.5.4	Handheld Readers for Capillarie Circuits . . . . .	69
3.5.5	Rapid Prototyping of Capillarie Circuits . . . . .	71
	Xurography (razor writing) . . . . .	71
	Laser cutting . . . . .	72

3D-printing . . . . .	74
3.6 Conclusions and Outlook . . . . .	75
<b>4 Capillarie Circuits replicated from 3D-printed molds</b>	<b>90</b>
4.1 Preface . . . . .	90
4.2 Introduction . . . . .	91
4.2.1 Capillarie circuits for autonomous liquid delivery . . . . .	92
4.2.2 Rapid prototyping of passive microfluidic devices . . . . .	93
4.2.3 3D-Printed Microfluidics . . . . .	93
4.2.4 Capillarie circuits from 3D-printed molds . . . . .	94
4.3 Materials and Methods . . . . .	95
4.3.1 Process flow for 3D-printing capillarie circuits . . . . .	95
4.3.2 PDMS replication from 3D-printed molds . . . . .	95
4.3.3 Procedure for capillary-driven flow experiments . . . . .	96
4.4 Results and Discussion . . . . .	96
4.4.1 Trigger Valves . . . . .	98
Cleanroom-fabricated versus 3D-printed trigger valves . . . . .	98
Effect of trigger valve geometry on success rate . . . . .	100
Effect of surfactant concentration on trigger valve performance . . . . .	102
4.4.2 Retention Burst Valves . . . . .	103
Capillarie circuit for autonomous delivery of four liquids . . . . .	103
Requirements for sequential RBV bursting . . . . .	105
Capillarie circuit for autonomous delivery of eight liquids . . . . .	109
Comparison between 3D-printed and cleanroom-fabricated capillarie circuits . . . . .	111
4.5 Conclusions . . . . .	113
4.6 Acknowledgements . . . . .	115
<b>5 Capillarie Circuit for Rapid Bacteria Detection</b>	<b>123</b>
5.1 Preface . . . . .	123

5.2	Introduction	124
5.3	Design and working principle of capillarie circuit	126
5.3.1	Design of microbead column	128
5.4	Experimental	129
5.4.1	Verifying pre-programmed liquid delivery	129
5.4.2	Validating assay operation and specificity	130
5.4.3	Serial dilution experiments	130
	Bacteria counts and calculation of limit of detection	131
	Algorithm for automated bacteria counts	132
5.5	Results and discussion	133
5.5.1	Pre-programmed liquid delivery in capillarie circuit	134
	Reproducibility of bead packing and liquid delivery	136
5.5.2	Validating assay principle and specificity	136
5.5.3	Limit of detection of <i>E. coli</i> in synthetic urine	137
	Algorithm for automated bacteria counts	139
	Trade-off between sensitivity and time-to-result	140
	3D-printing and mass production	141
	Ease of use of the CC	142
5.6	Conclusion	143
<b>6</b>	<b>Domino Capillarie Circuits</b>	<b>151</b>
6.1	Preface	151
6.2	Introduction	152
6.2.1	Capillary microfluidics for preprogrammed multistep liquid delivery	153
6.2.2	Capillarie circuits for autonomous liquid delivery	154
	Challenges in scaling up capillarie circuits	154
	Domino capillarie circuits for scalable preprogrammed liquid delivery	155

6.3	Materials and Methods	155
6.4	Results and Discussion	156
6.4.1	Operating Principle of Domino Capillarie Circuits	156
6.4.2	Physical Realization of Domino Capillarie Circuit	159
6.4.3	Preprogrammed sequential delivery of 9 liquids	160
6.4.4	Preprogrammed sequential delivery of 17 liquids	162
6.4.5	Domino capillarics for simultaneous liquid delivery	163
6.4.6	Domino capillarics to limit effect of surface tension variations	165
6.5	Conclusion	166
<b>7</b>	<b>Conclusions and Outlook</b>	<b>171</b>
7.1	Summary of scientific contributions	171
7.2	Recommendations for future directions	173
7.2.1	Material choice and device storage	173
7.2.2	Making CCs more user-friendly	175
	Aliquoting/Overflow Structures	176
7.2.3	Simplifying assay readout	176
7.2.4	Improving sensitivity of CCs for bacteria detection	177
7.2.5	Testing clinical urine samples	178
	Presence of debris in clinical urine samples	178
	Detecting different bacteria species	180
	Detecting antibiotic resistance	181
7.2.6	Applications of Capillarie Circuits	181
7.2.7	Closing Remarks	183

# List of Figures

2.1	Pneumatic actuation . . . . .	11
2.2	Centrifugal actuation . . . . .	12
2.3	Electroosmotic actuation . . . . .	13
2.4	Examples of paper-based microfluidics . . . . .	16
2.5	Positive pressure capillary pumping . . . . .	18
3.1	Stages of development in microchannel-based capillary microfluidics . .	36
3.2	Examples of early mechanically micromachined devices that were patented decades ago by industrial labs with many of the ideas recently rediscov- ered and published in academic literature. . . . .	38
3.3	Illustration of capillary-driven flow in a wettable rectangular microchan- nel . . . . .	41
3.4	Symbolic and schematic representations of a typical capillary circuit . .	45
3.5	Capillary system with simple tree line capillary pumps . . . . .	47
3.6	Microstructures for simple and advanced capillary pumping . . . . .	48
3.7	Serpentine capillary pump . . . . .	49
3.8	Schematics and images of stop valves and trigger valves . . . . .	50
3.9	Capillary retention valve . . . . .	53
3.10	Delay valve . . . . .	54
3.11	Capillary soft valve . . . . .	56
3.12	Array of 11 CCs for manual, multi-step assays . . . . .	58
3.13	Triage chip for immunoassays from whole blood . . . . .	59
3.14	Microfabricated silicon chip for one-step immunoassay . . . . .	60

3.15	Microchip with serially arranged reservoirs for multiplexed immunoassay	61
3.16	Air vents connected to microchannel inlets to control sequential delivery	66
3.17	Capillarie circuit for sequential liquid delivery . . . . .	67
3.18	Dissolvable Polyvinylalcohol (PVA) barriers for multi-step liquid delivery	70
3.19	Rapid prototyping of capillary systems using CO <sub>2</sub> laser cutting and 3D-printing . . . . .	73
4.1	Comparison between cleanroom-fabricated and 3D-printed TVs . . . . .	99
4.2	Effect of geometry and surfactant concentration on success rate of TVs .	101
4.3	Design, mold, PDMS replica and operation of CCs for autonomous sequential delivery of four liquids . . . . .	104
4.4	Design and experimental validation of CC for autonomous delivery of four liquids . . . . .	107
4.5	CC for autonomous delivery of eight liquids . . . . .	112
5.1	Design and working principle of CC for bacteria detection . . . . .	127
5.2	Fabrication and testing of CC for bacteria detection . . . . .	135
5.3	Validating bacteria capture assay principle and specificity . . . . .	137
5.4	Results of bacteria capture assay in CC - standard curve and automated algorithm validation . . . . .	138
6.1	Domino capillarie circuit with 8 side branches . . . . .	158
6.2	3D-printed hydraulic and PDMS-replicated pneumatic layers of the domino capillarie circuit . . . . .	159
6.3	Sequential delivery of 9 liquids by domino capillarie circuit . . . . .	161
6.4	Sequential drainage of 16 reservoirs by domino capillarie circuit . . . . .	162
6.5	Domino capillarie circuit with simultaneous reservoir drainage for silver enhancement . . . . .	164

# List of Tables

2.1	Comparison between fibrous and microchannel-based capillary microfluidics . . . . .	21
3.1	Examples of applications of capillarie circuits . . . . .	63
4.1	Geometry of retention burst valves (RBVs) for autonomous delivery of four liquids . . . . .	109
4.2	RBVs designed for autonomous delivery of eight liquids . . . . .	111
4.3	Design rules for capillarie circuits made from 3D-printed molds . . . . .	114
5.1	Geometry of retention burst valves (RBVs) in CC for detection of bacteria	133

# Abstract

Capillary microfluidic devices move liquids without external pumps and valves relying instead on surface tension effects defined by geometry and surface chemistry. This makes them well-suited for miniaturization and automation of biochemical assays in diagnostic and research settings. We introduced the term Capillarie Circuits (CCs) to refer to advanced capillary microfluidic systems composed of individual capillary fluidic elements like pumps, stop valves, and retention valves. CCs are usually micro-fabricated in cleanroom facilities limiting accessibility, increasing costs, and slowing down prototyping time.

Recently, there was a surge in the application of 3D-printing technologies to fabrication of microfluidic devices. However, the minimum feature size achievable by most commercial 3D-printers ( $\approx 100 \mu\text{m}$ ) is an order of magnitude larger than the typical features sizes required for functional capillary valves ( $\approx 10 \mu\text{m}$ ). Similarly, the large surface roughness ( $\pm 1 \mu\text{m}$ ) and layer-by-layer structure ( $\geq 50 \mu\text{m}$  layer thicknesses) of 3D-printed materials also call into question the feasibility of manufacturing functional 3D-printed capillary microfluidic devices.

In this thesis, we develop 3D-printed CCs and introduce clear design rules for pre-programmed liquid delivery in such circuits. 3D-printing allows us to rapidly and systematically investigate design parameters that control liquid delivery within capillary microfluidic systems. First, we manufactured molds for CCs using 3D-printing, then made functional device replicas in polydimethylsiloxane (PDMS). Then we tested the functionality of trigger valves, retention burst valves, and CCs manufactured from 3D-printed molds. After demonstrating reliable operation of these CCs, we developed large volume ( $> 100 \mu\text{L}$ ) devices to automate a sandwich immunoassay for rapid and

facile bacteria detection. The assay in the CC was completed in  $< 7$  min with a limit of detection of  $7.1 \times 10^3$  CFU/mL of *E. coli* in synthetic urine, which is well below the traditional diagnostic criterion for urinary tract infections ( $10^5$  CFU/mL).

Finally, we introduced a new design paradigm, called domino capillaric circuits (DCCs), for simple and scalable pre-programmed liquid delivery. DCCs use identical air conduits in a hydrophobic sealing layer to control the sequential and/or simultaneous reservoir drainage from a 3D-printed device. DCCs are simple to design and operate since they move liquids using a domino effect where reservoirs are opened to air and able to drain only after the preceding reservoir has completely drained.

3D-printing allowed rapid design iterations of CCs with functional devices available in only 10 min. The design rules, fabrication details, and clinically relevant application of the capillary microfluidic devices here suggest clearly that 3D-printed microfluidics enable simple and scalable design of devices for sequential and simultaneous liquid delivery. These devices may find many applications in clinical and industrial settings.

# Résumé

Les dispositifs microfluidiques capillaires déplacent des liquides sans pompes, ni valves. Ils s'appuient sur les effets de tension de surface, définis par la géométrie et la chimie de surface. Cela les rend parfaitement adaptés à la miniaturisation et à l'automatisation des analyses biochimiques afin d'établir un diagnostic et dans le cadre de la recherche. Les systèmes microfluidiques capillaires sont composés d'éléments fluidiques capillaires individuels, tel que les pompes passives et les valves d'arrêts. Ces éléments sont typiquement micro-fabriqués dans des salles blanches. Cela limite l'accessibilité, augmente les coûts et ralentit le temps de prototypage.

Récemment, il y a eu un afflux de l'application des technologies d'impression 3D pour la fabrication de dispositifs microfluidiques. Cependant, la résolution atteinte par la plupart des imprimantes 3D commerciales est un ordre de grandeur plus élevé que celle requise pour la fonctionnalité des valves capillaires. D'une manière similaire, la rugosité de la surface et la structure couche par couche des matériaux imprimés en 3D mettent également en doute la faisabilité de la fabrication par impression 3D de dispositifs microfluidiques capillaires fonctionnels.

Dans cette thèse, nous avons développé des règles de conception analytiques et empiriques pour les dispositifs microfluidiques capillaires imprimés en 3D. L'impression 3D nous a permis d'étudier rapidement et systématiquement les paramètres de conception qui contrôlent la distribution des liquides dans les systèmes microfluidiques capillaires. Pour commencer, nous avons conçu des circuits capillaires à partir d'éléments fluidiques capillaires individuels, tel que des pompes, des valves d'arrêt et des valves de rétention. Ces éléments ont été répliqués à partir de moules imprimés en 3D. Après

démonstration d'un fonctionnement fiables de ces circuits capillaires, nous avons développés des dispositifs à larges volumes afin d'automatiser un dosage immunologique en sandwich pour une détection rapide et facile des bactéries. Le dosage dans le circuit capillaire a été complété en moins de 7 minutes avec une limite de détection de  $7.1 \times 10^3$  UFC (Unité formant colonies) /mL d'E. coli dans un échantillon d'urine synthétique. Cette valeur est bien en dessous du seuil de diagnostique utilisé traditionnellement pour les infections urinaires ( $10^5$  UFC/mL).

Finalement, nous avons introduit un nouveau paradigme de conception, appelé microfluidique en domino, pour une distribution de liquides simples (and scalable) et pré-programmés. Les systèmes microfluidiques en domino imprimés en 3D utilisent des conduits d'air identiques, conçus dans une couche hydrophobe venant sceller la puce microfluidique, afin de contrôler le drainage séquentiel et/ou simultané de réservoirs. Les dispositifs microfluidiques en domino sont simples à concevoir et à opérer puisqu'ils utilisent un effet domino où les réservoirs sont ouverts à l'air et capables de s'écouler seulement après que le réservoir précédent soit complètement vidé.

L'impression 3D a permis des itérations rapides de conception de circuits capillaires et de systèmes microfluidiques domino fonctionnels en seulement 10 minutes. Les règles de conception, les détails de fabrication et les applications cliniques pertinentes des dispositifs microfluidiques capillaires indiquent sans ambiguïté que ces systèmes imprimés en 3D permettent la génération simple (and scalable) de distribution des liquides séquentiel et simultanés. Ces dispositifs microfluidiques peuvent trouver de nombreuses applications dans des environnements cliniques et industriels.

# Acknowledgements

I thank everyone who has contributed academically to this PhD thesis. First, I want to thank my supervisor, Dr. David Juncker, for giving me the opportunity to work in his lab. I am very grateful for your enthusiasm and interest in exploring different research ideas and for your candid feedback. I thank my PhD committee: Dr. Brian Ward, Dr. Jay Nadeau, and Dr. Maryam Tabrizian for their scientific guidance and advice on work ethic. I am also grateful for scientific and editorial feedback from my thesis defence committee: Dr. Delphine Bouilly, Dr. Henrietta Galiana, Dr. Anne Kietzig, Dr. Barry Lutz, and Dr. Sebastian Waschmann-Hogiu. I acknowledge the support of the agencies who funded my PhD: the NSERC CREATE Training Program in Integrated Sensor Systems, the CIHR Systems Biology Training Program, the Quebec Merit Scholarship for Foreign Students (PBEEE), and the Biomedical Engineering Department at McGill for an entrance award.

The PhD was a long, and sometimes difficult, journey. I would not have finished it without the support of a great group of colleagues running alongside me. Veronique Laforte, thank you for providing perspective in my early days, and reminding me that I could do this. Dr. Andy Ng, our many brainstorming sessions and your gentle encouragement to try new ideas gave me the courage to look beyond my initial project definition. Mathias Aebersold, our regular chats and your peer-review of my initial 3D printing project proposal helped to get this work off the ground. Philippe DeCorwin-Martin, our regular walks from campus, time spent flying kites in the park, and our time in student council provided much needed respite from the rigour of grad school. I also want to thank the Biomedical Engineering Department's administrative staff: Ms. Pina Sorrini, Mr. Daniel Caron, and Ms. Nancy Abate for helping with my various

requests, scheduling progress meetings and exams, and making sure that I stayed on track in my PhD.

Without a strong social network outside the lab, I would have been miserable and burned out. Iwasam Agube, our regular phone calls were an anchor through many of life's tough moments. Steven Jim, my brother from another mother, our long conversations about life and science provided perspective, and barely decipherable doodles provided reassurance and actionable ideas. Yaw Amoako-Tuffour, thank you for letting me knock on your door when I first moved to Montreal, and helping me get to the gym regularly. Jessica - thank you for your support in the difficult early days of the comprehensive exam. Paula - thank you for all you taught me, not least of which was to take holidays and to visit my family. Caitlin - thank you for bringing joy and hope as I tried to cross the finish line. The endless love and support of my brothers, Tope, Ayobami, and Timilehin helped me remember who I am and how far I've come no matter how far I may be from home. My dad remains a role model, a reminder of the power of hard work, and a valued counsellor. My mom is the source of so much of my joy, love, and vibrance. Thank you, all, for everything!

# Preface and Contribution of Authors

Following the “Guidelines for Thesis Preparation”, this thesis is presented as a collection of manuscripts written by the candidate with the collaboration of co-authors. The first chapter is an introduction to microfluidic liquid handling with a focus on self-powered liquid delivery in devices powered by capillary forces. Chapter 2 is a detailed literature review that provides historical perspective and highlights recent trends in the development of capillaric circuits (CCs) for preprogrammed liquid delivery. The third, fourth, and fifth chapters detail the results obtained and include the fabrication of CCs using 3D-printing (chapter 3), their application to rapid and sensitive bacteria detection (chapter 4), and the development of a novel and scalable capillaric liquid delivery strategy using 3D-printing (chapter 5). The final chapter summarizes the contributions of this thesis, articulating their impacts, and discuss potential avenues for future work.

In this dissertation, we developed microfluidic capillaric circuits (CCs) manufactured by 3D-printing. Prior to this work, the conventional view was that capillary microfluidic devices required the high precision ( $\approx 10 \mu\text{m}$ ) and sub-micron surface roughness provided by cleanroom fabrication to obtain functional capillaric valves and circuits. The reliance on cleanroom fabrication increased the time required to develop new design iterations to advance the understanding of capillaric valves and circuits, and employ them in clinically-relevant applications. In this thesis, we developed analytical and empirical design rules for rapid prototyping of functional capillaric valves and circuits using 3D-printing. We applied CCs from 3D-printed molds to a clinically relevant problem - rapid and user-friendly detection of bacteria in urine. We also introduced a new design paradigm, called Domino Capillaric Circuits (DCCs)

that enables robust and scalable design of CCs for sequential and/or simultaneous liquid delivery.

The manuscripts are based on experiments designed and conducted by the candidate who also collected and analyzed the data. The candidate also interpreted the data and wrote the presented articles. Professor Juncker, the PhD supervisor, appears as a co-author on all the manuscripts to reflect his supervisory role and involvement with result interpretation and manuscript editing.

In Chapter 2 where we review progress in CCs, Arya Tavakoli and Mohamed Yafia appear as co-authors. I reviewed the literature and wrote the manuscript and prepared/collected the figures with feedback from Professor Juncker. The co-authors contributed an image used in the timeline of progress in CCs, suggested including the summary table of applications of CCs, and provided editorial feedback on the manuscript.

In Chapter 3 where we introduce CCs replicated from 3D-printed molds, I designed, completed, and analyzed the experiments in the paper, wrote the manuscript, and revised it based on reviewer comments, with feedback from Professor Juncker. Alessandra Robillard appears as a co-author due to her contributions to experiments and data analysis for trigger valve reliability testing. Milad Dagher appears as a co-author due to his help with setting up and developing a protocol for high-resolution printing from our lab's 3D-printer.

In Chapter 4, where we apply CCs for rapid and sensitive bacteria detection, I designed, completed, and analyzed the experiments, wrote the manuscript, and revised the manuscript with feedback from Professor Juncker. Dr. Andy Ng appears as a co-author due to his contributions to experiment design for bacteria capture and his editorial input on the manuscript. Philippe DeCorwin-Martin appears as a co-author for writing the MATLAB algorithm for automated spot analysis, and Alessandra Robillard appears as a co-author for helping to conduct serial dilution experiments to determine the limit of detection of the CC.

In Chapter 5, where we develop domino capillarie circuits (DCCs) for scalable sequential and simultaneous liquid delivery, I designed, completed, and analyzed the experiments, wrote the manuscript, and revised the manuscript with feedback from Professor Juncker. Florian Possel appears as a co-author for helping to design and conduct initial experiments to validate the principle of DCCs. Mohamed Yafia and Maiwenn Beaugrand appear as co-authors for helping to conduct experiments with 3D-printed DCCs for sequential and simultaneous liquid delivery.

# List of Abbreviations

<b>CC</b>	<b>Capillarie Circuit</b>
<b>CS</b>	<b>Capillary System</b>
<b>DCC</b>	<b>Domino Capillarie Circuit</b>
<b>PDMS</b>	<b>Polydimethylsiloxane</b>
<b>PCR</b>	<b>Polymerase Chain Reaction</b>
<b>COC</b>	<b>Cyclic Olefin Copolymer</b>
<b>TV</b>	<b>Trigger Valve</b>
<b>RBV</b>	<b>Retention Burst Valve</b>
<b>PMMA</b>	<b>Polymethylmethacrylate</b>
<b>μTAS</b>	<b>micro Total Analysis System</b>

Mom, this one is for you. Thank  
you for all the ways you inspire  
me. I miss you.

# Chapter 1

## Introduction

Miniaturization and automation has revolutionized our everyday lives. The microelectronics revolution that started in the 1960s resulted in a world where almost everyone has access to miniaturized computing technologies in their pockets. It is difficult to imagine what life was like before smartphones, laptop computers, and ubiquitous internet access. This high level of miniaturization and automation was enabled by the development of microfabrication technologies that enabled large scale integration of billions of nanometer-scale transistors into handheld devices.

The field of microfluidics takes inspiration from the microelectronics industry and aims to harness the benefits of miniaturization and automation to offer rapid and scalable liquid handling technologies with a variety of applications, particularly in the life sciences.[1] Microfluidic devices enable manipulation of small volumes of liquids at micrometer length scales. Microfluidic systems are a promising platform for point-of-care tests because they have predictable and controllable flow paths, require only small sample and reagent volumes, have large surface area to volume ratio for analyte capture, can be automated within a small device footprint, and have small dimensions that improve the efficiency of mass transport.

The origin of liquid handling in microfabricated devices dates back to the development of inkjet nozzle heads used in printers.[2] Early work at IBM, Canon, and Kodak on the development of miniaturized inkjet heads from the 1950s till the 1970s paved the way for the development of liquid handling devices at the micrometer scale. The

first integrated microfluidic chip was a silicon micromachined device for gas chromatography developed by Terry *et al* in 1979.[3] In the early 1990s, Andreas Manz and co-workers articulated the vision of *micro-total analysis system* ( $\mu$ TAS) which they envisioned as integrated systems for chemical analysis within a single microchip.[4] Such *lab-on-a-chip* devices are developed using microfabrication technologies from the microelectronics industry and aim to bring the benefits of miniaturization and automation to the medical world. There was an explosion of interest and development in microfluidics in both academic and industrial settings in the 1990s. Varieties of liquid handling technologies and applications have been developed. The progress and potential of microfluidics has been reviewed by Whitesides[5] and more recently by Beebe and colleagues.[6]

However, nearly three decades since Manz envisioned  $\mu$ TAS, most microfluidic systems have not yet realized the dream of a functional *lab-on-a-chip*. Instead, most systems tend to be more of a *lab-around-a-chip* that relies heavily on external, macroscopic equipment such as syringe pumps for liquid transport. As such, there is a lot of interest in minimally-instrumented and user-friendly microfluidic systems for use in point-of-care settings.[7, 8]

The subfield of capillary microfluidics focuses on developing pumps,[9, 10] valves, [11, 12], and integrated systems[9, 13, 14] that achieve self-powered and self-regulated liquid delivery using only capillary forces defined by a material's geometry and surface chemistry.

Traditionally microfluidic devices are fabricated by photolithography in cleanroom environments with filtered ventilation to control the presence of particulate matter in the environment since even a 100- $\mu$ m wide hair could obstruct the microchannels required for flow control. Photolithography refers to the generation of patterns using light, reminiscent of photography in the early 1900s, and typically requires prior design of photomasks to define micropatterns, and relies on large and expensive photomasks aligners, and chemical etching equipment to achieve high resolution and small feature sizes. Consequently, cleanroom fabrication is costly and time-consuming

and results in long design iteration times for microchannel-based capillary microfluidic devices.

Another limitation of capillary microfluidic devices fabricated using conventional cleanroom techniques is that the volume capacity is typically limited to only a few microliters due to manufacturing limitations. This can be a challenge when applications require the screening of large sample volumes ( $> 100 \mu\text{L}$ ) for trace amounts of a target analyte, for example when detecting bacteria in urine. 3D-printing can help to address this concern since it enables simple multi-level fabrication.

## 1.1 Scope of the thesis

The aim of my thesis is to develop strategies for rapid prototyping of large-volume capillary microfluidics using 3D-printing, to characterize and develop detailed design rules for valves and circuits, and apply them to clinically-relevant applications. Finally, we also leverage the speed and rapid design iteration time available with 3D-printing to develop new design paradigms for preprogrammed liquid delivery.

In **Chapter 2**, we introduce liquid handling techniques in microfluidic systems. We briefly highlight actively-powered devices, which require peripheral equipment for actuation, such as: pneumatic, centrifugal, or electroosmotic forces. Then we discuss self-powered capillary microfluidic devices that do not require external equipment for actuation including: gravity-driven, vacuum-driven, and capillary-driven microfluidic devices. We focus on capillary microfluidics and classify it into 2 categories, namely: (1) fibrous capillary microfluidics that move liquids using negative pressure in porous materials like paper or thread, and (2) microchannel-based capillary microfluidics that wick liquids using capillary effects in microfabricated conduits. We further sub-divide microchannel-based capillary microfluidics into positive pressure

capillary microfluidics that move liquids in microchannels using Laplace pressure gradients generated by differences in droplet size, and negative pressure capillary microfluidics that wick liquids solely using the capillary forces defined by the geometry and surface chemistry of a substrate. We conclude by comparing fibrous and microchannel-based capillary microfluidics highlighting the strengths and limitations of both approaches. This chapter provides background and context for work presented in this thesis on negative pressure capillary microfluidic devices designed using electrical analogies.

In **Chapter 3**, we provide a detailed literature review on negative pressure capillary microfluidics using the framework of capillanic circuits (CCs). We define CCs as integrated systems for capillary-driven liquid handling in microchannels that can be assembled from modular fluidic elements and used to implement preprogrammed flow control. We provide a historical perspective of the development CCs starting with early work on mechanically micromachined pumps and stop valves in industry that is described in patents from the 1970s and 1980s and has not been described elsewhere. Next we discuss the principles of operation of individual fluidic elements such as capillary pumps, stop valves, trigger valves, retention valves, and retention burst valves that were developed following the explosion of the interest in cleanroom-fabricated microfluidic systems in the 1990s. We describe emerging trends in the field including CCs for preprogrammed delivery of multiple liquids and rapid prototyping of CCs. Our review, for the first time, summarizes progress over the past 30 years in the development of valves and circuits for self-regulated and self-powered capillary flow in microfabricated conduits and is timely given recent progress in establishing design rules and rapid prototyping techniques that could enable wider adoption of such systems.

In **Chapter 4**, we introduce the rapid prototyping of CCs by 3D-printing of molds. We describe the design and fabrication of capillanic circuits (CCs) - advanced capillary microfluidic devices assembled from capillary fluidic elements in a modular manner similar to the design of electric circuits. 3D-printing enabled rapid prototyping and

design iterations of CCs. We established empirical and analytical design rules for capillary fluidic elements like trigger valves, and retention burst valves. Functional trigger valves were obtained with 3D-printed molds with up to 80-fold larger geometry than the traditional cleanroom microfabrication. In addition, CCs for autonomous sequential delivery of eight liquids in a < 7 min were developed. CCs from 3D-printed molds lower the bar for other researchers to develop and apply capillary microfluidic valves and CCs for autonomous liquid delivery in a variety of applications. The use of 3D-printing allows fast and inexpensive design and fabrication of self-powered devices that could have many applications in the clinic or in industry.

In **Chapter 5**, we use CCs to address a major healthcare challenge - rapid and user-friendly detection of bacteria in urine. Urinary tract infections are one of the most common bacterial infections and causes of emergency room visits. Current clinical UTI diagnosis is slow and time-consuming. Although significant progress has been made in developing microfluidic systems for bacteria detection, their practical application is often limited by complex protocols, bulky peripherals, and slow operation. We present CCs optimized for rapid and automated bacteria detection in urine. For sensitive bacteria capture, microbeads functionalized with capture antibodies were packed on-the-spot within the CC in < 20 s. The CC automated preprogrammed delivery of 100  $\mu\text{L}$  of bacteria sample, biotinylated antibodies, fluorescent streptavidin conjugate, and wash buffer for a total volume  $\approx 115 \mu\text{L}$ . The automated assay was completed in < 7 min and captured bacteria were visible as fluorescent spots that were easily counted by the user or with an automated algorithm. The limit of detection (**LOD**) of *E. coli* in synthetic urine was  $7.1 \times 10^3$  colony-forming-units per mL (**CFU/mL**) which is well below the traditional clinical threshold for UTI ( $> 10^5$  CFU/mL). The CC for bacteria detection is one of the fastest demonstrations of rapid and sensitive bacteria detection to date, and has potential for use in rapid point-of-care UTI screening.

In **Chapter 6**, we introduce a new design paradigm for CCs, called Domino Capillary Circuit (**DCC**), that enables simpler design and greater number of liquid delivery steps. Previously, it was difficult to scale up the number of liquid delivery steps in

CCs because of limitations in 3D-printer resolution and accuracy. DCCs enable simple scaling up of the number of liquid delivery steps by using air conduits to separate liquid reservoirs. DCCs were designed such that air conduits connect the exit of one reservoir to the entrance of another reservoir. With this design, DCCs enable preprogrammed liquid delivery in a manner that resembles a domino effect where emptying of one reservoir allows drainage of a subsequent reservoir connected via an air conduit. Air conduits can be connected across multiple reservoirs enabling simultaneous liquid delivery similar to using one domino to knock over two other dominos. DCCs are an exciting approach for preprogrammed sequential and/or simultaneous liquid delivery with easy design and scaling up of the number of liquid delivery steps that could be open up many new applications in research, clinic, or industry.

In **Chapter 7**, we conclude by summarizing the contributions of this thesis to science, namely:

- rapid prototyping of CCs using 3D-printing
- rapid and user-friendly bacteria detection using CCs
- introduction of DCCs for simple and scalable design of devices for preprogrammed sequential and/or simultaneous liquid delivery.

We discuss the limitations of the 3D-printed CCs as well as avenues for potential future work that could address those limitations.

# Bibliography

- [1] T. M. Squires, "Microfluidics : Fluid physics at the nanoliter scale," *Rev. Mod. Phys.*, vol. 77, no. July, pp. 977–1026, 2005.
- [2] E. Bassous, H. H. Taub, and L. Kuhn, "Ink jet printing nozzle arrays etched in silicon," *Appl. Phys. Lett.*, vol. 31, no. 2, pp. 135–137, Jul. 1977.
- [3] S. C. Terry, J. H. Jerman, and J. B. Angell, "A gas chromatographic air analyzer fabricated on a silicon wafer," *IEEE Trans. Electron Devices*, vol. 26, no. 12, pp. 1880–1886, 1979.
- [4] A. Manz, N. Graber, and H. M. Widmer, "Miniaturized total chemical analysis systems: A novel concept for chemical sensing," *Sensors & Actuators: B. Chemical*, vol. 1, no. 1-6, pp. 244–248, Jan. 1990.
- [5] G. M. Whitesides, "The origins and the future of microfluidics," *Nature*, vol. 442, no. 7101, pp. 368–373, Jul. 2006.
- [6] E. K. Sackmann, A. L. Fulton, and D. J. Beebe, "The present and future role of microfluidics in biomedical research." *Nature*, vol. 507, no. 7491, pp. 181–189, Mar. 2014.
- [7] B. Weigl, G. Domingo, P. LaBarre, and J. Gerlach, "Towards non- and minimally instrumented, microfluidics-based diagnostic devices," *Lab Chip*, vol. 8, no. 12, p. 1999, 2008.
- [8] C. D. Chin, T. Laksanasopin, Y. K. Cheung, D. Steinmiller, V. Linder, H. Parsa, J. Wang, H. Moore, R. Rouse, G. Umvilighozo, E. Karita, L. Mwambarangwe, S. L. Braunstein, J. van de Wijgert, R. Sahabo, J. E. Justman, W. El-Sadr, and S. K. Sia,

- “Microfluidics-based diagnostics of infectious diseases in the developing world,” *Nature Medicine*, vol. 17, no. 8, pp. 1015–1019, Jul. 2011.
- [9] D. Juncker, H. Schmid, U. Drechsler, H. Wolf, M. Wolf, B. Michel, N. de Rooij, and E. Delamarche, “Autonomous Microfluidic Capillary System,” *Anal. Chem.*, vol. 74, no. 24, pp. 6139–6144, Dec. 2002.
- [10] M. Zimmermann, H. Schmid, P. Hunziker, and E. Delamarche, “Capillary pumps for autonomous capillary systems,” *Lab Chip*, vol. 7, no. 1, pp. 119–125, 2007.
- [11] M. Zimmermann, P. Hunziker, and E. Delamarche, “Valves for autonomous capillary systems,” *Microfluid Nanofluid*, vol. 5, no. 3, pp. 395–402, Sep. 2008.
- [12] J. Melin, N. Roxhed, G. Gimenez, P. Griss, W. van der Wijngaart, and G. Stemme, “A liquid-triggered liquid microvalve for on-chip flow control,” *Sensors & Actuators: B. Chemical*, vol. 100, no. 3, pp. 463–468, Jan. 2004.
- [13] L. Gervais and E. Delamarche, “Toward one-step point-of-care immunodiagnostics using capillary-driven microfluidics and PDMS substrates.” *Lab Chip*, vol. 9, no. 23, pp. 3330–3337, Dec. 2009.
- [14] R. Safavieh and D. Juncker, “Capillarics: Pre-programmed, self-powered microfluidic circuits built from capillary elements,” *Lab Chip*, vol. 13, no. 21, pp. 4180–4189, Nov. 2013.

## Chapter 2

# Background on Microfluidic Liquid Handling

### 2.1 Preface

In this chapter, we introduce liquid handling techniques in microfluidic systems. We briefly highlight actively-powered devices, which require peripheral equipment for actuation, such as: pneumatic, centrifugal, or electroosmotic forces. Then we discuss self-powered capillary microfluidic devices that do not require external equipment for actuation including: gravity-driven, vacuum-driven, and capillary-driven microfluidic devices. We focus on capillary microfluidics and classify it into 2 categories, namely: (1) fibrous capillary microfluidics that move liquids using negative pressure in porous materials like paper or thread, and (2) microchannel-based capillary microfluidics that wick liquids using capillary effects in microfabricated conduits. We further sub-divide microchannel-based capillary microfluidics into positive pressure capillary microfluidics that move liquids in microchannels using Laplace pressure gradients generated by differences in droplet size, and negative pressure capillary microfluidics that wick liquids solely using the capillary forces defined by the geometry and surface chemistry of a substrate. We conclude by comparing fibrous and microchannel-based capillary microfluidics highlighting the strengths and limitations of both approaches. This chapter provides background and context for work

presented in this thesis on negative pressure capillary microfluidic devices designed using electrical analogies.

## 2.2 Introduction to Microfluidic Liquid Handling

Microfluidics is the study of the manipulation of liquids using conduits at sub-millimeter size scales. The field is now well established with many developments aimed at applying microfluidics to biomedical research and point-of-care diagnostics.[1, 2, 3] Microfluidic devices may be divided into two main categories according to the mechanism of liquid actuation, namely:

1. actively-powered systems that require external power sources (such as pneumatic pressure, centrifugal forces, or electric or acoustic fields) for liquid manipulation,
2. self-powered systems that do not require external power sources and rely solely on forces defined by the geometry and material properties of a microfluidic device (such as surface tension, air permeability, or gravity) for liquid manipulation.

## 2.3 Actively-Powered Microfluidics

Actively-powered microfluidic devices move liquids using external equipment and power supplies. There are a wide variety of actively-powered microfluidic pumping and valving schemes including: pneumatic, electroosmotic, centrifugal, and acoustic methods. The breadth of microfluidic pumping and valving schemes was well reviewed previously.[4, 5, 6] Here we briefly describe some of the most common actively-powered microfluidic devices.

Pneumatic actuation is one of the most common approaches for manipulating fluids in microfluidic devices. By connecting air and vacuum lines to the inlets and outlets of microchannels, pneumatic pressure can be used to precisely manipulate liquids

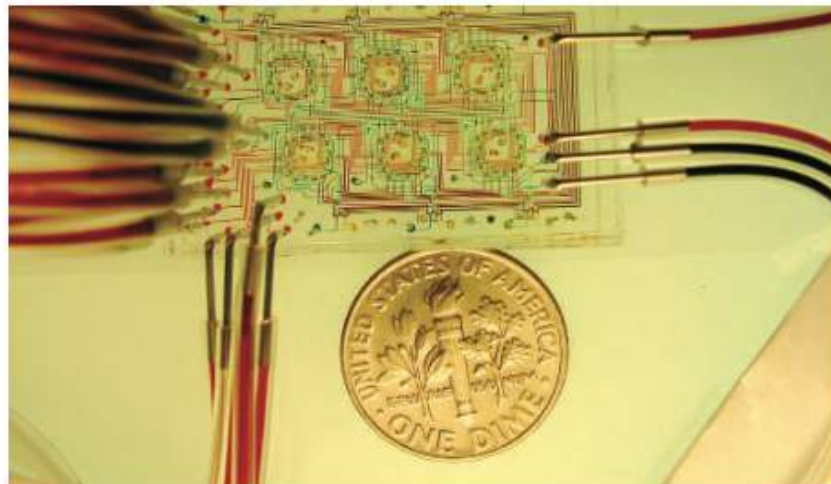


FIGURE 2.1: Microfluidic chip with pressure and vacuum lines for pneumatic actuation. Adapted from ref. [12] © 2005 American Association for the Advancement of Science

(Fig. 2.1). Pneumatic valves can also be manufactured by multilayer soft lithography wherein polydimethylsiloxane (PDMS) microchannels are constructed as the fluidic layer.[7] Air and/or vacuum is passed through a thin, flexible PDMS control layer that can be used to open or close microchannels on the fluidic layer. This enables precise control over flow in microchannels and complex networks of pneumatically actuated valves and circuits have been developed including devices for fluidic shift registers or logic circuits that demonstrate the versatility of this approach.[8, 9] Pneumatically-powered microfluidic devices have also been commercialized, for example the single cell analysis systems developed by Fluidigm.[10] Pneumatic valves can be readily integrated within microfluidic devices fabricated using mass production methods like injection molding,[11] and can be automated to offer robust and flexible flow control over a wide range of applications. However, the requirement for air and vacuum connections to the microfluidic chip generally limits the use of pneumatic actuation to centralized laboratories and precludes their use in point-of-care settings.

Centrifugal microfluidics, or Lab-on-a-CD is another common microfluidic liquid handling mechanism. Disk-shaped microfluidic devices are loaded with liquid and spun at high speeds, sometimes with a CD or a DVD player, to provide centrifugal forces for liquid manipulation (Fig. 2.2).[15] Centrifugal microfluidics have been applied for a variety of applications, and are already commercially available and were

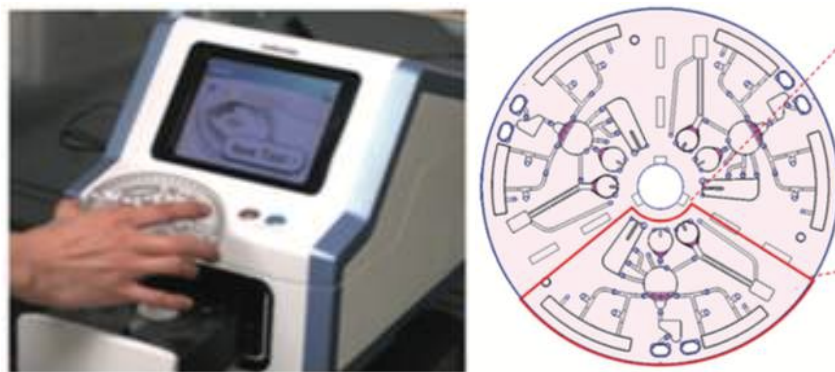


FIGURE 2.2: A microchip and supporting instrument for centrifugal actuation of microfluidic flow. Adapted from ref. [13] © 2009 Royal Society of Chemistry

recently used for detection of Ebola virus during the West African outbreak from 2013 - 2016.[16] Centrifugal microfluidics are advantageous since they use disposable, mass-producible, plastic substrates. They can also be used to automate multi-step assays that can be easily multiplexed along various branches or sectors of the CD substrate. However, real-time sensing and readout is challenging due to the need to spin the substrate to control flow. In addition, the size of the motor/spinner required tends to limit portability of centrifugal systems.

Electroosmosis is another phenomenon manipulated to move fluidics within microfabricated channels. Electroosmotic flow is important in chemical separation systems. Fig. 2.3 shows a capillary electrophoresis device commonly used in molecular biology for separation of analytes such as DNA based on size. Capillary electrophoresis systems were one of the first commercial applications of microfluidics in the 1990s.[17] Electroosmotic methods enable high precision flow control and are capable of manipulating nanoliter sample volumes. They also do not require any moving parts in the microchip, which simplifies fabrication. However, operation of electroosmotic methods is susceptible to changes in buffer composition and surface properties. In addition, the requirement for high voltage power supplies limits the portability of such systems.

Another huge category of microfluidic devices are powered by electrowetting.[18]

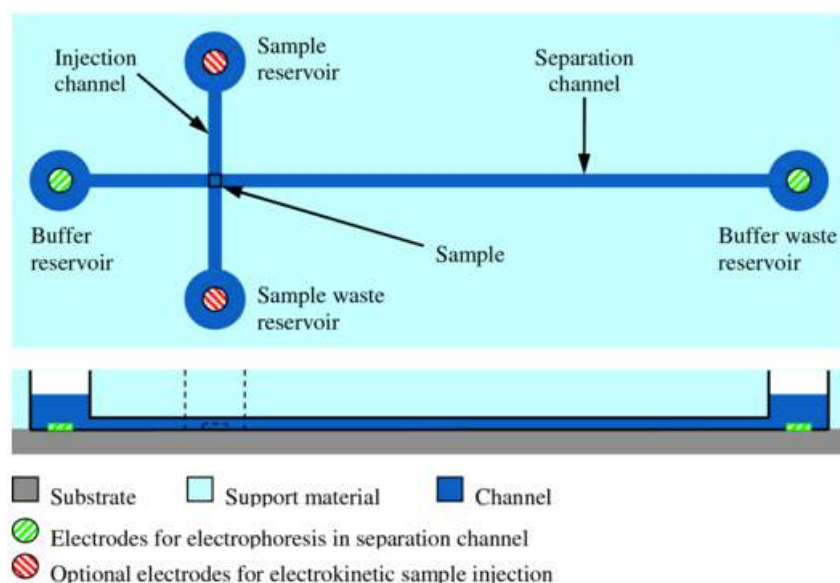


FIGURE 2.3: A schematic describing capillary electrophoresis in a microfluidic device. Electric voltages are used for chemical separation in the microchannel. Adapted from ref. [14] © 2013 IOP Publishing Ltd.

Liquids are moved in individual droplets using arrays of electrodes to control the wettability of the surface. We do not discuss electrowetting here because it does not fit within the scope of this thesis (i.e. channel-based microfluidics).

Actively-powered systems are very well-established and versatile tools for automation of biochemical assays. They may be used as high-throughput screening systems for a variety of assays and some systems have found commercial success as enabling technologies behind DNA sequencing platforms. However, actively-powered systems are not very suitable for applications where point-of-care or minimally instrumented operation is a priority, such as rapid diagnosis.

## 2.4 Self-Powered Microfluidics

Self-powered microfluidic devices do not require external equipment for liquid manipulation. Self-powered systems move liquids using driving forces encoded in the design or material properties of the microfluidic device. There are many different techniques for self-powered liquid delivery in microfluidic devices, including: vacuum, gravity, and capillary effects.

Vacuum-driven microfluidics moves liquids using a vacuum that is typically stored within the material that is used to fabricate the microfluidic chip. For example, microchannels made out of poly(dimethylsiloxane) (PDMS) are air permeable and can be degassed in a vacuum chamber and sealed in an air-tight chamber so that when flow is desired, liquids are loaded into the inlets of the PDMS device and the device is exposed to atmospheric air. Suction of air into the PDMS drives flow in the microchannels in a power-free manner.[19, 20] Progress and applications of vacuum-driven microfluidics was recently reviewed.[21] Vacuum-driven microfluidics is simple and power-free and requires no external connections or tubing. However, vacuum-driven flow requires air-tight storage of devices and offers only limited valving capabilities.

Gravity-driven flow in microfluidic devices uses the hydrodynamic pressure difference between vertical inlet and outlet reservoirs of a microfluidic device to drive flow.[22, 23] The difference in gravitational potential energy creates a hydraulic pressure difference that drives flow through microchannels. For example, DiagonSwiss developed a gravity-driven system that tilts a microfluidic chip to control flow rates within microfluidic channels to perform automated immunoassays with results available in < 10 min.[24] Gravity-driven flow has also been combined with separation schemes such as deterministic lateral displacement for size-specific particle sorting[25] and magnetic-bead based assays for specific analyte capture.[26] Advanced gravity-driven microfluidic systems have been developed that enable self-switching synchronous flows, analogous to synchronous electric circuits, with a wide range of flow frequencies and flow rates with the potential to automate multiple parallel operations without external controllers.[27] Nevertheless, the capability to implement fluidic valving operations like delaying or stopping flow has not yet been shown.

## 2.5 Capillary Microfluidics

Capillary microfluidics manipulate liquids using surface tension effects defined by the geometry and surface chemistry of a substrate. Capillary forces enable self-powered

wicking of liquid without external peripherals or power supplies. Capillary microfluidics can be broadly classified into two categories: (1) fibrous capillary microfluidics that wick using porous membranes and fibres, and (2) microchannel-based capillary microfluidics that wick liquids using microfabricated conduits.

### 2.5.1 Fibrous capillary microfluidics

Fibrous capillary microfluidic devices wick liquids using porous substrates such as paper[28] or thread[29]. The study of liquid transport in patterned paper dates back to paper chromatography in the 1940s.[30, 31] Between the 1930s and the 1980s, paper and membrane-based devices found practical applications such as glucose and pregnancy test strips with widespread adoption in everyday life. Lateral flow test strips where assay reagents were immobilized on porous membranes were developed and addition of sample resulted in visual assay results on a test line as well as a change in a control line to indicate proper liquid delivery in the test (Fig. 2.4A). Lateral flow tests are still the most widely commercially successful “microfluidic” devices.[1, 32]

Paper-based microfluidics as a research area was developed by the Whitesides group in 2007.[28] Rapid prototyping techniques such as craft cutting, laser cutting, and wax printing enabled design and manufacture of new devices within a few hours and at low cost. There are a wide variety of fluid control strategies and applications of paper-based microfluidics with many recent reviews.[30, 35, 36, 37] We briefly describe two approaches for preprogrammed sequential delivery of liquids in paper-based devices. One approach is folding of paper-devices into 3-dimensional structures that enable parallel addition of sample and reagents to different test zones without mixing (Fig. 2.4B).[33] Vertical flow in 3-dimensional paper devices enables parallel delivery of liquid to multiple reaction zones while retaining a compact device area. Such 3-dimensional paper-based microfluidics were applied in point-of-care settings to detect liver disease.[38, 39] Another fluid delivery strategy in paper-based microfluidics is

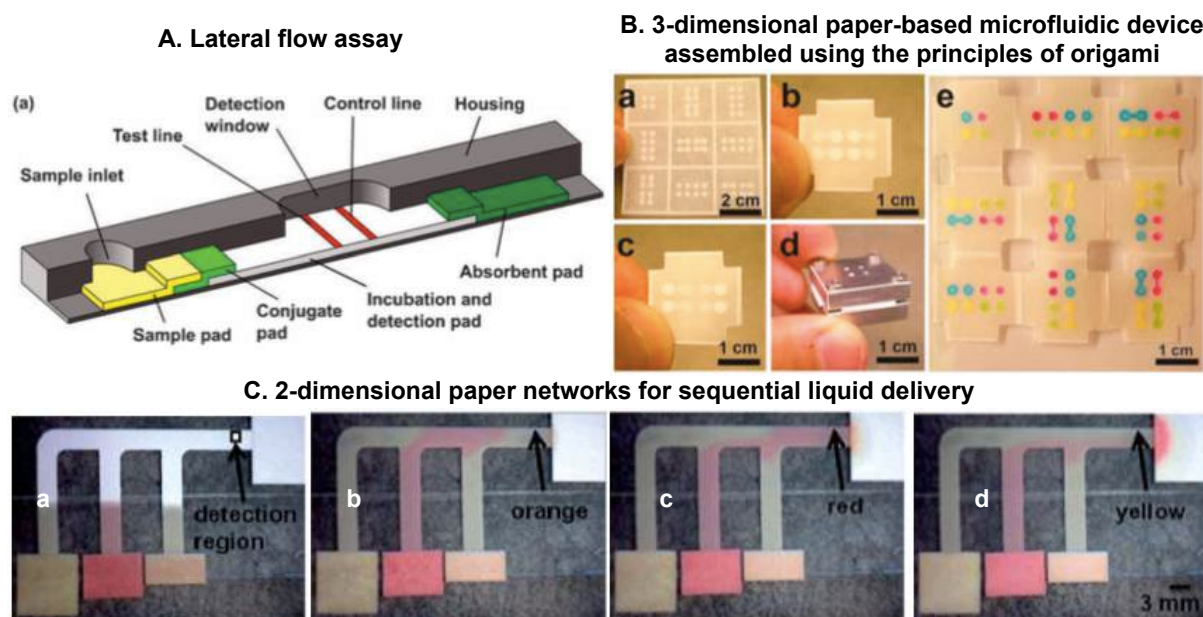


FIGURE 2.4: Examples of paper-based microfluidics. (A) Schematic of a lateral flow test showing key components. Liquid is added to the sample pad and reconstitutes antibodies stored on the conjugate pad moving them downstream towards the test line and control line. The absorbent pad wicks liquid driving flow downstream. (B) Three-dimensional paper-based microfluidics with photolithographically-defined channels, reservoirs, and a folding frame. Devices were cut, folded and clamped within an aluminum housing and loaded with liquid through four injection holes. An unfolded nine-layer device is shown after injection of liquids. (C) Two-dimensional paper microfluidic network with different flow path lengths used to obtain pre-programmed sequential delivery of multiple liquids through the detection region. Adapted from: (A) ref. [1] © 2010 Royal Society of Chemistry, (B) ref. [33] © 2011 American Chemical Society, (C) ref. [34] © 2010 Royal Society of Chemistry.

the fabrication of devices with converging flow paths with different path lengths to obtain sequential delivery of liquids to a detection zone (Fig. 2.4C).[34] Two-dimensional paper networks were used for sequential delivery of signal amplification and wash reagents to improve assay sensitivity.[40] Recently, paper-based devices with integrated sample collection, preparation, and analysis have also been developed.[41, 42] The benefits and drawbacks of paper-based and microchannel-based capillary microfluidics are compared in section 2.5.2.

## 2.5.2 Microchannel-based capillary microfluidics

Microchannel-based capillary microfluidics wick liquid through precisely micromachined conduits. There are two main categories of microchannel-based capillary microfluidics: (1) positive pressure capillary microfluidics, and (2) negative pressure capillary microfluidics.

### Positive pressure capillary microfluidics

Positive pressure capillary microfluidics use positive Laplace pressure acting on a liquid droplet to move liquids through microchannels. The capillary pressure difference,  $\Delta P$  acting on a hemispheric droplet of radius  $r$  (see Fig. 2.5A) can be calculated as:[43]

$$\Delta P = \frac{2\gamma}{r} \quad (2.1)$$

where  $\gamma$  is the surface tension of liquid. As seen in Fig. 2.5B, liquid moves from a smaller “pumping port” to a larger “receiving port” driven by Laplace pressure differences at the liquid inlets.[44] Flow in these passive pumps was characterized[43] and used to implement microfluidic logic operations[45]. Droplets with different sizes and Laplace pressures have also been applied in open platforms to passively direct flow for hanging drop cell culture.[46] This is an elegant and simple pumping scheme. The need for pipetting exact liquid volumes and shielding devices from evaporation are important considerations when using such systems.

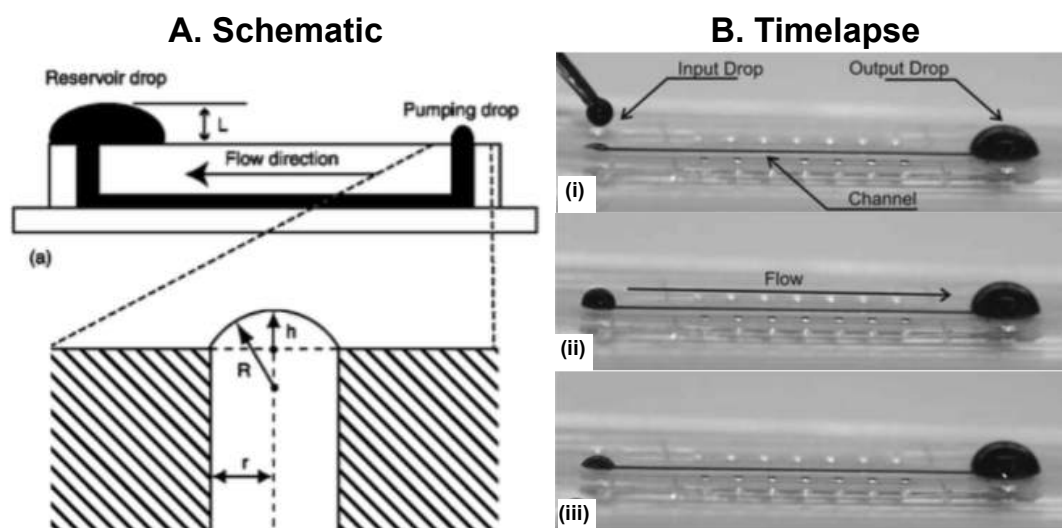


FIGURE 2.5: Capillary pump mechanism that propels liquid using both negative (wicking) surface tension and positive (Laplace) pressure differences governed by inlet and droplet size. (A) Schematic of positive capillary pumping mechanism. Adapted from ref. 44 © 2002 Royal Society of Chemistry. (B) Timelapse images showing flow of liquid from smaller pumping drop to larger reservoir drop. Adapted from ref. 43. © 2007 Royal Society of Chemistry.

Positive pressure capillary pumping can be combined with other capillary microfluidic elements to automate parallel bioassays.[47] For example, Kim et al. developed a microfluidic device that used positive pressure capillary pumping to control flow direction and also incorporated additional fluidic components such as timing channels, synchronization channels, and stop valves to implement pre-programmed multiplexed immunoassays to detect two protein biomarkers.[47] This approach also included a system-level design and electrical notation that guided development of microfluidic designs. The aim of the automated device developed by Kim et al. was to improve the user-friendliness and automation of conventional immunoassays within a portable self-filling microfluidic device. Indeed, the number of pipetting steps was decreased from the 48 required in a conventional microwell plate to 10 in the capillary system.[47] Nevertheless, the user needed to add liquids to inlets at specific times to ensure sequential liquid delivery, which limits the user-friendliness of the microfluidic device.

### **Negative pressure capillary microfluidics**

Negative pressure capillary microfluidics are powered solely by surface tension effects that result in wicking of liquids in microchannels. The capillary pressure that wicks liquid into wettable microchannels is a negative pressure that drives flow in sub-millimeter conduits. The driving force for negative pressure capillary microfluidics is the same as that in fibrous capillary microfluidics, except instead of moving liquids through porous membranes with heterogeneous pore structures, microchannel-based devices move liquids through precisely defined microfabricated conduits. By modifying the geometry of microstructures, capillary-driven microfluidic elements such as capillary pumps,[48] stop valves,[49] and trigger valves[50] were developed. When these capillary microfluidic elements were combined into integrated circuits powered solely by capillary pressure they were originally referred to as “autonomous microfluidic capillary systems” or “capillary systems” (CSs).[51] Our research group introduced the concept of Capillaric Circuits (CCs) - which are microfluidic systems assembled from individual capillaric fluidic elements in much the same way that electronic circuits are assembled from individual electronic components.[52] Framing the design and development of negative pressure capillary microfluidics in terms of CCs enables modular design of such systems for preprogrammed sequential liquid delivery. Chapter 3 provides a detailed description of the history of CCs, the operating principles of individual capillaric microfluidic elements, and CCs for preprogrammed sequential liquid delivery.

### **Fibrous vs. microchannel-based capillary microfluidics**

Fibrous capillary microfluidics and microchannel-based capillary microfluidics are both often proposed as platforms for self-powered and self-regulated bioassays at the point-of-care. In this section we briefly compare the strengths and weaknesses of both approaches (Table 2.1). We compare fabrication complexity, material choice, surface

treatment, surface properties for bioassays, fluidic control capability, dead volume, and suitability for mass production.

Paper-based devices have long benefited from fast and simple fabrication at low cost. There is a wide range of commercially available paper products that are typically hydrophilic.[30, 35] Flow control has been demonstrated with variations in geometry and surface chemistry of paper substrates allowing fluid velocity change, on/off flow control, and sequential delivery of multiple liquids (Fig. 2.4B).[36, 40] Nevertheless, some drawbacks of paper-based devices include relatively large dead volumes (microliter range) since the entire fluid flow path must be wetted for every liquid delivery step. This could increase the time and sample volume required to implement biochemical assays. In addition, the heterogeneity of paper substrates with component fibres that are often irregularly structured and arranged can make surface functionalization challenging and also limit the range of geometric modifications and flow control capabilities.

On the other hand, microchannel-based capillary systems are traditionally manufactured in cleanroom environments using silicon substrates.[51] Recently, rapid prototyping technologies such as laser cutting and 3D-printing have enabled fast and inexpensive fabrication of capillary systems.[56, 57, 59, 60] Microchannel-based capillary microfluidics are typically manufactured using silicon substrates or replicated into polymers such as polydimethylsiloxane (PDMS) by soft lithography[52] or thermoplastic polymers like cyclic olefin copolymer (COC) by injection molding.[55] Precise control over microchannel geometries in two and three dimensions allows a broad range of fluid control capabilities including capillary pumps with guided liquid filling fronts,[48, 61] capillary stop valves and trigger valves,[49, 62], and pre-programmed multi-step liquid sequencing using encoded capillary pressures.[52, 63] Surface treatment to maintain stable hydrophilic surfaces in microchannel-based devices is usually more challenging than with paper-based devices. This is because paper-based substrates like nitrocellulose are typically treated during the manufacturing process to obtain stable hydrophilic surfaces. Meanwhile with microchannel-based devices,

TABLE 2.1: Comparison between fibrous and microchannel-based capillary microfluidics

	<b>Fibrous capillary microfluidics</b>	<b>Microchannel-based capillary microfluidics</b>
<b>Fabrication complexity</b>	Fast and simple e.g. laser cutting, wax patterning, craft cutting [30, 37]	Mostly made by conventional cleanroom fabrication which is complex and time-consuming [52, 53]
<b>Material choice</b>	Commercially available filter paper and chromatography paper usually made of nitrocellulose or glass fibre [30, 35]	Typically silicon,[51, 54] PDMS,[44, 52] and thermoplastics (e.g. Cyclic Olefin Copolymer[55], PMMA[56])
<b>Surface properties</b>	Substrate surface is heterogeneous making analyte capture challenging to model and characterize.	Homogeneous and regular surface properties allowing greater capability to model analyte capture.
<b>Surface treatment</b>	Wetting agents are added to commercial nitrocellulose and glass fibre membranes to render them hydrophilic.	Microfabricated substrates typically require surface treatment for hydrophilicity e.g. polyethylene glycol silane coating[51, 54] or plasma treatment.[52, 57]
<b>Fluidic control capabilities</b>	Several flow control techniques using geometry and surface chemistry modification[36, 37] but precise control over microscale geometries is largely dependent on suppliers.	Greater capability for precise flow control with well-defined microchannel geometries and chemical surface treatment.
<b>Dead volume</b>	Typically larger ( $\mu\text{L}$ range) since entire flow path must be wetted[40]	Relatively low. Can work with nanoliter volumes given micro-scale control over channel geometry[51, 58]
<b>Volume capacity</b>	Typically larger (up to mL) since fibre can be easily stacked, and pore size and thickness varied.	Typically low (few $\mu\text{L}$ ) given typical dimensions of microchannels ( $\approx 10 - 100 \mu\text{m}$ )
<b>Cost of mass production</b>	Inexpensive to mass produce given existing industrial infrastructure and inexpensive substrate, although two- and three-dimensional devices might require custom modifications	Depends on substrate. Silicon is mass produced in the semiconductor industry but requires large-scale mass production to reduce cost. Polymers can be hot embossed or injection molded for low-cost mass production[55]

the user/researcher often must implement their own surface treatment protocols for microchannel-based devices, often leading to a wide range of surface treatments, many of which were developed without manufacturability in mind.

While there are benefits and drawbacks of both fibrous and microchannel-based capillary microfluidics, the microfluidics community can benefit from applying all the fluidic control elements at our disposal to solve real world problems. As such, it is important to carefully consider the application of both fibrous and microchannel-based capillary microfluidics. In fact, there are a few demonstrations of hybrid capillary microfluidics that combine paper and microchannels to leverage the benefits of both porous and non-porous substrates.[53, 57, 64, 65] For example, microchannel-based capillary pumps in microchannel-based devices typically have relatively low sample volumes ( $nL$  range) and are relatively complex to fabricate. To address this concern, porous materials (such as paper) were used as pumps in microchannel-based devices.[57, 64, 65] Such porous pumps provide large volume capacity while retaining small device footprints. Paper pumps can be patterned to provide variable and pre-programmed flow rates.[65, 66]

## 2.6 Summary

In this chapter, we introduced microfluidic liquid handling techniques. We briefly discussed actively-powered and self-powered liquid handling techniques with a focus on capillary microfluidics. We described fibrous, positive pressure, and negative pressure capillary microfluidics. Then we concluded with a brief comparison of fibrous and microchannel-based capillary microfluidics to provide context for upcoming work in the thesis. In the next chapter, we provide a detailed literature review on CCs - modular capillary microfluidic networks for preprogrammed liquid delivery. We discuss fundamental parameters, the historical progress, and operating principles of capillary microfluidic elements and circuits.

# Bibliography

- [1] D. Mark, S. Haeberle, G. Roth, F. von Stetten, and R. Zengerle, "Microfluidic lab-on-a-chip platforms: requirements, characteristics and applications," *Chem. Soc. Rev.*, vol. 39, no. 3, pp. 1153–1182, 2010.
- [2] E. K. Sackmann, A. L. Fulton, and D. J. Beebe, "The present and future role of microfluidics in biomedical research," *Nature*, vol. 507, no. 7491, pp. 181–189, Mar. 2014.
- [3] G. M. Whitesides, "The origins and the future of microfluidics," *Nature*, vol. 442, no. 7101, pp. 368–373, Jul. 2006.
- [4] A. K. Au, H. Lai, B. R. Utela, and A. Folch, "Microvalves and Micropumps for BioMEMS," *Micromachines*, vol. 2, no. 2, pp. 179–220, Jan. 2011.
- [5] K. W. Oh and C. H. Ahn, "A review of microvalves," *J. Micromech. Microeng.*, vol. 16, no. 5, pp. R13–R39, Mar. 2006.
- [6] D. J. Laser and J. G. Santiago, "A review of micropumps," *J. Micromech. Microeng.*, vol. 14, no. 6, pp. R35–R64, Apr. 2004.
- [7] N. S. G. K. Devaraju and M. A. Unger, "Pressure driven digital logic in PDMS based microfluidic devices fabricated by multilayer soft lithography." *Lab Chip*, vol. 12, no. 22, pp. 4809–4815, Nov. 2012.
- [8] M. Rhee and M. A. Burns, "Microfluidic pneumatic logic circuits and digital pneumatic microprocessors for integrated microfluidic systems," *Lab Chip*, vol. 9, no. 21, p. 3131, 2009.

- [9] J. A. Weaver, J. Melin, D. Stark, S. R. Quake, and M. A. Horowitz, "Static control logic for microfluidic devices using pressure-gain valves," *Nature Physics*, vol. 6, no. 3, pp. 218–223, Jan. 2010.
- [10] J. S. Jang, V. A. Simon, R. M. Feddersen, F. Rakhshan, D. A. Schultz, M. A. Zschunke, W. L. Lingle, C. P. Kolbert, and J. Jen, "Quantitative miRNA Expression Analysis Using Fluidigm Microfluidics Dynamic Arrays," *BMC Genomics* 2011 12:1, vol. 12, no. 1, p. 144, Mar. 2011.
- [11] A. F. Sauer-Budge, P. Mirer, A. Chatterjee, C. M. Klapperich, D. Chargin, and A. Sharon, "Low cost and manufacturable complete microTAS for detecting bacteria." *Lab Chip*, vol. 9, no. 19, pp. 2803–2810, Oct. 2009.
- [12] F. K. Balagaddé, L. You, C. L. Hansen, F. H. Arnold, and S. R. Quake, "Long-Term Monitoring of Bacteria Undergoing Programmed Population Control in a Microchemostat," *Science*, vol. 309, no. 5731, pp. 137–140, Jul. 2005.
- [13] B. S. Lee, J.-N. Lee, J.-M. Park, J.-G. Lee, S. Kim, Y.-K. Cho, and C. Ko, "A fully automated immunoassay from whole blood on a disc," *Lab Chip*, vol. 9, no. 11, pp. 1548–1555, Jun. 2009.
- [14] A. P. Lewis, A. Cranny, N. R. Harris, N. G. Green, J. A. Wharton, R. J. K. Wood, and K. R. Stokes, "Review on the development of truly portable and in-situ capillary electrophoresis systems," *Meas. Sci. Technol.*, vol. 24, no. 4, p. 042001, Apr. 2013.
- [15] R. Gorkin, J. Park, J. Siegrist, M. Amasia, B. S. Lee, J.-M. Park, J. Kim, H. Kim, M. Madou, and Y.-K. Cho, "Centrifugal microfluidics for biomedical applications," *Lab Chip*, vol. 10, no. 14, pp. 1758–1773, 2010.
- [16] W. E. Owen, J. E. Caron, and J. R. Genzen, "Liver function testing on the Abaxis Piccolo Xpress: Use in Ebola virus disease protocols," *Clinica Chimica Acta*, vol. 446, pp. 119–127, Jun. 2015.

- [17] N. J. Panaro, P. K. Yuen, T. Sakazume, P. Fortina, L. J. Kricka, and P. Wilding, "Evaluation of DNA fragment sizing and quantification by the agilent 2100 bio-analyzer." *Clin. Chem.*, vol. 46, no. 11, pp. 1851–1853, Nov. 2000.
- [18] K. Choi, A. H. C. Ng, R. Fobel, and A. R. Wheeler, "Digital Microfluidics," *Annual Review of Analytical Chemistry*, vol. 5, no. 1, pp. 413–440, Jul. 2012.
- [19] K. Hosokawa, K. Sato, N. Ichikawa, and M. Maeda, "Power-free poly(dimethylsiloxane) microfluidic devices for gold nanoparticle-based DNA analysis," *Lab Chip*, vol. 4, no. 3, pp. 181–185, 2004.
- [20] K. Hosokawa, M. Omata, and M. Maeda, "Immunoassay on a power-free microchip with laminar flow-assisted dendritic amplification." *Anal. Chem.*, vol. 79, no. 15, pp. 6000–6004, Aug. 2007.
- [21] L. Xu, H. Lee, D. Jetta, and K. W. Oh, "Vacuum-driven power-free microfluidics utilizing the gas solubility or permeability of polydimethylsiloxane (PDMS)," *Lab Chip*, vol. 15, no. 20, pp. 3962–3979, 2015.
- [22] D. Huh, J. H. Bahng, Y. Ling, H.-H. Wei, O. D. Kripfgans, J. B. Fowlkes, J. B. Groberg, and S. Takayama, "Gravity-driven microfluidic particle sorting device with hydrodynamic separation amplification." *Anal. Chem.*, vol. 79, no. 4, pp. 1369–1376, Feb. 2007.
- [23] B. S. Cho, T. G. Schuster, X. Zhu, D. Chang, G. D. Smith, and S. Takayama, "Passively Driven Integrated Microfluidic System for Separation of Motile Sperm," *Anal. Chem.*, vol. 75, no. 7, pp. 1671–1675, Apr. 2003.
- [24] J. Rossier, S. Baranek, P. Morier, C. Vollet, F. Vulliet, Y. Dechastonay, and F. Raymond, "GRAVI: Robotized Microfluidics for Fast and Automated Immunoassays in Low Volume," *Journal of the Association for Laboratory Automation*, vol. 13, no. 6, pp. 322–329, Dec. 2008.

- [25] R. Devendra and G. Drazer, "Gravity Driven Deterministic Lateral Displacement for Particle Separation in Microfluidic Devices," *Anal. Chem.*, vol. 84, no. 24, pp. 10 621–10 627, Dec. 2012.
- [26] S. Laschi, R. Miranda-Castro, E. González-Fernández, I. Palchetti, F. Reymond, J. S. Rossier, and G. Marrazza, "A new gravity-driven microfluidic-based electrochemical assay coupled to magnetic beads for nucleic acid detection," *Electrophoresis*, vol. 31, no. 22, pp. 3727–3736, Oct. 2010.
- [27] S.-J. Kim, R. Yokokawa, S. C. Lesher-Perez, and S. Takayama, "Multiple independent autonomous hydraulic oscillators driven by a common gravity head." *Nature Communications*, vol. 6, p. 7301, Jun. 2015.
- [28] A. W. Martinez, S. T. Phillips, M. J. Butte, and G. M. Whitesides, "Patterned paper as a platform for inexpensive, low-volume, portable bioassays." *Angew. Chem. Int. Ed.*, vol. 46, no. 8, pp. 1318–1320, 2007.
- [29] R. Safaviieh, G. Z. Zhou, and D. Juncker, "Microfluidics made of yarns and knots: from fundamental properties to simple networks and operations," *Lab Chip*, vol. 11, no. 15, pp. 2618–2624, Jul. 2011.
- [30] A. K. Yetisen, M. S. Akram, and C. R. Lowe, "Paper-based microfluidic point-of-care diagnostic devices," *Lab Chip*, vol. 13, no. 12, pp. 2210–2251, May 2013.
- [31] R. H. Müller and D. L. Clegg, "Automatic paper chromatography," *Anal. Chem.*, vol. 21, no. 1, p. 192, Dec. 1949.
- [32] G. A. G. Posthuma-Trumpie, J. J. Korf, and A. A. van Amerongen, "Lateral flow (immuno)assay: its strengths, weaknesses, opportunities and threats. A literature survey." *Anal Bioanal Chem*, vol. 393, no. 2, pp. 569–582, Jan. 2009.
- [33] H. Liu and R. M. Crooks, "Three-Dimensional Paper Microfluidic Devices Assembled Using the Principles of Origami," *J. Am. Chem. Soc.*, vol. 133, no. 44, pp. 17 564–17 566, Nov. 2011.

- [34] E. Fu, B. Lutz, P. Kauffman, and P. Yager, "Controlled reagent transport in disposable 2D paper networks," *Lab Chip*, vol. 10, no. 7, pp. 918–920, 2010.
- [35] X. Li, D. R. Ballerini, and W. Shen, "A perspective on paper-based microfluidics: Current status and future trends," *Biomicrofluidics*, vol. 6, no. 1, p. 011301, Mar. 2012.
- [36] E. Fu and C. Downs, "Progress in the development and integration of fluid flow control tools in paper microfluidics." *Lab Chip*, vol. 17, no. 4, pp. 614–628, Feb. 2017.
- [37] M. M. Gong and D. Sinton, "Turning the Page: Advancing Paper-Based Microfluidics for Broad Diagnostic Application." *Chem. Rev.*, pp. in press, DOI: 10.1021/acs.chemrev.7b00024, Jun. 2017.
- [38] N. R. Pollock, J. P. Rolland, S. Kumar, P. D. Beattie, S. Jain, F. Noubary, V. L. Wong, R. A. Pohlmann, U. S. Ryan, and G. M. Whitesides, "A paper-based multiplexed transaminase test for low-cost, point-of-care liver function testing." *Sci Transl Med*, vol. 4, no. 152, pp. 152ra129–152ra129, Sep. 2012.
- [39] A. A. Kumar, J. W. Hennek, B. S. Smith, S. Kumar, P. Beattie, S. Jain, J. P. Rolland, T. P. Stossel, C. Chunda-Liyoka, and G. M. Whitesides, "From the bench to the field in low-cost diagnostics: two case studies." *Angew. Chem. Int. Ed. Engl.*, vol. 54, no. 20, pp. 5836–5853, May 2015.
- [40] E. Fu, T. Liang, P. Spicar-Mihalic, J. Houghtaling, S. Ramachandran, and P. Yager, "Two-Dimensional Paper Network Format That Enables Simple Multistep Assays for Use in Low-Resource Settings in the Context of Malaria Antigen Detection," *Anal. Chem.*, vol. 84, no. 10, pp. 4574–4579, May 2012.
- [41] L. K. Lafleur, J. D. Bishop, E. K. Heiniger, R. P. Gallagher, M. D. Wheeler, P. Kauffman, X. Zhang, E. C. Kline, J. R. Buser, S. Kumar, S. A. Byrnes, N. M. J. Vermeulen, N. K. Scarr, Y. Belousov, W. Mahoney, B. J. Toley, P. D. Ladd, B. R. Lutz, and

- P. Yager, "A rapid, instrument-free, sample-to-result nucleic acid amplification test," *Lab Chip*, vol. 16, no. 19, pp. 3777–3787, 2016.
- [42] J. R. Choi, J. Hu, R. Tang, Y. Gong, S. Feng, H. Ren, T. Wen, X. Li, W. A. B. Wan Abas, B. Pingguan-Murphy, and F. Xu, "An integrated paper-based sample-to-answer biosensor for nucleic acid testing at the point of care," *Lab Chip*, vol. 16, no. 3, pp. 611–621, 2016.
- [43] E. Berthier and D. J. Beebe, "Flow rate analysis of a surface tension driven passive micropump," *Lab Chip*, vol. 7, no. 11, p. 1475, 2007.
- [44] G. M. Walker and D. J. Beebe, "A passive pumping method for microfluidic devices," *Lab Chip*, vol. 2, no. 3, pp. 131–134, Aug. 2002.
- [45] M. W. Toepke, V. V. Abhyankar, and D. J. Beebe, "Microfluidic logic gates and timers," *Lab Chip*, vol. 7, no. 11, p. 1449, 2007.
- [46] T. E. de Groot, K. S. Veserat, E. Berthier, D. J. Beebe, and A. B. Theberge, "Surface-tension driven open microfluidic platform for hanging droplet culture," *Lab Chip*, vol. 16, no. 2, pp. 334–344, 2016.
- [47] S.-J. Kim, S. Paczesny, S. Takayama, and K. Kurabayashi, "Preprogrammed, Parallel On-Chip Immunoassay Using System-Level Capillarity Control," *Anal. Chem.*, vol. 85, no. 14, pp. 6902–6907, Jul. 2013.
- [48] M. Zimmermann, H. Schmid, P. Hunziker, and E. Delamarche, "Capillary pumps for autonomous capillary systems," *Lab Chip*, vol. 7, no. 1, pp. 119–125, 2007.
- [49] P. Man, C. H. Mastrangelo, M. A. Burns, and D. T. Burke, "Microfabricated capillarity-driven stop valve and sample injector," in *Proceedings of the the IEEE MEMS Conference*, Jan. 1998, pp. 45–50.
- [50] J. Melin, N. Roxhed, G. Gimenez, P. Griss, W. van der Wijngaart, and G. Stemme, "A liquid-triggered liquid microvalve for on-chip flow control," *Sensors & Actuators: B. Chemical*, vol. 100, no. 3, pp. 463–468, Jan. 2004.

- [51] D. Juncker, H. Schmid, U. Drechsler, H. Wolf, M. Wolf, B. Michel, N. de Rooij, and E. Delamarche, "Autonomous Microfluidic Capillary System," *Anal. Chem.*, vol. 74, no. 24, pp. 6139–6144, Dec. 2002.
- [52] R. Safavieh and D. Juncker, "Capillarics: Pre-programmed, self-powered microfluidic circuits built from capillary elements," *Lab Chip*, vol. 13, no. 21, pp. 4180–4189, Nov. 2013.
- [53] L. Gervais, M. Hitzbleck, and E. Delamarche, "Capillary-driven multiparametric microfluidic chips for one-step immunoassays." *Biosensors and Bioelectronics*, vol. 27, no. 1, pp. 64–70, Sep. 2011.
- [54] E. Delamarche, A. Bernard, H. Schmid, B. Michel, and H. Biebuyck, "Patterned delivery of immunoglobulins to surfaces using microfluidic networks." *Science*, vol. 276, no. 5313, pp. 779–781, May 1997.
- [55] C. Jönsson, M. Aronsson, G. Rundström, C. Pettersson, I. Mendel-Hartvig, J. Bakker, E. Martinsson, B. Liedberg, B. MacCraith, O. Öhman, and J. Melin, "Silane–dextran chemistry on lateral flow polymer chips for immunoassays," *Lab Chip*, vol. 8, no. 7, p. 1191, 2008.
- [56] M. I. Mohammed and M. P. Y. Desmulliez, "The manufacturing of packaged capillary action microfluidic systems by means of CO<sub>2</sub> laser processing," *Microsyst Technol*, pp. 1–10, Mar. 2013.
- [57] A. O. Olanrewaju, A. Robillard, M. Dagher, and D. Juncker, "Autonomous microfluidic capillary circuits replicated from 3D-printed molds." *Lab Chip*, vol. 16, no. 19, pp. 3804–3814, Sep. 2016.
- [58] L. Gervais and E. Delamarche, "Toward one-step point-of-care immunodiagnostics using capillary-driven microfluidics and PDMS substrates." *Lab Chip*, vol. 9, no. 23, pp. 3330–3337, Dec. 2009.

- [59] M.-I. Mohammed and M. P. Y. Desmulliez, "Characterization and theoretical analysis of rapidly prototyped capillary action autonomous microfluidic systems," *J. Microelectromech. Syst.*, vol. 23, no. 6, pp. 1408–1416, Dec. 2014.
- [60] A. O. Olanrewaju, A. Ng, P. Decorwin-Martin, A. Robillard, and D. Juncker, "Microfluidic Capillary Circuit for Rapid and Facile Bacteria Detection." *Anal. Chem.*, vol. 89, no. 12, pp. 6846–6853, Jun. 2017.
- [61] R. Safavieh, A. Tamayol, and D. Juncker, "Serpentine and leading-edge capillary pumps for microfluidic capillary systems," *Microfluid Nanofluid*, vol. 18, no. 3, pp. 357–366, Jul. 2014.
- [62] M. Zimmermann, P. Hunziker, and E. Delamarche, "Valves for autonomous capillary systems," *Microfluid Nanofluid*, vol. 5, no. 3, pp. 395–402, Sep. 2008.
- [63] S.-J. Kim, S. Paczesny, S. Takayama, and K. Kurabayashi, "Preprogrammed capillarity to passively control system-level sequential and parallel microfluidic flows." *Lab Chip*, vol. 13, no. 11, pp. 2091–2098, Jun. 2013.
- [64] M. Wolf, D. Juncker, B. Michel, P. Hunziker, and E. Delamarche, "Simultaneous detection of C-reactive protein and other cardiac markers in human plasma using micromosaic immunoassays and self-regulating microfluidic networks." *Biosensors and Bioelectronics*, vol. 19, no. 10, pp. 1193–1202, May 2004.
- [65] X. Wang, J. A. Hagen, and I. Papautsky, "Paper pump for passive and programmable transport." *Biomicrofluidics*, vol. 7, no. 1, pp. 14 107–14 107, 2013.
- [66] B. M. Cummins, R. Chinthapatla, B. Lenin, F. S. Ligler, and G. M. Walker, "Modular pumps as programmable hydraulic batteries for microfluidic devices," *Technology*, vol. 05, no. 01, pp. 21–30, Mar. 2017.

## Chapter 3

# Capillary microfluidics in microchannels: from microfluidic networks to capillanic circuits

Microfluidics offer economy of reagents, rapid liquid delivery, and potential for automation of many reactions. Microchannel-based capillary microfluidics can deliver and drain liquids in a pre-programmed and autonomous manner without peripheral equipment by exploiting surface tension effects encoded by the geometry and surface chemistry of the microchannel. Here, we review the history, progress, challenges, and opportunities of microchannel-based capillary microfluidics, spanning over three decades, with names evolving from microfluidic networks, capillary systems, and most recently capillanic circuits (CCs). We deconstruct CCs into basic principles and circuit elements, and benchmark CCs within the framework of sequential delivery of reagents to a reaction chamber, a fundamental requirement for many biological and chemical reactions. The first capillary microfluidics were developed in industry using lamination and replication of mechanically micro-machined molds as recorded in numerous patents filed as early as in the 1980s. The second wave of capillary microfluidics grew in academia in the context of  $\mu$ TAS and lab-on-a-chip devices, and was supported by advances in clean-room microfabrication, leading to development of a myriad of sub-100  $\mu\text{m}$  capillary elements including: pumps, stop valves, trigger

valves, delay valves, retention valves, and so on. Next, more advanced CCs were developed based on the combination of multiple capillary fluidic elements, analogously to electronic circuits, for sequentially delivering reagents. We conclude by discussing emerging trends including in particular rapid prototyping as a manufacturing technique that is paving the way for the 3rd wave of CCs. Buoyed by better models and lower entry barriers thanks to advances in manufacturing, CCs are on one hand presenting themselves as a fertile research area, and on the other hand as an increasingly powerful technology for creating laboratory and diagnostic tests that combine ease of use, hands-off operation, and high performance

This chapter is a manuscript of an invited review paper to be submitted for publication to *Lab on a Chip*: “**Capillary microfluidics in microchannels: from microfluidic networks to capillary circuits**” A.O. Olanrewaju, A. Tavakoli, M. Yafia, and D. Juncker.

### 3.1 Introduction

Microfluidic devices are miniaturized liquid handling systems with potential for biomedical applications for a variety of reasons including small sample and reagent volume requirements, potential for efficient mass transport to functionalized surfaces, ease of automation, low-cost, and disposability of devices.[1, 2] Capillary microfluidics is a sub-field that manipulate liquids using capillary effects (also called capillary action or capillary force) governed by the liquid surface tension, geometry, and surface chemistry of the support.[3] Capillary microfluidics are sometimes characterized as ‘passive’ because they often afford no real-time control over the flow. Yet this passive operation can also be understood as an advantage compared to ‘active’ devices since it eliminates the need for external pumps, valves, or other peripheral control. Hence, capillary microfluidic devices are not subject to the ‘lab-around-a-chip’ predicament that limits the deployment of many ‘active’ microfluidic systems.[4] Instead, instrument-free operation naturally constrains capillary microfluidics as actual

lab-on-a-chip devices that are especially suitable for rapid and minimally-instrumented biochemical assays.

Capillary microfluidics has become strongly associated with porous materials such as paper-based (and to a lesser extent thread-based) devices in academia and industry. Porous capillary microfluidics rely on non-deterministic capillary flow within the network of pores and have been reviewed elsewhere.[5, 6, 7, 8, 9, 10] However, capillary microfluidics as a *bona fide* academic research theme started as microfabricated, deterministic hydrophilic self-filling microchannels that generate negative capillary pressures at the filling front and that were initially called microfluidic networks. The term "capillary" was introduced in the context of microfabricated devices that were labelled as autonomous microfluidic capillary systems, both to avoid confusion with glass capillary-based microfluidics that were still quite prevalent at the beginning of this millennium, and to convey the concept of an autonomous system fulfilling a pre-programmed task.[11] The success and widespread adoption of paper-based capillary microfluidics can be explained by their low cost and hence potential for global health applications, and the ability to rapidly prototype new circuits using simple cutters and scissors and common printers.

On the other hand, microfabricated capillary systems were dependent on cleanroom and expensive microfabrication systems and photomasks, thus increasing the time and cost between design and testing. Conversely, cleanroom technology allowed fabrication of capillary systems with micrometer-scale resolution and deterministic control of capillary pressure and liquid interface during filling. An increasing number of functional capillary elements were designed, and increasingly complex fluidic circuits assembled from them in a modular manner, allowing for an analogy to electronic circuits, and leading us to propose the term "capillary circuits" (CCs) for microchannel-based circuits for several reasons: (i) to help resolve confusion around the word "capillary" which is used both as a noun, and lacking an adjective, as a

noun adjunct for many different applications and uses, such as capillary action, paper-based and microchannel (or capillary)-based capillary microfluidics, or capillary electrophoresis (which is a term used to describe electrophoresis in both capillaries and microchannels) etc. Indeed, the overuse of *capillary* makes it difficult to distinguish these concepts when used simultaneously, and confounds search engines, (ii) In addition to conveying the idea of a circuit assembled from basic elements[12], *capillarics* affords the nuance existing between *electric* and *electronic*, and (iii) can function both as an adjective *capillary* that is distinguishable from the noun *capillarics* in much the same way that *microfluidic* is distinguishable from *microfluidics*. We thus adopt *capillary* and CC for this review.

There are many different approaches for using capillary effects for flow control in microchannel-based microfluidics. An interesting, and perhaps the structurally simplest form of capillary microfluidics, are devices that use the positive pressure generated by droplets deposited at different inlets and outlets to control the flow.[13, 14] Such positive pressure capillary microfluidic devices can perform complex operations with minimal user intervention[15] Positive capillary microfluidics can operate with a small device footprint, and are compatible with robotic pipetting equipment; however, the pressures generated are small, and the number of sequential liquid delivery has been limited to just 5-steps, and require manual timing of pipetting steps for more complex operations.[16]. Capillary flow is also applicable to open microconduits and to virtual microchannels with liquid confined between horizontal, hydrophilic stripes [17], or suspended between side walls.[18]

Capillary forces have also been combined with other effects for flow control in microfluidic devices. Electrochemical and electrostatic effects were also combined with capillary forces for flow regulation in microchannels.[19, 20, 21] In addition, capillary valving using hydrophobic features can also be used to regulate flow with subsequent fluid actuation using active means such as centrifugal or pneumatic force needed as the primary driving force for flow.[22, 23, 24] For example, a wearable microfluidic device for chronological sweat sampling was developed by using capillary burst valves

for sequential guiding of liquids into reservoirs, with device filling driven by pressure induced by sweat glands and subsequent liquid recovery using centrifugal forces.[25] There are also non-biological applications of capillary-driven microfluidics such as their use in cooling systems,[26] self-assembly,[27] manufacture of electric circuits,[28] and electronic packaging.[29]

This review is focused on CCs that use negative capillary pressures to wick liquids into microchannels with deterministic control over filling. We discuss them from the perspective of a system assembled from ‘capillary elements’. We begin with a brief historical perspective that covers pioneering work on capillary flow and capillaric elements performed in industry that has not been reviewed so far. Next, the physical properties governing microchannel-based capillary flow, and the principles of operation of individual capillaric elements such as capillary pumps and valves are discussed. Then we describe the integration of capillaric elements into self-regulated CCs for pre-programmed liquid delivery operations. We do not provide an exhaustive discussion of all the literature in microchannel-based capillary microfluidics, instead we provide a perspective on key developments and upcoming trends, such as rapid prototyping, that may dictate future directions in the field.

## 3.2 Brief Historical Perspective

Microfluidic CCs have a history that stretches back over 30 years. As shown in Figure 3.1, there are two established waves of development that can be distinguished based on the dominant manufacturing technologies used, namely: (1) classical mechanical micro-machining, and (2) photolithography-based chemical micromachining. More recently, a third emerging wave fuelled by additive manufacturing and rapid prototyping is emerging.

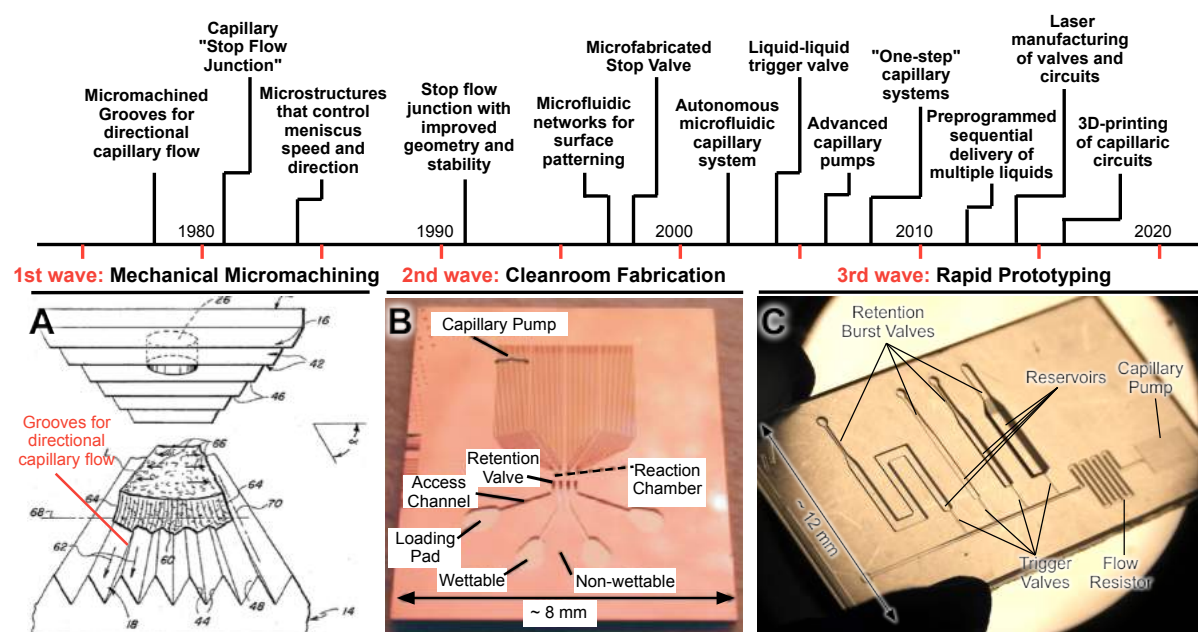


FIGURE 3.1: **Stages of development in microchannel-based capillary microfluidics.** Some notable developments are highlighted in the timeline. (A) The 1st wave of capillary microfluidics was developed largely in industrial labs and prevalently relied on mechanical micromachining. (B) The 2nd wave was developed in the late 1990s following the emergence of microfluidics, micro total analysis systems ( $\mu T A S$ ) and lab-on-a-chip as distinct research fields, and the availability of photolithography, micromachining and soft lithography for making microfluidics with features with to sub-micrometer resolution. (C) The 3rd emerging wave of microchannel-based capillary microfluidics is taking shape following the emergence of rapid prototyping systems with resolution now reaching  $100 \mu m$ , adequate for capillary flow, enabling rapid design and optimization cycles, paving the way for enhancing CCs with new functionalities enabled by 3D printing. Adapted from (A) ref. 30, (B) ref. 31 © 2005 WILEY-VCH Verlag GmbH & Co. KGaA, Weinheim. (C) directly 3D-printed capillarie circuit from our lab.

### 3.2.1 1st wave capillary microfluidics: Mechanical Micromachining and Lamination

The first wave of CCs can be associated with the development of microstructures for capillary-driven fluid transport in industrial research labs, and is documented in a variety of patents detailing ideas and developments in capillary transport from the late 1970s till the early 1990s. These developments primarily appear in the patent literature rather than in the academic literature and so are not widely known - in part because patents are often written to be tedious to read, while also lacking experimental demonstration in many cases as it was not required then. Micromachined grooves for promoting directional capillary-driven transport[30] and abrupt geometry changes to halt flow[32, 33] are among the earliest microchannel-based capillary flow control elements described in the patent literature. For example, Fig 3.2A illustrates the use of microstructures to guide liquid filling fronts to avoid bubble entrapment in capillary pumps, which was originally patented in 1986[34] while capillary pumps based on similar ideas were published in the scientific peer-reviewed literature over 20 years later.[35, 36] Other contributions include development and optimization of capillary stop valves that passively halt flow at abrupt geometric changes (Fig. 3.2B), self-powered dilution devices that combine capillary effects and gravity (Fig. 3.2C), matrix plugs for delay and sequential drainage of liquids (Fig. 3.2D), and advanced capillary pumps with gaps that prevent liquid back flow (Fig. 3.2E).

Details about the fabrication of early CC ideas presented in patents was often lacking, or merely hinted at, and were described in the context of lamination (allowing fabrication of thin gaps), or imprinting into polymers. Considering that many patents precede advanced silicon microfabrication techniques, it seems safe to assume that they were designed for fabrication using conventional mechanical machining in most cases. Although often unproven, many of the ideas in the early patents appear sound

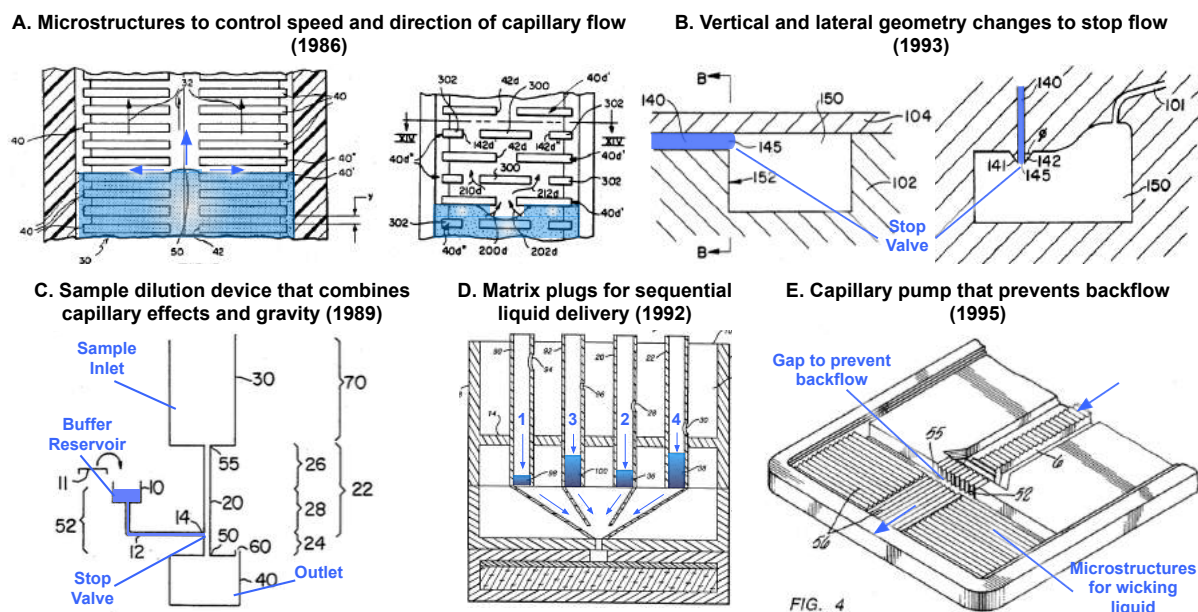


FIGURE 3.2: Examples of early mechanically micromachined devices that were patented decades ago by industrial labs with many of the ideas recently rediscovered and published in academic literature. (A) Two examples of microstructures that guide the speed and direction of liquid preventing bubble trapping. (B) Examples of capillary stop valve geometries with abrupt geometric changes to halt flow. Flow stoppage results from the pressure barrier created due to the abrupt geometric change at a stop valve. (C) Device for dilution and mixing of liquid samples that holds buffer in a reservoir using a capillary stop valve and enables subsequent sample dilution by additional of liquid from an inlet at a higher gravitational potential. (D) Use of porous matrix plugs for preprogrammed sequential drainage of liquids based on properties of porous matrix. (E) Capillary pump structure with microstructures for directional filling and a gap to prevent backflow of liquid towards the inlet. The gap in the capillary pump ensures unidirectional flow in the capillary pump since the wicking structures can completely empty liquid from the gap and prevent flow of liquid back up towards the inlet. Adapted from: (A) ref. 34, (B) ref. 33, (C) ref. 37, (D) ref 38, (E) ref. 39.

and should not be discounted. In fact, these early patents may inspire the development of capillary elements and systems, notably in the context of additive manufacturing with resolution limitations currently within the same range as that of historical machining technologies.

### 3.2.2 2nd wave capillary microfluidics: Cleanroom Fabrication

The emergence of micro total analysis systems ( $\mu$ TAS) in the 90s,[40] was empowered by advances in microfabrication technologies that enabled high-precision fabrication of microstructures in silicon and photoresists. The second wave of development followed the widespread adoption of photolithography and cleanroom processes for  $\mu$ TAS applications. Capillary force-driven flows in microchannels followed suit with early applications not in assays, but micromolding[41]. Capillary microfluidics for chemical and biological applications were first proposed by Delamarche and colleagues by patterning surfaces with proteins for immunoassays.[42] using 1.5- $\mu$ m-deep microchannels and refined for multiplexed immunoassays.[43] Microfabricated capillary fluidic elements were proposed to add functionality, such as stop valves[44], and the analogy to trees and water transport in plants noted, leading to the introduction of evaporation to drive liquids, [45]. More advanced systems were developed for autonomous, controlled delivery of reagents sequentially applied to the inlet [11] and more advanced applications in immunoassays were explored[46]. Subsequently, CCs for hands-off, pre-programmed, sequential delivery of samples and reagents for immunoassays were developed[47, 48, 49, 50, 51] and the concept of capillarie circuits was proposed [12].

Si substrates were the most popular material for CCs owing to the wide range of microfabrication tools and technologies available to microstructure it.[36, 42, 47, 52] Some CCs were made using patterned photoresist and then replicated into PDMS by soft lithography for rapid production of more devices without returning to the cleanroom.[12, 48] CCs were also manufactured by mass producible means such as

injection molding in thermoplastics (e.g. cycloolefin-copolymer) and treated with silane-dextran chemistry to obtain a stable hydrophilic surface.[53] CCs are typically rendered hydrophilic by plasma activation and silane chemistry. Si substrates maintain a highly stable and wettable surface since an oxide layer is formed after plasma treatment. Whereas, PDMS rapidly becomes hydrophobic again unless special, advanced surface treatments are used. CC fabrication by programmable proximity aperture lithography using 9- $\mu\text{m}$  thick PMMA films on a Si substrate and sealed with 50- $\mu\text{m}$  thick PMMA sheets so that the closed channels were wettable and did not require surface treatment.[54] Progress in microfabricated capillary elements and integrated circuits is described in greater detail in section 3.4 (“Capillary microfluidic elements”).

### 3.2.3 3rd wave capillary microfluidics: Rapid prototyping

Rapid prototyping technologies such as simple craft cutting of tape, laser etching of polymers, and 3D-printing are now widely available and have been applied for rapid and inexpensive microfabrication of CSs.[55, 56, 57] Functional capillary elements and systems were manufactured using CO<sub>2</sub> laser cutting[56, 58]. Stereolithographic 3D-printing was used to manufacture molds for capillary valves and systems that were replicated into PDMS.[57, 59] However, laser cutting is usually limited to microchannel sizes  $> 200 \mu\text{m}$ , while the lateral resolution of commercial 3D-printers is usually  $> 100 \mu\text{m}$  while the vertical resolution is typically  $> 20 \mu\text{m}$ . [60] Despite these size limitations, rapidly prototyped microfluidic devices with complex channel architectures for deterministic flow control can be made in  $< 1 \text{ h}$ , and can be used directly, or serve as molds for replica molding in the lab or for mass manufacturing by injection molding. In particular, CCs stand to gain from 3D-printing and digital multi-layer design of modular capillary fluidic elements that can be tailored for specific applications.[57, 59] Progress, challenges, and opportunities in rapid prototyping of CCs is discussed in detail in section 3.5.5.

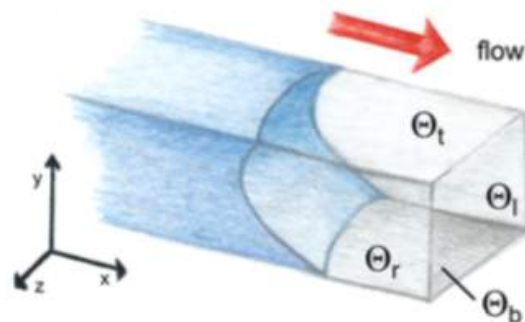


FIGURE 3.3: Illustration of capillary-driven flow in a wettable rectangular microchannel. Contact angles of liquid with each of the four microchannel walls are denoted. Adapted from ref. 61

### 3.3 Fundamentals Parameters and Equations

Before describing the operating principles of capillary microfluidic elements, we briefly summarize fundamental parameters and equations that govern capillary flow in microchannels.

#### 3.3.1 Capillary Pressure

Capillary pressure is a pressure that arises at the liquid-air interface in a microchannel as a result of surface tension of the liquid, geometry and surface chemistry at the immediate location of the interface. A surface is considered wettable if the contact angle of liquid is less than  $90^\circ$ , as it will generate a concave interface and a negative capillary pressure that will spontaneously draw the liquid into the conduit by capillary action; for angles greater than  $90^\circ$ , the interface is convex, and the pressure positive, pushing the liquid out of the channel. Most microfabricated channels used in capillary-driven microfluidics have a rectangular geometry due to the use of planar photolithographic fabrication technologies. Fig. 3.3 illustrates capillary-driven transport of liquid in a rectangular microchannel.

The Young-Laplace equation gives the relationship between capillary pressure, contact angle, and microchannel geometry for a rectangular microchannel as:[62]

$$P = -\gamma \left[ \frac{\cos \theta_t + \cos \theta_b}{h} + \frac{\cos \theta_l + \cos \theta_r}{w} \right] \quad (3.1)$$

where  $P$  is the capillary pressure,  $\gamma$  is the surface tension of liquid in the microchannel,  $h, w$  are the channel height and width respectively, and  $\theta_t, \theta_b, \theta_l, \theta_r$  are the top, bottom, left, and right contact angles of liquid with the corresponding microchannel walls.

For very wettable surfaces with contact angle  $< 45^\circ$ , corner flow - the rapid imbibition of liquid along the corners of microchannels forming a precursor film along the channel walls that precedes bulk flow - is an important effect that could result in deviations from the expected behaviour in equation 3.1.[63, 64] Corner flow is especially pronounced in microchannels with heterogenous surfaces where the contact angles for all the channel walls are not identical especially when the channel has a very high (or low) height-to-width ratio.[65, 66]

### 3.3.2 Flow Resistance

Another important parameter to consider is the flow rate of liquid in a microchannel. Most microfabricated channels have a rectangular structure. An expression for the flow rate of liquid in a rectangular microchannel can be obtained by solving Navier-Stokes equations. Laminar flow in microfluidic channels assuming steady state flow with no gravitational effects enables us to obtain a simplified analytical expression for the flow rate of liquid in a rectangular microchannel.[67] A further simplified form of the flow rate can be obtained for a flat and very wide channel in the limit  $\frac{h}{w} \rightarrow 0$ :

$$Q \approx \frac{h^3 w \Delta P}{12 \eta L} \left[ 1 - 0.630 \frac{h}{w} \right] \quad (3.2)$$

where  $h$  is microchannel height,  $w$  is microchannel width,  $\eta$  is the viscosity of liquid,  $\Delta P$  is the difference in capillary pressure across the microchannel, and  $L$  is microchannel length. This approximation differs from the exact analytical value of flow resistance by up to 13% when  $h = w$  (the worst case scenario deviation for the approximation in Eqn 3.2) and differs by only 0.2% when  $h = w/2$ .[67]

Microfluidic networks can be analyzed using electrical analogies. Based on Eqn. 3.2, we can express the relationship between the capillary pressure and flow rate as

follows:

$$Q = \frac{\Delta P}{R} \quad (3.3)$$

where  $R$  is the flow resistance of the microchannel.

Studying the flow resistance and the capillary pressure provides understanding of the scaling laws at play in capillary microfluidic systems. Note that for a rectangular microchannel with  $h$  significantly smaller than  $w$ , the capillary pressure is proportional to  $1/h$ , meanwhile the flow resistance is proportional to  $1/h^3$ . Thus, decreasing microchannel height has a much greater effect on the flow resistance than the capillary pressure. Such considerations based on scaling laws are important in the design of capillary elements and integrated systems. In contrast, when  $h = w$ , the capillary pressure is proportional to  $2/h$  while the flow resistance is proportional to  $1/h^4$ .

Equation 3.3 can be used to predict the expected filling time of capillary microfluidic devices. For example, a multi-parametric microfluidic chip for parallel immunoassays was developed by systematically designing the flow resistances along parallel flow paths to obtain filling times ranging from 10 to 72 min.[68] However, in that demonstration the experimental filling time exceeded the calculated filling time by up to 35% (i.e. calculated filling time of 47 min and experimental filling time of 72 min). This indicates that the theoretical model for flow rate is accurate to within a factor of two, but not accurate enough to provide an exact prediction of the expected flow rate. Dynamic models with time-dependent analytical expressions for the velocity of capillary-driven flow in microchannels more closely match experimental data; [58, 69] however, dynamic models are more complex to derive and have only been presented for microchannels with uniform wettability on all microchannel walls. Dynamic models need to be adapted for microchannels with heterogeneous surfaces e.g. hydrophobic top cover and hydrophilic bottom and side walls.

## 3.4 Capillary Microfluidic Elements

Keeping with the concept of microfluidic circuits assembled from basic fluidic elements, we review the various capillary (or capillary) elements that have been developed to generate and regulate capillary flow. A representative CC is shown using symbolic representation borrowed from electronics and schematic representation (Fig. 3.4). CCs are designed by combining various capillary elements thus creating *autonomous* microfluidics capable of self-powered and self-regulated liquid delivery. The different elements shown in the CC will be described in detail below. Flow is generated by the self-filling property of the microchannels until they are filled, and then sustained by capillary pumps. Stop valves, trigger valves, and retention valves regulate flow. Note that the functionality of various elements is realized only when the liquid-air interface reaches those elements during either filling or draining of different branches of the CC. The flow resistance on the other hand is a function of the filling level and gradually increases as liquid fills a conduit reaching its maximum value once filled (under the condition that viscosity is constant of course).

In this section, we summarize and critically analyze the properties of commonly used capillary microfluidic elements to understand the operation and application of CCs.

### 3.4.1 Flow Resistors

Flow resistors naturally arise from the viscous flow resistance of liquid flowing through a microchannel, and are an important design consideration for any microfluidic chip, and can be readily calculated (see Eqn. 3.2). Flow resistors may be employed in several ways within a CC for biochemical assays. The flow resistance in a CC can be varied systematically to investigate the effects of longer incubation time on the detected signal after an assay.[68] Serpentine flow resistors can also be used as mixers within CCs [68, 70]. Systematic differences in flow resistance of parallel microchannels branching from the same flow path can also be used to create “reagent integrators” for

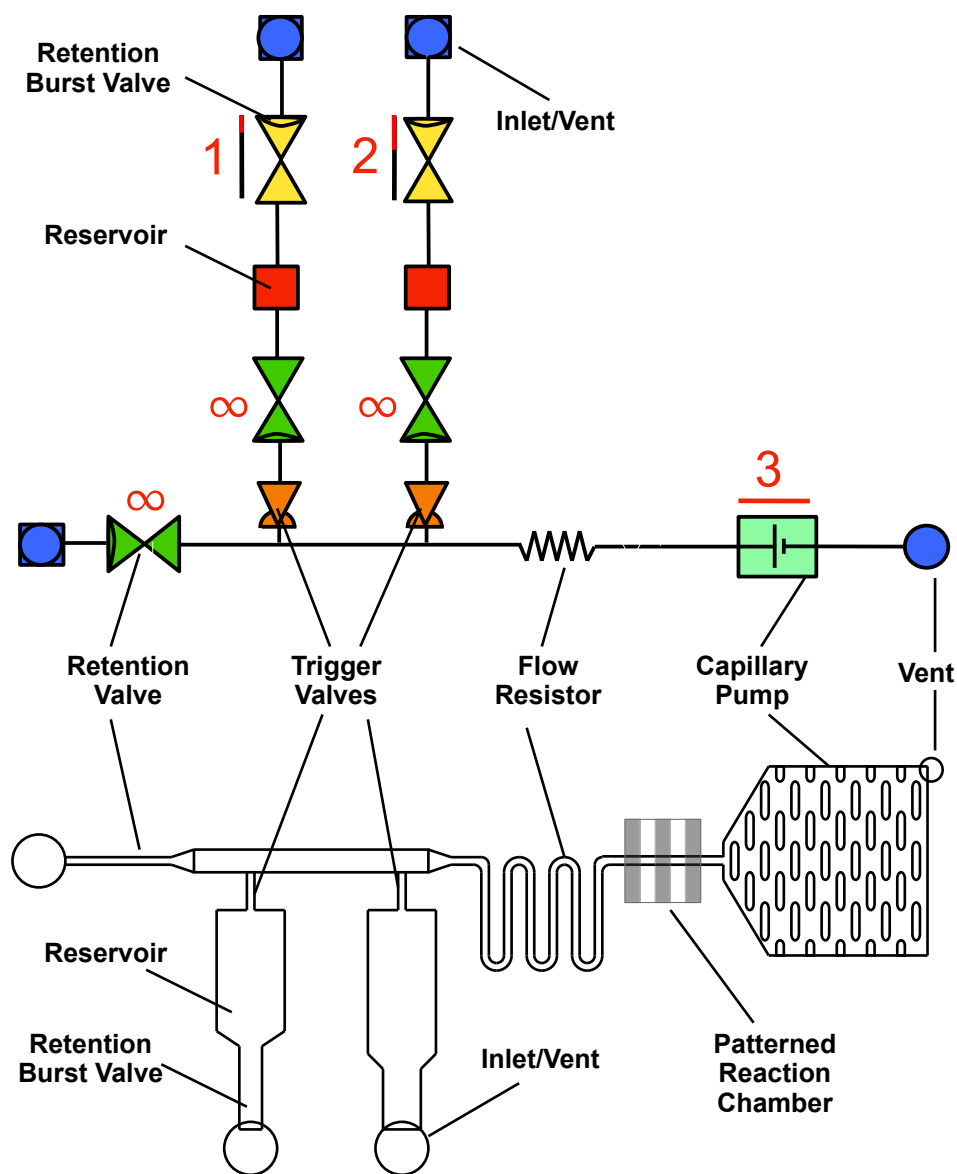


FIGURE 3.4: Symbolic (top) and schematic (bottom) representations of a microfluidic circuit consisting of several capillary fluidic elements including: capillary pump, trigger valve, retention valve, retention burst valve, flow resistor, inlets, and vents.

rapid and efficient dissolution of dried reagents while retaining a small footprint for the mixing structure.[52] In addition, flow resistors can be used to provide a capillary pressure drop, similar to the voltage drop across an electric resistor, to regulate capillary pressures in a CC and regulate sequential bursting of Retention Burst Valves (RBVs).[12, 57] Berthier et al. recently analytically and experimentally studied flow resistors and referred to microchannel constrictions as “global” flow resistors that reduce the overall flow rate in all downstream sections of a conduit, while microchannel expansions act as “local” flow resistors that only temporarily decrease the flow rate and do not affect the flow rate downstream of the enlargement. [71] It is important to clarify that microchannel expansions in fact decrease flow velocity by reducing the capillary pressure driving flow in a circuit, rather than increasing the flow resistance of the channel, yet in this context they are referred to as “local flow resistors” because they have the net effect of slowing down flow velocity in a microchannel.

### 3.4.2 Capillary pumps

Capillary pumps are one of the earliest capillary microfluidic elements developed. Capillary pumps wick liquids spontaneously into wettable microchannels using capillary pressure and are placed at the outlet of a CC to pump additional liquid through the channels and reaction chambers upstream. Capillary pumps fulfill essential functions in a CC, and are used to draw sufficient reagent to complete a reaction. Often capillary pumps also simultaneously serve as a waste compartment for reagents after completion of biochemical assays on-chip.

Capillary pumps need to meet two specific requirements depending on the application. First, to ensure constant (or a predetermined) flow throughout the experiment, they should provide a constant, predetermined pressure irrespective of filling level, implying that the pump should not add to the resistance of the overall circuit. Early designs aimed at minimizing flow resistance used branching to link the microchannel outlet to multiple parallel channels, thus forming arborescent structures reminiscent

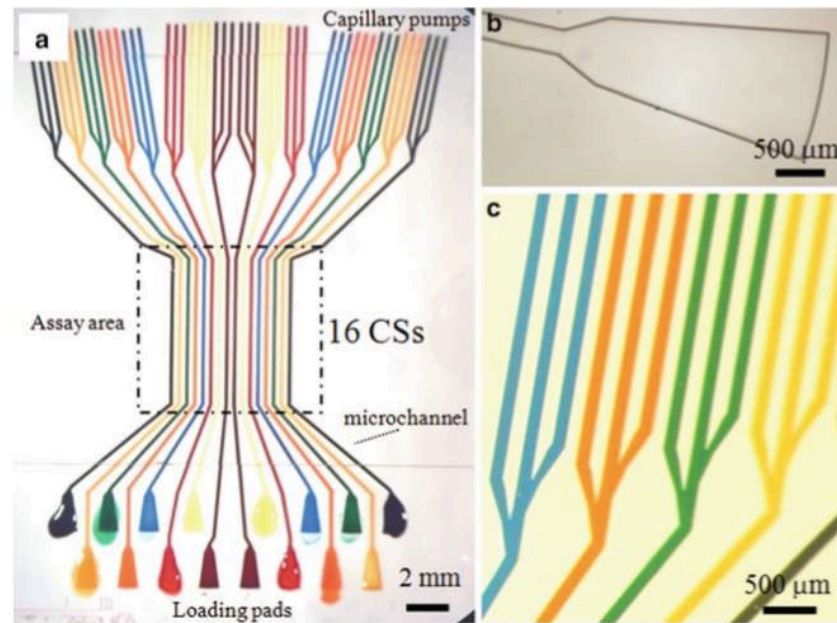


FIGURE 3.5: **Capillary system with simple tree line capillary pumps.** Overview of capillary system (left), close-up of inlet (top right), and close-up of capillary pump (bottom right). Adapted from from ref. 72 © 2010 Springer

of trees (Fig. 3.5).[11, 72]

A second important function of many capillary pumps is liquid metering defined by the volume of the pump so as to precisely control the amount of reagent drawn through the circuit. However, the capillary pressure of pumps is often high, requiring features only a few tens of micrometers wide, which cannot be etched more than 100 to 200  $\mu\text{m}$  in depth. Hence to accommodate volumes of the order of a few nanoliters, the footprint of capillary pumps rapidly reaches several  $\text{mm}^2$  in size, while at the same time the pumps need to be covered to minimize evaporation. Given these requirements, bubble trapping arises as an issue because the liquid often follows the edges, and reaches the outlet quickly before filling the centre, thus trapping an air bubble, and introducing significant metering errors based on the liquid volume displaced by the bubble within the capillary pump. To provide some control over the filling front of the liquid and help reduce bubble trapping, designs shifted from microchannels to arrays of posts - which lead to stochastic capillary flow that is more similar to paper than to deterministic microchannels - with regular spacing to provide some control over the speed and position of the liquid meniscus[12, 36, 53, 73]. (see Fig. 3.6) Also,

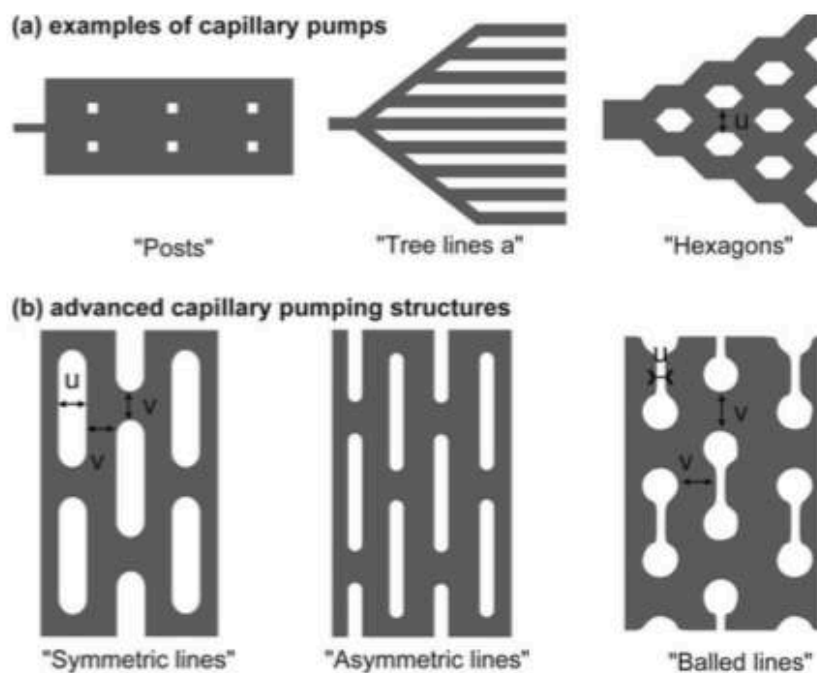


FIGURE 3.6: **Microstructures for simple and advanced capillary pumping.** Microstructure shape and arrangement can be adjusted to guide liquid filling front. Adapted from ref. 36, © 2007 Royal Society of Chemistry.

microchannel outlet geometries with redundant flow paths, i.e. multiple conversation microchannels leading to a single outlet, and low capillary pressure could help to further mitigate the risk of bubble trapping by delaying flow along the edges of the capillary pump and merging them together into a single central stream.[36]

Deterministic control of the filling front using the microstructures was realized by creating zones of high and low capillary pressure and thus predictably guiding the direction of the liquid meniscus (Fig 3.7).[35, 73] Microstructure arrangements within the capillary pump guide the liquid meniscus along well-defined paths to avoid bubble trapping and row skipping. These advanced capillary pumps improve reliability but at the cost of greater design and microfabrication complexity.

To increase the capacity of capillary pumps with volumes typically limited to the  $nL$  range, evaporation[45, 74, 75] and porous materials (such as paper) were used.[46, 57, 76] Porous pumps provide large volume capacity while retaining small device footprints. Paper pumps can be patterned to provide variable and pre-programmed flow rates.[76, 77] Synthetic microfluidic paper with well-controlled arrays of interlocked

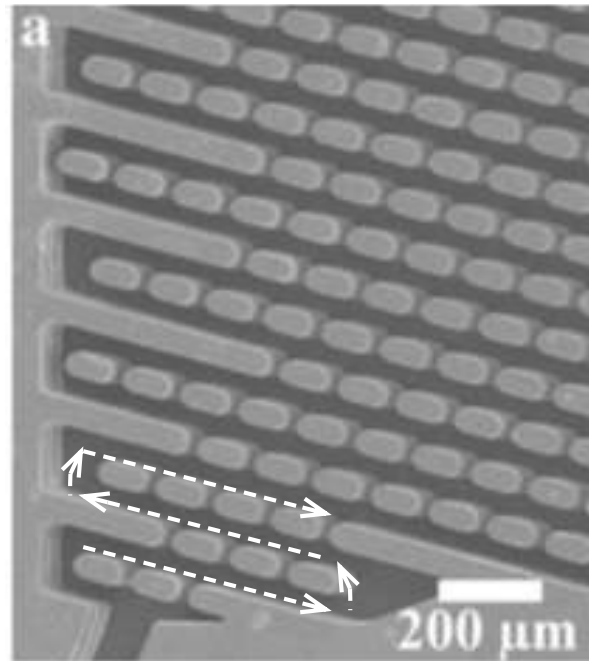


FIGURE 3.7: Scanning electron micrograph of serpentine capillary pump with microposts that guide direction of liquid meniscus to avoid bubble entrapment thereby minimizing variations in pumping pressure and flow rate. Adapted from ref. 35 © 2014 Springer.

micropillars was developed in polymer and demonstrated to provide improved performance compared to conventional porous materials.[78] Hydrogels[79] and superabsorbent polymers[80, 81] have also been used as pumps to drive capillary-driven flow. It is noteworthy that paper-plastic hybrid devices typically require an initial priming step to ensure proper contact between the membrane and the microchannel.[76]

### 3.4.3 Stop valves

Stop valves are another one of the earliest capillary microfluidic elements developed. Stop valves halt the flow of liquid in microchannels without external intervention using an abrupt change in microchannel geometry.[44, 82] Liquid is stopped by abruptly enlarging the microchannel cross-section.

The theoretical principles behind the operation of the capillary stop valve have also been described in detail.[22, 44, 82, 86] Fig. 3.8A shows the geometric parameters that affect the pressure barrier provided by a 2-dimensional stop valve. The pressure barrier,  $\Delta P$ , for a 2-dimensional stop valve (depth  $\gg$  width) can be calculated as:[44]

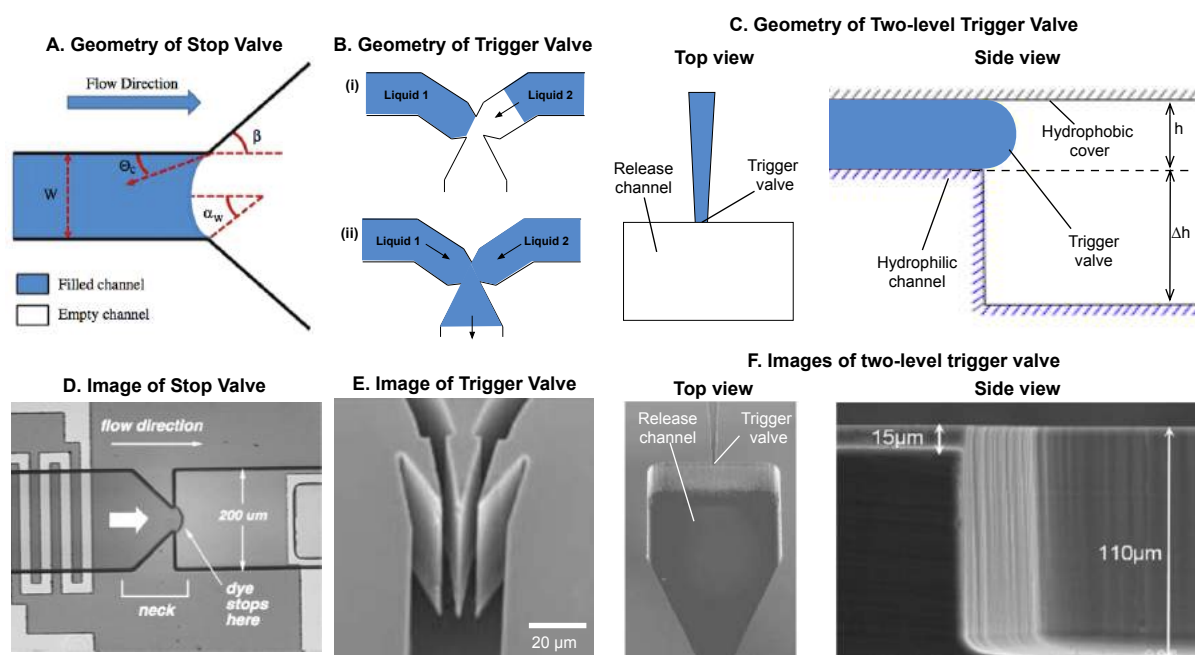


FIGURE 3.8: **Schematics and images of stop valves and trigger valves.** (A) Schematic showing geometry of a 2-dimensional stop valve (depth  $\gg$  width) illustrating the relevant parameters in analytical models (Equation 3.4). (B) Operating principle of liquid-liquid trigger valve showing how liquid is released when fluid is present at both sides of the trigger valve junction. (C) Schematic of two-level trigger valve showing abrupt geometry change in both lateral and vertical directions. (D) Image of liquid stopped at abrupt 2-dimensional geometry change in microchannel. (E) Scanning electron micrograph showing trigger valve with large height-to-width ratio (aspect ratio). (F) Scanning electron micrograph images of two-level trigger valve. Adapted from: (A) ref. 83 © 2013 IOP Publishing Ltd., (B) ref. 84 © 2004 Elsevier B.V., (D) ref. 44 © 1998 IEEE, (E) ref. 82 © 2007 Springer-Verlag, (F) ref. 85 © 2005 Elsevier B.V.

$$\Delta P = \frac{2\gamma}{w} \left( \frac{\cos \theta_c - \frac{\alpha_w \sin \beta}{\sin \alpha_w}}{-\cos \beta + \frac{\sin \beta}{\sin \alpha_w} \left( \frac{\alpha_w}{\sin \alpha_w} - \cos \alpha_w \right)} \right) \quad (3.4)$$

where  $w$  and  $h$  are the width and height of the microchannel leading into the stop valve,  $\theta_c$  is the contact angle assuming all walls have the same surface energy,  $\alpha_w$  is the liquid meniscus curvature in the lateral direction,  $\beta$  is the change in curvature of the liquid meniscus as illustrated in Fig. 3.8A.

Although stop valves are reliable and simple to incorporate within actively powered hydrophobic systems,[22, 44, 87] their reliability in capillary-driven systems is rarely reported or only described for short durations (e.g. 5 min[58, 82]). Glière and Delattre numerically and empirically characterized the burst pressure of two-level trigger valves as a function of microchannel hydraulic diameter.[85]

### 3.4.4 Trigger valves

Stop valves have only limited use in CCs as they typically require external actuation to overcoming the flow stoppage.[44] Stop valves can readily be turned into capillary trigger valves by implementing the flow stop at an intersection with a second (orthogonal) microchannel, thus allowing flow of the stopped liquid to be resumed simply by the application of a liquid in the other conduit (Fig 3.8B). One trigger valve design was based on joining microchannels, requiring all conduits to be filled for flow to progress, in effect realizing an "AND" function with two or more reagents. [82, 84]

Early trigger valves were made from Silicon and required very high height-to-width ratios (e.g.  $h/w = 12.5$ )[84] to successfully stop liquid (Fig. 3.8). To reduce fabrication constraints and improve reliability, two-level trigger valves with lower aspect ratios were developed that replicated the design of the robust two-level stop valve[85] with a hydrophobic cover (typically PDMS), and hydrophilic side and bottom walls, and that could be actuated by flowing liquid in the microchannel that formed the valve. (Fig. 3.8C).[12] "Two-level" refers to the fact that the stop/trigger valve has a different (and shallower) depth than the release channel that it is connected

to. This vertical height change also contributes to the capillary pressure barrier on the liquid and helps to stop liquid at the stop/trigger valve. Two-level trigger valves are more reliable than one level-trigger valves and robustly stopped liquids for up to 30 min.[12, 57] Two-level trigger valves can be made with larger dimensions without compromising functionality using rapid prototyping as discussed in section 3.5.5 (Rapid prototyping). Further study is required to ascertain the influence of parameters such as liquid surface tension and contact angle on the reliability of trigger valves.

### 3.4.5 Retention valves

Retention valves are capillary elements that pin liquids at microchannel constrictions, and prevent drainage of liquids from downstream reaction chambers. By placing a retention valve at the inlet of a closed microchannel, it is possible to simply load reagents one after the other as they are drained by the capillary pump, while the retention valves prevent entry of air and drying of the reaction chamber.[11, 46, 88] Retention valves are realized simply by reducing the microchannel cross-section and generating a capillary pressure that exceeds the one of the capillary pump, ensuring that they cannot be emptied during operation (Fig. 3.9). A 16-step bioassay with sample addition, washing, blocking, and detection steps, can be performed in a capillary system.[11] Although eliminating the need to remove liquid from the reaction chamber manually, retention valves require manual addition of the liquids at predetermined times in accordance with the needs of the assay. In addition, the need for creating constrictions by changing microchannel heights requires high resolution microfabrication ( $\approx 10 \mu\text{m}$ ) which can lead to increased cost and complexity.

### 3.4.6 Delay valves

Delay valves are used for distribution of liquids through different zones in a capillary system. Liquids fill narrower, higher capillary pressure, gaps first before filling wider,

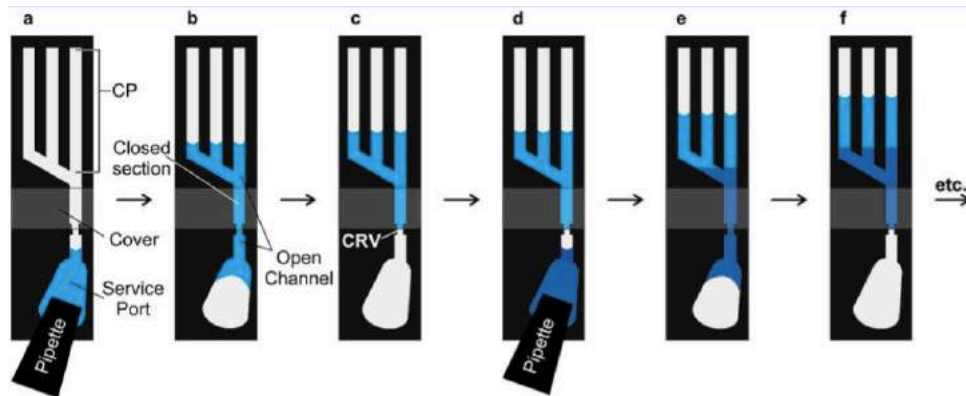


FIGURE 3.9: **Capillary retention valve (CRV) that allows sequential loading of a capillary microfluidic system.** Liquid is pinned at the CRV (step c) because it has a higher capillary pressure than the capillary pump. Adapted from ref. 11 © 2002

lower capillary pressure, gaps. Thus, by carefully tuning the spacing between microchannels reliable delay valves can be developed. For example, Zimmermann et al. implemented delay valves to ensure proper filling of 30- $\mu\text{m}$  wide side channels before filling a 60- $\mu\text{m}$  wide central channel (Fig. 3.10).[82]

Another approach to delaying flow in microchannels is to use dissolvable thin films as preprogrammed time delays within microchannels. This idea is reminiscent of past work using porous matrices to regulate flow (see Fig. 3.2D) Similar dissolvable valves were also implemented in paper-based microfluidics.[89] Lenk et al. used polyvinylalcohol (PVA) as a dissolvable barrier to control the sequence of liquid delivery in laminated capillary microfluidic devices.[51] The design incorporated dead-end channels to reduce PVA concentration and prevent saturation at the liquid leading edge which could result in slow drainage time.

Phaseguides are a fluidic component for routing liquids in microchannels.[90, 91] Phaseguides are formed using small bumps or dips in microchannels that create a capillary pressure barrier within a microchannel. Using phaseguides with different pressure barriers determined by geometry, one can obtain selective routing of liquid through microchannel networks and perform otherwise challenging operations such as filling corners while avoiding bubble trapping.[91]

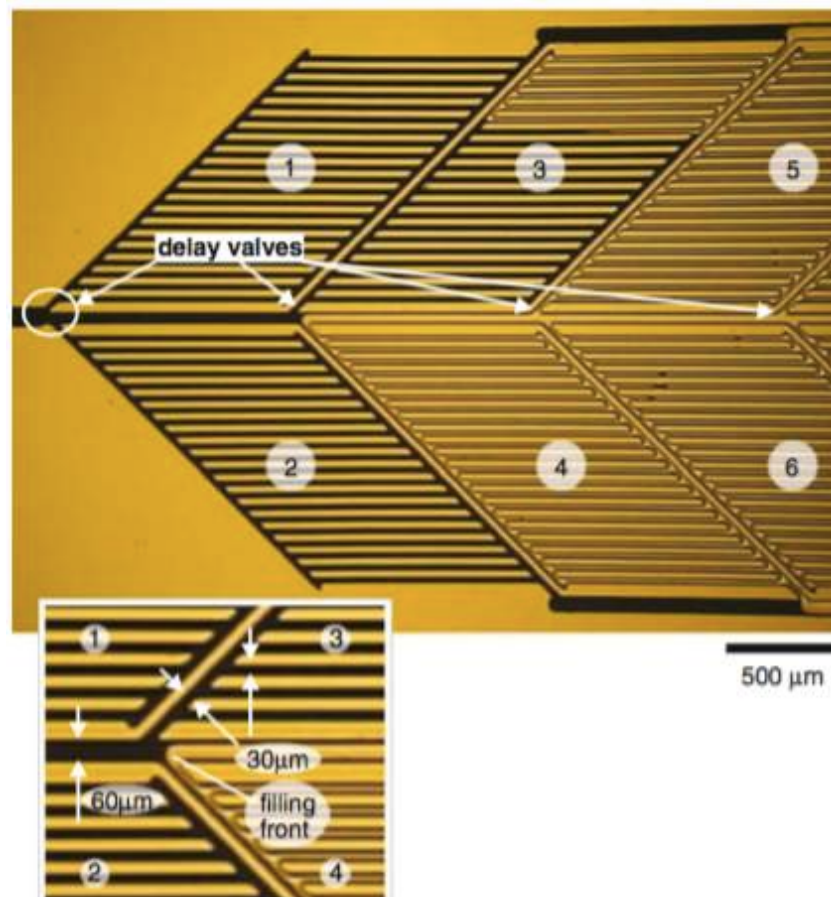


FIGURE 3.10: Delay valves for sequential distribution of liquid into six zones (1) - (6). Zones filled with liquid appear dark. The inset shows a closeup of the delay valve structure with gap sizes between microstructures resulting in preferential filling of narrow ( $30\ \mu\text{m}$ ) gaps before wider ( $60\ \mu\text{m}$ ) gaps. Adapted from: ref. 82 © 2008 Springer-Verlag

### 3.4.7 Capillary soft valves

Capillary soft valves can be used to stop liquids at precise locations within a CS as a result of a capillary pressure barrier imposed by an abrupt microchannel enlargement. A distinguishing feature of soft valves from stop valves is that flow can be resumed simply by manual actuation because the valves are designed to be wide and covered with a soft and flexible PDMS membrane (Fig. 3.11).[92, 93] When a user pushes down on the PDMS cover, the channel height is reduced resulting in a local increase in the magnitude of the wicking/negative pressure driving flow thereby restarting flow in the microchannel. Although capillary soft valves are relatively easy to fabricate, flow actuation is dependent on user intervention, which on one hand creates a constraint and limits scalability, but on the other hand allows for interactive control of the flow, which can be desirable depending on the application.

### 3.4.8 Retention burst valves

Retention burst valves (RBVs) are capillary fluidic components that work as programmable pressure fuses, allowing drainage of a reservoir based on a predefined capillary burst pressure encoded by RBV geometry. The sequence of reservoir drainage, and hence the sequence of reagent flowing through to a downstream reaction chamber can be pre-programmed by connecting each of the reservoirs to a RBV with a different burst pressure as will be discussed below. Similar to capillary retention valves, RBVs are realized by reducing the cross-section of a channel and the precise burst pressure calculated using the Young-Laplace equation (Eqn 3.1).[12, 57] The range of burst pressures that can be encoded is limited by the pressure of the capillary pump which needs to generate a higher negative pressure than the strongest RBV, and by the largest dimension that can still generate significant capillary pressure.

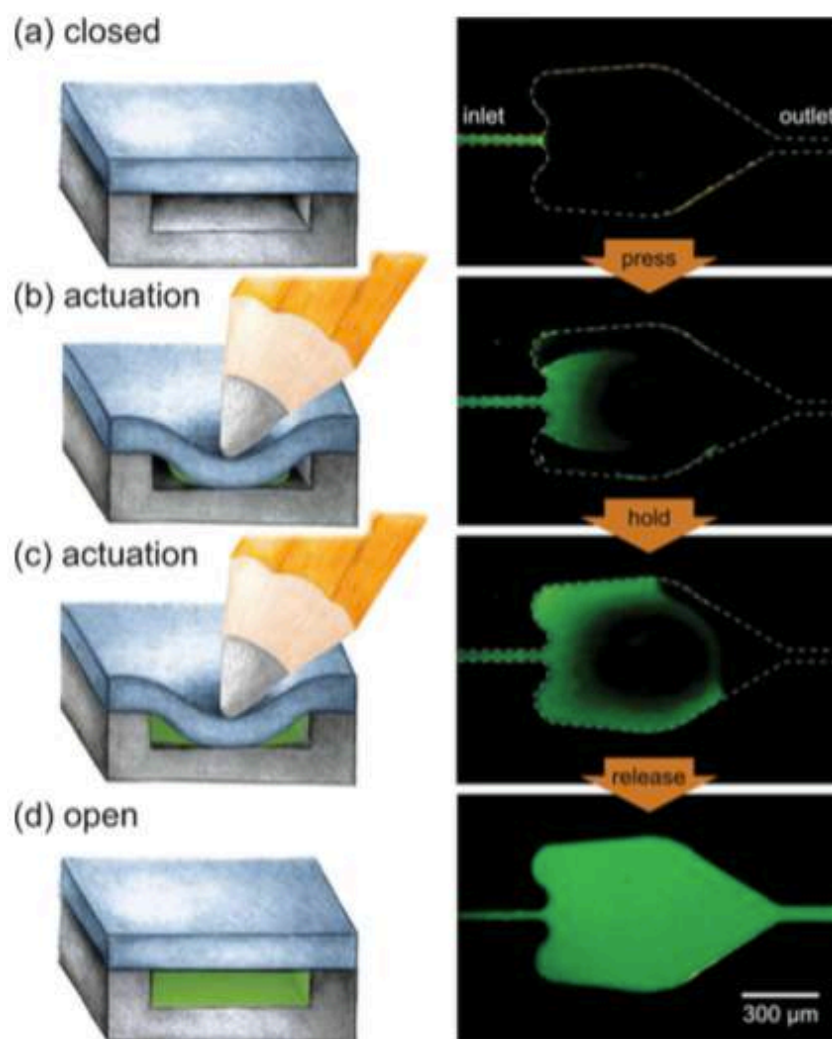


FIGURE 3.11: **Capillary soft valve stops liquid at a capillary pressure barrier posed by a wide channel with a hydrophobic PDMS cover.** Manual actuation decreases microchannel height, decreasing the pressure barrier, and restarting flow. Adapted from ref. 92 © 2012 Royal Society of Chemistry.

## 3.5 Capillarie Circuits for Preprogrammed Liquid Delivery

After discussing the principle of operation of individual capillarie elements, we now discuss capillarie circuits (CCs) that combine multiple capillarie elements to implement self-powered and self-regulated liquid delivery. Microfluidic networks for preprogrammed liquid delivery using capillary forces were first referred to as “capillary systems.”[11] However, here we will refer to them as CCs to emphasize the modular nature of these systems and to provide consistent terminology across different demonstrations.

### 3.5.1 Capillarie Circuits for Immunoassays

The earliest and most common application of CCs is to automate sandwich immunoassays. [11, 46, 47, 48, 53, 68, 70, 94] Sandwich immunoassays in microfluidic networks typically require a capture agent (typically an antibody) that is immobilized on a surface to capture a target analyte (typically a protein) that is flowed through the functionalized reaction zone. Next, a detection agent (typically a labeled antibody) is flowed through the reaction zone, and often followed by a wash step to reduce background signal due to non-specific binding.

CCs have several advantages in immunoassay automation, including: (1) small sample and reagent volume requirements (can process nL reagent volumes), (2) precise control over liquid flow speed and direction, (3) self-powered and user-friendly operation, (4) compatible with precise patterning (e.g. inkjet printing) of reagents within microchannels, and (5) compatible with transparent substrates enabling sensitive fluorescence or chemiluminescence detection.

The concept of realizing a CC (or a capillary system as it was named then) was proposed in 2002, and used a series of capillarie elements including capillary pumps, retention valves, inlets, and vents (Fig. 3.12).[11, 46, 88] The reaction zone of the CC

was patterned with capture antibodies using the CC [11] or a simple microfluidic network[42, 72] to deposit lines of antibodies onto a PDMS cover layer. Liquids were retained at inlets using retention valves enabling sequential loading of multiple liquids. The circuit by Juncker *et al* with retention valves was used to perform 16 sequential assay steps (including sample and antibody delivery as well as multiple wash and block steps) for the detection of C-reactive protein (CRP) from 0.2  $\mu\text{L}$  of sample volume within 25 min. Similar CC designs were used to automate micromosaic immunoassays wherein multiple lines of capture antibodies were patterned onto the reaction zone and exposed to orthogonal flow of analytes within the CC, allowing simultaneous detection of multiple analytes with fluorescently labeled detection antibodies within a small device footprint.[43, 46, 72] Using 8 parallel CCs, CRP and other cardiac biomarkers (including cardiac troponin I and myoglobin) were detected at clinically relevant concentrations from 1  $\mu\text{L}$  of serum within 10 min.[46]

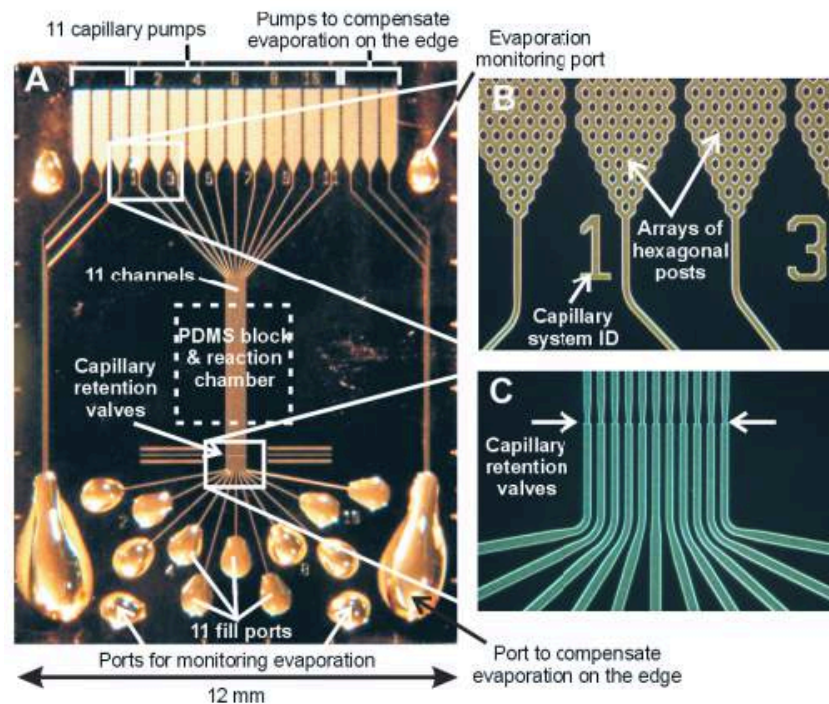


FIGURE 3.12: **Array of 11 CCs for manual, multi-step assays.** CCs consist of capillary pumps, retention valves, inlets, patterned reaction chambers on PDMS, and vents. Capillary retention valves pin liquid near inlets and enable liquid re-loading to accomplish multi-step assays. Multiple capillary systems were placed side-by-side for parallel assays. Adapted from ref. 31

One-step immunoassays that only require sample addition, and that come with

dried reagents spotted along the flow path, were first realized in membrane-based lateral flow assays, and then in microchannel-based microfluidic devices using laminated polymers; both of these technologies were developed in industry and both led to successful commercial products. For example, the Triage™ chip from Biosite (now part of Alere) detects cardiac biomarkers in whole blood (Fig. 3.13).[95, 96] The Triage™ chip incorporates a blood filter to separate blood cells from plasma. It also has a hydrophobic barrier (or time gate) that is used to control sample incubation time. Proteins from the blood sample bind to the hydrophobic surface to render it hydrophilic and the time gate typically provides an incubation time of  $\approx 2$  min that can be varied depending on the degree of hydrophobicity of the surface. There are control and assay zones where the immunoassay takes place as well as a waste reservoir for excess liquid. Notably, the laminated microfluidic device provided quantitative readout with high sensitivity and was accompanied by a hand-held reader.

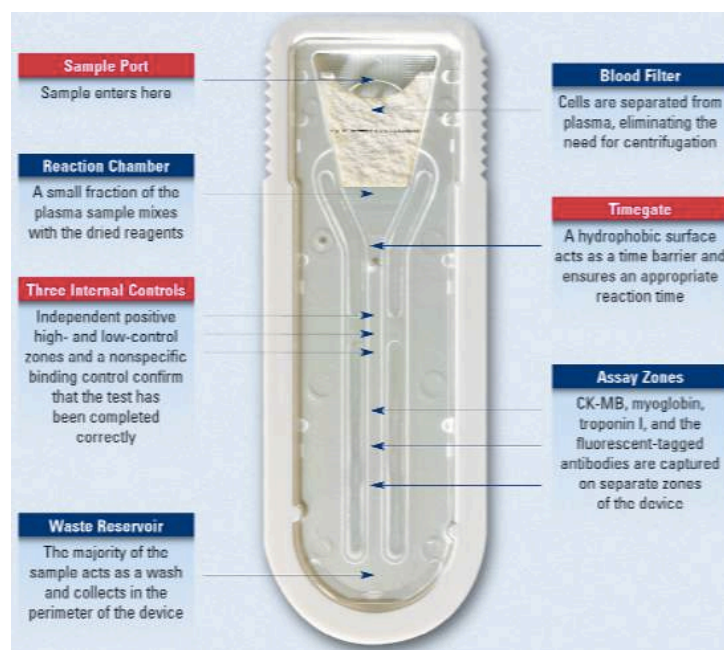


FIGURE 3.13: **Triage™ chip for one-step immunoassay.** Biosite (now part of Alere) Triage™ chip uses capillary-driven flow in plastic microchannels for one-step immunoassays from whole blood consisting of filter to separate blood cells, hydrophobic time gate to regulate sample incubation time, as well as control and assay zones to carry out immunoassays. Adapted from 95 © 2002 Lippincott Williams & Wilkins, Inc.

In 2008, the first demonstration of a full assay with pre-immobilized reagents in a microfabricated silicon chip was published[47, 94] using microscale reagent zones

and very small amounts of detection antibodies. Specifically, 200- $\mu\text{m}$  wide deposition zones were used to hold 3.6 nL of detection antibody along the flow path of a CC used to implement one-step detection of CRP from 5  $\mu\text{L}$  of human serum within 15 min, and read out using a fluorescence microscope (Fig. 3.14).[47]

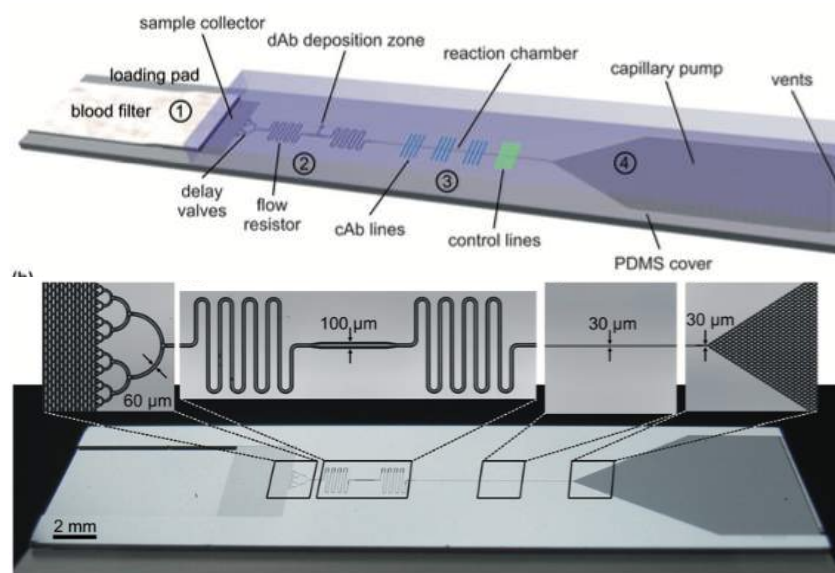


FIGURE 3.14: **Microfabricated silicon chip for one-step immunoassay.** Detection antibodies were spotted along the flow path, reconstituted by the sample, and autonomously delivered to the reaction chamber where capture antibodies were patterned onto the surface of the PDMS cover. Adapted from ref.47 © 2009 Royal Society of Chemistry.

Another demonstration of immunoassays in a microfluidic chip powered with capillary forces employed serially arranged reservoirs along the flow path such that liquids were delivered to the capillary pump in the required sequence for assay implementation (Fig. 3.15).[48]. This approach does not make use of advanced capillary fluidic elements, but instead relies on high flow resistance between subsequent reservoirs to promote serial drainage and reagent delivery. Micropost arrays provided flow resistance and also acted as filters to separate blood cells from the whole blood sample. The microchannels leading to the reaction chamber were also designed such that they provided focusing of inertial flow focusing effects to further separate blood cells from plasma (Fig. 3.15). Interestingly, the authors used the optical adhesive NOA 63

(Norland opticals) instead of PDMS as it was found to be hydrophilic after UV curing and unlike PDMS, stably retains its hydrophilicity. Blood sample and immunoassay reagents (biotinylated detection antibodies, fluorescently labeled streptavidin, and wash buffer) were sequentially delivered through a patterned reaction zone over a 40-minute period using filter paper as a capillary pump. The self-powered microchip was used to implement a multiplexed assay for detection of 11 proteins in blood using a DNA barcode assay. The simple design however faced some trade-offs, such as a need for rapid filling to avoid leaking into adjacent reservoirs, observable mixing of reagents between reservoirs, and difficulty adjusting flow rates for different reagents (in fact, flow rates are expected to increase for each reagent).

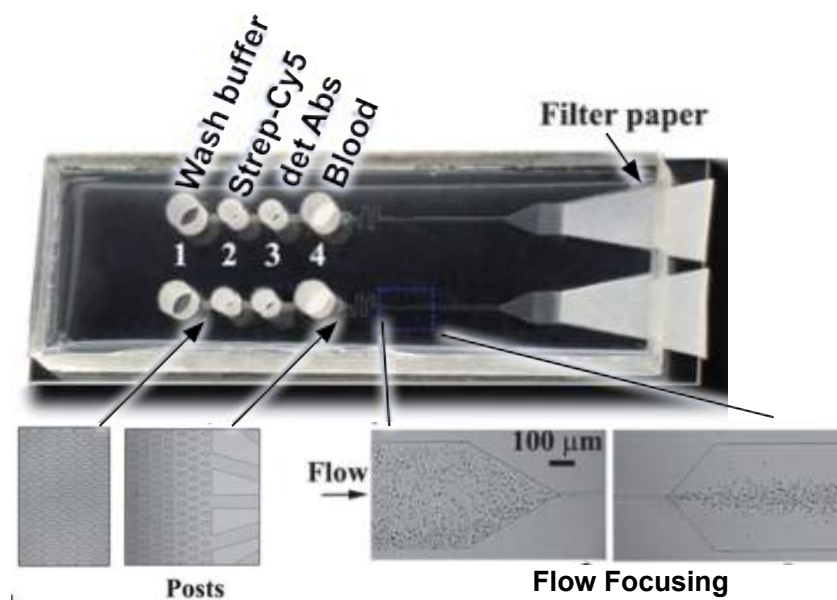


FIGURE 3.15: **Microchip with serially arranged reservoirs for multiplexed immunoassay.** Reservoirs were pre-loaded with immunoassay reagents and blood. Microposts act as flow resistors between reservoirs while filter paper is used as a capillary pump. Microchannels near the reaction chamber were designed to provide inertial flow focusing effects that helped to separate blood cells from plasma. Adapted from ref.48 © 2010 Royal Society of Chemistry.

There are numerous demonstrations of CCs for automated immunoassays. Table 3.1 summarizes a few key examples of capillary systems demonstrated in the literature. It is clear that the most common application of capillary systems is immunoassay automation for protein detection typically targeting cardiac biomarkers. Other immunoassay targets detected with CCs include botulinum toxin[70] and whole bacteria

cells.[59]

### 3.5.2 Capillary Circuits for DNA analysis

Beyond immunoassays, CCs have also been used for DNA analysis. For example, CCs consisting of loading pads, reagent deposition zones, capillary soft valves, patterned reaction chambers, and capillary pumps were used for DNA hybridization assays.[92] Double-stranded DNA was detected from 0.7  $\mu\text{L}$  of sample within 10 min. Biotinylated capture probes and fluorescent intercalating dye were spotted into reagent deposition zones along the flow path prior to the start of the assay. Addition of sample reconstituted these reagents and capillary soft valves were used to stop the sample at a precise location within the CC. This enabled completion of the DNA hybridization assay that required DNA denaturation at 95 °C, annealing to biotinylated probes at 50 °C, and intercalation of fluorescent dye at 25 °C. The CC was pressured at  $\approx 1.5$  bar over ambient pressure to eliminate air bubbles generated during heating and push those air bubbles into the PDMS sealing layer. After completion of the DNA hybridization assay, the capillary soft valve was manually actuated resulting in the flow of the DNA target-probe-dye complexes over 100- $\mu\text{m}$  streptavidin receptor lines patterned over the reaction chamber facilitating unambiguous readout.

More recently, microfluidic devices with flow regulated by capillary forces have also been developed for DNA amplification.[98, 99, 100, 101] Real-time Polymerase Chain Reaction (PCR) in closed chambers was carried out using capillary-driven reagent delivery.[98, 101] The microchannels were not wettable (contact angle  $> 90^\circ$ ) but self-filling was assisted by the presence of surfactant which lowers the surface tension of liquid and provides moderate wetting that is sufficient to fill the microchannels.[98, 101] Microchannel expansions that form stop valves were used at reaction chamber exits to meter the volume of sample added. Different approaches were taken to avoid evaporation during temperature cycling (between 95 °C and 55 °C) required for PCR. In one case, PDMS microchannels were bonded to glass on either side leaving only

TABLE 3.1: **Examples of applications of capillary circuits.** Most circuits were used for sandwich immunoassays for protein detection. We present a few representative examples to show typical assay time, sample volume, and limit of detection (LOD). DNA analysis is also an emerging application of CCs.

Application	Target(s)	Assay time (min)	Sample volume ( $\mu\text{L}$ )	LOD	Comments	Ref.
Sandwich immunoassay	C-reactive protein (CRP)	25	0.2	$\approx 1 \mu\text{g}/\text{mL}$	Retention valve enabled 16 sequential filling steps	11
	CRP	14	5	1 ng/mL	One-step assay with detection antibodies dried along the flow path and re-constituted and delivered to the downstream reaction chamber.	47
	11 protein panel (CRP, IL-8, MMP-3, serpin etc.)	40	10	20 pg/mL for IL-8	Antibody-DNA barcode arrays to capture proteins from serum.	48
	Troponin I	9	15	24 pg/mL	Preprogrammed sequential delivery of sample and assay reagents Integrated on-chip planar lenses for portable fluorescence readout.	97
	Whole <i>E. coli</i> O157:H7 cells	7	100	$1.2 \times 10^2$ CFU/mL	Large-volume capillary circuit (CC) for preprogrammed assay with packed microbeads for rapid and sensitive bacteria capture.	59
DNA hybridization	997-bp PCR product (double-stranded DNA)	10	0.7	20 nM	Uses capillary soft valves - stop valves with simple manual actuation to restart flow - to implement DNA hybridization assay with fluorescence readout.	92
DNA amplification (real-time PCR)	BNI-1 fragment of SARS cDNA (and 12 other human gene targets)	30	0.8	10 pg/mL of SARS cDNA	Surfactant-assisted flow of PCR reagents. Liquid stationary in reaction chamber. Temperature cycling through 94 °C, 55 °C, and 72 °C	98

the microchannel inlets open. To seal the inlets after loading the PCR mixture, liquid PDMS pre-polymer was added to the channels and cured at 72 °C for 10 min prior to the start of the PCR amplification.[98] In other cases, cyclic olefin copolymer (COP) - which is a transparent mass producible material with low water absorption - was used for device fabrication to avoid evaporation during PCR.[100, 101] Temperature cycling was carried out either with thin film heaters embedded within the microfluidic chip[101] or with heating elements placed underneath the chip.[98, 99, 100] In one case, PCR was implemented by continuous flow of PCR mixture through 2 different temperature zones established by placing two hot plates (at 95 °C and 60 °C) on opposite ends of the microfluidic chip that had a long serpentine reaction channel winding between both zones.[99, 100] PCR results were visualized in real-time by measuring the fluorescence from a DNA intercalating dye. PCR was typically completed within minutes with the fastest PCR in a CC reported to date being completed within 8.5 min.[101] Most of these demonstrations of PCR powered by capillary-driven flows use relatively simple channel designs and stop valves, and do not yet leverage the more advanced liquid handling capabilities available with other capillarie elements.

### 3.5.3 Preprogrammed Multi-Step Liquid Delivery

Within the past five years, there has been a lot of interest and development of CCs capable of preprogrammed multi-step liquid delivery operations.[12, 49, 50, 102] Preprogrammed sequential operations may enable additional wash steps or chemical signal amplification to increase the signal-to-noise ratio of assay results.[12, 103, 104] Preprogrammed multi-step liquid delivery in microchannel-based capillary microfluidics was inspired by innovations in paper-based microfluidics where two-dimensional networks with varied flow path lengths were used to implement sequential liquid delivery.[103, 105] There are multiple approaches to achieving preprogrammed multi-step liquid delivery within CCs. We discuss a few examples below.

### Air vents connected to inlets

One approach to preprogrammed multistep liquid delivery in CCs is to connect reservoirs to one another and to a common outlet channel, and to use air vents connected between the reservoirs to control sequential drainage.[50] Fig. 3.16 shows part of the device designed with 3 reservoirs arranged such that the inlet of the first reservoir also acted as the only air vent for the flow path of the second reservoir, while the inlet of the second reservoir was the only air vent of the third reservoir. When the reservoirs were filled sequentially starting with the first reservoir, the air vents to reservoirs 2 and 3 were blocked preventing displacement of liquid by air and flow of liquid from reservoirs 2 and 3 into the channel outlets (Fig. 3.16i). An important design element was the use of passive valves, arrays of narrow passageways at the intersections of the microchannels exiting from inlets 1, 2, and 3. These passageways act as passive valves that prevent back flow of liquid from channel 1 into channel 2 or channel 3, while allowing flow towards the pump when liquid is present in two interconnected channels. When the inlet to reservoir 1 was completely emptied, the air vent to reservoir 2 was opened allowing flow of liquid from reservoir 2 into the channel out leading to the capillary pump (Fig. 3.16ii). This sequence repeated when reservoir 2 emptied allowing drainage of reservoir 3 into the capillary pump thereby achieving sequential liquid drainage using air vents. This is a subtle and elegant approach to achieving sequential liquid delivery; however, the technique depends on the sequence of loading of reservoirs by the user and might also be susceptible to evaporation from open reservoirs that serve as air vents. In addition, the shape of the liquid meniscus at inlets 2 and 3 suggests that the channel needed to be somewhat hydrophobic (or only mildly wettable) to ensure that liquid did not fill the narrow air vents, yet this is not described in the paper.

The same group demonstrated preprogrammed multi-step liquid delivery using air bubbles as spacers between orthogonal microchannels connected to a single capillary pump.[49] Liquids were delivered sequentially based on their proximity to the

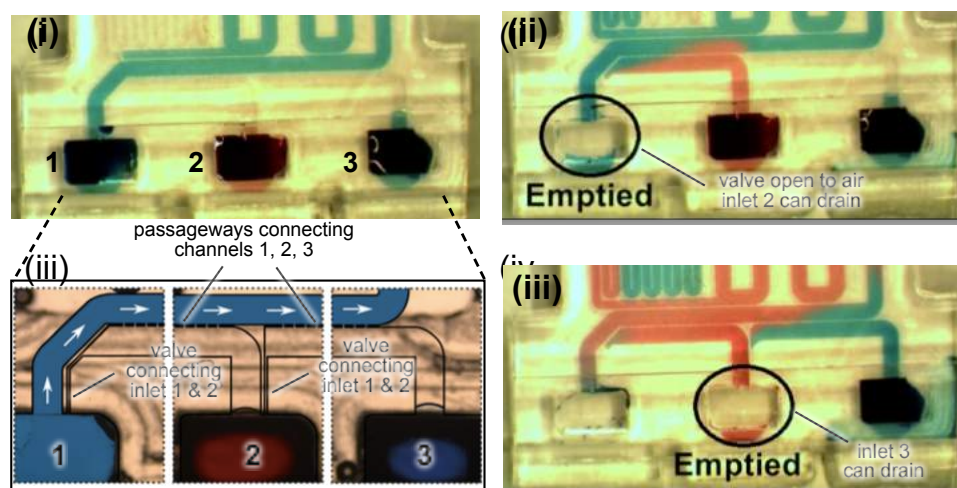


FIGURE 3.16: **Air vents connected to microchannel inlets to control sequential delivery.** Air vents connected to microchannel inlets can be used to control sequence of liquid delivery. When the inlet empties, the air vent is opened allowing drainage of the next inlet. Adapted from ref. 50 © 2014 Elsevier B.V.

capillary pump and the system was used to implement a pre-programmed immunoassay. [49] However, there was limited discussion of the reliability of creating the air bubble spacers and how sensitive device operation was to user manipulation especially given that the presence of air bubbles in microchannels and capillary pumps can be a major source of variation in CCs. Also, it appears that precise pipetting was required to ensure that channels fill to the right position and trap bubbles between adjacent solutions.

### Combining Retention Burst Valves and Trigger Valves

Our research group introduced a technique for preprogrammed liquid delivery within CCs by combining retention burst valves (RBVs) and trigger valves. [12] As described earlier, each RBV has a unique burst pressure based on its microchannel height and width and can be calculated using the Young-Laplace equation (eqn. 3.1). By incorporating both trigger valves and RBVs within CCs, one can implement multi-step liquid operations without precise timing by the user, where liquids are pre-loaded into reservoirs and stopped by two-level trigger valves.[12] When the user is ready to start the assay, they fill a release channel that connects all the reservoirs to the capillary pump, at which point pre-programmed drainage and sequential bursting of RBVs proceeds

according to increasing order of capillary pressure (Fig. 3.17). Safavieh and Juncker developed a CC with a flow reversal architecture that enabled precise metering of the volume and incubation time of sample flowed through a reaction chamber using one capillary pump, and using a trigger valve and second capillary pump enabled sequential drainage of 4 pre-loaded reagents through the reaction chamber at a different flow rate.[12] This flow reversal circuit was used to implement a sandwich immunoassay for proof-of-principle detection of CRP from 1  $\mu\text{L}$  of sample within 5 min.

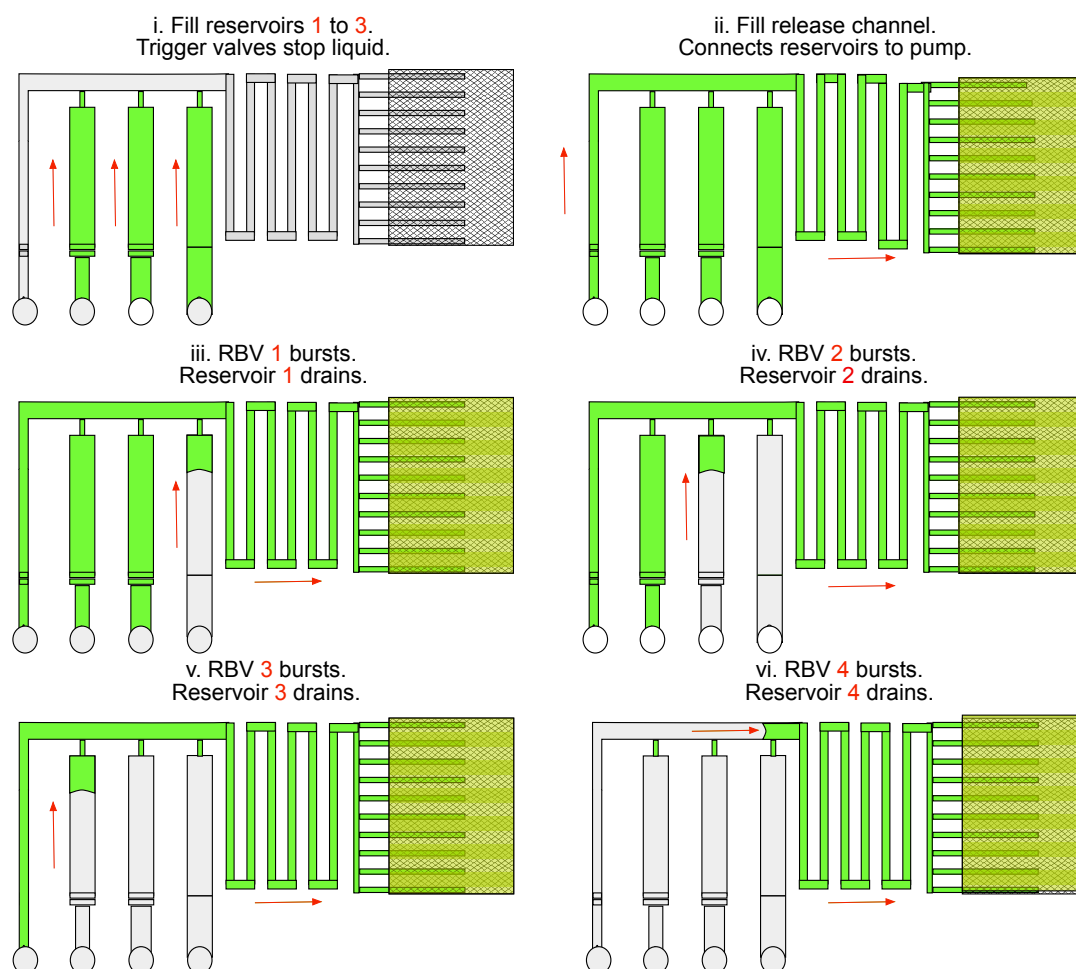


FIGURE 3.17: **Capillary circuit with trigger valves and retention burst valves to implement sequential liquid delivery.** Trigger valves hold liquid in place in reservoirs and RBVs burst sequentially in increasing order of capillary pressure encoded by microchannel geometry. Adapted from ref. 57 © 2016 Royal Society of Chemistry.

Sequential bursting of RBVs depends not only on the capillary pressure difference between RBVs but also on the flow resistance within the CC. It is important to consider the entire circuit architecture when designing CCs with RBVs.[57] Sequential delivery

of reagents is realized by connecting reservoirs, each with its own unique RBV, to a main microchannel by a trigger valve (Fig. 3.17). Following filling of all reservoirs with reagents in an arbitrary order, the sequential drainage is initiated by triggering the flow via a liquid flowed through the main microchannel which is outfitted with a retention valve at the inlet. As the liquid reaches the capillary pump, and is drained from the inlet, the flow comes momentarily to a halt. As the pressure of the capillary pump propagates through the entire network (as in a hydraulic circuit), the RBV with the lowest capillary pressure bursts leading to rapid drainage of the first reservoir. Importantly, as the reservoir drains, there is a pressure loss in the circuit due to appropriately designed resistances, so that the pressure is below the threshold of the second weakest RBV. Once the first reservoir is drained, a capillary retention valve positioned intermediately upstream of the trigger valve, stops the flow, leading to a rise in pressure in the circuit and bursting of the RBV with the second lowest pressure, and so on. Note that for successful sequential bursting of RBVs several conditions must be met: (i) the capillary pressure difference between individual RBVs must be increased monotonically, (ii) the difference in capillary pressure between RBVs must be large enough for only one RBV to burst at a time, and (iii) the overall circuit must be designed such that during flow, the pressure at each reservoir remains below the bursting pressure.[57] The second condition can be calculated using an electrical equivalent circuit for the CC.

Reliability of RBV performance depends on the precision of fabrication techniques in creating geometric differences between RBVs. RBV reliability may also be affected by surface tension differences between liquids in different RBVs since the surface tension directly influences capillary pressure (equation 3.1). Also, the reliance of initial RBV designs on high-resolution ( $\approx 10 \mu\text{m}$ ) differences in microchannel width required conventional cleanroom fabrication that makes design iteration slow and expensive. We discuss rapid prototyping of RBVs using 3D-printing to vary both the height and width of microchannels in section 3.5.5.

### Dissolvable barriers

Dissolvable barriers can be used to control the sequence of liquid delivery in parallel microchannels connected to a single capillary pump either by modifying properties (such as the thickness) of the thin film, or by arranging multiple identical thin films in sequence.[51] To enable pre-loading of liquids into parallel channel inlets and simultaneously activate liquid delivery, channel vents were temporarily blocked by sealing them with parafilm. The user pre-loads reservoirs with liquid and when ready to start liquid delivery, removes the parafilm to open up the vents and start the liquid delivery process. Sequential drainage of four different liquids from parallel reservoirs was demonstrated (Fig. 3.18). In addition, 19 serial valves were stacked to obtain a delay of up to 11 minutes. One of the challenges with implementing dissolvable barriers is the need to get rid of excess dissolved material at the filling front of liquid which can build up over time and slow down flow or interfere with immunoassays. To address this concern, Lenk et al. incorporated dead-end channels to diverting PVA at the leading edge of liquid away from the main flow path. Fabrication of individual delay valves was tedious since different thin film thicknesses need to be manually transferred to specific locations on-chip to achieve sequential drainage.

### 3.5.4 Handheld Readers for Capillaric Circuits

CCs were integrated with handheld optical readers by Biosite[95, 96] and more recently by academic research groups.[50, 97] For example, Novo et al. developed a CC with a microfabricated photodiode array and electronic instrumentation for chemiluminescence Enzyme Linked Immunosorbent Assay (ELISA) detection of antibody-antigen interactions within 15 min.[50] PDMS microfluidic devices were integrated with amorphous silicon photodiode chips within an integrated handheld unit that also housed a microcontroller and electronic readout circuitry. Another example of a CC with integrated optical detection was developed by Mohammed and Desmulliez who embedded on-chip planar lenses within PMMA devices.[97] LED illumination

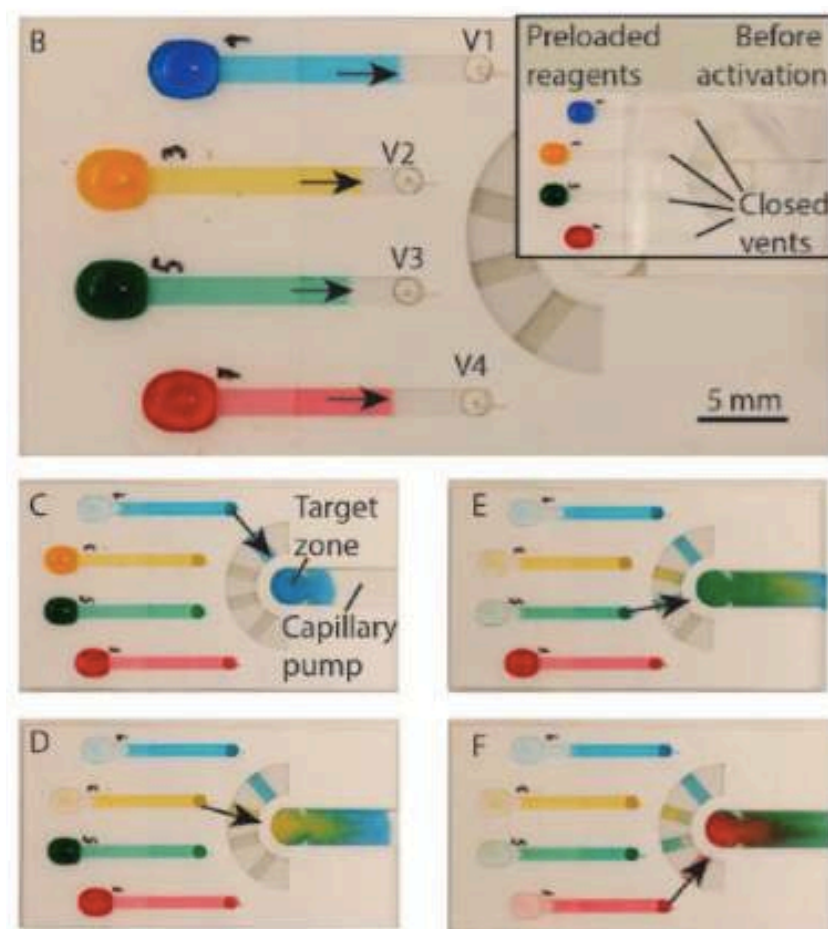


FIGURE 3.18: **Dissolvable Polyvinylalcohol (PVA) barriers for multi-step liquid delivery.** Liquid is placed at each of the inlets with PVA barriers downstream. The thickness of PVA barriers downstream determines the sequence of drainage of each liquid into the central target zone. Adapted from ref. [51] © 2014 Chemical and Biological Microsystems Society.

and filters for fluorescence detection were integrated within a custom-made handheld reader.[97] These examples demonstrate that CCs can be readily integrated with portable detection systems and that microfabrication techniques can also be leveraged to include optical detection components directly while achieving sensitivities that could be useful for clinically relevant assays.[50, 97]

### 3.5.5 Rapid Prototyping of Capillarie Circuits

Another emerging area of research is the rapid prototyping of CCs. Fabrication of microchannel-based capillary systems is predominantly carried out by photolithography in cleanroom environments. [11, 12, 49, 68, 82, 102] This is because the generally accepted view is that capillarie elements, such as stop valves or trigger valves, require high resolution ( $\approx 10\mu\text{m}$  feature sizes) and smooth surfaces (with submicron roughness) to achieve reliable capillary valving and flow control. Yet this reliance on high precision fabrication within cleanrooms results in slow and expensive fabrication processes with long design iteration times, and limits the adoption and application of CCs. Lately, there have been demonstrations of rapid prototyping of functional capillarie elements and circuits. In this section, we briefly describe these demonstrations of rapid prototyping and highlight their potential to drive a third wave of development of CCs driven by short design iteration cycles and simple fabrication of multi-level structures. The minimum feature sizes achievable with these rapid prototyping techniques is usually practically  $> 100\ \mu\text{m}$ ; however, by using thin layers ( $\approx 50\text{-}\mu\text{m}$  thickness) or by fabricating multi-level structures, advanced capillarie elements such as trigger valves and RBVs were demonstrated.

#### **Xurography (razor writing)**

Xurography is an inexpensive fabrication technique originally used in the graphic arts industry and consists of using a plotter fit with a knife or a scalpel to cut patterns in

thin polymer films such as tape or transparencies. Xurography has been used for inexpensive fabrication of microfluidic devices and/or molds with resolutions down to  $\approx 10 \mu\text{m}$ .<sup>[106, 107]</sup> Xurography was used for fabrication of molds by stacking layers of commercial tape to obtain channel heights ranging from 100 to 400  $\mu\text{m}$ , followed by PDMS replication to obtain microchannels for capillary-driven flow.<sup>[55]</sup> Xurography was also used to cut hydrophilic polymer films and spacers that were laminated together with dissolvable polymer films to form CCs for preprogrammed liquid delivery.<sup>[51]</sup> While xurography is inexpensive and accessible, it involves a lot of manual operations and alignment to obtain multi-level structures. This has limited the application of xurography for the design of more complex CCs that rely on precise geometry changes. As such, xurography has so far only been used to cut relatively simple microchannel structures and not been used for more advanced capillaric elements.

### Laser cutting

CO<sub>2</sub> laser cutting was recently used to fabricate CCs consisting of capillary pumps with micropillar arrays, timing channels, trigger valves, and integrated microlenses (Fig. 3.19B).<sup>[56]</sup> Laser cutting enables fabrication of functional devices in PMMA within 30 min to 3 hours. Laser cutting allows simple fabrication of multi-level structures, enabling the generation of two-level trigger valve structures.<sup>[58, 83]</sup> Mohammed and Desmulliez experimentally investigated the reliability of two-level trigger valves manufactured by CO<sub>2</sub> laser cutting as a function of geometry and obtained functional trigger valves with widths up to 670  $\mu\text{m}$ .<sup>[58]</sup> However, the feature sizes obtained with CO<sub>2</sub> laser cutting were limited to  $> 150 \mu\text{m}$  with narrower channels having more triangular 'Gaussian' profiles as a result of the shape of the laser beam (Fig. 3.19A). These limitations of laser micromachining should be readily resolved using femtosecond lasers and different optics that can achieve  $\approx 1 \mu\text{m}$  resolution, and using beam shaper technology with top hat profile to avoid the triangular microchannel shape.<sup>[108]</sup>

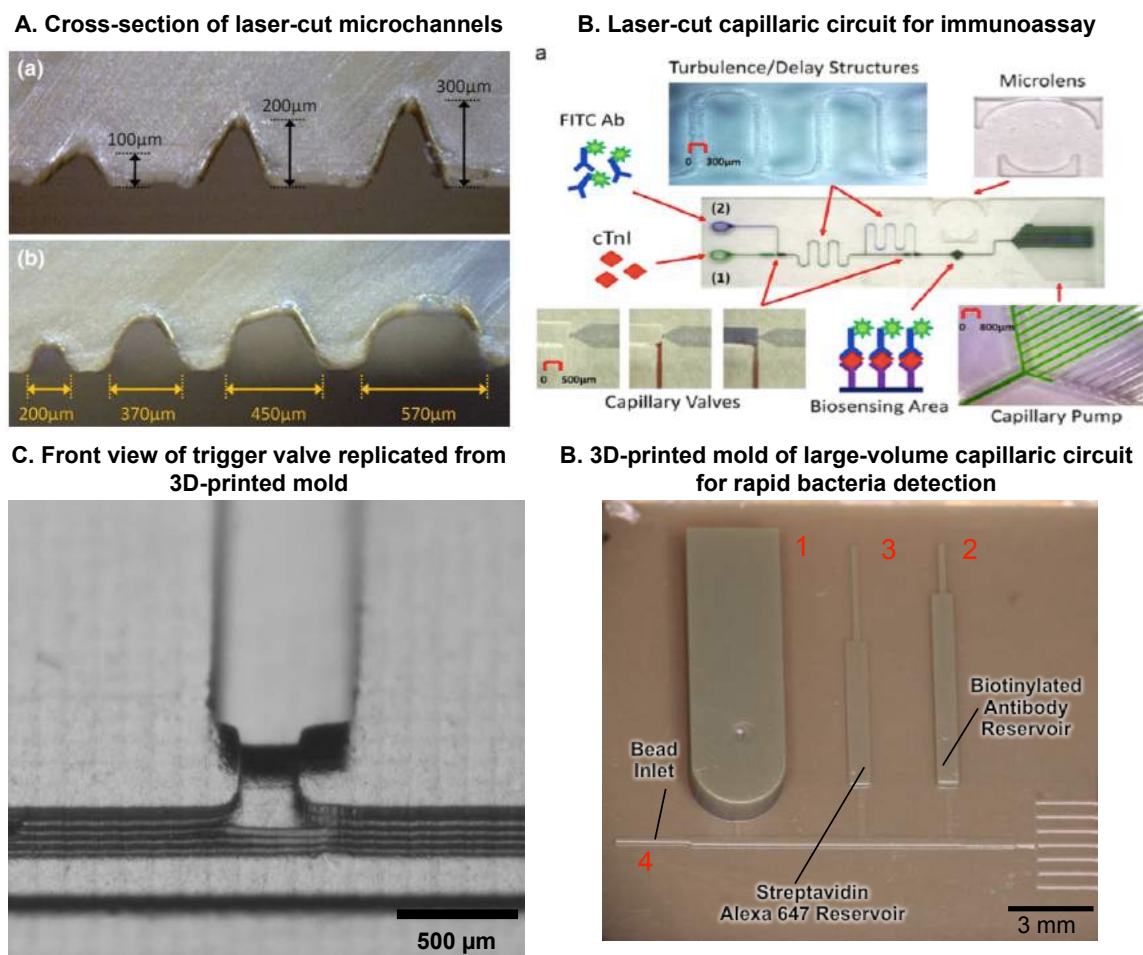


FIGURE 3.19: **Rapid prototyping of capillary systems using CO<sub>2</sub> laser cutting and 3D-printing.** (A) Cross-sections of microchannels fabricated using laser cutting. Smaller microchannels (a) take on a triangular “Gaussian” profile as a result of repeated scanning of the laser beam, while (b) wider microchannels have a more triangular shape. (B) Integrated CC for detection of cardiac troponin I (cTnI) with various fluidic elements including capillary pumps, inlets, timing channels, and integrated optical lenses. (C) Comparison between resolution and surface roughness of cleanroom-fabricated and 3D-printed features. Cleanroom-fabricated trigger valves have smaller features ( $\approx 20 \mu\text{m}$ ) and sub-micron roughness while 3D-printed trigger valves are larger ( $300 \mu\text{m}$ ) and have layered structures with micron-scale ( $\approx \pm 1 \mu\text{m}$ ) roughness, (D) 3D-printed mold for CC for bacteria detection showing physical realization of structures. Adapted from: (A) ref. 56 © 2013 Springer-Verlag Berlin Heidelberg, (B) ref. 97 © 2014 Elsevier B.V., (C) ref. 57 © 2016 Royal Society of Chemistry, (D) ref 59 © 2017 American Chemical Society.

### 3D-printing

Over the past five years, there has been an explosion of in 3D-printing of microfluidic devices in polymeric resins given the potential for rapid and inexpensive fabrication of multi-layer structures.[109, 110, 111] However, the minimum feature sizes achievable with commercial 3D-printers is  $\approx 100 \mu\text{m}$  which is an order of magnitude larger than the typical feature sizes in cleanroom-fabricated trigger valves.[112] Surface roughness in 3D-printed microchannels can readily approach  $\approx 10 \mu\text{m}$  and result in deviations from the predicted dynamics of capillary-driven flow in open microchannels.[113] Surface roughness of microchannels obtained with state-of-the-art stereolithographic 3D-printers is typically  $\approx \pm 1 \mu\text{m}$  with microchannels having a stratified layer-by-layer structure due to the 3D-printing process.[57, 112] 3D-printed features are much larger and rougher than those obtained with cleanroom fabrication (see Fig. 3.19C) and we were concerned that such structures could lead to creeping flows and leakage in stop valves and trigger valves.

Nevertheless, we recently demonstrated functional capillarie valves and circuits replicated from 3D-printed molds.[57] New designs for CCs were printed in  $< 30$  min, followed by PDMS replication. Trigger valves with geometries up to 80-fold larger than cleanroom-fabricated ones functioned reliably. In addition, RBVs with variations in both the microchannel height and width were designed using analytical and empirical design rules for preprogrammed delivery of up to 8 liquids in CCs.[57] The digital multi-layer fabrication available with 3D-printing provided a new degree of freedom when designing channel geometries. In addition, 3D-printing enabled fabrication of millimeter-scale ( $13 \times 4 \times 2 \text{ mm}^3$ ) conduits with large volume capacity ( $\approx 100 \mu\text{L}$ ) within CCs with integrated trigger valves and RBVs for screening large sample volumes. We leveraged this large-volume capacity to design a CC for rapid and sensitive detection of *E. coli* in synthetic urine using microbeads assembled on-the-fly to provide large surface area and ensure contact of bacteria to functionalized surfaces within the CC.[59] The CC for bacteria detection provided results in  $< 7$  min, making it one of

the fastest demonstrations of bacteria detection so far, while meeting the sensitivity requirements for clinical diagnosis of urinary tract infections.

Yet, the resolution limitations of commercially available 3D-printers limits the development and application of 3D-printed CCs. For example, the minimum feature size currently achievable with commercial 3D-printers ( $> 100 \mu\text{m}$ )[60] limits the highest capillary pressure that can be attained as well as the range of applications that may be pursued as smaller microstructures ( $\approx 10 \mu\text{m}$ ) that could be used as cell or microbead traps cannot yet be fabricated with 3D-printing.

## 3.6 Conclusions and Outlook

We discussed capillary flow in microchannels within the frame work of circuits that consist of individual fluidic elements for capillary-driven flow control. We traced the early history of capillary elements highlighting two waves of past development with the first wave starting with mechanically micromachined and laminated capillary elements described in industrial patents from the 1980s, while the second wave followed the  $\mu\text{TAS}$  revolution in the 1990s that brought about cleanroom-fabricated microstructures. Then we discussed capillary elements such as capillary pumps, flow resistors, and trigger valves, that can be designed in a modular fashion and combined into integrated circuits for preprogrammed liquid delivery. We also highlighted emerging trends in the field such as different strategies for preprogrammed multi-step liquid delivery with minimal user intervention, as well as rapid prototyping of functional CCs. As increasingly complex CC designs are developed, they have the potential to open up new avenues of research and application. Despite their use so far to automate immunoassays in blood, CCs are an application-agnostic liquid handling tool and could be applied wherever there is a need for hands-off liquid handling with small to medium throughput, including diagnostics, education, chemical synthesis or drug screening. With the recent rise of rapid prototyping and 3D-printing of microfluidic devices, we believe that the field of capillary microfluidics is on the edge of a third

wave of development with potential for greater accessibility, affordability, and applicability. It is our view that rapid prototyping of CCs will spark wider development and application similar to the resurgence of paper microfluidics in the late 2000s.[114] New design paradigms and detailed design rules are already available and we envisage a future where capillarie elements and circuits could be designed as readily as electrical circuits and components, with parts easily fabricated to suit custom needs. Directly 3D-printed CCs would rival the fabrication speed and low-cost of paper-based devices while providing deterministic control over microchannel geometry and flow paths. In addition, the digital and standardized “.STL” file format of 3D-printing could allow easy sharing of files and designs within databases and modular design of fluidic components.

## Acknowledgements

We thank Arya Tavakoli, Mohamed Yafia, and Maiwenn Beaugrand for helpful discussions.

# Bibliography

- [1] G. M. Whitesides, "The origins and the future of microfluidics," *Nature*, vol. 442, no. 7101, pp. 368–373, Jul. 2006.
- [2] D. J. Beebe, G. A. Mensing, and G. M. Walker, "Physics and applications of microfluidics in biology," *Annu. Rev. Biomed. Eng.*, vol. 4, pp. 261–286, 2002.
- [3] J. C. T. Eijkel and A. Van den Berg, "Young 4ever—the use of capillarity for passive flow handling in lab on a chip devices," *Lab Chip*, vol. 6, no. 11, pp. 1405–1408, Oct. 2006.
- [4] B. Weigl, G. Domingo, P. LaBarre, and J. Gerlach, "Towards non- and minimally instrumented, microfluidics-based diagnostic devices," *Lab Chip*, vol. 8, no. 12, p. 1999, 2008.
- [5] A. K. Yetisen, M. S. Akram, and C. R. Lowe, "Paper-based microfluidic point-of-care diagnostic devices," *Lab Chip*, vol. 13, no. 12, pp. 2210–2251, May 2013.
- [6] E. Fu and C. Downs, "Progress in the development and integration of fluid flow control tools in paper microfluidics." *Lab Chip*, vol. 17, no. 4, pp. 614–628, Feb. 2017.
- [7] X. Li, D. R. Ballerini, and W. Shen, "A perspective on paper-based microfluidics: Current status and future trends," *Biomicrofluidics*, vol. 6, no. 1, p. 011301, Mar. 2012.
- [8] Y. Yang, E. Noviana, M. P. Nguyen, B. J. Geiss, D. S. Dandy, and C. S. Henry, "Paper-Based Microfluidic Devices: Emerging Themes and Applications," *Anal. Chem.*, vol. 89, no. 1, pp. 71–91, Jan. 2017.

- [9] K. Yamada, H. Shibata, K. Suzuki, and D. Citterio, "Toward practical application of paper-based microfluidics for medical diagnostics: state-of-the-art and challenges," *Lab Chip*, vol. 17, no. 7, pp. 1206–1249, 2017.
- [10] A. Nilghaz, D. R. Ballerini, and W. Shen, "Exploration of microfluidic devices based on multi-filament threads and textiles: A review," *Biomicrofluidics*, vol. 7, no. 5, p. 051501, Sep. 2013.
- [11] D. Juncker, H. Schmid, U. Drechsler, H. Wolf, M. Wolf, B. Michel, N. de Rooij, and E. Delamarche, "Autonomous Microfluidic Capillary System," *Anal. Chem.*, vol. 74, no. 24, pp. 6139–6144, Dec. 2002.
- [12] R. Safavieh and D. Juncker, "Capillarics: Pre-programmed, self-powered microfluidic circuits built from capillary elements," *Lab Chip*, vol. 13, no. 21, pp. 4180–4189, Nov. 2013.
- [13] G. M. Walker and D. J. Beebe, "A passive pumping method for microfluidic devices," *Lab Chip*, vol. 2, no. 3, pp. 131–134, Aug. 2002.
- [14] E. Berthier and D. J. Beebe, "Flow rate analysis of a surface tension driven passive micropump," *Lab Chip*, vol. 7, no. 11, p. 1475, 2007.
- [15] M. W. Toepke, V. V. Abhyankar, and D. J. Beebe, "Microfluidic logic gates and timers," *Lab Chip*, vol. 7, no. 11, p. 1449, 2007.
- [16] S.-J. Kim, S. Paczesny, S. Takayama, and K. Kurabayashi, "Preprogrammed, Parallel On-Chip Immunoassay Using System-Level Capillarity Control," *Anal. Chem.*, vol. 85, no. 14, pp. 6902–6907, Jul. 2013.
- [17] B. Zhao, J. S. Moore, and D. J. Beebe, "Surface-directed liquid flow inside microchannels." *Science*, vol. 291, no. 5506, pp. 1023–1026, Feb. 2001.
- [18] B. P. Casavant, E. Berthier, A. B. Theberge, J. Berthier, S. I. Montanez-Sauri, L. L. Bischel, K. Brakke, C. J. Hedman, W. Bushman, N. P. Keller, and D. J. Beebe,

- "Suspended microfluidics." *Proceedings of the National Academy of Sciences*, vol. 110, no. 25, pp. 10 111–10 116, Jun. 2013.
- [19] B. S. Gallardo, V. K. Gupta, F. D. Eagerton, L. I. Jong, V. S. Craig, R. R. Shah, and N. L. Abbott, "Electrochemical Principles for Active Control of Liquids on Submillimeter Scales," *Science*, vol. 283, no. 5398, pp. 57–60, Jan. 1999.
- [20] M. W. J. Prins, W. J. J. Welters, and J. W. Weekamp, "Fluid Control in Multi-channel Structures by Electrocapillary Pressure," *Science*, vol. 291, no. 5502, pp. 277–280, Jan. 2001.
- [21] F. He and S. R. Nugen, "Automating fluid delivery in a capillary microfluidic device using low-voltage electrowetting valves," *Microfluid Nanofluid*, pp. 1–8, Jan. 2014.
- [22] H. Cho, H.-Y. Kim, J. Y. Kang, and T. S. Kim, "How the capillary burst microvalve works," *Journal of Colloid and Interface Science*, vol. 306, no. 2, pp. 379–385, Jan. 2007.
- [23] M. R. McNeely, M. K. Sputea, N. A. Tusneem, and A. R. Oliphant, "Sample Processing with Hydrophobic Microfluidics," *Journal of the Association for Laboratory Automation*, vol. 4, no. 4, pp. 1–4, Dec. 1999.
- [24] A. Kazemzadeh, P. Ganesan, F. Ibrahim, S. He, and M. J. Madou, "The Effect of Contact Angles and Capillary Dimensions on the Burst Frequency of Super Hydrophilic and Hydrophilic Centrifugal Microfluidic Platforms, a CFD Study," *PLoS ONE*, vol. 8, no. 9, p. e73002, 2013.
- [25] J. Choi, D. Kang, S. Han, S. B. Kim, and J. A. Rogers, "Thin, Soft, Skin-Mounted Microfluidic Networks with Capillary Bursting Valves for Chrono-Sampling of Sweat." *Adv Healthc Mater*, vol. 6, no. 5, p. 1601355, Mar. 2017.
- [26] B. Suman and R. Savino, "Capillary flow-driven heat transfer enhancement," *Journal of Thermophysics and Heat Transfer*, vol. 25, no. 4, pp. 553–560, Oct. 2011.

- 
- [27] C. J. Morris and B. A. Parviz, "Micro-scale metal contacts for capillary force-driven self-assembly," *J. Micromech. Microeng.*, vol. 18, no. 1, p. 015022, Jan. 2008.
- [28] F. Shao, T. W. Ng, J. Fu, W. Shen, and W. Y. L. Ling, "Electrical circuits from capillary flow driven evaporation deposition of carbon nanotube ink in non-porous V-grooves," *Journal of Colloid and Interface Science*, vol. 363, no. 1, pp. 425–430, Nov. 2011.
- [29] Y. Ding, L. Hong, B. Nie, K. S. Lam, and T. Pan, "Capillary-driven automatic packaging," *Lab Chip*, vol. 11, no. 8, pp. 1464–1469, Apr. 2011.
- [30] R. L. Columbus, "Liquid transport device and method," *US Patent*, no. 4233029, 1980.
- [31] E. Delamarche, D. Juncker, and H. Schmid, "Microfluidics for Processing Surfaces and Miniaturizing Biological Assays," *Angew. Chem. Int. Ed.*, vol. 17, no. 24, pp. 2911–2933, Dec. 2005.
- [32] R. L. Columbus, "Capillary transport device having connected transport zones," *US Patent*, no. 4271119, 1981.
- [33] R. Shartle, D. Besemer, and M. Gorin, "Capillary stop-flow junction having improved stability against accidental fluid flow," *US Patent*, no. 5230866, Jun. 1993.
- [34] R. L. Columbus, "Capillary transport device having speed and meniscus control means," *US Patent*, no. 4618476, 1986.
- [35] R. Safavieh, A. Tamayol, and D. Juncker, "Serpentine and leading-edge capillary pumps for microfluidic capillary systems," *Microfluid Nanofluid*, vol. 18, no. 3, pp. 357–366, Jul. 2014.
- [36] M. Zimmermann, H. Schmid, P. Hunziker, and E. Delamarche, "Capillary pumps for autonomous capillary systems," *Lab Chip*, vol. 7, no. 1, pp. 119–125, 2007.

- [37] I. Gibbons, R. S. Hillman, and C. R. Robertson, "Apparatus and method for dilution and mixing of liquid samples," *US Patent*, no. 4868129, Sep. 1989.
- [38] K. F. Buechler, "Diagnostic devices for the controlled movement of reagents without membranes," *US Patent*, no. 5458852, 1995.
- [39] P. J. Pouletty and T. Ingalz, "Matrix controlled method of delayed fluid delivery for assays," *US Patent*, no. 5135872, Aug. 1992.
- [40] A. Manz, N. Graber, and H. M. Widmer, "Miniaturized total chemical analysis systems: A novel concept for chemical sensing," *Sensors & Actuators: B. Chemical*, vol. 1, no. 1-6, pp. 244–248, Jan. 1990.
- [41] E. Kim, Y. Xia, and G. M. Whitesides, "Polymer microstructures formed by moulding in capillaries," *Nature*, vol. 376, no. 6541, pp. 581–584, Aug. 1995.
- [42] E. Delamarche, A. Bernard, H. Schmid, B. Michel, and H. Biebuyck, "Patterned delivery of immunoglobulins to surfaces using microfluidic networks." *Science*, vol. 276, no. 5313, pp. 779–781, May 1997.
- [43] André Bernard, B. Michel, and E. Delamarche, "Micromosaic Immunoassays," *Anal. Chem.*, vol. 73, no. 1, pp. 8–12, Nov. 2000.
- [44] P. Man, C. H. Mastrangelo, M. A. Burns, and D. T. Burke, "Microfabricated capillarity-driven stop valve and sample injector," in *Proceedings of the the IEEE MEMS Conference*, Jan. 1998, pp. 45–50.
- [45] N. Goedecke, J. Eijkel, and A. Manz, "Evaporation driven pumping for chromatography application," *Lab Chip*, vol. 2, no. 4, pp. 219–223, 2002.
- [46] M. Wolf, D. Juncker, B. Michel, P. Hunziker, and E. Delamarche, "Simultaneous detection of C-reactive protein and other cardiac markers in human plasma using micromosaic immunoassays and self-regulating microfluidic networks." *Biosensors and Bioelectronics*, vol. 19, no. 10, pp. 1193–1202, May 2004.

- [47] L. Gervais and E. Delamarche, "Toward one-step point-of-care immunodiagnos-  
tics using capillary-driven microfluidics and PDMS substrates." *Lab Chip*, vol. 9,  
no. 23, pp. 3330–3337, Dec. 2009.
- [48] J. Wang, H. Ahmad, C. Ma, Q. Shi, O. Vermesh, U. Vermesh, and J. Heath, "A  
self-powered, one-step chip for rapid, quantitative and multiplexed detection of  
proteins from pinpricks of whole blood," *Lab Chip*, vol. 10, no. 22, p. 3157, 2010.
- [49] P. Novo, F. Volpetti, V. Chu, and J. P. Conde, "Control of sequential fluid delivery  
in a fully autonomous capillary microfluidic device." *Lab Chip*, vol. 13, no. 4, pp.  
641–645, Feb. 2013.
- [50] P. Novo, V. Chu, and J. P. Conde, "Integrated optical detection of autonomous  
capillary microfluidic immunoassays: a hand-held point-of-care prototype,"  
*Biosensors and Bioelectronics*, vol. 57, no. C, pp. 284–291, Jul. 2014.
- [51] G. A. Lenk, G. Stemme, and N. Roxhed, "Delay valving in capillary driven de-  
vices based on dissolvable thin films," in *Proceedings of The 18th International Con-  
ference on Miniaturized Systems for Chemistry and Life Sciences ( $\mu$ TAS)*, Jan. 2014,  
pp. 216–218.
- [52] M. Hitzbleck, L. Gervais, and E. Delamarche, "Controlled release of reagents  
in capillary-driven microfluidics using reagent integrators." *Lab Chip*, vol. 11,  
no. 16, pp. 2680–2685, Aug. 2011.
- [53] C. Jönsson, M. Aronsson, G. Rundström, C. Pettersson, I. Mendel-Hartvig,  
J. Bakker, E. Martinsson, B. Liedberg, B. MacCraith, O. Öhman, and J. Melin,  
"Silane–dextran chemistry on lateral flow polymer chips for immunoassays,"  
*Lab Chip*, vol. 8, no. 7, p. 1191, 2008.
- [54] N. Puttaraksa, H. J. Whitlow, M. Napari, L. Meriläinen, and L. Gilbert, "Devel-  
opment of a microfluidic design for an automatic lab-on-chip operation," *Mi-  
crofluid Nanofluid*, vol. 20, no. 10, p. 142, Oct. 2016.

- [55] W. Wu and A. Manz, "Rapid manufacture of modifiable 2.5-dimensional (2.5D) microstructures for capillary force-driven fluidic velocity control," *RSC Adv.*, vol. 5, no. 87, pp. 70 737–70 742, Aug. 2015.
- [56] M. I. Mohammed and M. P. Y. Desmulliez, "The manufacturing of packaged capillary action microfluidic systems by means of CO<sub>2</sub> laser processing," *Microsyst Technol*, pp. 1–10, Mar. 2013.
- [57] A. O. Olanrewaju, A. Robillard, M. Dagher, and D. Juncker, "Autonomous microfluidic capillary circuits replicated from 3D-printed molds." *Lab Chip*, vol. 16, no. 19, pp. 3804–3814, Sep. 2016.
- [58] M.-I. Mohammed and M. P. Y. Desmulliez, "Characterization and theoretical analysis of rapidly prototyped capillary action autonomous microfluidic systems," *J. Microelectromech. Syst.*, vol. 23, no. 6, pp. 1408–1416, Dec. 2014.
- [59] A. O. Olanrewaju, A. Ng, P. Decorwin-Martin, A. Robillard, and D. Juncker, "Microfluidic Capillary Circuit for Rapid and Facile Bacteria Detection." *Anal. Chem.*, vol. 89, no. 12, pp. 6846–6853, Jun. 2017.
- [60] M. J. Beauchamp, G. P. Nordin, and A. T. Woolley, "Moving from millifluidic to truly microfluidic sub-100- $\mu\text{m}$  cross-section 3D printed devices," *Anal Bioanal Chem*, vol. 409, no. 18, pp. 4311–4319, Jun. 2017.
- [61] M. Hitzbleck, "Advanced Capillary-Driven Microfluidic Chips for Diagnostic Applications," Ph.D. dissertation, ETH Zurich, Oct. 2013.
- [62] E. Delamarche, A. Bernard, H. Schmid, A. Bietsch, B. Michel, and H. Biebuyck, "Microfluidic Networks for Chemical Patterning of Substrates: Design and Application to Bioassays," *J. Am. Chem. Soc.*, vol. 120, no. 3, pp. 500–508, Jan. 1998.
- [63] M. Dong and I. Chatzis, "The Imbibition and Flow of a Wetting Liquid along the Corners of a Square Capillary Tube," *Journal of Colloid and Interface Science*, vol. 172, no. 2, pp. 278–288, Jun. 1995.

- [64] P. Concus and R. Finn, "On the behavior of a capillary surface in a wedge." *Proc. Natl. Acad. Sci. U.S.A.*, vol. 63, no. 2, pp. 292–299, Jun. 1969.
- [65] E. Kim and G. M. Whitesides, "Imbibition and flow of wetting liquids in non-circular capillaries," *Journal of Physical Chemistry B*, vol. 101, no. 6, pp. 855–863, 1997.
- [66] V. Jokinen and S. Franssila, "Capillarity in microfluidic channels with hydrophilic and hydrophobic walls," *Microfluid Nanofluid*, vol. 5, no. 4, pp. 443–448, Feb. 2008.
- [67] H. Bruus, *Theoretical microfluidics*, ser. Oxford Masters Series in Physics. OUP Oxford, Mar. 2008.
- [68] L. Gervais, M. Hitzbleck, and E. Delamarche, "Capillary-driven multiparametric microfluidic chips for one-step immunoassays." *Biosensors and Bioelectronics*, vol. 27, no. 1, pp. 64–70, Sep. 2011.
- [69] H. Song, Y. Wang, and K. Pant, "System-level simulation of liquid filling in microfluidic chips," *Biomicrofluidics*, vol. 5, no. 2, p. 024107, 2011.
- [70] P. B. Lillehoj, F. Wei, and C.-M. Ho, "A self-pumping lab-on-a-chip for rapid detection of botulinum toxin," *Lab Chip*, vol. 10, no. 17, p. 2265, 2010.
- [71] J. Berthier, D. Gosselin, A. Pham, G. Delapierre, N. Belgacem, and D. Chaussy, "Capillary Flow Resistors: Local and Global Resistors," *Langmuir*, vol. 32, no. 3, pp. 915–921, Jan. 2016.
- [72] M. Pla-Roca and D. Juncker, "PDMS Microfluidic Capillary Systems for Patterning Proteins on Surfaces and Performing Miniaturized Immunoassays," in *Methods in Molecular Biology*, A. Khademhosseini, K.-Y. Suh, and M. Zourob, Eds. Totowa, NJ: Humana Press, Sep. 2010, pp. 177–194.
- [73] H. J. Kim, W. K. Jang, B. H. Kim, and Y. H. Seo, "Advancing liquid front shape control in capillary filling of microchannel via arrangement of microposts for

- microfluidic biomedical Sensors," *Int. J. Precis. Eng. Manuf.*, vol. 17, no. 1, pp. 59–63, Jan. 2016.
- [74] M. Zimmermann, S. Bentley, H. Schmid, P. Hunziker, and E. Delamarche, "Continuous flow in open microfluidics using controlled evaporation." *Lab Chip*, vol. 5, no. 12, pp. 1355–1359, Dec. 2005.
- [75] N. S. Lynn and D. S. Dandy, "Passive microfluidic pumping using coupled capillary/evaporation effects," *Lab Chip*, vol. 9, no. 23, p. 3422, 2009.
- [76] X. Wang, J. A. Hagen, and I. Papautsky, "Paper pump for passive and programmable transport." *Biomicrofluidics*, vol. 7, no. 1, pp. 14 107–14 107, 2013.
- [77] B. M. Cummins, R. Chinthapatla, B. Lenin, F. S. Ligler, and G. M. Walker, "Modular pumps as programmable hydraulic batteries for microfluidic devices," *Technology*, vol. 05, no. 01, pp. 21–30, Mar. 2017.
- [78] J. Hansson, H. Yasuga, T. Haraldsson, and W. van der Wijngaart, "Synthetic microfluidic paper: High surface area and high porosity polymer micropillar arrays," *Lab Chip*, vol. 16, no. 2, pp. 298–304, Jan. 2016.
- [79] Y. M. Bae, K.-H. Lee, J. Yang, D. Heo, and H. J. Cho, "Hydrogel-based capillary flow pumping in a hydrophobic microfluidic channel," *Jpn. J. Appl. Phys.*, vol. 53, no. 6, p. 067201, May 2014.
- [80] Y.-C. Lee and W.-H. Hsieh, "Absorbent-force-driven microflow cytometer," *Sensors & Actuators: B. Chemical*, vol. 202, pp. 1078–1087, Oct. 2014.
- [81] Y. Oyama, T. Osaki, K. Kamiya, M. Sawai, M. Sakai, and S. Takeuchi, "A sensitive point-of-care testing chip utilizing superabsorbent polymer for the early diagnosis of infectious disease," *Sensors & Actuators: B. Chemical*, vol. 240, pp. 881–886, Mar. 2017.
- [82] M. Zimmermann, P. Hunziker, and E. Delamarche, "Valves for autonomous capillary systems," *Microfluid Nanofluid*, vol. 5, no. 3, pp. 395–402, Sep. 2008.

- [83] M. I. Mohammed, E. Abraham, and M. P. Y. Desmulliez, "Rapid laser prototyping of valves for microfluidic autonomous systems," *J. Micromech. Microeng.*, vol. 23, no. 3, p. 035034, Mar. 2013.
- [84] J. Melin, N. Roxhed, G. Gimenez, P. Griss, W. van der Wijngaart, and G. Stemme, "A liquid-triggered liquid microvalve for on-chip flow control," *Sensors & Actuators: B. Chemical*, vol. 100, no. 3, pp. 463–468, Jan. 2004.
- [85] A. Glière and C. Delattre, "Modeling and fabrication of capillary stop valves for planar microfluidic systems," *Sensors & Actuators: A. Physical*, vol. 130-131, pp. 601–608, Aug. 2006.
- [86] J. M. Chen, P.-C. Huang, and M.-G. Lin, "Analysis and experiment of capillary valves for microfluidics on a rotating disk," *Microfluid Nanofluid*, vol. 4, no. 5, pp. 427–437, Jul. 2007.
- [87] K. Kistrup, C. E. Poulsen, P. F. Østergaard, K. B. Haugshøj, R. Taboryski, A. Wolff, and M. F. Hansen, "Fabrication and modelling of injection moulded all-polymer capillary microvalves for passive microfluidic control," *J. Micromech. Microeng.*, vol. 24, no. 12, p. 125007, Nov. 2014.
- [88] S. Cesaro-Tadic, G. Dernick, D. Juncker, G. Buurman, H. Kropshofer, B. Michel, C. Fattinger, and E. Delamarche, "High-sensitivity miniaturized immunoassays for tumor necrosis factor  $\alpha$  using microfluidic systems," *Lab Chip*, vol. 4, no. 6, pp. 563–569, 2004.
- [89] B. Lutz, T. Liang, E. Fu, S. Ramachandran, P. Kauffman, and P. Yager, "Dissolvable fluidic time delays for programming multi-step assays in instrument-free paper diagnostics." *Lab Chip*, vol. 13, no. 14, pp. 2840–2847, Jul. 2013.
- [90] P. Vulto, S. Podszun, P. Meyer, C. Hermann, A. Manz, and G. A. Urban, "Phaseguides: A paradigm shift in microfluidic priming and emptying," *Lab Chip*, vol. 11, no. 9, pp. 1596–1602, May 2011.

- [91] E. Yildirim, S. J. Trietsch, J. Joore, A. van den Berg, T. Hankemeier, and P. Vulto, "Phaseguides as tunable passive microvalves for liquid routing in complex microfluidic networks," *Lab Chip*, vol. 14, no. 17, pp. 3334–3340, Jun. 2014.
- [92] M. Hitzbleck, L. Avrain, V. Smekens, R. D. Lovchik, P. Mertens, and E. Delamarche, "Capillary soft valves for microfluidics," in *Lab Chip*, vol. 12, May 2012, pp. 1972–1978.
- [93] M. Hitzbleck and E. Delamarche, "Advanced Capillary Soft Valves for Flow Control in Self-Driven Microfluidics," *Micromachines*, vol. 4, no. 1, pp. 1–8, Mar. 2013.
- [94] M. Zimmermann, P. Hunziker, and E. Delamarche, "Autonomous capillary system for one-step immunoassays." *Biomed Microdevices*, vol. 11, no. 1, pp. 1–8, Feb. 2009.
- [95] T. J. Clark, P. H. McPherson, and K. F. Buechler, "The triage cardiac panel: Cardiac markers for the triage system," *Point of Care*, vol. 1, no. 1, pp. 42–46, 2002.
- [96] K. F. Buechler, P. McPherson, J. Anderberg, K. Nakamura, S. Lesefko, and B. Noar, "Microarray Immunoassays in the Microfluidic Triage® Protein Chip," in *Micro Total Analysis Systems 2001*. Dordrecht: Springer Netherlands, 2001, pp. 42–44.
- [97] M. I. Mohammed and M. P. Y. Desmulliez, "Biosensors and Bioelectronics," *Biosensors and Bioelectronics*, vol. 61, no. C, pp. 478–484, Nov. 2014.
- [98] N. Ramalingam, H.-B. Liu, C.-C. Dai, Y. Jiang, H. Wang, Q. Wang, K. M Hui, and H.-Q. Gong, "Real-time PCR array chip with capillary-driven sample loading and reactor sealing for point-of-care applications." *Biomed Microdevices*, vol. 11, no. 5, pp. 1007–1020, Oct. 2009.

- [99] H. Tachibana, M. Saito, K. Tsuji, K. Yamanaka, L. Q. Hoa, and E. Tamiya, "Self-propelled continuous-flow PCR in capillary-driven microfluidic device: Microfluidic behavior and DNA amplification," *Sensors & Actuators: B. Chemical*, vol. 206, pp. 303–310, Jan. 2015.
- [100] H. Tachibana, M. Saito, S. Shibuya, K. Tsuji, N. Miyagawa, K. Yamanaka, and E. Tamiya, "On-chip quantitative detection of pathogen genes by autonomous microfluidic PCR platform." *Biosensors and Bioelectronics*, vol. 74, pp. 725–730, Dec. 2015.
- [101] A. Sposito, V. Hoang, and D. L. DeVoe, "Rapid real-time PCR and high resolution melt analysis in a self-filling thermoplastic chip," *Lab Chip*, vol. 16, no. 18, pp. 3524–3531, 2016.
- [102] S.-J. Kim, S. Paczesny, S. Takayama, and K. Kurabayashi, "Preprogrammed capillarity to passively control system-level sequential and parallel microfluidic flows." *Lab Chip*, vol. 13, no. 11, pp. 2091–2098, Jun. 2013.
- [103] E. Fu, T. Liang, J. Houghtaling, S. Ramachandran, S. A. Ramsey, B. Lutz, and P. Yager, "Enhanced sensitivity of lateral flow tests using a two-dimensional paper network format." *Anal. Chem.*, vol. 83, no. 20, pp. 7941–7946, Oct. 2011.
- [104] C. D. Chin, T. Laksanasopin, Y. K. Cheung, D. Steinmiller, V. Linder, H. Parsa, J. Wang, H. Moore, R. Rouse, G. Umvilighozo, E. Karita, L. Mwambarangwe, S. L. Braunstein, J. van de Wijert, R. Sahabo, J. E. Justman, W. El-Sadr, and S. K. Sia, "Microfluidics-based diagnostics of infectious diseases in the developing world," *Nature Medicine*, vol. 17, no. 8, pp. 1015–1019, Jul. 2011.
- [105] E. Fu, S. A. Ramsey, P. Kauffman, B. Lutz, and P. Yager, "Transport in two-dimensional paper networks," *Microfluid Nanofluid*, vol. 10, no. 1, pp. 29–35, Jun. 2010.

- [106] D. A. Bartholomeusz, R. W. Boutté, and J. D. Andrade, "Xurography: Rapid prototyping of microstructures using a cutting plotter," *J. Microelectromech. Syst.*, vol. 14, no. 6, pp. 1364–1374, Dec. 2005.
- [107] J. I. Martínez-López, M. Mojica, C. A. Rodríguez, and H. R. Siller, "Xurography as a Rapid Fabrication Alternative for Point-of-Care Devices: Assessment of Passive Micromixers," *Sensors (Basel, Switzerland)*, vol. 16, no. 5, p. 705, May 2016.
- [108] L. Cerami, E. Mazur, S. Nolte, and C. B. Schaffer, "Femtosecond Laser Micromachining," in *Ultrafast Nonlinear Optics*. Heidelberg: Springer International Publishing, Jan. 2013, pp. 287–321.
- [109] A. K. Au, W. Huynh, L. F. Horowitz, and A. Folch, "3D-Printed Microfluidics." *Angew. Chem. Int. Ed.*, vol. 55, no. 12, pp. 3862–3881, Mar. 2016.
- [110] S. Waheed, J. M. Cabot, N. P. Macdonald, T. Lewis, R. M. Guijt, B. Paull, and M. C. Breadmore, "3D printed microfluidic devices: enablers and barriers." *Lab Chip*, vol. 16, no. 11, pp. 1993–2013, May 2016.
- [111] B. Gross, S. Y. Lockwood, and D. M. Spence, "Recent Advances in Analytical Chemistry by 3D Printing." *Anal. Chem.*, vol. 89, no. 1, pp. 57–70, Jan. 2017.
- [112] N. P. Macdonald, J. M. Cabot, P. Smejkal, R. M. Guijt, B. Paull, and M. C. Breadmore, "Comparing Microfluidic Performance of Three-Dimensional (3D) Printing Platforms," *Anal. Chem.*, vol. 89, no. 7, pp. 3858–3866, Mar. 2017.
- [113] R. K. Lade, E. J. Hippchen, C. W. Macosko, and L. F. Francis, "Dynamics of Capillary-Driven Flow in 3D Printed Open Microchannels." *Langmuir*, vol. 33, no. 12, pp. 2949–2964, Mar. 2017.
- [114] A. W. Martinez, S. T. Phillips, M. J. Butte, and G. M. Whitesides, "Patterned paper as a platform for inexpensive, low-volume, portable bioassays." *Angew. Chem. Int. Ed.*, vol. 46, no. 8, pp. 1318–1320, 2007.

## Chapter 4

# Capillarie Circuits Replicated from 3D-Printed Molds

### 4.1 Preface

Our research group recently developed capillarie circuits (CCs) – advanced capillary microfluidic devices assembled from capillary fluidic elements in a modular manner similar to the design of electric circuits (Safavieh & Juncker, *Lab Chip*, 2013, 13, 4180-4189). CCs choreograph liquid delivery operations according to pre-programmed capillary pressure differences with minimal user intervention. CCs were thought to require high-precision micron-scale features manufactured by conventional photolithography, which is slow and expensive. Here we present CCs manufactured rapidly and inexpensively using 3D-printed molds. Molds for CCs were fabricated with a benchtop 3D-printer, Poly(dimethylsiloxane) replicas were made, and fluidic functionality was verified with aqueous solutions. We established design rules for CCs by a combination of modelling and experimentation. The functionality and reliability of trigger valves – an essential fluidic element that stops one liquid until flow is triggered by a second liquid – was tested for different geometries and different solutions. Trigger valves with geometries up to 80-fold larger than cleanroom-fabricated ones were found to function reliably. We designed retention burst valves that encode sequential liquid delivery using capillary pressure differences encoded by systematically varied

heights and widths. Using an electrical circuit analogue of the CC, we established design rules to ensure strictly sequential liquid delivery. CCs autonomously delivered eight liquids in a pre-determined sequence in <7 min. Taken together, our results demonstrate that 3D-printing lowers the bar for other researchers to access capillary microfluidic valves and CCs for autonomous liquid delivery with applications in diagnostics, research and education.

This chapter is based on: **Autonomous Microfluidic Capillary Circuits Replicated from 3D-Printed Molds**, A.O. Olanrewaju, A. Robillard, M. Dagher, and D. Juncker, *Lab on a Chip*, 2016.

## 4.2 Introduction

Capillary-driven microfluidic devices move liquids using capillary forces defined by the geometry and surface chemistry of microchannels. This allows liquid delivery without using external pumps and valves. A wide range of capillary fluidic control elements were developed over the years including: stop valves,[1] retention valves,[2] trigger valves,[3] and capillary pumps.[2, 4, 5] Autonomous capillary microfluidic systems capable of self-powered and self-regulated completion of biochemical assays were also developed.[2, 6, 7, 8] Yet these autonomous capillary microfluidic systems were fabricated using silicon wafers and cleanroom processes with multiple photomasks, thereby increasing their cost and complexity. Paper-based microfluidics and lateral flow assays were also re-discovered as inexpensive approaches to autonomous capillary-driven flow;[9, 10] nevertheless, paper-based methods rely on heterogeneous porous substrates with statistical flow paths and cannot accomplish some of the valving capabilities that require the deterministic and predictable flow paths of microchannel-based devices. As such, there is a need for rapid and inexpensive fabrication of microchannel-based capillary microfluidics.

### 4.2.1 Capillarie circuits for autonomous liquid delivery

More recently, advanced capillary microfluidic devices capable of preprogrammed delivery of multiple liquids were developed to enable autonomous multi-step processes, for instance to incorporate wash or signal amplification steps for improved bioassay sensitivity and specificity.[11, 12, 13] Our research group proposed capillarie circuits (CCs) – advanced capillary circuits that are assembled from individual capillarie elements in the same way that electric circuits are assembled from individual electric components.[13] CCs enable the operator to pre-load each reservoir, without worrying about the timing or sequence of these operations – instead, capillary microfluidic elements choreograph liquid delivery operations with minimal user intervention. This makes CCs a desirable platform for automating biochemical assays in point-of-care settings with minimal instrumentation.

The words *capillary* and *capillarie* are meant to emulate the distinction between *electric* and *electronic* whereas the former pertains to basic principles and the latter is used in the context of advanced circuits integrating multiple functionalities. In addition, the term *capillary* is ambiguous, as it is both used in reference to physical capillaries (including artificial and natural capillaries such as blood vessels) and in reference to surface tension-driven flow either within capillaries, microfluidic conduits or porous media, which can lead to confusion. The term *capillarie* is restricted to surface-tension driven microfluidic circuits, and thus helps resolve the ambiguity.

Our group introduced two new fluidic elements to enable deterministic flow control with CCs. First, we developed two-level trigger valves (TVs) that stop liquids for over 30 minutes using an abrupt geometry change and a hydrophobic PDMS cover, thereby enabling pre-loading of reservoirs and subsequent liquid release when flow is triggered by a connected channel.[13] We also developed retention burst valves (RBVs) that have a burst pressure encoded by their geometry. When integrated with other capillary fluidic elements within a CC, RBVs allow autonomous delivery of liquids in a pre-programmed sequence according to increasing order of RBV capillary

pressure.[13]

## 4.2.2 Rapid prototyping of passive microfluidic devices

Although CCs enable sophisticated and automated fluidic operations, the prevailing view is that deterministic capillary microfluidics require high-precision and small-scale ( $\approx 10\mu\text{m}$ ) features for proper operation. As such, fabrication of CCs was dependent on cleanrooms, and was resource-intensive, time-consuming and expensive. Coupled with the need of photomasks for photolithography, a high cost and slow turnaround time for new design iterations limits the development of new devices and their widespread adoption.

To overcome the limitations of cleanroom fabrication, rapid and inexpensive prototyping of capillary microfluidic valves and integrated devices has been explored. Rapid prototyping techniques used for developing capillary microfluidic devices include micromilling[14] and laser cutting[15]. These techniques have successfully been used for making capillary stop valves using primarily hydrophobic surface coatings that greatly relax the design constraints on the valve, but at the expense of autonomy and thus require syringe pumps or centrifugal forces to move the liquids within the microchannels.[16, 17, 18, 19] More recently, a simple, autonomous self-filling capillary system comprising a capillary TV was fabricated by CO<sub>2</sub> laser cutting.[15, 15, 20] These results suggested that larger scale capillary circuits may be possible, however the laser cutting created triangular shaped conduits with limited control over the channel dimension, thus preventing the integration of more advanced elements such as retention burst valves for making more advanced capillary circuits.

## 4.2.3 3D-Printed Microfluidics

Lately, there has been a surge of interest in 3D-printing for microfluidics applications due to the speed, accessibility, and low cost required to fabricate multilayer microfluidic structures. Recent reviews describe state of the art 3D-printing for microfluidics

applications.[21, 22] All demonstrations of 3D-printed microfluidics so far employ active flow control (usually pneumatic or centrifugal pumps). The resolution currently available with consumer grade 3D-printers is typically  $\geq 200\mu\text{m}$ [23, 24] with  $\approx 1\mu\text{m}$  surface roughness.[25] Capillary microfluidics however have traditionally been made with channels in the 1 – 100  $\mu\text{m}$  range because the capillary pressure is inversely proportional to the smallest dimension, and becomes very small for large microchannels. Moreover, valving and flow control depend on the surface topography and abrupt geometric changes and low surface roughness are considered necessary to prevent edge wetting and creeping flows. Hence the prevailing perception is that current 3D-printing technology may not be suitable for making capillary microfluidics because the smallest dimensions are too large to obtain adequate capillary pressure, the resolution and precision insufficient for making abrupt changes needed for reliable valves – notably due to the layered structure of stereolithographic printing forming steps that lend themselves to edge wetting effects – and the high surface roughness may lead to creeping of liquid. High surface roughness could also lead to pinning of liquid that could result in flow stoppage or intermittent flow.[26]

#### 4.2.4 Capillarie circuits from 3D-printed molds

Here we present microfluidic capillarie circuits made from 3D-printed molds fabricated by stereolithographic 3D-printing with geometries scaled up > 20-fold compared to cleanroom-fabricated circuits. 3D-printing allows rapid and inexpensive fabrication of CCs. This enables investigation and engineering of CCs with greater capabilities and increased accessibility in research and point-of-care settings. First, we 3D-print molds for TVs and characterize their performance as a function of geometry and surfactant concentration. Then we investigate design rules for CCs composed of TVs, RBVs, flow resistors, and capillary pumps using a proof of principle circuit with four reservoirs. Finally, we demonstrate the capabilities of our CCs by developing a circuit for autonomous delivery of eight liquids in < 7 minutes.

## 4.3 Materials and Methods

### 4.3.1 Process flow for 3D-printing capillary circuits

First, we developed a symbolic representation for CCs using electrical analogies, as described in our previous work.[13] Next, the symbolic circuit was converted into a computer-aided schematic design that was exported into the standard stereolithography (STL) format for 3D-printing. We 3D-printed molds of CCs in polymeric resin using a stereolithography-based printer (Perfactory MicroEDU, EnvisionTEC Inc., USA) with  $96\ \mu\text{m}$  XY pixel size and  $50\ \mu\text{m}$  Z layer height. Microfluidic features were aligned to the pixel grid of the 3D-printer projector to ensure accurate realization of features. The 3D-printer's default settings were used. Device designs included 2 mm thick bases for easier handling. The typical printing time for capillary microfluidic devices, with multiple devices arranged to cover nearly the entire  $100 \times 75\ \text{mm}^2$  print area of the 3D-printer, was  $\approx 30$  minutes. After 3D-printing, molds were washed in isopropanol for 5 minutes and dried with nitrogen gas. 3D-printed molds were inspected under the microscope to check for defects during the printing process.

### 4.3.2 PDMS replication from 3D-printed molds

To obtain multiple copies of capillary microfluidic devices from the same 3D-printed mold, we made Poly(dimethylsiloxane) (PDMS) replicas of devices by soft lithography. [27] We 3D-printed molds using a high temperature molding resin (EnvisionTEC Inc., Germany) with a manufacturer-specified heat deflection temperature of  $140\ ^\circ\text{C}$  to allow replica molding of 3D-printed structures. Prior to PDMS replication, molds were pre-treated with a silicone spray (Ease Release 200™, Mann Formulated Products, USA) to prevent PDMS from sticking to the mold. The spray was applied in two passes uniformly over the surface of the mold from a height of about 10 cm. To make PDMS replicas, elastomer base and curing agent (Sylgard 184, Paisley Products Inc., Canada) were mixed in a 10:1 ratio. The PDMS mixture was degassed for 1 hour and

poured onto the 3D-printed mold placed in a petri dish. PDMS was cured overnight at 60 °C and then peeled from the mold. First PDMS replicas were discarded because they were sticky due to the presence of silicone spray residue; subsequent replicas were used for capillary microfluidics experiments.

### 4.3.3 Procedure for capillary-driven flow experiments

To obtain hydrophilic surfaces for capillary-driven flow, PDMS replicas were activated for 12 seconds at 200 mTorr and 150 W in a plasma chamber (PE-50, PlasmaEtch, USA). To characterize the plasma-treated surfaces, advancing and receding contact angles of deionized water were measured using a video-based optical contact angle measurement instrument (OCA 15EC, Dataphysics Instruments GmbH, Germany). Plasma-treated PDMS devices were sealed with flat, untreated PDMS covers to provide closed microchannels for capillary-driven flow. The PDMS covers were made with a 1:20 ratio of curing agent to elastomer base to obtain soft and flexible PDMS surfaces that sealed well, despite their hydrophobicity. Flow in CCs was tested using aqueous food dye solutions and visualized under a stereomicroscope (SMZ-8, Leica Microsystems Inc., Canada) with a video camera (Lumix GH3 DSLR, Panasonic Inc., Canada). During TV testing, when devices were tested for  $\geq 30$  min, we humidified the area around the capillary microfluidic chips with wet Kimwipes™ and covered with a petri dish to prevent evaporation.[28]

## 4.4 Results and Discussion

CCs operate using a series of functional elements including inlets, channels, flow resistors, capillary pumps, trigger valves (TV), capillary retention valves, and retention burst valves (RBVs) that can be combined for encoding the autonomous delivery of multiple liquids.[13] The capillary pressure of each RBV is calculated using the Young-Laplace equation:

$$P = -\gamma \left[ \frac{\cos \theta_t + \cos \theta_b}{h} + \frac{\cos \theta_l + \cos \theta_r}{w} \right] \quad (4.1)$$

where  $P$  is the capillary pressure,  $\gamma$  is the surface tension of liquid in the microchannel, and  $h, w$  are the height and width of the microchannel respectively.  $\theta_t, \theta_b, \theta_l, \theta_r$  are the top, bottom, left, and right channel wall contact angles, respectively. Contact angle hysteresis must be considered when calculating capillary pressures of microchannels in the CC. For the hydrophobic top PDMS surface, advancing and receding contact angles were measured as  $114$  and  $89 \pm 2^\circ$  respectively. While for the hydrophilic bottom and side surfaces, advancing and receding contact angles were  $45$  and  $31 \pm 2^\circ$  respectively. Advancing contact angles are relevant when a channel is filled while the receding contact angles are relevant when a channel is drained. Likewise, the resistance  $R$  for a conduit with a rectangular cross-section is given by:[29]

$$R = \frac{12\eta L}{\left[1 - 0.630 \frac{h}{w}\right]} \frac{1}{h^3 w} \quad (4.2)$$

where  $\eta$  is the viscosity of liquid in the channel, and  $L$  is length of the microchannel. The cross section of channels and various elements for microfabricated CCs reported by Safavieh *et al*[13] ranged from  $15 \times 100 \mu\text{m}^2$  to  $200 \times 200 \mu\text{m}^2$ . Thus, using measured contact angles for the hydrophobic top PDMS surface and hydrophilic side and bottom surfaces, and a surface tension of  $72 \text{ N/m}$ , the capillary pressures of microchannels (calculated using equation 4.1) in the cleanroom-fabricated circuits ranged from  $-7948 \text{ Pa}$  to  $-1264 \text{ Pa}$ . These capillary pressures would correspond to water column heights of  $810 \text{ mm}$  and  $129 \text{ mm}$  respectively in capillary rise experiments. Since our microchannel lengths were on the order of  $5 \text{ mm}$ , capillary forces dominated gravity in our microfabricated CCs and our devices could be operated without considering gravity effects.

We first tested whether 3D-printed channels and capillary pumps replicated into PDMS could be filled by a liquid, and found that this worked reliably up to  $1000 \times 1000 \mu\text{m}^2$  constituting the upper limit for capillary elements in this study. The lower

size limit for fluidic elements was set by the resolution of the 3D printer. The vertical resolution was set by the thickness of each printed layer and was  $50\ \mu\text{m}$ . The lateral resolution was  $100\ \mu\text{m}$  under the best circumstances, but was limited to  $200\ \mu\text{m}$  when taking into consideration fabrication yield. Hence, for 3D-printed circuits, the cross-sectional dimensions range from  $50 \times 200\ \mu\text{m}^2$  to  $1000 \times 1000\ \mu\text{m}^2$ , and the capillary pressure ranges from  $-955\ \text{Pa}$  to  $-188\ \text{Pa}$ , or a water column height from  $97\ \text{mm}$  to  $19\ \text{mm}$ . These type of conduits filled spontaneously with aqueous solutions and remain in a microfluidic regime where gravity and inertia within the conduits are negligible.

Next, we set out to test whether critical functional elements such as the TV and the RBV could also be 3D printed, whether surface roughness might affect their functionality, and to determine the design rules for making them.

#### 4.4.1 Trigger Valves

In order to develop functional CCs, the first step is to have functional and reliable trigger valves (TVs) to robustly hold liquids in reservoirs.[13] Consequently, we first characterized TVs on a standalone basis, before developing more complex CCs.

##### Cleanroom-fabricated versus 3D-printed trigger valves

Cleanroom fabrication is generally considered the gold standard for manufacturing capillary stop valves and TVs because of the small feature sizes and smooth channel surfaces attainable.[1, 12, 13, 30, 31] Cleanroom-fabricated TVs have small features ( $\approx 20\ \mu\text{m}$ ) and smooth, vertical channel walls (Fig. 4.1a and 4.1c). Meanwhile, 3D-printed trigger features have larger minimum widths ( $\geq 100\ \mu\text{m}$ ) and rough, layered channel walls (Fig. 4.1b and 4.1d). The surface roughness of 3D-printed molds was measured to be  $\pm 1\ \mu\text{m}$  using contact profilometry, compared to the typical submicron roughness (tens of nanometers) for cleanroom-fabricated devices. These stark geometry differences call into question the functionality and reliability of 3D-printed TVs.

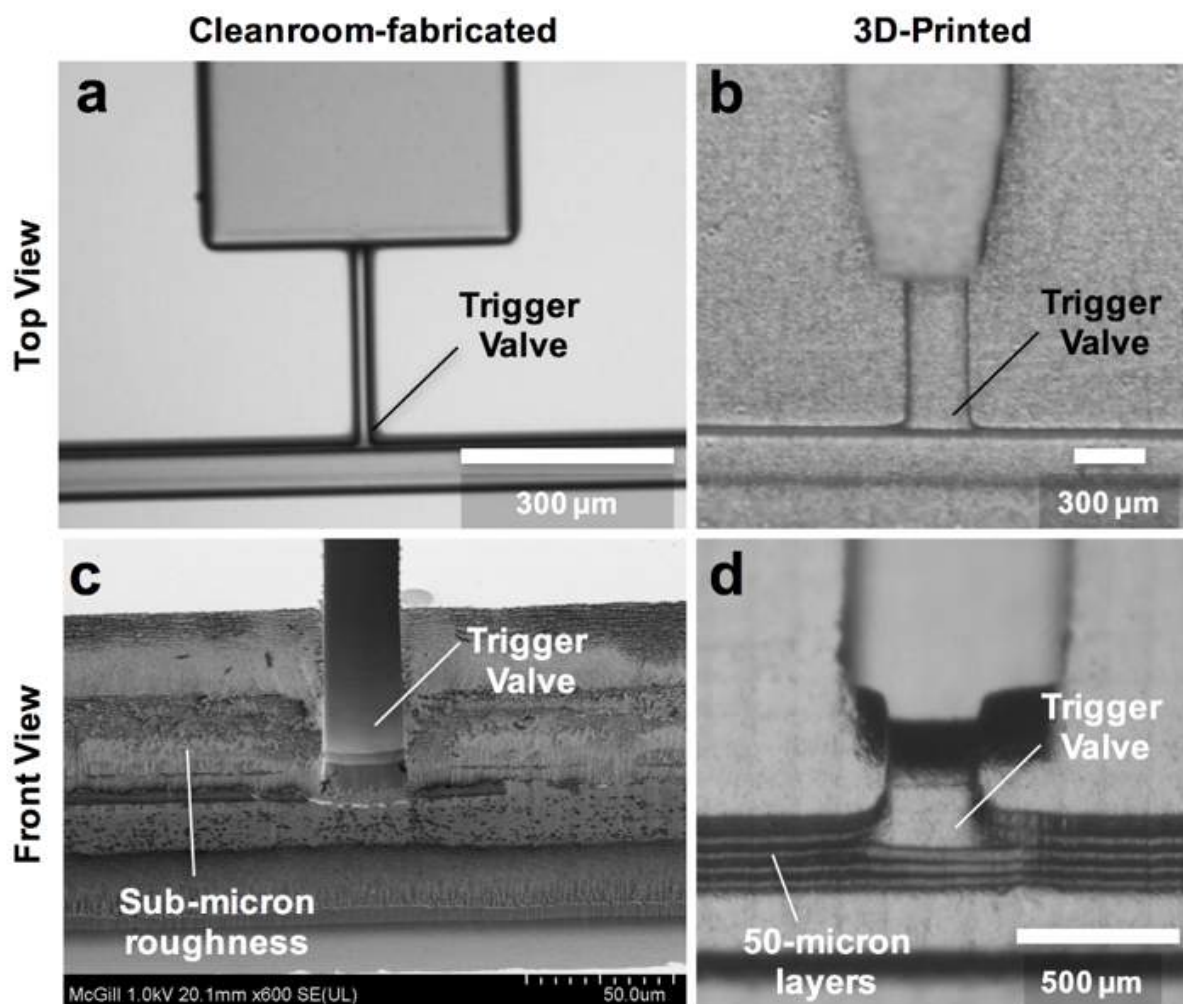


FIGURE 4.1: **Comparison between cleanroom-fabricated and 3D-printed TVs.** (A) Top view of TV fabricated by photolithography in the cleanroom showing smooth, high-precision features. (B) Top view of TV fabricated by stereolithography-based 3D printing showing rough, large features. (C) Scanning electron micrograph of TV fabricated by deep reactive ion etching of silicon showing vertical channel walls with sub-micron roughness. (D) Front view of PDMS replica of 3D-printed TV showing 50- $\mu\text{m}$  thick ridges on the channel wall due to the layer-by-layer printing process.

We 3D-printed TV molds and tested a wide range of geometries and surfactant concentrations to assess their functionality and reliability. Previously, the success rate of capillary stop valves and TVs was only reported over a 5-minute period.[15, 30] Here we defined TV success as when a valve holds liquid for at least 30 minutes without leakage. This allowed autonomous microfluidic operations where the user pre-loads samples and reagents onto the chip and subsequently starts the assay at a time of their choosing, without needing to fit their operations to a strict 5-minute window.

### Effect of trigger valve geometry on success rate

The geometry of TVs influences their success rate.[18, 30, 31] Fig. 4.2a shows the geometric parameters known to affect the performance of capillary TVs: the height of the TV, width of the TV, and the height difference between the TV and its release channel. To determine which geometries provide high TV success rates, we tested valves with widths of 96  $\mu\text{m}$ , 192  $\mu\text{m}$ , 288  $\mu\text{m}$ , 480  $\mu\text{m}$ , 672  $\mu\text{m}$ , 960  $\mu\text{m}$ , and 2016  $\mu\text{m}$ . TV heights were fixed at either 400  $\mu\text{m}$  or 1000  $\mu\text{m}$  to obtain different height-to-width ratios for these experiments. As summarized in Fig. 4.2b, all TVs tested were at least 75 % successful (N=8). The few failures were due to difficulties while loading valves with low (< 1) or high (> 5) aspect ratios (i.e. height-to-width ratios) that required the user to apply additional positive pressure when filling the valves. We found that 3D-printed TVs were reliable with dimensions up to 3 times larger than reported with CO<sub>2</sub> laser cutting[15] and up to 80 times larger than typical cleanroom-fabricated valves.[13, 30]

Since the minimum z-layer thickness of the microchannels was limited to 50  $\mu\text{m}$  by the 3D-printer resolution, we tested height differences of 100  $\mu\text{m}$ , 150  $\mu\text{m}$ , 200  $\mu\text{m}$ , 250  $\mu\text{m}$ , 300  $\mu\text{m}$ , 400  $\mu\text{m}$ , and 500  $\mu\text{m}$  between the TV and the release channel. The TVs used for these height difference tests were 300  $\mu\text{m}$  wide and 50  $\mu\text{m}$  deep, since our TV characterizations showed reliable functionality over a wide range of geometries (Fig. 4.2b). As seen in Fig. 4.2c, the height difference between the TV and the release channel had a threshold effect on TV success. When the height difference was  $\geq 300$   $\mu\text{m}$ , TVs were 100 % successful (N = 6).

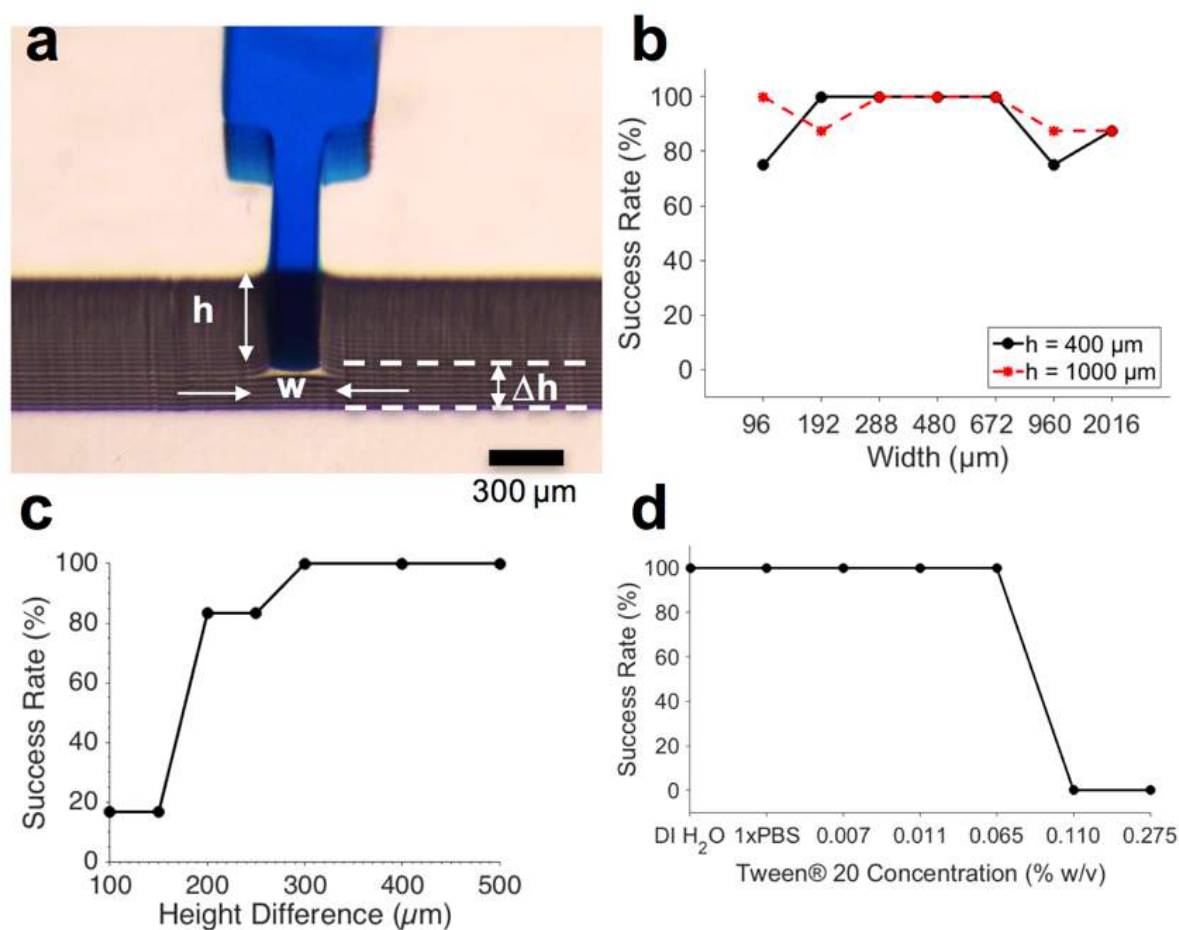


FIGURE 4.2: Effect of geometry and surfactant concentration on success rate of TVs. (A) Front view of food dye solution stopped at TV showing the TV height ( $h$ ), width ( $w$ ), and the height difference between TV and release channel ( $\Delta h$ ). (B) Success rates for TVs over a wide range of widths and heights.  $N = 8$ . (C) Above a height difference ( $\Delta h$ ) of  $300\ \mu\text{m}$ , TVs were 100 % successful.  $N = 6$ . (D) TVs were 100 % successful at Tween® 20 concentrations  $\leq 0.0650$  % weight by volume in  $1\times\text{PBS}$ .  $N = 3$ .

This is a useful initial characterization; however, it is important to note that there are several other factors that influence trigger valve performance including: channel height, contact angle, and 3D-printed layer height. Future work is required to systematically investigate the effect of these parameters on trigger valve performance. The capillary pressure barrier of trigger valves may be estimated analytically[1] or numerically[31] allowing comparison of trigger valve success rate directly with the capillary pressure barrier imposed by the valve. This would provide a deterministic design rule that encompasses the different geometry and surface chemistry parameters that affect trigger valve performance. A challenge with achieving such a generalizable design rule is that surface roughness and 3D-printed layer heights might be affected by the choice of 3D-printer and material used to fabricate the CCs. As such, comparisons must be made between different 3D-printers to determine how generalizable the design rules.

#### **Effect of surfactant concentration on trigger valve performance**

Despite the fact that the most common application of capillary microfluidics is to automate biological assays that often require the use of surfactant-containing reagents, the effect of surfactant concentration on TV performance is not well reported in the literature. To determine the effect of surfactant on TVs, we tested aqueous solutions with different concentrations of Tween® 20, a surfactant commonly used in immunoassay wash buffers and for cell lysis. The critical micelle concentration of Tween® 20, is 0.0074% w/v. Consequently, we tested the following concentrations of Tween® 20: 0.0074, 0.0110, 0.0650, 0.1100, and 0.2750 % weight/volume. As shown in Fig.2d, we found that the TVs were 100 % reliable when Tween® 20 concentrations were  $\leq 0.0650$  % weight/volume (N=3), a suitable surfactant concentration for use in wash buffers during immunoassays that commonly use 0.05%. [32, 33]

#### 4.4.2 Retention Burst Valves

After establishing that functional trigger valves could be obtained by 3D-printing, we designed CCs with Retention burst valves (RBVs) to control sequential liquid delivery. The burst pressure of each RBV was calculated using Eq. 1.

##### Capillary circuit for autonomous delivery of four liquids

As a proof of principle that we could 3D-print molds for capillary circuits, we designed a circuit with 4 RBVs (Fig. 4.3a and b). PDMS replicas of the 3D-printed mold were made (Fig. 4.3c), plasma-treated for hydrophilicity, and sealed with a hydrophobic PDMS cover (Fig. 4.3d). The expected pre-programmed operation of the CC is illustrated in Fig. 4.3e. First reservoirs were filled and TVs held each liquid in place. Next, a solution was added to the release channel, connecting the reservoirs to the pump and starting the pre-programmed liquid delivery sequence. Subsequently, the RBVs burst sequentially according to increasing capillary pressure.

The TVs in the CC were designed to have the smallest cross section in the circuit and the highest capillary pressure in the CC since they play a dual role – stopping liquids during initial filling of reservoirs, and acting as retention valves with higher capillary pressure than the capillary pump during reservoir drainage (see Fig. 4.3a). These retention valves ensure that the side branches are not completely emptied (with minimal dead volume), thereby allowing sequential liquid delivery without bubble trapping.[2, 13]

In cleanroom-fabricated devices, multiple masks are needed for making structures with multiple depths; hence only the microchannel widths were used as a free parameter to adjust the RBV threshold.[13] RBVs were typically 100  $\mu\text{m}$  deep and had widths of 200  $\mu\text{m}$ , 130  $\mu\text{m}$ , 110  $\mu\text{m}$ , and 90  $\mu\text{m}$  corresponding to capillary pressures of  $-1264$  Pa,  $-1601$  Pa,  $-1847$  Pa, and  $-2028$  Pa respectively.

With 3D-printing both the width and depth can be adjusted independently and fabricated in one shot. Consequently, we encoded the capillary pressure differences

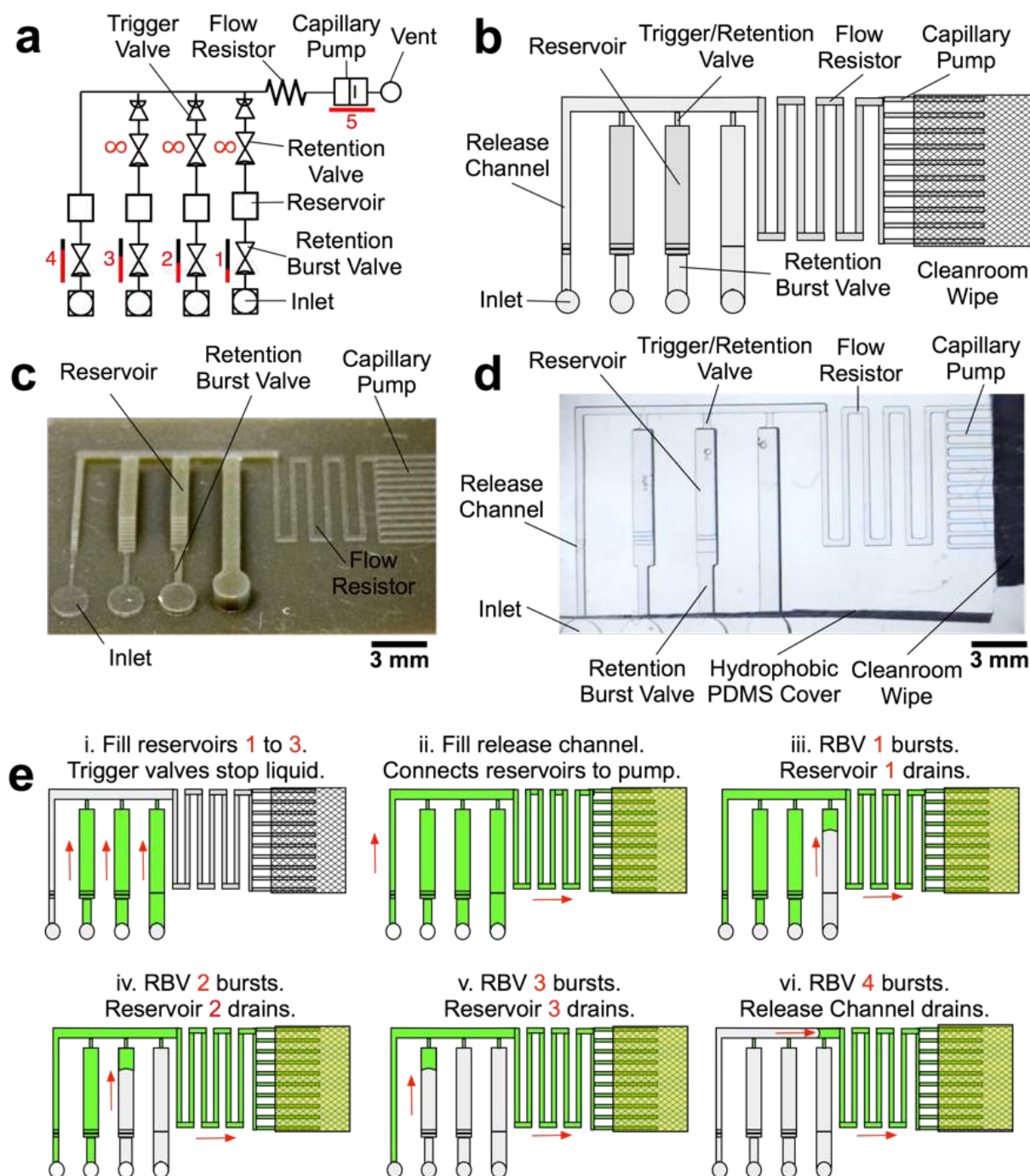


FIGURE 4.3: **Design, mold, PDMS replica and operation of CCs for autonomous sequential delivery of four liquids.** (A) Symbolic representation of CC with main fluidic elements labelled. (B) Schematic of CC. (C) 3D-printed mold of the CC and (D) PDMS replica with transparent PDMS cover and clean room wipe contacting the capillary pump. (E) Schematic illustrating expected operation of RBVs. Solutions loaded into the reservoirs are delivered in pre-programmed manner according to RBV capillary pressure.

between RBVs by modifying both the height and widths of the microchannels. The lower size limit of our microchannels was set by 3D-printer resolution. The pixel size for the EnvisionTEC Perfactory MicroEDU 3D-printer is listed as  $96\ \mu\text{m}$ , the smallest features that we were able to print with a high yield were  $200\ \mu\text{m}$  wide and  $50\ \mu\text{m}$  deep open channels. This resolution obtained is similar to that reported for other state of the art stereolithographic 3D-printers in the literature.[34] The reservoirs were  $960\ \mu\text{m}$  wide,  $1000\ \mu\text{m}$  deep, and  $6250\ \mu\text{m}$  long with a volume of  $6\ \mu\text{L}$ , corresponding to 60 times the volume of typical microfabricated reservoirs.[13] Due to the change in the size of the RBV, there were minor changes in volume for each reservoir (Fig. 4.3c and d) that could be compensated for by adjusting the reservoir size.

To accommodate the large volumes in the reagent reservoirs without significantly increasing device footprint, we placed a cleanroom wipe made of paper (Durx 670, Berkshire Corporation, USA) atop the capillary pump.[35] The combination of 3D-printing and off-the-shelf, low cost paper saves costs without compromising performance. The driving capillary pressure in the circuit is defined by capillary pump because the gap between the edge of the PDMS and the paper forms an open microchannel that can be drained. Hence, the capillary pressure is dictated by the capillary pressure of the capillary pump, allowing use of paper pumps with higher, but sometimes ill-defined capillary pressures, without impacting the accuracy and functionality of the CCs.

### Requirements for sequential RBV bursting

It is not sufficient to simply increase the burst pressure of the RBV to achieve sequential drainage. In fact the architecture of the CC must be designed to ensure that an RBV only bursts after complete drainage of the reservoir connected to the previous RBV. To illustrate this point, the proof of concept CC shown in Fig. 4.3a when filled with liquid is modeled by an electrical equivalent circuit shown in Fig. 4.4a.

Considering the circuit at the instant when all reservoirs are filled, but still under static conditions, without flow, the junction pressure  $P_J$  will be equal to the pressure

$P_C$  of the capillary pump. Given that the capillary pressure of the pump is larger than the capillary pressure of the side branches, liquid will be drawn towards the junction  $P_J$ , leading to flow in the CC. The first side branch to be drained in the CC is the one connected to the RBV with the lowest burst pressure, which here is RBV1 with pressure  $P_1$ . As liquid drains from side branch 1, there is a pressure drop across  $R_1$  and  $R_{RV}$  on one hand and across the main resistor  $R_M$  on the other hand, which will lead to a reduction of the pressure  $P_J$  at the juncture between the side-branch and the main channel. The high resistance of  $R_{RV}$  and  $R_M$  compared to the low resistance of the release channel ensures that pressure  $P_J$  is replicated across all 4 junctions (red dot in Fig. 4.4a). To avoid bursting of RBV2 while branch 1 is draining, it is imperative that  $|P_J| < |P_2|$  at all times. Assuming a single branch drains at any given time, the pressure  $P_J$  during drainage of the RBV can be calculated from the electrical circuit analogue using Kirchhoff's law and Ohm's law yielding:

$$P_J = \frac{P_i \cdot R_M + P_C \cdot (R_{RV} + R_i)}{(R_M + R_{RV} + R_i)} \quad (4.3)$$

where the index  $i$  represents the side branch that is being drained in the capillary circuit,  $P_i$  is the capillary pressure of the liquid meniscus on the end of the side branch,  $R_i$  is the flow resistance of the RBV and reservoir of the side branch,  $R_{RV}$  is the resistance of the retention valve, is the flow resistance of the main resistor, and  $P_C$  is the pressure of the capillary pump (see Fig. 4.4a).

As the liquid drains, the resistance in the side branch is expected to change. However, the retention/trigger valve structure has the smallest cross-section ( $300 \times 50 \mu\text{m}^2$ ) in the side branch and its associated resistance  $R_{RV} > 100R_i$ . Consequently, changes in the resistance of the side branch during drainage are negligible and do not need to be considered in the calculation of  $P_J$ . Moreover, after the RBV drains,  $P_J$  decreases since the capillary pressure at the end of the side branch now becomes the capillary pressure of the reservoir rather than the capillary pressure of the RBV. This drop in  $P_J$  does not adversely affect sequential liquid delivery since the condition for sequential

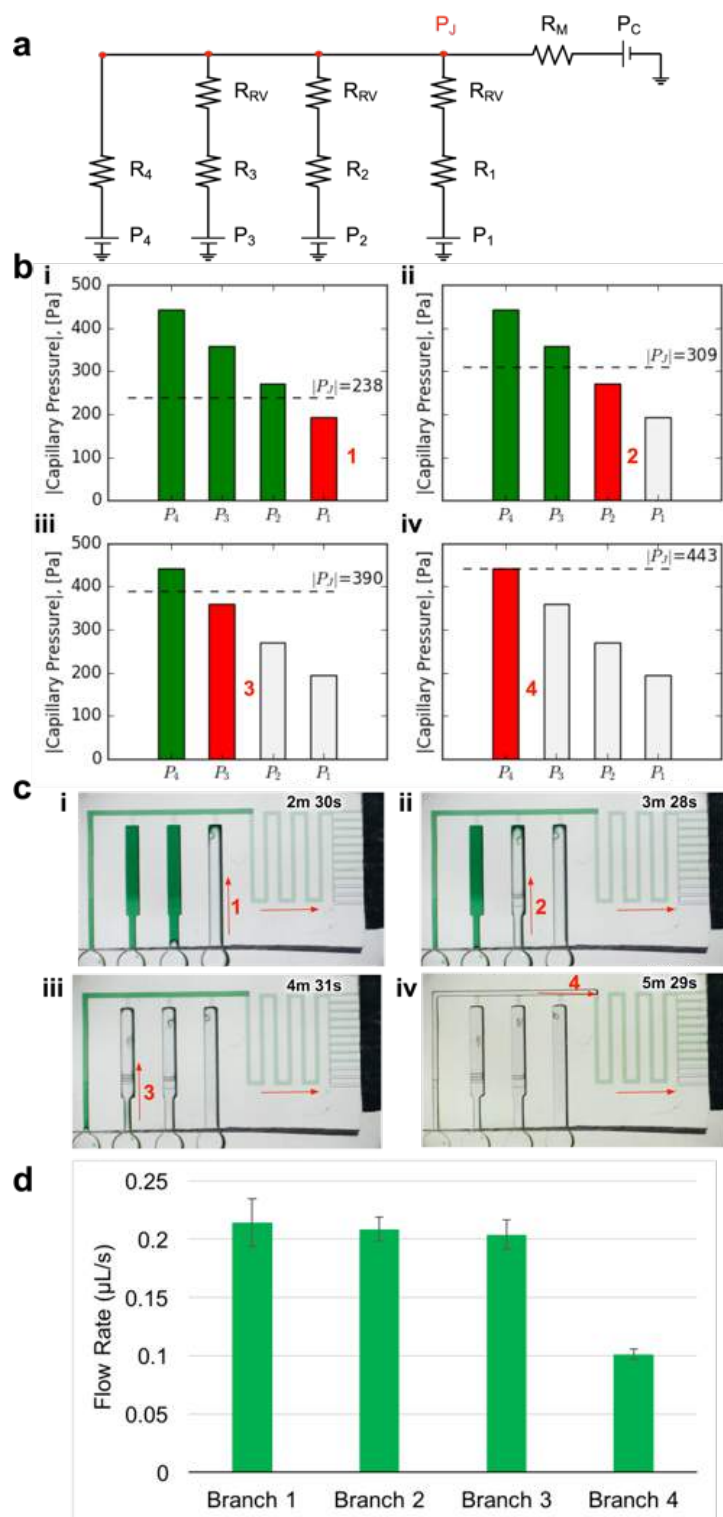


FIGURE 4.4: **Design and experimental validation of CC for autonomous delivery of four liquids.** (A) Electric circuit analogue showing the flow resistances and capillary pressures in the CC. (B) Graphs showing the calculated junction pressures during bursting of each RBV. Junction pressures were designed to ensure that RBVs burst sequentially. (C) Time-lapse images showing autonomous and sequential drainage of reservoirs in the CC. Arrows represent sequence and flow direction. Text labels show time during liquid delivery. A video of the autonomous liquid delivery operation is provided in supplementary movie S3.1. (D) Flow rates for different branches of the capillary circuit.  $N = 3$  devices from different 3D-printed molds. Error bars represent standard deviation.

liquid delivery is still met; in fact, during reservoir drainage the junction pressure is lower thereby further reducing the chance of bursting other RBVs. Hence the most stringent condition on  $P_J$  is given by the situation described by the electrical circuit with fully filled conduits, which can thus be used to establish the conditions for sequential drainage of each of the side branches.

The required condition for junction pressure to ensure that only one RBV in the CC bursts can be generalized as follows:

$$P_J < P_{i+1} \quad \text{during drainage of branch } i \quad (4.4)$$

where  $P_{i+1}$  is the capillary pressure of the next RBV to burst in the circuit. This condition can be satisfied by balancing the flow resistance in the circuit, and in particular adjusting the main flow resistance ( $R_M$ ) in front of the capillary pump to ensure that  $P_J$  during drainage is lower than the pressure of the subsequent RBVs (see Fig. 4.4a). This calculation is applicable to CCs where the resistance of the channel linking the side branches is negligible compared to  $R_{RV}$ , or else that resistance must also be considered and the appropriate analogous electrical model derived and resolved. The calculation holds for the model CC and can be used to calculate the pressure  $P_J$  during drainage of branch  $i$  and ensure that it is smaller than the retention pressure  $P_{i+1}$  of branch  $i + 1$  Fig. 4.4b.

The geometries of the RBVs in the CC are summarized in Table 4.1. We designed our proof-of-principle device to obtain uniform capillary pressure differences of  $80 \pm 5$  Pa between successive valves. All RBVs were 2.6 mm long. We designed a 4.2 mm long, 290  $\mu\text{m}$  wide, and 100  $\mu\text{m}$  deep main resistor so that the junction pressure during each liquid delivery step satisfied our condition for sequential liquid delivery (see Fig. 4.4b).

Contact angle hysteresis must be taken into account when designing the capillary pump to ensure that the capillary pressure threshold for all RBVs can be overcome. Since the filling of the capillary pump is dictated by the advancing contact

TABLE 4.1: **Geometry of retention burst valves (RBVs) for autonomous delivery of four liquids.** Junction pressures during drainage of RBVs were calculated using Equation 4.3.

	RBV1	RBV2	RBV3	RBV4
<b>Width (<math>\mu\text{m}</math>)</b>	960	670	480	380
<b>Height (<math>\mu\text{m}</math>)</b>	1000	750	650	550
<b>Calculated RBV Pressure <math>P_i</math> (Pa)</b>	-194	-271	-358	-441
<b>Calculated <math>P_j</math> during drainage (Pa)</b>	-238	-309	-390	-443

angles on the microchannel walls while the bursting of the RBVs is dictated by the receding contact angles on the microchannel walls, the dimensions of the capillary pump must be significantly smaller than the smallest dimension of RBVs to ensure drainage.[13] Thus, the capillary pump in our proof-of-principle 4-valve circuit was using microchannels that were  $200 \times 100 \mu\text{m}^2$ , providing a wicking capillary pressure of  $-736 \text{ Pa}$  that is large enough to drain each RBV in the circuit.

To experimentally validate our design, we 3D-printed the CC mold with our calculated dimensions for the main resistor and made PDMS replicas as described earlier (see Fig.4.3). Then we tested liquid delivery using aqueous food dye solutions. As expected, each side branch drained sequentially without drainage of the other RBVs (Fig. 4.4c). Pre-programmed drainage of the side branches was completed within 4 min. The sequence of RBV drainage was 100% successful over four repeated tests with devices made from four different 3D-printed molds. As shown in Fig. 4.4d, the flow rates for liquid drainage from branches 1, 2, 3, and 4 were  $0.21 \pm 0.02$ ,  $0.21 \pm 0.01$ ,  $0.20 \pm 0.01$ , and  $0.10 \pm 0.01 \mu\text{L}/\text{s}$  respectively. Next we tested whether reproducibility of flow rate could be further improved by using three replicates from a single mold, but the variability remained comparable, suggesting that user manipulations and other parameters, but not the 3D-printer imprecision, are the main source of variability.

### Capillarie circuit for autonomous delivery of eight liquids

After establishing general guidelines for designing RBVs to obtain sequential liquid delivery, we designed a CC with eight liquid delivery steps, double the number in

our proof-of-principle CC and exceeding the number of sequentially-encoded, self-regulated microfluidic drainage events in our previous work with cleanroom-fabricated CCs.[13]

As described earlier, the smallest microchannel width that we could print without a high incidence of defects was 200  $\mu\text{m}$ . We designed the capillary pump region of the CC to be 300  $\mu\text{m}$  wide and 50  $\mu\text{m}$  deep to ensure reliable printing since the capillary pump has a larger pressure than all the RBVs in the circuit. To encode capillary pressure differences, we systematically varied the heights and widths of microchannels in each side branch (see Table 4.2). We designed RBVs according to the junction pressure criterion (see equation 4.4) to ensure that valves were drained sequentially.

Although in theory, very small differences in capillary pressure between successive RBVs should ensure serial drainage, empirical tests yield that designed capillary pressure differences of  $\approx 40$  Pa provided reliable sequential drainage of RBVs. This empirical value likely depends on the resolution and accuracy of features produced by the 3D printer and might be reduced with a more accurate printer, or conversely might need to be increased for experiments that require solutions with different surface tensions that will affect the contact angle and the capillary pressure  $P_i$  of the RBV and branch loaded with this solution.

Another parameter that could contribute to the need for a 40 Pa safety margin between theoretical designs and experimental measurements is the presence of surface inhomogeneities due to roughness that could result in local contact angle variations due to local imperfections. Further research is required to assess the impact of local variations in surface roughness on flow in CCs and the reliability of RBVs.

The main resistor was 18.5 mm long, 300  $\mu\text{m}$  wide, and 50  $\mu\text{m}$  deep to obtain a calculated drainage time of  $\approx 10$  min for all 8 liquid delivery steps based on the capillary pressures, resistances, and volumes of the microchannels in the circuit. The smallest RBV in the circuit was 380  $\mu\text{m}$  wide and 200  $\mu\text{m}$  deep. Since this valve was much shallower than the reservoir (960  $\mu\text{m}$  wide and 1000  $\mu\text{m}$  deep), connecting it directly to the reservoir would result in the formation of an unwanted stop valve. To prevent liquid

TABLE 4.2: RBVs designed for autonomous delivery of eight liquids.

	RBV1	RBV2	RBV3	RBV4	RBV5	RBV6	RBV7	RBV8
Width ( $\mu\text{m}$ )	770	670	580	480	380	380	380	380
Height ( $\mu\text{m}$ )	900	750	650	600	600	400	300	200
RBV Pressure $P_i$ (Pa)	-233	-270	-314	-365	-430	-483	-536	-642
$P_J$ during drainage (Pa)	-250	-286	-329	-379	-442	-493	-544	-643

from stopping at the abrupt geometric change between the RBV and the reservoir, we designed a gently sloped transition (or staircase) with 50  $\mu\text{m}$  height increments to prevent from liquid stopping due to the formation of an undesired stop valve. We set the maximum channel height in our CCs to 1mm to stay within a regime where capillary forces are dominant. These geometric constraints limited the number of RBVs, and by extension the number of liquid delivery steps that we could automate in our CCs.

We experimentally validated the operation of the 8-step circuit by 3D-printing a mold and making PDMS replicas as described previously. Fig. 4.5 shows time-lapse images of autonomous and sequential delivery of 8 liquids in the CC. Liquids were initially pre-loaded into the reagent reservoirs, and then the central release channel was filled with 10  $\mu\text{L}$  of liquid to start the autonomous drainage operations. Following drainage of the solution from inlet 8 and pinning of the air-liquid interface at RBV8 in the trigger channel, RBV1 is the first to start bursting at  $t = 3 \text{ min } 11 \text{ s}$ . Each RBV with its attendant reservoir take  $\approx 50 \text{ s}$  to drain and the autonomous drainage of the 8 solutions was completed in  $< 7 \text{ min}$ .

### Comparison between 3D-printed and cleanroom-fabricated capillarie circuits

Cleanroom fabrication allows microchannel height and width specifications down to 1  $\mu\text{m}$  and less, whereas with the 3D printer used here the resolution was limited  $\approx 200 \mu\text{m}$  in XY and 50  $\mu\text{m}$  in Z. Consequently, can more finely vary the capillary pressures of microfabricated CCs, which in theory could allow sequential drainage of more channels. However, sequential drainage is constrained by the whole circuit architecture to ensure that the condition for sequential drainage of all the retention burst valves in the capillary circuit is still met (Equations 4.2 and 4.4 and Fig. 4.4A).

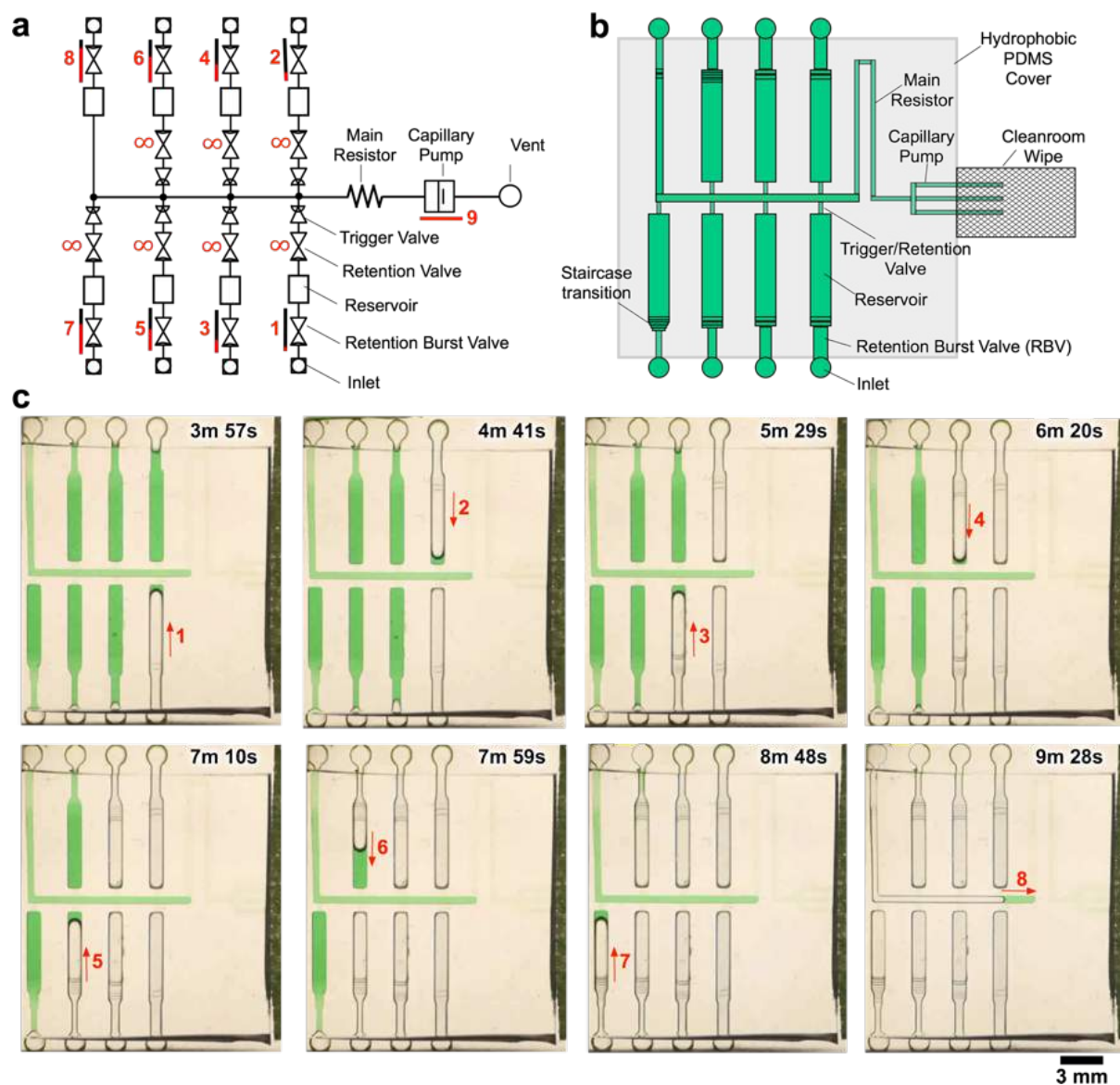


FIGURE 4.5: **CC for autonomous delivery of eight liquids.** (A) Symbolic representation of CC showing modular assembly of fluidic elements. (B) Schematic representation of CC. (C) Time-lapse images showing autonomous delivery of 8 liquids in the CC. Arrows indicate flow direction and numbers highlight the time and sequence of liquid delivery. A video of liquid delivery is provided in supplementary movie S3.2.

A strength of 3D printing is the capability to print multi-height features in a single run, whereas when using classical photolithography each different depth level would require a photolithographic and processing step with precise alignment which would make fabrication excessively slow, costly and at the same time reduce the yield. For example, the CC for the autonomous delivery of eight liquids used seven different depths on the same mold (see Fig. 4.5).

Capillary forces are dominant over gravitational and inertial forces at the scale of the conduits used for the CCs shown here. However, the 3D-printed conduits extend over several tens of millimetres in some cases, and if a chip is not horizontal, or in the most extreme case if it is positioned such that the channel is vertical, then the hydrostatic pressure could disrupt the functionality of the CC and notably the pre-programmed drainage order. For the 8-valve CC the difference between two sequential retention burst valves is 40 Pa, which corresponds to the pressure of a water column height of 4 mm. The footprint of the 8-valve CC is much larger, and by placing it on one of the sides at a 90 °tilt, the sequence of drainage was disrupted, as predicted. Hence, for the reliable operation of CCs with large conduits and incremental differences in capillary pressure it is important to consider the position of the CC, and ideally to position the devices horizontally.

## 4.5 Conclusions

Taken together, our results indicate that 3D-printing allows rapid and inexpensive fabrication of reliable capillarie valves and circuits.

We established design rules for CCs, TVs, and RBVs (see Table 4.3). The empirically-derived TV design rule provides an important proof-of-principle demonstration. Future work is required to provide analytical design rules based on calculated pressure barriers of TVs and including other relevant parameters that affect TV performance, such as: TV height, contact angle, surface roughness, and 3D-printed layer height.

TABLE 4.3: **Design rules for capillary circuits made from 3D-printed molds.** Summary of empirical and analytical design rules for CCs with TVs and RBVs. The design rules presented here are specific to CCs printed using the EnvisionTEC MicroEDU 3D-printer. Empirically-derived design rules were obtained by systematic variation of geometric parameters and may depend more strongly on the choice of 3D-printer. Analytically-derived design rules were obtained by calculating capillary pressures of fluidic elements in the CC and should be more generalizable between 3D-printers.

<p><b>Maximal conduit size to stay within capillary microfluidic regime:</b></p> <p>Channel width: <math>w \leq 1</math> mm Channel height: <math>h \leq 1</math> mm</p>	<p><b>Minimal feature size imposed by EnvisionTEC MicroEDU 3D-printer:</b></p> <p>Channel width: <math>w &gt; 200</math> <math>\mu\text{m}</math> Channel height: <math>h \geq 50</math> <math>\mu\text{m}</math> Max. Device footprint: <math>75 \times 100</math> <math>\text{mm}^2</math> Min. step between two widths: <math>\Delta w = 100</math> <math>\mu\text{m}</math> Min. step between two heights: <math>\Delta h = 50</math> <math>\mu\text{m}</math></p>
<p><b>Empirically-derived design rules:</b></p> <ol style="list-style-type: none"> <li>1. Height difference between TV and release channel: <math>\Delta h \geq 300</math> <math>\mu\text{m}</math></li> <li>2. Difference in capillary pressure between successive RBVs: <math>\Delta P &gt; 40</math> Pa</li> </ol>	<p><b>Analytically-derived design rules:</b></p> <ol style="list-style-type: none"> <li>1. Condition for sequential delivery of liquids in CC with side branches with high-resistance retention valves connected to a main channel with pressure <math>P_j</math>: <math> P_j  &lt;  P_{i+1} </math> during drainage of branch <math>i</math></li> </ol>

In addition, the analytically-derived RBV design rule was based on electrical analogies and clearly explains the required conditions for sequential bursting of RBVs. The empirically-determined RBV design rule depends on the variability of feature sizes produced by the 3D-printer, which could result in unexpected capillary pressure differences between RBVs. For us, a safety margin of 40 Pa between consecutive RBVs, in addition to the analytical RBV design rule based on junction pressures, ensured sequential liquid delivery.

These design rules are specific to our 3D-printer and the PDMS replicas with a hydrophobic top surface (advancing and receding contact angles of  $114^\circ$  and  $89^\circ$ , respectively) and hydrophilic bottom and side surfaces (advancing and receding contact angles  $45^\circ$  and  $31^\circ$ , respectively). However, the design rules should be generalizable to other 3D-printers provided that the 3D-printed features have similar resolution, surface roughness, and surface chemistry.

The resolution reliably achievable with the consumer grade 3D printer used here

was limited to  $\approx 200 \mu\text{m}$ . The design of a CC must consider multiple, sometimes competing, conditions for achieving the desired number of sequential events, flow rates, and time of delivery. With further improvements and better 3D-printers and resolution, higher capillary pressures could be generated, and more RBVs and liquid delivery steps could be included in the CC, thus increasing the possibilities of CCs.

The skill and resources needed to make CCs from 3D-printed molds lies between paper microfluidics and cleanroom-fabricated capillary microfluidics. In the future, it would be desirable to replace PDMS – which gradually reverts back to its inherent hydrophobic form after plasma treatment[36] – with alternate polymers with more stable hydrophilic surfaces,[37] either by directly 3D printing them, or by replication into stable polymers.

3D-printed molds may be used as intermediate step to manufacture silicone molds for injection molding.[38, 39] As 3D-printing of metals[40, 41] improves, one could envision direct 3D-printing of metal molds for durable high-volume injection molding. The design of CCs is also compatible with conventional mold machining in metal that would allow injection molding into polymers like Cyclic Olefin Copolymer (COC) that are inexpensive to mass produce and can be chemically treated to obtain stable hydrophilic surfaces.[42]

With the widespread adoption of 3D-printers, CCs could be readily printed by many researchers, and the design rules presented here will facilitate the fabrication of functional circuits. 3D-printing of CCs is especially appealing as a way to rapidly iterate through multiple designs and test new functions. 3D-printed autonomous CCs may be developed for large-volume and multi-step biochemical assays to be used for point-of-care diagnosis, for research in a lab, as well as for educational purposes.

## 4.6 Acknowledgements

We acknowledge NSERC and CIHR for funding. A.O. acknowledges financial support from the NSERC CREATE Integrated Sensor Systems Training Program, the CIHR

---

Systems Biology Training Program, and an FRQNT PBEEE Scholarship. D.J. acknowledges a Canada Research Chair. We acknowledge support from the McGill Nanotools Microfab. We thank Nicolas Brodich and Professor Raynald Gauvin in the Department of Materials Engineering at McGill University for Scanning Electron Microscopy support. A.O. also acknowledges helpful discussions with Arya Tavakoli, Donald MacNearney, Jeffrey Munzar, and Philippe DeCorwin-Martin at McGill University, Steven Jim at the University of California, Irvine, and writing feedback from members of his McGill Graphos Peer Writing Group.

# Bibliography

- [1] P. Man, C. H. Mastrangelo, M. A. Burns, and D. T. Burke, "Microfabricated capillarity-driven stop valve and sample injector," in *Proceedings of the the IEEE MEMS Conference*, Jan. 1998, pp. 45–50.
- [2] D. Juncker, H. Schmid, U. Drechsler, H. Wolf, M. Wolf, B. Michel, N. de Rooij, and E. Delamarche, "Autonomous Microfluidic Capillary System," *Anal. Chem.*, vol. 74, no. 24, pp. 6139–6144, Dec. 2002.
- [3] J. Melin, N. Roxhed, G. Gimenez, P. Griss, W. van der Wijngaart, and G. Stemme, "A liquid-triggered liquid microvalve for on-chip flow control," *Sensors & Actuators: B. Chemical*, vol. 100, no. 3, pp. 463–468, Jan. 2004.
- [4] R. Safavieh, A. Tamayol, and D. Juncker, "Serpentine and leading-edge capillary pumps for microfluidic capillary systems," *Microfluid Nanofluid*, vol. 18, no. 3, pp. 357–366, Jul. 2014.
- [5] M. Zimmermann, H. Schmid, P. Hunziker, and E. Delamarche, "Capillary pumps for autonomous capillary systems," *Lab Chip*, vol. 7, no. 1, pp. 119–125, 2007.
- [6] L. Gervais, M. Hitzbleck, and E. Delamarche, "Capillary-driven multiparametric microfluidic chips for one-step immunoassays." *Biosensors and Bioelectronics*, vol. 27, no. 1, pp. 64–70, Sep. 2011.
- [7] L. Gervais and E. Delamarche, "Toward one-step point-of-care immunodiagnostics using capillary-driven microfluidics and PDMS substrates." *Lab Chip*, vol. 9, no. 23, pp. 3330–3337, Dec. 2009.

- 
- [8] M. Zimmermann, P. Hunziker, and E. Delamarche, "Autonomous capillary system for one-step immunoassays." *Biomed Microdevices*, vol. 11, no. 1, pp. 1–8, Feb. 2009.
- [9] E. Fu, S. A. Ramsey, P. Kauffman, B. Lutz, and P. Yager, "Transport in two-dimensional paper networks," *Microfluid Nanofluid*, vol. 10, no. 1, pp. 29–35, Jun. 2010.
- [10] X. Li, D. R. Ballerini, and W. Shen, "A perspective on paper-based microfluidics: Current status and future trends," *Biomicrofluidics*, vol. 6, no. 1, p. 011301, Mar. 2012.
- [11] P. Novo, F. Volpetti, V. Chu, and J. P. Conde, "Control of sequential fluid delivery in a fully autonomous capillary microfluidic device." *Lab Chip*, vol. 13, no. 4, pp. 641–645, Feb. 2013.
- [12] S.-J. Kim, S. Paczesny, S. Takayama, and K. Kurabayashi, "Preprogrammed capillarity to passively control system-level sequential and parallel microfluidic flows." *Lab Chip*, vol. 13, no. 11, pp. 2091–2098, Jun. 2013.
- [13] R. Safavieh and D. Juncker, "Capillarics: Pre-programmed, self-powered microfluidic circuits built from capillary elements," *Lab Chip*, vol. 13, no. 21, pp. 4180–4189, Nov. 2013.
- [14] J. Berthier, D. Gosselin, and E. Berthier, "A generalization of the Lucas–Washburn–Rideal law to composite microchannels of arbitrary cross section," *Microfluid. Nanofluid.*, vol. 19, no. 3, pp. 497–507, May 2015.
- [15] M. I. Mohammed and M. P. Y. Desmulliez, "The manufacturing of packaged capillary action microfluidic systems by means of CO<sub>2</sub> laser processing," *Microsyst Technol*, pp. 1–10, Mar. 2013.
- [16] A. Kazemzadeh, P. Ganesan, F. Ibrahim, S. He, and M. J. Madou, "The Effect of Contact Angles and Capillary Dimensions on the Burst Frequency of Super

- Hydrophilic and Hydrophilic Centrifugal Microfluidic Platforms, a CFD Study,” *PLoS ONE*, vol. 8, no. 9, p. e73002, 2013.
- [17] K. Ellinas, A. Tserepi, and E. Gogolides, “Superhydrophobic, passive microvalves with controllable opening threshold: exploiting plasma nanotextured microfluidics for a programmable flow switchboard,” *Microfluid Nanofluid*, vol. 17, pp. 489–498, Jan. 2014.
- [18] K. Kistrup, C. E. Poulsen, P. F. Østergaard, K. B. Haugshøj, R. Taboryski, A. Wolff, and M. F. Hansen, “Fabrication and modelling of injection moulded all-polymer capillary microvalves for passive microfluidic control,” *J. Micromech. Microeng.*, vol. 24, no. 12, p. 125007, Nov. 2014.
- [19] J. L. Moore, A. McCuiston, I. Mittendorf, R. Ottway, and R. D. Johnson, “Behavior of capillary valves in centrifugal microfluidic devices prepared by three-dimensional printing,” *Microfluid Nanofluid*, vol. 10, no. 4, pp. 877–888, Nov. 2010.
- [20] M. I. Mohammed, E. Abraham, and M. P. Y. Desmulliez, “Rapid laser prototyping of valves for microfluidic autonomous systems,” *J. Micromech. Microeng.*, vol. 23, no. 3, p. 035034, Mar. 2013.
- [21] A. K. Au, W. Huynh, L. F. Horowitz, and A. Folch, “3D-Printed Microfluidics.” *Angew. Chem. Int. Ed.*, vol. 55, no. 12, pp. 3862–3881, Mar. 2016.
- [22] B. C. Gross, J. L. Erkal, S. Y. Lockwood, C. Chen, and D. M. Spence, “Evaluation of 3D Printing and Its Potential Impact on Biotechnology and the Chemical Sciences,” *Anal. Chem.*, vol. 86, no. 7, pp. 3240–3253, Apr. 2014.
- [23] A. I. Shallan, P. Smejkal, M. Corban, R. M. Guijt, and M. C. Breadmore, “Cost-Effective Three-Dimensional Printing of Visibly Transparent Microchips within Minutes,” *Anal. Chem.*, vol. 86, no. 6, pp. 3124–3130, Mar. 2014.

- [24] A. K. Au, W. Lee, and A. Folch, "Mail-order microfluidics: evaluation of stereolithography for the production of microfluidic devices." *Lab Chip*, vol. 14, no. 7, pp. 1294–1301, Apr. 2014.
- [25] D. J. Guckenberger, T. E. de Groot, A. M. D. Wan, D. J. Beebe, and E. W. K. Young, "Micromilling: a method for ultra-rapid prototyping of plastic microfluidic devices," *Lab Chip*, vol. 15, no. 11, pp. 2364–2378, 2015.
- [26] R. K. Lade, E. J. Hippchen, C. W. Macosko, and L. F. Francis, "Dynamics of Capillary-Driven Flow in 3D Printed Open Microchannels." *Langmuir*, vol. 33, no. 12, pp. 2949–2964, Mar. 2017.
- [27] D. Qin, Y. Xia, and G. M. Whitesides, "Soft lithography for micro- and nanoscale patterning." *Nature Protocols*, vol. 5, no. 3, pp. 491–502, Mar. 2010.
- [28] M. Pla-Roca and D. Juncker, "PDMS Microfluidic Capillary Systems for Patterning Proteins on Surfaces and Performing Miniaturized Immunoassays," in *Methods in Molecular Biology*, A. Khademhosseini, K.-Y. Suh, and M. Zourob, Eds. Totowa, NJ: Humana Press, Sep. 2010, pp. 177–194.
- [29] H. Bruus, *Theoretical microfluidics*, ser. Oxford Masters Series in Physics. OUP Oxford, Mar. 2008.
- [30] M. Zimmermann, P. Hunziker, and E. Delamarche, "Valves for autonomous capillary systems," *Microfluid Nanofluid*, vol. 5, no. 3, pp. 395–402, Sep. 2008.
- [31] A. Glière and C. Delattre, "Modeling and fabrication of capillary stop valves for planar microfluidic systems," *Sensors & Actuators: A. Physical*, vol. 130-131, pp. 601–608, Aug. 2006.
- [32] S. Cesaro-Tadic, G. Dernick, D. Juncker, G. Buurman, H. Kropshofer, B. Michel, C. Fattinger, and E. Delamarche, "High-sensitivity miniaturized immunoassays for tumor necrosis factor  $\alpha$  using microfluidic systems," *Lab Chip*, vol. 4, no. 6, p. 563, 2004.

- [33] S. Bergeron, V. Laforte, P.-S. Lo, H. Li, and D. Juncker, "Evaluating mixtures of 14 hygroscopic additives to improve antibody microarray performance," *Anal Bioanal Chem*, vol. 407, no. 28, pp. 8451–8462, Sep. 2015.
- [34] A. K. Au, W. Huynh, L. F. Horowitz, and A. Folch, "3D-Printed Microfluidics." *Angew. Chem. Int. Ed.*, vol. 55, no. 12, pp. 3862–3881, Mar. 2016.
- [35] M. Wolf, D. Juncker, B. Michel, P. Hunziker, and E. Delamarche, "Simultaneous detection of C-reactive protein and other cardiac markers in human plasma using micromosaic immunoassays and self-regulating microfluidic networks." *Biosensors and Bioelectronics*, vol. 19, no. 10, pp. 1193–1202, May 2004.
- [36] D. Bodas and C. Khan-Malek, "Hydrophilization and hydrophobic recovery of PDMS by oxygen plasma and chemical treatment—An SEM investigation," *Sensors & Actuators: B. Chemical*, vol. 123, no. 1, pp. 368–373, Apr. 2007.
- [37] C. F. Carlborg, T. Haraldsson, K. Öberg, M. Malkoch, and W. van der Wijngaart, "Beyond PDMS: off-stoichiometry thiol-ene (OSTE) based soft lithography for rapid prototyping of microfluidic devices." *Lab Chip*, vol. 11, no. 18, pp. 3136–3147, Sep. 2011.
- [38] T. Mueller, "Stereolithography-based prototyping: case histories of applications in product development," in *IEEE Technical Applications Conference and Workshops. Northcon/95. Conference Record.* IEEE, 1995, pp. 305–310.
- [39] P. Chung, J. A. Heller, M. Etemadi, P. E. Ottoson, J. A. Liu, L. Rand, and S. Roy, "Rapid and Low-cost Prototyping of Medical Devices Using 3D Printed Molds for Liquid Injection Molding," *JoVE*, no. 88, p. e51745, 2014.
- [40] C. Ladd, J. H. So, J. Muth, and M. D. Dickey, "3D printing of free standing liquid metal microstructures," *Adv. Mater.*, vol. 25, no. 36, pp. 5081–5085, 2013.

- 
- [41] D. P. Parekh, C. Ladd, L. Panich, K. Moussa, and M. D. Dickey, "3D printing of liquid metals as fugitive inks for fabrication of 3D microfluidic channels," *Lab Chip*, vol. 16, no. 10, pp. 1812–1820, 2016.
- [42] C. Jönsson, M. Aronsson, G. Rundström, C. Pettersson, I. Mendel-Hartvig, J. Bakker, E. Martinsson, B. Liedberg, B. MacCraith, O. Öhman, and J. Melin, "Silane–dextran chemistry on lateral flow polymer chips for immunoassays," *Lab Chip*, vol. 8, no. 7, p. 1191, 2008.

## Chapter 5

# Capillarie Circuit for Rapid and Facile Bacteria Detection

### 5.1 Preface

In this chapter, we apply CCs to a clinically-relevant application that benefits from the capability to 3D-print large-volume ( $> 100 \mu\text{L}$ ) devices. Urinary tract infections (UTI) are one of the most common bacterial infections and would greatly benefit from a rapid point-of-care diagnostic test. Although significant progress has been made in developing microfluidic systems for nucleic acid and whole bacteria immunoassay tests, their practical application is limited by complex protocols, bulky peripherals, and slow operation. Here we present a microfluidic capillarie circuit (CC) optimized for rapid and automated detection of bacteria in synthetic urine. Molds for CCs were constructed using previously-established design rules, then 3D-printed and replicated into poly(dimethylsiloxane). CCs autonomously and sequentially performed all liquid delivery steps required for the assay. For efficient bacteria capture, on-the-spot packing of antibody-functionalized microbeads was completed in  $< 20$  s followed by autonomous sequential delivery of  $100 \mu\text{L}$  of bacteria sample, biotinylated detection antibodies, fluorescent streptavidin conjugate, and wash buffer for a total volume  $\approx 115 \mu\text{L}$ . The assay was completed in  $< 7$  min. Fluorescence images of the microbead column revealed captured bacteria as bright spots that were easily counted manually

or using an automated script for user-independent assay readout. The limit of detection of *E. coli* in synthetic urine was  $7.1 \times 10^3$  colony-forming-units per mL (CFU/mL), which is well below the clinical diagnostic criterion ( $> 10^5$  CFU/mL) for UTI. The self-powered, peripheral-free CC presented here has potential for use in rapid point-of-care UTI screening.

This chapter is based on: “**Microfluidic Capillary Circuit for Rapid and Facile Bacteria Detection**”, A.O. Olanrewaju, A. Ng, P. Decorwin-Martin, A. Robillard, and D. Juncker, *Analytical Chemistry*, 2017.

## 5.2 Introduction

Up to 50 % of women will get a urinary tract infection (UTI) by age 32.[1] UTI is caused by the presence of bacteria in urine, with over 80 % of cases caused by *E. coli*.[2] The gold standard for detecting bacteria in urine is plate culture and the traditional clinical diagnostic threshold is  $\geq 10^5$  colony-forming units per mL (CFU/mL).[2, 3] However, plate culture is slow (24 - 72 hours to provide results), labour intensive, and centralized. Although dipstick tests are sometimes used in doctors’ offices for rapid UTI detection, they are indirect tests that detect nitrites and leukocytes - symptoms that might be indicative of infection, rather than the bacterial pathogens themselves - thus, dipsticks have low specificity and sensitivity.[4] Another approach for bacteria diagnosis in clinical microbiology labs is real-time PCR from urine samples.[5] But conventional PCR requires extensive sample preparation to purify nucleic acids and bulky equipment for nucleic acid amplification.

Microfluidic devices offer the promise of rapid, miniaturized, and automated biochemical assays.[6, 7] The use of microfluidic devices for detection of bacteria in urine has been recently reviewed.[8, 9] Many microfluidic devices for bacteria detection aim

to miniaturize and automate nucleic-acid detection methods. For example, paper-based devices for integrated nucleic acid extraction, isothermal amplification, and visual detection were developed.[10, 11] Yet nucleic-acid based detection methods require sample preparation steps including cell lysis and nucleic acid purification. These steps slow down the bacteria detection assay and increase test complexity, challenging integration and automation at the point of care. Recently, DNA-based bacteria detection was accelerated by skipping the sample preparation and DNA amplification processes. Lam et al. developed a test with on-chip electrical bacterial lysis followed by electrochemical detection in  $< 30$  min.[12] Nevertheless, for rapid screening at a doctor's office or patient's home, it is desirable to further reduce both the test time and complexity.

Immunoassays that target whole bacterial cells using affinity binders such as antibodies enable bacteria detection without cell lysis.[13] Sandwich immunoassays, commonly used for specific protein detection, can be adapted to whole bacteria detection and even implemented in a multiplexed microarray format.[14, 15] The availability of multiple bacterial extracellular receptors allows sensitive and specific capture of whole cells in immunoassays. However, the typical planar configuration of microfluidic immunoassays requires bacterial cells to diffuse to the sensing surface, which is slow given the relatively large size and low diffusivity of bacterial cells.[16] Consequently, to reduce assay time immunoaffinity columns consisting of packed microbeads functionalized with antibodies are used to provide large and distributed areas for bacterial capture.[17, 18, 19, 20, 21] The reported limit of detection in immunoaffinity columns for bacteria capture is as low as  $10^4$  CFU/mL,[18] thus meeting the diagnostic requirement for UTI.

However, bacteria capture with packed beads typically uses peripheral equipment such as syringe pumps for bead packing and subsequent sample and reagent delivery. To enable point-of-care immunoaffinity columns for rapid bacteria capture, there is a need for minimally-instrumented and user-friendly liquid handling in microfluidic devices. Autonomous capillary microfluidic systems are an attractive platform

for minimally-instrumented and self-powered immunoassays.[22] Our lab developed capillary circuits (CCs) for pre-programmed and self-powered delivery of multiple liquids.[23]. More recently, we presented analytical and empirical design rules for CCs manufactured by rapid prototyping of molds with a bench-top 3D-printer.[24] Here we optimize and apply CCs for rapid and facile detection of bacteria that requires only 4 pipetting steps and performs 5 functional steps. Pre-assembled microbead columns are not compatible with capillary flow as they can lead to bubble entrapment. Thus, we introduce on-the-spot assembly of microbead columns in CCs, followed by autonomous, and sequential delivery of bacteria sample and sandwich immunoassay reagents in < 7 min. Captured bacteria are detected using biotinylated antibodies and fluorescent streptavidin conjugates with fluorescence results that are easily interpreted by the user or an automated image analysis algorithm.

### 5.3 Design and working principle of capillary circuit

Our goal was to develop a self-powered microfluidic device for rapid and simple detection of bacteria. To accomplish this, we integrated a microbead column within the CC to increase the surface area available for bacteria detection while simultaneously ensuring contact of bacteria to the surface, thereby improving detection sensitivity.

Based on our previous work,[24] a CC with a constriction to assemble a microbead column and 4 sequential retention burst valves (RBVs) was designed to capture and detect bacteria. The design of the modular CC was optimized and guided using a combination of symbolic (Fig. 5.1A) and schematic layouts (Fig. 5.1B).

Operation of the CC for bacteria detection is illustrated in Fig. 5.1C. An assay is prepared by first pre-loading the sample and the two assay reagents to their respective inlets thereby filling the reservoirs. Pre-loading sample and reagent reservoirs is a preparatory step that can be completed up to 30 min before the start of the assay and in any order since liquids are held in place by capillary trigger valves (Fig. 5.1C0).[24]

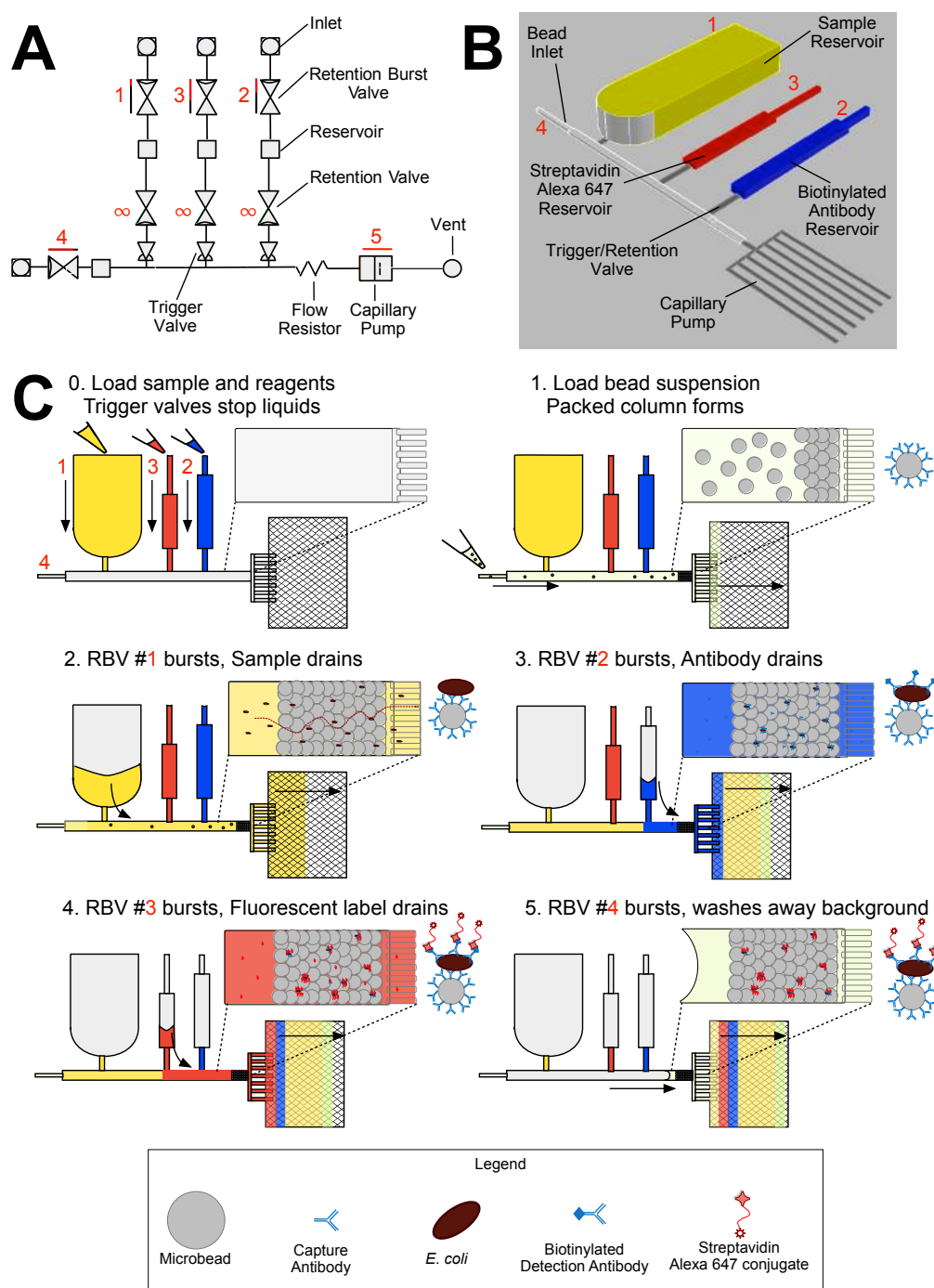


FIGURE 5.1: **Design and working principle of CC for bacteria detection.** A) Symbolic layout showing modular design with individual capillary fluidic elements.[23, 24] B) 3D schematic of CC showing the relative physical dimensions of various fluidic elements. C) The assay is completed in 4 pipetting steps (C0) and 5 autonomous liquid delivery steps (C1-C5). Insets show close-ups of the packed bead column and individual assay steps on the bead surface (not to scale).

The pre-programmed assay is then initiated by the fourth pipetting step, which is loading the buffer containing beads. This triggers the automated five steps required for the bacteria capture assay in the CC without need for further user intervention. First, microbeads are assembled on-the-spot in the microchannel at a physical barrier (Fig. 5.1C1) immediately followed by bacteria sample which is flowed through the microbead column resulting in the capture of whole bacterial cells by antibodies on the microbead surface (Fig. 5.1C2). Next, biotinylated detection antibodies are flowed through the microbead column and bind to captured bacteria (Fig. 5.1C3), followed by fluorescent streptavidin Alexa 647 conjugate which binds to biotinylated detection antibodies (Fig. 5.1C4). Finally, wash buffer, which is comprised of the residual buffer from step #1, is flowed through the microbead column to remove unbound streptavidin (Fig. 5.1C5).

### 5.3.1 Design of microbead column

The microbead column is a crucial component that influences the detection limit of this bacteria capture assay. There are several factors that affect bacteria capture in a microbead column including: bacteria size, microbead size, sample volume, and sample flow rate. In the absence of accurate mathematical models that describe the influence of all these parameters, we empirically designed the microbead column for bacteria capture, in line with past work.[17, 18, 19, 20, 21]

Trapping microbeads with a physical constriction that is smaller than the microbead diameter is a simple and reliable way to pack beads in a microchannel.[17, 18, 19, 20] The minimum feature size of the 3D-printer used to make the mold was a 50  $\mu\text{m}$  vertical step,[24] which sets a lower limit on the size of microbeads that can be used. Although the “keystone effect” can be used to pack beads with a constriction that is larger than the microbead diameter,[25] it is sensitive to surface roughness (greater in 3D-printed channels than microfabricated ones) and requires a high temperature (115

°C) stabilization step to securely trap beads at the constriction. Thus, beads with a diameter  $\geq 50 \mu\text{m}$  were used to ensure predictable and reliable bead packing at a  $50 \mu\text{m}$  deep channel forming the constriction.

## 5.4 Experimental

Device molds were 3D-printed (Fig 5.2A) and replicated into PDMS (Fig 5.2B) as described in our past work.[24] Subsequently, the CC was evaluated in three steps: (i) verify pre-programmed liquid delivery operations using aqueous food dye solutions, (ii) validate basic assay operation and specificity by comparing capture of *E. coli* O157:H7 and K12 serving as positive and negative control, respectively, and (iii) determine limit of detection using serial dilution experiments with *E. coli* O157:H7 spiked into synthetic urine.

### 5.4.1 Verifying pre-programmed liquid delivery

To test liquid delivery, the PDMS CCs were plasma-treated for hydrophilicity and sealed with flat hydrophobic PDMS covers prior to use. Aqueous food dye solutions were loaded in the reservoirs, and the pre-programmed liquid delivery verified.[24] To characterize the reproducibility of bead packing and liquid delivery, five PDMS replicas from five different 3D-printed molds were tested with aqueous food dye solutions. Microbead column lengths and drainage times for each reservoir were recorded.

### 5.4.2 Validating assay operation and specificity

*E. coli* O157:H7 ATCC strain 700728 (ATCC, USA) was used as the model organism in our bacteria capture experiments. Synthetic urine (Surine™ Negative Control, DynaTek, USA) with constituents that mimic human urine was used in on-chip experiments. Pre-activated Ultralink™ bis-acrylamide azlactone copolymer beads (ThermoFisher Scientific, USA) were used for bacteria capture. Beads were functionalized with 10  $\mu\text{g}/\text{mL}$  of anti-*E. coli* O157:H7 antibodies (BacTrace™ 01-95-90-MG, KPL, USA) following the microbead manufacturer's specifications. Biotinylated anti-*E. coli* O157:H7 antibodies (BacTrace™ 16-95-90, KPL, USA), and Streptavidin-Alexa Fluor™ 647 conjugate (S21374, ThermoFisher Scientific, USA) were used to label and detect bacteria during the sandwich immunoassay. Reagents were diluted in 1 $\times$  Phosphate Buffered Saline (1 $\times$  PBS, ThermoFisher Scientific, USA).

To validate the general principle of the assay and determine its specificity, 10<sup>6</sup> CFU/mL each of *E. coli* K12 and *E. coli* O157:H7 was run through a CC containing beads and reagents that target *E. coli* O157:H7. A laboratory strain of *E. coli* K12, which lacks the O157 antigen, was generously provided by the Tufenkji lab at McGill University. Spots were counted manually.

### 5.4.3 Serial dilution experiments

We carried out the bacteria capture assay using synthetic urine spiked with *E. coli* O157:H7. *E. coli* O157:H7 samples were grown overnight in LB medium at 37 °C. Subsequently, serial dilutions of bacteria suspension were prepared in synthetic urine. Samples with bacterial concentrations of 0, 10<sup>3</sup>, 10<sup>4</sup>, 10<sup>5</sup>, 10<sup>6</sup>, and 10<sup>7</sup> CFU/mL were prepared. Bacteria serial dilutions were plated on LB agar culture plates at room temperature for 24 hours to count and confirm the number of bacteria present in each sample. Subsequently, bacteria suspensions were used for on-chip experiments to characterize bacteria capture in CCs. To determine the sensitivity of the assay, a binding curve was established by plotting the number of spots observed in the microbead

column with the known bacterial count from plate culture.

### **Bacteria counts and calculation of limit of detection**

After completion of the assay in the CC, the microbead column was imaged at 20× magnification using an inverted fluorescence microscope (TE-2000-E Inverted Microscope, Nikon, USA) equipped with a CCD camera (QuantEM 512SC, Photometrics, USA). Manual counts of the number of bacteria in each bead column were carried out by 5 volunteers blinded to the true test results. One labeled image with 5 spots ( $10^4$  image in Fig. 5.4A) was presented as a training image to the volunteers who were instructed to identify similar spots in all other images. All images, including the negative controls, were presented in a random order. At higher concentrations (i.e.  $10^5$ ,  $10^6$ ,  $10^7$  CFU/mL), the number of spots was estimated by counting the number of spots in a quarter of the bead column and multiplying by 4. This is similar to the colony counting technique employed in standard microbiology. Spot counts from the 5 volunteers were averaged for each image. Subsequently, average spots counts were obtained for each bacteria concentration using images from 3 different CCs.

All experiments were performed in triplicate unless otherwise stated. Log transforms of the concentration and spot count data from manual bacteria counts were fitted with a non-linear four-parameter logistic curve using GraphPad Prism 7 (GraphPad Software Inc., La Jolla, CA, USA). The limit of detection (LoD) was calculated using the EP17 guideline published by the Clinical and Laboratory Standards Institute (CLSI) that considers both the measured limit of blank (LoB) and variation from replicates of a sample known to contain a small concentration of analyte.[26] The LoD was calculated as follows:

$$\text{LoD} = \text{LoB} + 1.645 \cdot (\text{SD}_{\text{low concentration sample}}) \quad (5.1)$$

where the limit of blank (LoB) is given by:

$$\text{LoB} = \text{mean}_{\text{blank}} + 1.645 \cdot (\text{SD}_{\text{blank}}) \quad (5.2)$$

and  $\text{SD}_{\text{low concentration sample}}$  is the measured standard deviation of the low concentration sample,  $\text{SD}_{\text{blank}}$  is the measured standard deviation of the blank (zero) sample, and  $\text{mean}_{\text{blank}}$  is the measured average signal of the blank sample.

Assuming a Gaussian distribution of the low concentration samples, the LoD calculation presented in equation 5.1 ensures only 5% of low concentration samples will produce signal outputs lower than the previously defined LoB (equation 5.2) and incorrectly appear to be negative signals i.e. contain no analyte.

To determine the concentration corresponding to the calculated LoD, we interpolated the log transform of the calculated LOD value with the four-parameter logistic curve fit.

### Algorithm for automated bacteria counts

To provide automated bacteria counts, a MATLAB™ script was written to analyze assay images. The image analysis algorithm is provided in the electronic supplementary information. First, images were manually cropped to remove the edges of the bead column since they create artifacts in subsequent image processing steps. Next, a Gaussian filter was applied to normalize images. At 20x magnification, 1 pixel in each fluorescence micrograph corresponded to  $2 \mu\text{m}$  in size. Given that *E. coli* are expected to be  $\approx 2 \mu\text{m} \times 1 \mu\text{m}$ , we expected bacteria to appear as  $\approx 4$ -pixel diameter “spots” in the fluorescence micrographs. Consequently, spots were identified using an opening top-hat filter with a disk radius of 2 pixels and a Laplacian of Gaussian filter to match the expected size of detected bacteria in the bead column. Both the top-hat and the Laplacian of a Gaussian filters identify bright point-like features in which the 2-pixel radius disk can fit. An H-max transform was used to remove low regional peaks. A

TABLE 5.1: **Geometry of retention burst valves (RBVs) in CC for detection of bacteria.** RBV heights and widths were designed to ensure sequential delivery of sample and assay reagents according to previously established design rules.[24]

	Width ( $\mu m$ )	Height ( $\mu m$ )	Capillary Pressure (Pa)
RBV1	4000	2000	-93
RBV2	300	500	-667
RBV3	300	300	-834
RBV4	200	250	-1126
Capillary Pump	200	50	-2602

threshold was then applied based on the average signal of the image to form a black and white image.

In less than 20 % of the captured images, larger spots ( $\approx 20 - 50$  pixels in diameter) that appeared to come from dust or debris were splintered during the image thresholding step and counted as bacteria by the automated script. To avoid these spurious counts, an opening and closing by reconstruction operation was performed with a larger disk with a 5-pixel radius. By thresholding the resulting image, these large areas with bright fluorescence were ignored.

## 5.5 Results and discussion

A CC for rapid and facile bacteria detection was designed and tested. The cross-section and capillary pressure of each RBV required for pre-programmed liquid delivery in the CC is summarized in Table 5.1. Device molds were 3D-printed (Fig 5.2A) and replicated into PDMS (Fig 5.2B).[24] The sample reservoir (inlet 1) was designed to have a volume of  $100 \mu L$  while retaining a compact footprint ( $2 \times 4 \times 13 \text{ mm}^3$ ) as seen in Fig 5.2B. Meanwhile, the biotinylated antibody reservoir (inlet 2) and streptavidin conjugate reservoir (inlet 3) had volumes of  $4.7 \mu L$  and  $2.4 \mu L$  respectively. These volumes were empirically found to provide a good signal-to-noise ratio for bacterial imaging. The central branch (inlet 4) had a volume of  $1.4 \mu L$  and was used to introduce the microbead suspension to the circuit.

### 5.5.1 Pre-programmed liquid delivery in capillary circuit

We verified sequential liquid delivery using aqueous food dye solutions as shown in Fig. 5.2C. 100  $\mu\text{L}$  of liquid was added to the sample reservoir, 4.7  $\mu\text{L}$  was added to the biotinylated antibody reservoir, and 2.4  $\mu\text{L}$  was added to the Streptavidin-Alexa 647 reservoir (Fig. 5.2C,  $t = 1\text{m } 31\text{s}$ ). Trigger valves held the sample and reagents in place for at least 30 min allowing sufficient time to pre-load the chip and conveniently start the assay without worrying about the timing of the reagent loading steps.[23, 24]

In the CC design, flow of the sample and assay reagents is triggered by adding the microbead solution to inlet 4. This initiates on-the-spot packing of microbeads in front of the capillary pump as the first step in the on-chip immunoassay. We added 7  $\mu\text{L}$  containing a 1 % w/v bead suspension in 1xPBS to inlet 4 (Fig 5.2C,  $t = 3\text{m } 00\text{s}$ ). Adding the bead suspension to inlet 4 filled the central branch and connected all reservoirs in the CC to the capillary pump. At this point, the capillary pump and RBVs determined the sequence of liquid delivery without user intervention. The sample reservoir drained first since it had the lowest capillary pressure (Fig 5.2C,  $t = 8\text{m } 03\text{s}$ ). It is noteworthy that the position of the RBVs relative to the capillary pump does not determine their drainage sequence; instead it is the capillary pressure of the microchannel (set by its geometry and surface chemistry) that controls the drainage sequence. Next, RBV2 burst and the biotinylated antibody reservoir drained (Fig. 5.2C,  $t = 8\text{m } 35\text{s}$ ), then RBV3 and the streptavidin Alexa 647 conjugate reservoir (Fig. 5.2C,  $t = 8\text{m } 51\text{s}$ ) and finally, RBV4 and the central branch (Fig. 5.2C,  $t = 9\text{m } 00\text{s}$ ). Laminar flow in the CC ensures that the remaining sample and wash buffer in the central channel effectively washed away the streptavidin Alexa 647 conjugate solution from the bead column thereby reducing background fluorescence. The total liquid delivery time since microbead addition was 6m 00s.

The packed microbead column may be imaged in real-time during the assay or afterwards when the microchannels are dry. The microbeads were readily visible with a brightfield microscope and captured bacteria were readily visible with a fluorescence

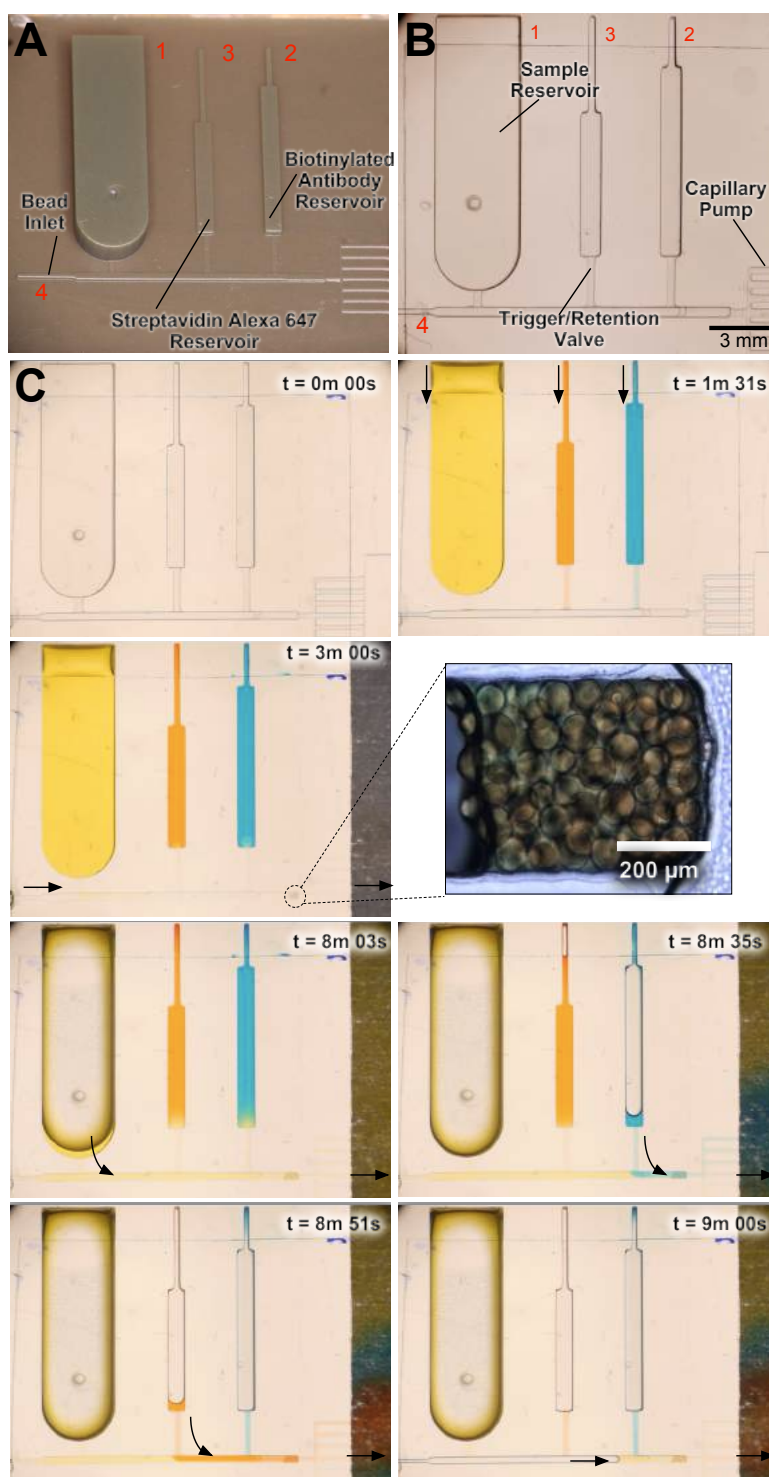


FIGURE 5.2: **Fabrication and testing of CC for bacteria detection.** A) 3D-printed mold of the CC. B) Final CC replicated into PDMS. C) Time-lapse images of pre-programmed liquid delivery in CC. Arrows indicate flow direction.

microscope.

### Reproducibility of bead packing and liquid delivery

To determine the reproducibility of liquid delivery in the circuit, we tested five PDMS replicas from five different 3D-printed molds. This represents the worst case scenario in reproducibility of liquid delivery since replicas can be made from a single mold to minimize mold-to-mold variability that arises during manufacturing. We recorded bead column lengths and liquid delivery times after pre-programmed drainage was initiated by adding the bead suspension to inlet 4. Over five experiments, the average bead column length was  $888 \pm 144 \mu\text{m}$ . Meanwhile the average flow rates for the sample, biotinylated antibody, streptavidin Alexa 647 conjugate, and wash buffer were  $0.36 \pm 0.07$ ,  $0.23 \pm 0.06$ ,  $0.21 \pm 0.04$  and  $0.18 \pm 0.05 \mu\text{L}/\text{s}$  respectively. The average assay time over all five experiments was  $5.5 \pm 1.0$  min. The coefficient of variation in liquid delivery times (18.7%) is consistent with observations in our previous work with 3D-printed CCs and is thought to arise primarily from variations in surface chemistry and handling of PDMS devices.[24]

### 5.5.2 Validating assay principle and specificity

As a proof of principle test of assay sensitivity and specificity,  $10^6$  CFU/mL each of the target *E. coli* O157:H7 and non-pathogenic *E. coli* K12 were run through bacterial capture assays in CCs with microbeads functionalized with anti-*E. coli* O157:H7 capture antibodies and detection antibodies that also target *E. coli* O157:H7. When the sample was *E. coli* O157:H7, multiple spots ( $238.1 \pm 62.5$ ,  $N = 3$ ) were observed in the microbead column (Fig. 5.3). This test was a positive control showing that the overall principle of the sandwich immunoassay with spot counting was viable. In contrast, when the sample was  $10^6$  CFU/mL of *E. coli* K12, very few spots ( $5.7 \pm 7.2$ ,  $N = 3$ ) were observed in the microbead column, demonstrating specificity of the sandwich immunoassay.

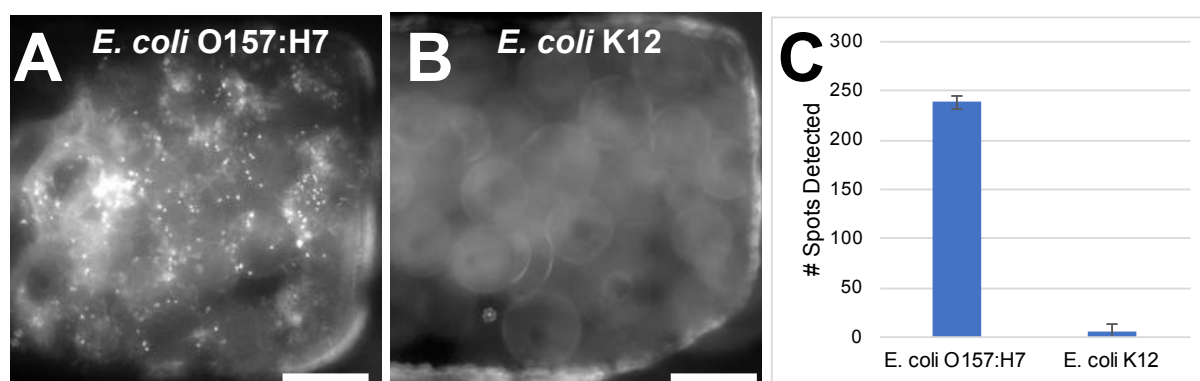


FIGURE 5.3: Validating assay principle and specificity by comparing bacteria capture after flowing  $10^6$  CFU/mL of *E. coli* O157:H7 and K12 through CCs designed for *E. coli* O157:H7 capture. A) Multiple spots in bead column after flowing *E. coli* O157:H7. B) Few spots in bead column after flowing *E. coli* K12. C) Bar graph quantifying specific capture of *E. coli* O157:H7. Bacteria spot counts were obtained by manual counting. Error bars indicate standard deviation.  $N = 3$ .

### 5.5.3 Limit of detection of *E. coli* in synthetic urine

As described in section 5.4.3, the limit of detection (LoD) was calculated using equation 5.1 according to guidelines from the Clinical and Laboratory Standards Institute to ensure that only 5% of low concentration samples will produce signal outputs that incorrectly appear to be negative signals.[26] To determine the limit of detection of the bacteria capture assay, the following concentrations of *E. coli* O157:H7 were spiked into synthetic urine and tested in the CC: 0,  $10^3$ ,  $10^4$ ,  $10^5$ ,  $10^6$ , and  $10^7$  CFU/mL. Fig. 5.4A shows raw data obtained from on-chip experiments. Captured bacteria were clearly visible as fluorescent spots that could be counted by the user. These “spots” were defined as bright fluorescence regions that are  $\approx 2 \mu\text{m}$  in diameter when viewed with a  $20\times$  objective, since the target *E. coli* are  $\approx 2 \times 1 \mu\text{m}^2$  in size. Such spots are easy to count in microscope images since they stood out from the background greyscale signal, as illustrated with arrows in Fig. 5.4A. Residual fluorescence of antibodies on the beads was visible as halos that were readily distinguished from bacterial spots. The results shown in Fig. 5.4A suggest that we could readily distinguish between low and high bacteria concentrations.

The number of spots detected at each bacteria concentration was plotted against the bacteria concentration determined by plate culture (the gold standard). Each bacterial

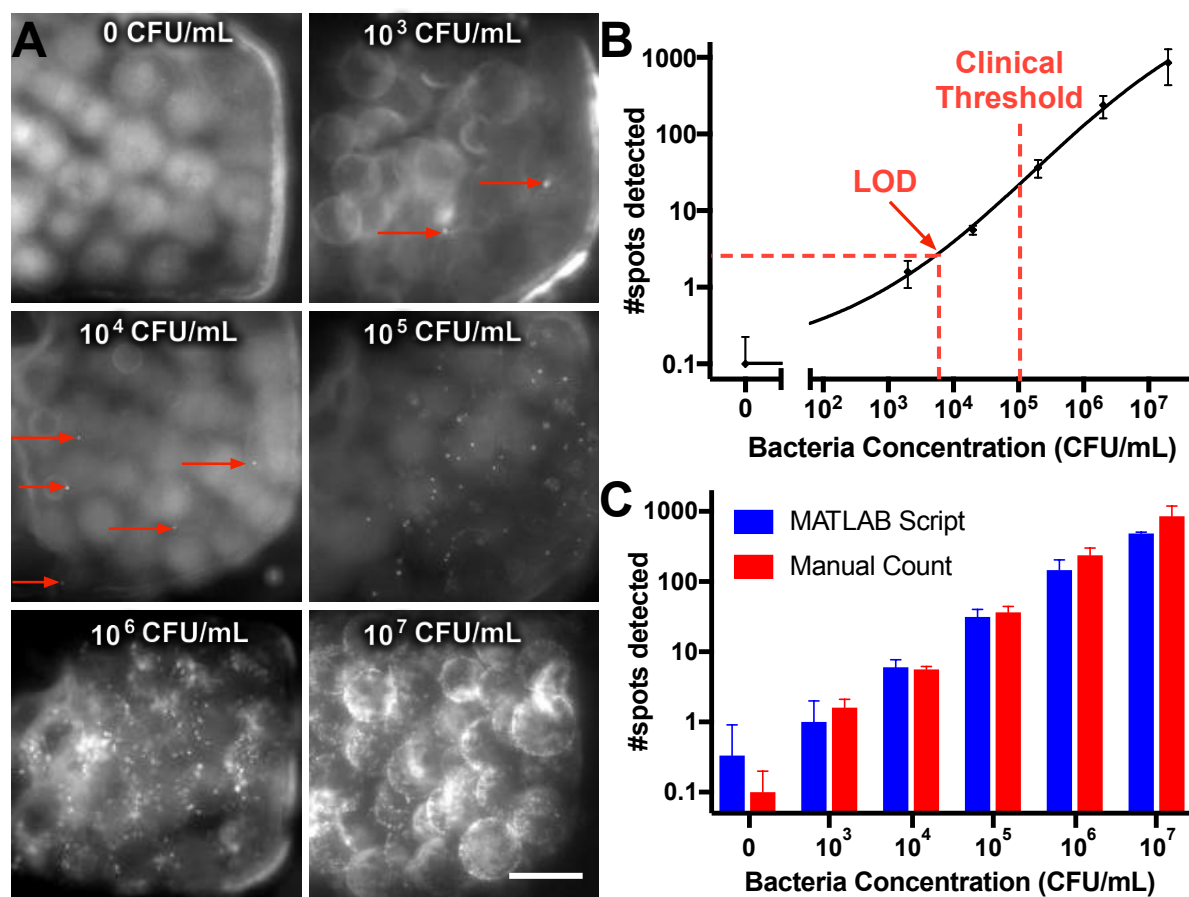


FIGURE 5.4: Results of bacteria capture assay in CC, standard curve for calculating limit of detection, and validation of automated script for bacteria counts. A) Fluorescence micrographs showing captured bacteria in the microbead column of the CC. Scale bar is  $100 \mu\text{m}$ . B) Log-log standard curve showing bacteria concentration versus # spots detected. The Limit of Detection (LoD) was  $7.1 \times 10^3$  CFU/mL. N = 3. Error bars indicate 95% Confidence Intervals. C) The MATLAB™ script provided similar results to manual counts performed by 5 individuals blinded to the true test results. Error bars indicate standard deviation. N = 3.

sample was tested on 3 separate CCs. Spots were counted by 5 volunteers blinded to the true test results. Average spot counts were 0.1, 1.6, 5.6, 36.5, 238.1, and 854.9 spots at 0,  $10^3$ ,  $10^4$ ,  $10^5$ ,  $10^6$ , and  $10^7$  CFU per mL respectively. The number of observed spots increased as the number of CFU in the bacteria sample increased; however, this increase was in a non-linear manner over the entire range of concentrations tested. The data was fitted with a non-linear four-parameter logistic curve with the sigmoidal shape characteristic of antibody-based immunoassays. The curve fit had good agreement with the data ( $R^2 = 0.9975$ ) and could enable quantification of results within the assay's linear range ( $\approx 10^4$  to  $10^6$  CFU/mL).

Given that 0.1 mL of sample is screened at each concentration, we observed that  $< 2\%$  of the available bacteria was captured by the CC. Strategies for improving the bacteria capture efficiency are described in section 5.5.3 where we discuss the trade off between sensitivity and time-to-result. Nevertheless, we observed a steady increase in the number of spots detected as the bacteria concentration increased (Fig. 5.4B). The LoD, calculated using equation 5.1, was  $7.1 \times 10^3$  CFU/mL which is well below the traditional clinical diagnostic threshold for bacteria in urine ( $10^5$  CFU/mL).

### Algorithm for automated bacteria counts

As described above, the number of bacteria captured in the CC can be readily counted by users with minimal training. To further facilitate ease of use at the point-of-care and to enable independent, quantitative, traceable, and comparable analysis, it is desirable to automate bacteria spot counting. As such, we developed a spot detection script using MATLAB.

To verify the bacteria counts by the automated algorithm, we compared the number of spots counted by the MATLAB algorithm with manual counts (Fig 5.4C). Good agreement was observed between the manual and automated bacteria counts with a few exceptions. The MATLAB script reported a higher average spot count for negative controls. Using the MATLAB script, individual spot counts of 0, 0, 1 were obtained the three images captured at 0 CFU/mL. Meanwhile, of the 5 individuals who performed

blinded manual spot counts, all users reported no spots in the 0 CFU/mL images, except for one user who reported 1 spot in only 1 of the 3 negative control images. As a result, the average spot counts at 0 CFU/mL for the MATLAB algorithm and the manual counts were  $0.33 \pm 0.58$  and  $0.1 \pm 0.1$  respectively. Also, at higher concentration ( $> 10^6$  CFU/mL), there was a large ( $\approx 50\%$ ) difference between the manual and automated counts. This is because the background intensity levels of images differed significantly between the low and high concentration images, making it difficult to find a single thresholding algorithm that performs well over the five orders of magnitude of bacteria concentration tested in our experiments. This discrepancy at very high concentrations is not a major concern as primarily a yes/no answer for bacteruria is sought with  $> 10^5$  CFU/mL as cut-off. If quantitative measures are required at high concentrations, it should be possible to use other metrics such as the average image intensity. These results establish that automated analysis could be used for assay read-out.

### **Trade-off between sensitivity and time-to-result**

Although the CC for bacteria detection meets the traditional diagnostic requirement for bacteriuria ( $10^5$  CFU/mL), recent reviews suggest that LODs as low as  $10^2$  CFU/mL may be required for some symptomatic patients with UTI, which is close to the LOD of our test.[2] The LOD of the CC may be further improved by 3D-printing CCs with finer features and using smaller microbeads to improve bacteria capture efficiency. As microbead diameter decreases, the bacteria capture efficiency increases[17, 27] since the gap size between beads decreases and bacteria cells are more likely to contact the functionalized sensing surface. In this work, bead diameter was limited to sizes  $\geq 50 \mu m$  - imposed by the resolution of the 3D-printer used. 3D-printers with minimum Z-feature sizes down to  $10 \mu m$  have recently become available at a cost of  $\approx$ US\$10,000, which is affordable for many research labs, and would allow trapping of much smaller beads.[28, 29] However, given a constant capillary pressure, the flow resistance in the CC increases rapidly with smaller bead size and the time required to flow  $100 \mu L$  of

sample through the CC would increase significantly. Increasing residence time of the bacteria in the bead chamber might also improve the capture efficiency of the assay; however, at the cost of longer assay time. The current CC design allowed processing of a large sample volume (i.e.  $100 \mu\text{L}$ ) in a short time with a capture efficiency of  $\approx 1$  in 100 bacteria. Applications that require bacteria detection at much lower concentrations could be addressed by using smaller beads, however at the expense of much longer flow times. Hence, for each application optimization will be needed to identify the desired trade-off between capturing of sufficient bacterial particles while permitting sample processing within a given time.

Although patients with UTI typically produce spontaneous urine volumes of 20 - 200 mL which is significantly less than the volume produced by healthy individuals (100 - 550 mL),<sup>[30]</sup> we do not anticipate any problems related to small urine sample volumes. This is because the CC requires only a small aliquot (0.1 mL) of the patient sample to achieve clinically-relevant sensitivity. In fact, we could increase the volume of urine sample screened to further improve the limit of detection of the assay. The sample volume screened could easily be doubled or tripled while keeping the same design and completing tests in  $< 30$  min fitting within the typical duration of a doctor's office visit. Flow resistances in the CC could also be redesigned to process a larger sample volume while still providing results within the 7-min time frame shown here.

### 3D-printing and mass production

3D-printing was used for rapid and simple prototyping despite the size limitations imposed by the 3D printer (i.e.  $\geq 200 \mu\text{m}$  lateral features and  $\geq 50 \mu\text{m}$  vertical features). Also, 3D-printing provided the capability to easily fabricate millimeter-scale ( $2 \times 4 \times 13 \text{ mm}^3$ ) reservoirs to hold large ( $100 \mu\text{L}$ ) sample volumes within the same device that contains micrometer-scale ( $200 \times 50 \mu\text{m}^2$ ) channels for capillary pumping. To implement mass production, the final mold design may be replicated into metal, or directly manufactured by conventional means such as Computer Numerical Control (CNC) micromachining, followed by injection molding to produce many functional

replicas. Alternatively, 3D-printing may be used as an initial step to generate silicone rubber molds for injection molding.[31, 32] In future, advances in 3D-printing technology, such as 3D-printing of metals,[33, 34] may provide sufficient resolution and smoothness for direct printing of metal molds for durable injection molding.

### **Ease of use of the CC**

Our aim was to develop a test that meets key criteria for use at the point-of-care, and we envision that the CC could be used by a medical practitioner (doctor, nurse, or technician) who would add liquids to on-chip reservoirs to start the test. Precise pipetting may not be required to operate the device and a disposable plastic liquid dropper could be used to fill reservoirs. Since trigger valves hold liquids in place, the chip could be designed to tolerate overfilling and excess liquids, which in the current design was simply wiped away from the inlets using a piece of paper, but which could be removed by overflow structures integrated into the CC.

Since the CC enables rapid and user-friendly processing of samples, a user can set up multiple experiments in parallel. A series of CCs can be loaded with reagents over a period of 30 min, without worrying about precise timing of pipetting steps or removing liquids from the chip. All chips could then be triggered sequentially by adding different samples, and the result simply read out as soon as 7 min after the first chip was loaded, within 30 min or so to minimize the risk of post-experiment drying artefacts.

One can envision further improvements to make operation of the CC even simpler. For example, it may be possible to reduce the number of pipetting steps using a simpler design where antibodies and microbeads are spotted and dried on the CC, and only require rehydration with a buffer. This would allow development of a CC that only requires two steps - addition of wash buffer and addition of sample.

To facilitate inexpensive visual readout at the point-of-care, low-cost and portable fluorescence microscopes[35, 36] or cell phones with optical adaptors[37] may be used

for quantitative, yet minimally instrumented detection. Similarly, chemical signal amplification may be used to provide colorimetric results that are visible to the naked eye.[38, 39]

Compared to DNA-based tests and other non-nucleic acid bacteria detection tests, the primary advantage of our approach is the simplicity and speed while still achieving clinically-relevant sensitivity. Most microfluidic-based approaches require external pumps and valves to automate each liquid handling step, making miniaturization and point-of-care use more challenging. In contrast, the CC automates sequential liquid delivery processes with minimal external equipment and without user intervention other than to start the assay.

## 5.6 Conclusion

In this paper, we demonstrate rapid and facile detection of bacteria in synthetic urine in  $< 7$  min using a self-powered and autonomous microfluidic CC with a LOD of  $7.1 \times 10^3$  CFU/mL which is well below the traditional clinical threshold for UTI detection ( $\geq 10^5$  CFU/mL). The CC features on-the-spot packing of functionalized microbeads in  $< 20$  s which proved to be compatible with subsequent capillary-driven flow of sample and reagents. The CC is user-friendly as it only requires 4 pipetting steps to initiate the self-powered assay procedure, and achieves clinically-relevant results in a fraction of the time that it takes with competing technologies and without requiring bulky peripherals. The speed, simplicity, and sensitivity of the CC meets key requirements for use as a triage tool for screening patients suspected of having UTI. Rapid tests could allow physicians to prescribe antibiotics only after confirmation of bacterial infection, thereby helping to reduce over-prescription and minimize the emergence of antibiotic-resistant pathogens. Although *E. coli* causes 80 - 85 % of UTI cases, other bacteria including *Klebsiella pneumoniae* and *Staphylococcus saprophyticus* also regularly cause UTI.[2] By combining different affinity binders, CCs may be adapted to detect multiple pathogenic bacteria causing UTI. The CC will need to be

validated using clinical urine samples to study the impact of matrix effects, patient-to-patient variation in urine properties, and the diversity of bacterial strains that cause UTI. Furthermore, the concept of CCs with packed microbeads should be suitable for other bacterial assays as well as for other analytes such as viruses or proteins.

## **Acknowledgements**

We thank NSERC and CIHR for funding. A.O. is grateful for funding from the NSERC CREATE Integrated Sensor Systems Training Program, the CIHR Systems Biology Training Program, and the Quebec Merit Scholarship for Foreign Students (PBEEE). D.J. acknowledges a Canada Research Chair. We are grateful for helpful discussions with Dr. Brian Ward, Dr. Nathalie Tufenkji, Arya Tavakoli, Sa Xiao, and Veronique Laforte at McGill University. We thank Edward Zhang, Eun Hae Oh, Maiwenn Beau-grand, Mcolisi Dlamini, Mohamed Yafia, and Rosalie Martel for their help with data analysis. A.O thanks his McGill Graphos Peer Writing Group.

# Bibliography

- [1] T. M. Hooton, "Uncomplicated Urinary Tract Infection," *N Engl J Med*, vol. 366, no. 11, pp. 1028–1037, 2012.
- [2] B. Foxman, "The epidemiology of urinary tract infection." *Nature Reviews Urology*, vol. 7, no. 12, pp. 653–660, Dec. 2010.
- [3] J. W. Warren, E. Abrutyn, J. R. Hebel, J. R. Johnson, A. J. Schaeffer, and W. E. Stamm, "Guidelines for Antimicrobial Treatment of Uncomplicated Acute Bacterial Cystitis and Acute Pyelonephritis in Women," *Clinical Infectious Diseases*, vol. 29, no. 4, pp. 745–758, Oct. 1999.
- [4] G. Schmiemann, E. Kniehl, K. Gebhardt, M. M. Matejczyk, and E. Hummers-Pradier, "The diagnosis of urinary tract infection: a systematic review." *Dtsch Arztebl Int*, vol. 107, no. 21, pp. 361–367, May 2010.
- [5] L. E. Lehmann, S. Hauser, T. Malinka, S. Klaschik, S. U. Weber, J.-C. Schewe, F. Stüber, and M. Book, "Rapid Qualitative Urinary Tract Infection Pathogen Identification by SeptiFast® Real-Time PCR," *PLoS ONE*, vol. 6, no. 2, p. e17146, Feb. 2011.
- [6] G. M. Whitesides, "The origins and the future of microfluidics." *Nature*, vol. 442, no. 7101, pp. 368–373, 2006.
- [7] E. K. Sackmann, A. L. Fulton, and D. J. Beebe, "The present and future role of microfluidics in biomedical research," *Nature*, vol. 507, no. 7491, pp. 181–189, Mar. 2014.

- [8] K. E. Mach, P. K. Wong, and J. C. Liao, "Biosensor diagnosis of urinary tract infections: a path to better treatment?" *Trends in Pharmacological Sciences*, vol. 32, no. 6, pp. 330–336, 2011.
- [9] M. S. Kumar, S. Ghosh, S. Nayak, and A. P. Das, "Recent advances in biosensor based diagnosis of urinary tract infection," *Biosensors and Bioelectronics*, vol. 80, pp. 497–510, Jun. 2016.
- [10] J. R. Choi, J. Hu, R. Tang, Y. Gong, S. Feng, H. Ren, T. Wen, X. Li, W. A. B. Wan Abas, B. Pingguan-Murphy, and F. Xu, "An integrated paper-based sample-to-answer biosensor for nucleic acid testing at the point of care," *Lab Chip*, vol. 16, no. 3, pp. 611–621, 2016.
- [11] L. K. Lafleur, J. D. Bishop, E. K. Heiniger, R. P. Gallagher, M. D. Wheeler, P. Kauffman, X. Zhang, E. C. Kline, J. R. Buser, S. Kumar, S. A. Byrnes, N. M. J. Vermeulen, N. K. Scarr, Y. Belousov, W. Mahoney, B. J. Toley, P. D. Ladd, B. R. Lutz, and P. Yager, "A rapid, instrument-free, sample-to-result nucleic acid amplification test," *Lab Chip*, vol. 16, no. 19, pp. 3777–3787, 2016.
- [12] B. Lam, Z. Fang, E. H. Sargent, and S. O. Kelley, "Polymerase Chain Reaction-Free, Sample-to-Answer Bacterial Detection in 30 Minutes with Integrated Cell Lysis," *Anal. Chem.*, vol. 84, no. 1, pp. 21–25, Jan. 2012.
- [13] J. H. Shin and J.-K. Park, "Functional Packaging of Lateral Flow Strip Allows Simple Delivery of Multiple Reagents for Multistep Assays," *Anal. Chem.*, vol. 88, no. 21, pp. 10 374–10 378, Nov. 2016.
- [14] A. G. Gehring, D. M. Albin, A. K. Bhunia, S. A. Reed, S.-I. TU, and J. Uknalis, "Antibody Microarray Detection of *Escherichia coli* O157:H7: Quantification, Assay Limitations, and Capture Efficiency," *Anal. Chem.*, vol. 78, no. 18, pp. 6601–6607, Sep. 2006.

- [15] A. Wolter, R. Niessner, and M. Seidel, "Detection of *Escherichia coli* O157:H7, *Salmonella typhimurium*, and *Legionella pneumophila* in water using a flow-through chemiluminescence microarray readout system." *Anal. Chem.*, vol. 80, no. 15, pp. 5854–5863, Aug. 2008.
- [16] T. M. Squires, "Microfluidics : Fluid physics at the nanoliter scale," *Rev. Mod. Phys.*, vol. 77, no. July, pp. 977–1026, 2005.
- [17] J. D. Brewster, "Isolation and concentration of *Salmonellae* with an immunoaffinity column," *Journal of Microbiological Methods*, vol. 55, no. 1, pp. 287–293, Oct. 2003.
- [18] X. Guan, H.-j. Zhang, Y.-n. Bi, L. Zhang, and D.-l. Hao, "Rapid detection of pathogens using antibody-coated microbeads with bioluminescence in microfluidic chips." *Biomed Microdevices*, vol. 12, no. 4, pp. 683–691, Aug. 2010.
- [19] J. H. Yoo, D. H. Woo, M.-S. Chun, and M.-S. Chang, "Microfluidic based biosensing for *Escherichia coli* detection by embedding antimicrobial peptide-labeled beads," *Sensors & Actuators: B. Chemical*, vol. 191, pp. 211–218, Jan. 2014.
- [20] M.-S. Chang, J. H. Yoo, D. H. Woo, and M.-S. Chun, "Efficient detection of *Escherichia coli* O157:H7 using a reusable microfluidic chip embedded with antimicrobial peptide-labeled beads," *Analyst*, vol. 140, no. 23, pp. 7997–8006, 2015.
- [21] P. Molloy, L. Brydon, A. J. Porter, and W. J. Harris, "Separation and concentration of bacteria with immobilized antibody fragments." *J. Appl. Bacteriol.*, vol. 78, no. 4, pp. 359–365, Apr. 1995.
- [22] D. Juncker, H. Schmid, U. Drechsler, H. Wolf, M. Wolf, B. Michel, N. de Rooij, and E. Delamarche, "Autonomous microfluidic capillary system." *Anal. Chem.*, vol. 74, pp. 6139–6144, 2002.

- [23] R. Safavieh and D. Juncker, "Capillarics: pre-programmed, self-powered microfluidic circuits built from capillary elements," *Lab Chip*, vol. 13, no. 21, p. 4180, Oct. 2013.
- [24] A. O. Olanrewaju, A. Robillard, M. Dagher, and D. Juncker, "Autonomous microfluidic capillary circuits replicated from 3D-printed molds," *Lab Chip*, vol. 16, no. 19, pp. 3804–3814, 2016.
- [25] L. Ceriotti, N. F. De Rooij, and E. Verpoorte, "An integrated fritless column for on-chip capillary electrochromatography with conventional stationary phases," *Anal. Chem.*, vol. 74, no. 3, pp. 639–647, 2002.
- [26] D. A. Armbruster and T. Pry, "Limit of blank, limit of detection and limit of quantitation." *The Clinical Biochemist Reviews*, vol. 29 Suppl 1, no. Suppl 1, pp. S49–52, Aug. 2008.
- [27] N. Tufenkji, "Modeling microbial transport in porous media: Traditional approaches and recent developments," *Advances in Water Resources*, vol. 30, no. 6-7, pp. 1455–1469, Jun. 2007.
- [28] A. K. Au, W. Huynh, L. F. Horowitz, and A. Folch, "3D-Printed Microfluidics." *Angewandte Chemie. International edition in English*, vol. 55, no. 12, pp. 3862–3881, 2016.
- [29] S. Waheed, J. M. Cabot, N. P. Macdonald, T. Lewis, R. M. Guijt, B. Paull, and M. C. Breadmore, "3D printed microfluidic devices: enablers and barriers," *Lab Chip*, vol. 16, no. 11, pp. 1993–2013, 2016.
- [30] J. C. I. Truzzi, F. M. R. Almeida, E. C. Nunes, and M. V. Sadi, "Residual Urinary Volume and Urinary Tract Infection—When are They Linked?" *The Journal of Urology*, vol. 180, no. 1, pp. 182–185, Jul. 2008.

- [31] T. Mueller, "Stereolithography-based prototyping: case histories of applications in product development," in *IEEE Technical Applications Conference and Workshops. Northcon/95. Conference Record*. IEEE, 1995, pp. 305–310.
- [32] P. Chung, J. A. Heller, M. Etemadi, P. E. Ottoson, J. A. Liu, L. Rand, and S. Roy, "Rapid and Low-cost Prototyping of Medical Devices Using 3D Printed Molds for Liquid Injection Molding," *JoVE*, no. 88, pp. 517 453 791–517 451 745, 2014.
- [33] C. Ladd, J. H. So, J. Muth, and M. D. Dickey, "3D printing of free standing liquid metal microstructures," *Adv. Mater.*, vol. 25, no. 36, pp. 5081–5085, 2013.
- [34] D. P. Parekh, C. Ladd, L. Panich, K. Moussa, and M. D. Dickey, "3D printing of liquid metals as fugitive inks for fabrication of 3D microfluidic channels," *Lab Chip*, vol. 16, no. 10, pp. 1812–1820, 2016.
- [35] A. R. Miller, G. L. Davis, Z. M. Oden, M. R. Razavi, A. Fateh, M. Ghazanfari, F. Abdolrahimi, S. Poorazar, F. Sakhaie, R. J. Olsen, A. R. Bahrmand, M. C. Pierce, E. A. Graviss, and R. Richards-Kortum, "Portable, Battery-Operated, Low-Cost, Bright Field and Fluorescence Microscope," *PLoS ONE*, vol. 5, no. 8, p. e11890, Aug. 2010.
- [36] M. M. Hasan, M. W. Alam, K. A. Wahid, S. Miah, and K. E. Lukong, "A Low-Cost Digital Microscope with Real-Time Fluorescent Imaging Capability," *PLoS ONE*, vol. 11, no. 12, p. e0167863, Dec. 2016.
- [37] A. Ozcan, "Mobile phones democratize and cultivate next-generation imaging, diagnostics and measurement tools," *Lab Chip*, vol. 14, no. 17, p. 3187, Feb. 2014.
- [38] E. Fu, T. Liang, J. Houghtaling, S. Ramachandran, S. A. Ramsey, B. Lutz, and P. Yager, "Enhanced sensitivity of lateral flow tests using a two-dimensional paper network format." *Anal. Chem.*, vol. 83, no. 20, pp. 7941–7946, Oct. 2011.

- [39] G. Zhou, S. Bergeron, and D. Juncker, "High-performance low-cost antibody microarrays using enzyme-mediated silver amplification," *J. Proteome Res.*, vol. 14, no. 4, pp. 1872–1879, 2015.

## Chapter 6

# Domino Capillarie Circuits: 3D-Printed Capillaries For Scalable, Sequential, And Simultaneous Liquid Delivery

### 6.1 Preface

We previously developed capillarie circuits (CCs) replicated from 3D-printed molds (Chapter 4) and applied them for rapid bacterial detection (Chapter 5). CCs enable preprogrammed sequential liquid delivery operations using retention burst valves (RBVs) that ‘burst’ at predefined capillarie pressures encoded by the height and width of microchannels. However, the number of sequential liquid delivery steps cannot be easily scaled up because of limitations in 3D printer resolution and reproducibility, as well as variability in the surface tensions of different reagents that could lead to wrong sequences. In this chapter, we introduce domino capillarie circuits (DCCs), a new scalable approach to preprogrammed liquid delivery in capillarie microfluidics. DCCs can be scaled up simply by adding another trigger unit, like a line of falling dominos that can be extended simply by adding an extra domino. DCCs use identical air conduits to control the preprogrammed drainage of liquids using a domino effect where reservoirs are opened to air and able to drain only after the preceding reservoir has completely

drained. Proof of principle testing of DCCs enabled 9 preprogrammed liquid delivery operations using only 2 RBV sizes instead of the 9 distinct RBV sizes that would have been required with conventional CC design. To demonstrate the scalability of DCCs, we demonstrated preprogrammed sequential delivery of 17 liquids also using only 2 RBV sizes by adding more identical air conduits and reservoirs. Furthermore, DCCs can also be used to implement simultaneous liquid delivery by triggering two reservoirs at once, akin to one domino hitting two dominos. Simultaneous delivery of two solutions was implemented by extending an air conduit over two reservoirs, and illustrated by synchronously delivering a silver salt and reducing agent to perform a silver enhancement reaction that requires simultaneous drainage. DCCs are robust as they are insensitive to surface tension and may be readily scaled up given the simple modular design. Hence they may find numerous applications in research, clinic, or industry.

This chapter is a manuscript of a research article intended for submission: “**Domino Capillarie Circuits: 3D-Printed Capillaries for Scalable, Sequential, and Simultaneous Liquid Delivery**”, A.O. Olanrewaju, M. Yafia, M. Beaugrand, F. Possel, and D. Juncker.

## 6.2 Introduction

Capillary-driven microfluidics move liquids using only surface tension effects defined by the geometry and surface chemistry of a substrate. Capillary flow control elements such as capillary pumps,[1] stop valves,[2] trigger valves,[3] retention valves,[4] and retention burst valves (RBVs)[5] have been developed. Autonomous capillary systems consisting of various capillary fluidic elements enable self-powered and user-friendly liquid delivery and are well-suited for performing bioassays in point-of-care settings.[4, 6, 7]

### 6.2.1 Capillary microfluidics for preprogrammed multistep liquid delivery

Recently, there has been a push towards developing capillary systems capable of preprogrammed sequential delivery of multiple liquids.[5, 8, 9, 10] Sequential delivery of multiple liquids enables implementation of additional liquid wash steps or signal amplification steps that can improve the sensitivity of an assay.[11, 12] These advanced capillary systems provide sophisticated control over the sequence and timing of liquid delivery with minimal user intervention. For example, *Novo et al.* used air bubbles as spacers between four microchannels connected to the same capillary pump.[8] Preprogrammed sequential drainage was obtained based on the proximity of the microchannels to the capillary pump. However, the use of air bubbles as liquid gaps is sensitive to the handling and loading sequence of the device and the reliability of preprogrammed operations was not characterized.

The same group demonstrated another approach where instead of using air bubbles, air vents were used for preprogrammed control of multi-step liquid delivery.[13] Three open reagent reservoirs were arranged such that the inlet of the first reservoir was the air vent of the second reservoir and the inlet of the second reservoir was the air vent of the third reservoir. All three reservoirs were connected to a central channel that led to a capillary pump. When all inlets were filled the blocked air vents ensure that only reservoir 1 could drain. Only after all the liquid from the inlet of reservoir 1 had drained could the narrow connecting channel between reservoirs 1 and 2 fill with liquid and result in drainage of reservoir 2 into the central channel leading to the capillary pump. This sequence repeats for reservoir 3 thereby achieving sequential drainage of the 3 liquids. This is a subtle and elegant approach to achieving sequential reservoir drainage; however, evaporation from the open reservoirs is a concern.

Another approach to implement preprogrammed liquid delivery in capillary microfluidics is to use dissolvable barriers as delay valves that regulate the sequence of liquid delivery in the microfluidic device.[10] By designing a microfluidic device with

multiple parallel paths connected to the same capillary pump and having different thicknesses of dissolvable delays along each path, one can obtain preprogrammed sequential liquid delivery. Integration of dissolvable barriers requires an additional step in device fabrication and device design must include dead-end channels to divert dissolved thin films away from the leading edge of liquid to prevent saturation and slow flow in the microfluidic device.

### 6.2.2 Capillaric circuits for autonomous liquid delivery

Our research group developed capillaric circuits (CCs) - advanced capillary microfluidic circuits assembled from individual capillary fluidic elements similar to the assembly of electric circuits from electronic components.[5] Sequential delivery of liquids in CCs depends on RBVs which have distinct burst pressures encoded by their geometry. 3D-printing allowed us to vary both the height and width of RBVs to encode a unique “burst” pressure for each valve.

For rapid and inexpensive fabrication, we developed empirical and analytical design rules that enable manufacture of CCs using 3D-printed molds.[14] Using those design rules, we developed a CC for preprogrammed sequential delivery 8 liquids.[14] To our knowledge this was the largest number of preprogrammed sequential liquid delivery steps demonstrated in an autonomous capillary system.

#### Challenges in scaling up capillaric circuits

Nevertheless, the number of sequential liquid delivery steps in CCs could not be easily increased beyond 8 because of limitations in 3D-printer resolution and reproducibility. The minimum lateral (XY) resolution that can be reliably printed using most commercially available stereolithographic 3D-printers is  $\approx 200 \mu\text{m}$ , while the minimum Z-dimension that can reliably printed is  $\approx 50 \mu\text{m}$ . Meanwhile, to stay within a size regime where capillary forces are dominant, microchannel dimensions must remain

< 1 mm. Practically we were only able to implement 8 unique RBV sizes while obtaining reliable performance within the upper and lower size limits imposed by 3D-printer resolution and maintenance of capillary force dominance.[14]

### **Domino capillarie circuits for scalable preprogrammed liquid delivery**

To address the concerns of scaling up the number of liquid delivery steps, we introduce a new paradigm for preprogrammed liquid delivery in capillary systems. Domino capillarie circuits (DCCs) are a new approach to capillary-driven liquid delivery that enable sequential liquid delivery and can be scaled up simply by adding another trigger unit, like a line of falling dominos that can be extended simply by adding an extra domino. DCCs can also be used to implement simultaneous liquid delivery by triggering two reservoirs at once, akin to one domino hitting two dominos.

## **6.3 Materials and Methods**

DCCs consist of two layers: a 3D-printed hydraulic layer and a PDMS pneumatic layer. Molds for microchannels in the pneumatic layer were designed, 3D-printed, and replicated into PDMS as described in our past work.[14] The pneumatic layer was made using a 1:20 base:curing agent ratio mixture of PDMS to obtain soft and flexible devices that adequately sealed the hydraulic layer. PDMS was cured overnight at 60 °C and then peeled from the mold. Pneumatic layers were hydrophobic (untreated PDMS, contact angle 120 °) to prevent filling of the air conduits with liquids. When designing molds for the PDMS pneumatic layer it is important to mirror the orientation of the microchannels so that when the PDMS devices are peeled off from their mold they can be placed directly on top of the hydraulic layer. This is because the devices are vertically mirrored when they are replicated into PDMS. This must be accounted for in the design to ensure proper alignment of the two device layers.

The hydraulic layer was 3D-printed using transparent resin (BV-007 resin, Miicraft) in a Miicraft 100 printer. Devices were designed in AutoCAD®, exported in the STL

file format, and then sliced into 25- $\mu\text{m}$  layers using software provided by the 3D-printer manufacturer. Exposure time for each 25- $\mu\text{m}$  thick 3D-printed layer was 0.9 seconds with 4 buffer layers included at the start of the 3D-print. Printing was completed in 10 min, after which time prints were washed with isopropanol and dried with nitrogen. To prepare 3D-printed hydraulic layers for capillary-driven flow, they were plasma-treated for 60 s at 150 W in a plasma chamber (PE-50, Plasma Etch) for hydrophilicity.

Cleanroom paper was used as a high volume, small footprint capillary pump and placed directly on top of the capillary pump structure within the hydraulic layer. The paper pump was wetted with 20  $\mu\text{L}$  of liquid prior to placing it on top of the plastic device to ensure proper contact. Liquid delivery was tested using aqueous food dye solutions and observed under a microscope.

For silver enhancement reactions to demonstrate simultaneous liquid delivery in DCCs, silver enhancement reagents (LI silver kit with silver salt solution, and reducing agent) were obtained from Nanoprobe Inc (NY, USA). 25 nm gold nanorods functionalized with neutravidin were obtained from Nanopartz (CO, USA). Deionized water was used as a wash buffer to stop the silver enhancement reaction.

## 6.4 Results and Discussion

### 6.4.1 Operating Principle of Domino Capillary Circuits

Instead of relying on geometric differences between microchannels to control sequential liquid delivery, we use identical air conduits to control sequential delivery of liquid in DCCs. Fig. 6.1A provides a symbolic view of a DCC for sequential liquid delivery of 9 liquids. There are 8 branches with liquid reservoirs (branches #1 - #8) and one central branch (branch #0) that connects the other branches to the capillary pump. Only two retention burst valve sizes are required in the design of any DCC. One RBV, the weaker one, is placed at the end of branch #1 and the other stronger RBV is placed at

the end of branch #0. All the other branches in the DCC are terminated with retention valves since they are designed not to drain.

In addition, each of the side branches #1 - #8 has a trigger valve at its intersection with the central branch #0. This allows pre-loading of liquids into the side branches up to 30 min before starting liquid delivery.[5, 14, 15] Branch #0 acts as the release channel that triggers preprogrammed drainage by connecting all the side branches to the capillary pump. Each side branch also has a retention valve just upstream of the trigger valve to ensure that the side branches do not completely empty resulting in the formation of bubbles in the microchannels and disruption of flow in the DCC.[5, 14]

A flow resistor is included in front of the capillary pump which has sufficient capillary pressure to drain both RBV #1 and #2 but not any of the retention valves in the circuit. The capillary pressures of the pump, RBVs, and retention valves were chosen according to design rules for RBVs presented in our previous work.[14]

The crucial design element that enables liquid delivery in DCCs using only 2 RBVs is the use of air conduits to connect liquid reservoirs. As seen in Fig. 6.1A, air conduits connect reservoirs in each of the side branches. When a reservoir is emptied, the air conduit acts as an air vent that allows the next reservoir to drain.

Fig. 6.1B shows the schematic layout of DCCs with physical realizations of individual fluidic components. Here we see clearly that air conduits connect the downstream end of one reservoir to the upstream end of the next reservoir. For example, an air conduit connects the downstream end of reservoir #1 to the upstream end of reservoir #2. That way, when RBV #1 bursts and reservoir #1 empties, the air conduit between reservoirs #1 and #2 acts as an air vent that allows drainage of reservoir #2 despite the presence of the retention valve at the side branch. The air conduit presents an alternate air vent to liquid in reservoir #2 enabling liquid drainage. The other air conduits are positioned accordingly connecting the downstream ends of preceding reservoirs to the upstream ends of succeeding reservoirs thereby enabling sequential drainage of reservoirs.

Fig. 6.1C shows the physical realization of the DCC for delivery of 8 liquids. Food

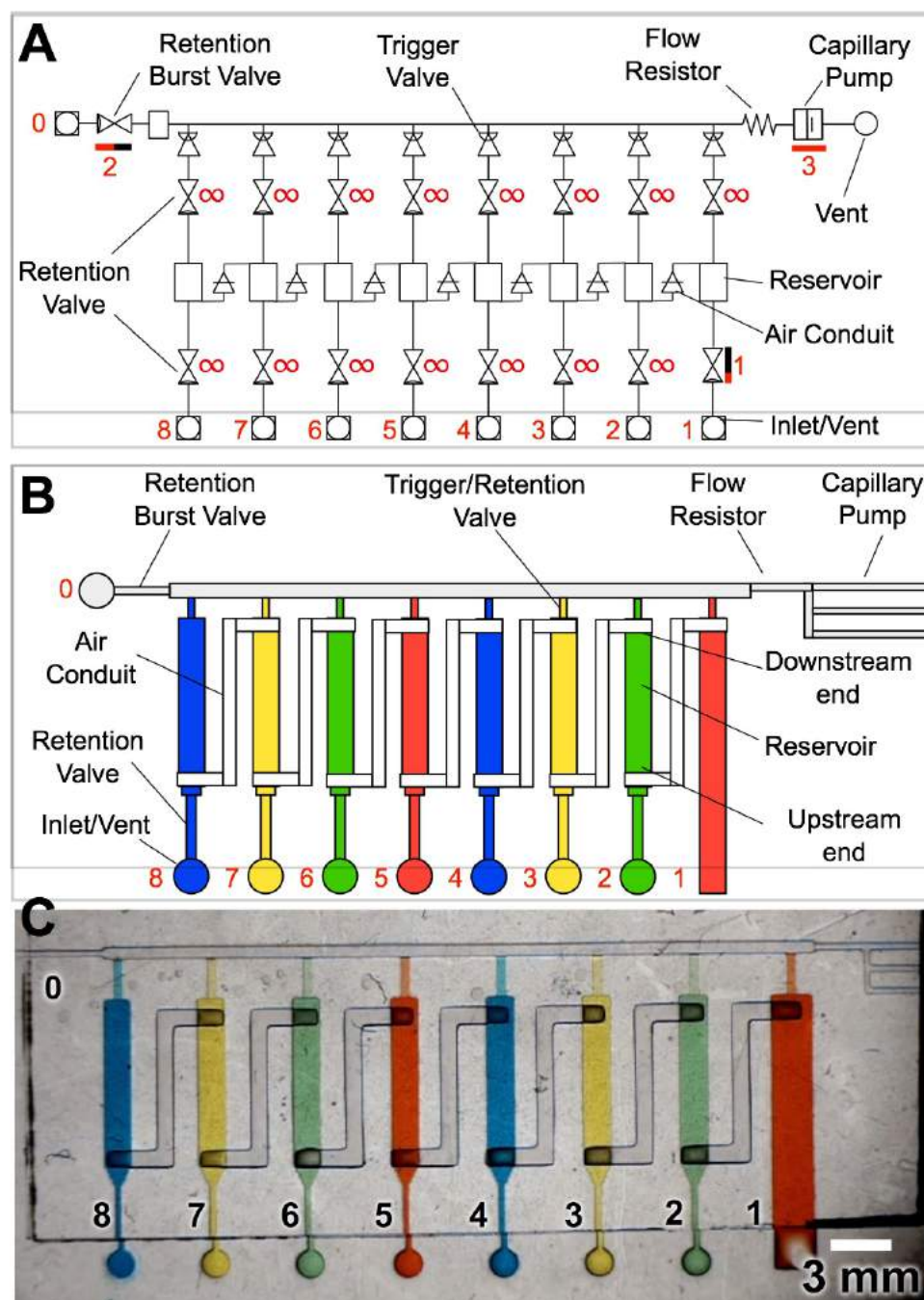


**FIGURE 6.1: Domino capillary circuit with 8 side branches.** (A) Symbolic layout showing capillary microfluidic elements in DCC design. Main branch 0 is the release channel that triggers liquid release from the 8 side branches. Branch 1 has a weak retention burst valve allowing it to drain first in the circuit. (B) Schematic layout showing assembled DCC. The air conduits are etched in the pneumatic layer and connect the downstream end of each reservoir to the upstream end of the subsequent reservoir, serially connecting each reservoir to ambient air. (C) Image of assembled DCC with the hydraulic layer sealed with the pneumatic layer. Reservoirs were filled with colored aqueous solutions held in place by trigger valves.

dye solutions are stopped at the trigger valves at the intersections between the side branches and the central release branch.

### 6.4.2 Physical Realization of Domino Capillary Circuit

DCCs consist of two layers (Fig. 6.2): (1) a hydrophilic hydraulic layer with reservoirs, trigger valves, retention valves, inlets, vents, and a capillary pump, and (2) a hydrophobic pneumatic layer with microchannels that act as air conduits serially linking the downstream end of a reservoir to the upstream end of the next reservoir.

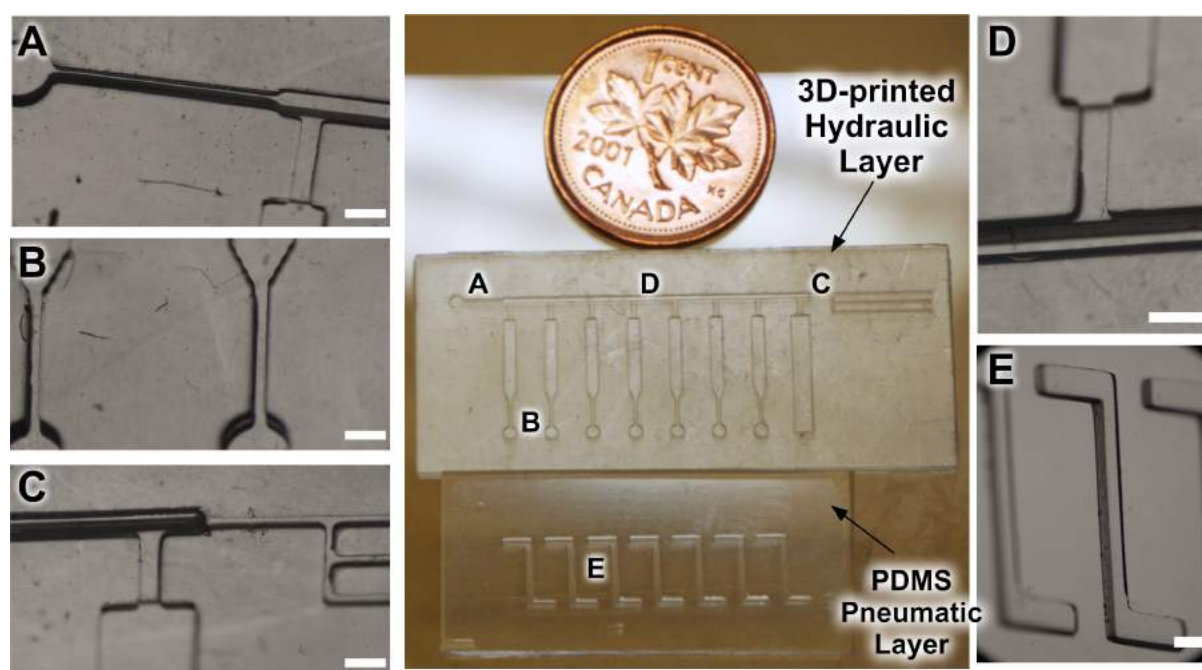


FIGURE 6.2: **3D-printed hydraulic and PDMS-replicated pneumatic layers of the domino capillary circuit.** Close-up images of: (A) Branch 0 that acts as release channel, (B) Inlets and upstream ends of reservoirs, (C) Flow resistor and capillary pump, (D) Front view of trigger valve, and (E) Air conduit. Microchannel sizes on the hydraulic layer range from  $50 \times 150 \mu\text{m}^2$  for the trigger valve to  $500 \times 1000 \mu\text{m}^2$  for the reservoirs. Air conduits on the pneumatic layer were  $300 \times 1000 \mu\text{m}^2$ . Scale bars are 1mm.

The insets in Fig. 6.2 show close-ups of different sections of the directly 3D-printed structures in the hydraulic and pneumatic layers of the DCC. The air conduits on the pneumatic layer were  $300 \mu\text{m}$  deep and  $1,000 \mu\text{m}$  wide and arranged in L-shapes so that when overlapped with the hydraulic layer, they connected the downstream end of one reservoir to the upstream end of the next reservoir to drain as shown in Fig. 6.1C.

Microchannel sizes in the 3D-printed hydraulic layer range from  $50 \times 150 \mu\text{m}^2$  (for trigger valves) to  $500 \times 1000 \mu\text{m}^2$  for the reservoirs. The capillary pump had a cross-section of  $150 \times 200 \mu\text{m}^2$  to provide high capillary pressure for wicking liquids. RBV #1, connected to the reservoir #1, had a cross-section of  $1000 \times 500 \mu\text{m}$  which is identical to the cross-section of the reservoirs and had the lowest capillary pressure in the DCC. Therefore, RBV #1 was the first microchannel to drain when all the channels in the DCC were filled. For simplicity, all the other branches (branches #2 - #8, and branch #0) in the DCC were terminated with microchannels that had cross-sections of  $500 \times 200 \mu\text{m}$ . These narrower microchannels were designed to retain liquid in branches #2 - #8, and in fact behave like retention valves in these side branches since they retained liquid without bursting or draining. The narrower channel connected to branch #0 does not drain until all the side branches are emptied since drainage of wider RBV #1 and the reservoirs in branches #2 - #8 occurs first as predicted by the design rules for RBVs.[14] The requirement for only two RBV sizes allows us to design two RBVs with a large capillary pressure difference between them - in this case, RBV #1 was  $1000 \mu\text{m}$  wide while RBV #2 was  $200 \mu\text{m}$  wide with both RBVs being  $500 \mu\text{m}$  deep.

### 6.4.3 Preprogrammed sequential delivery of 9 liquids

As a proof of concept demonstration of DCCs, a device for preprogrammed sequential delivery of 9 liquids was designed (Fig. 6.3). There are 8 reservoirs (branches 1 - 8) and one central branch (#0) that connects the reservoirs to the capillary pump. After fabrication of the two layers, the DCC was assembled by placing the hydrophobic PDMS pneumatic layer on top of the hydrophilic hydraulic layer as shown in Fig. 6.3. At this point, reservoirs were preloaded with coloured food dye solutions and the DCC was ready to test (Fig. 6.3,  $t = 0\text{s}$ ). Preprogrammed liquid delivery was triggered by adding a solution to branch #0 (Fig. 6.3,  $t = 5\text{s}$ ). When all the reservoirs are connected to the capillary pump, RBV #1 connected to branch #1 bursts and reservoir #1 drains

(Fig. 6.3,  $t = 8\text{s}$ ). Following bursting of the RBV upstream of reservoir #1, the air conduit between the downstream end of reservoir #1 and the upstream end of reservoir #2 opens allowing drainage of reservoir #2 (Fig. 6.3,  $t = 9\text{s}$ ). This is the domino effect that enables preprogrammed sequential opening of air vents and reservoir drainage. Next, reservoir #3 drains (Fig. 6.3,  $t = 10\text{s}$ ) followed by #4, #5, etc. When all the reservoirs are empty, RBV #2 connected to branch #0 bursts and branch #0 empties to complete the liquid delivery process (Fig. 6.3,  $t = 21\text{s}$ ). Movie 5.1 shows the preprogrammed drainage of 9 liquids in the DCC.



FIGURE 6.3: **Sequential delivery of 9 liquids by domino capillary circuit.** Time-lapse images showing sequential drainage of 8 reservoirs using repeats of an identical air conduit. The DCC is triggered by loading the release channel (branch 0) at  $t = 5\text{s}$ . Once the retention burst valve upstream of reservoir 1 bursts, the air conduit connecting the downstream end of reservoir 1 to the upstream end of reservoir 2 opens allowing drainage of reservoir 2 ( $t=9\text{s}$ ). Subsequently, air conduit 2 opens leading to drainage of reservoir 3 ( $t = 10\text{s}$ ), and so on. In total 9 liquids are drained (including branch #0). A video of 8-reservoir DCC is included in the Electronic Supplementary Information for this thesis (Movie 6.1)

#### 6.4.4 Preprogrammed sequential delivery of 17 liquids

To demonstrate how easily DCCs can be scaled, we designed a device with double the number of liquid delivery steps in our proof of principle demonstration. This scaled-up DCC has 16 reservoirs and was designed for sequentially flowing 17 solutions (including solution #0) (Fig. 6.4). This was accomplished also using only 2 RBV sizes and with 15 air conduits. The sizes of RBV #1 and #2 are identical to the previous design shown in Fig. 6.3. To reduce device footprint, reservoirs are arranged in two rows opposite each other. Devices were tested with aqueous food dye solutions and preprogrammed drainage of reservoirs in the expected sequential order was obtained (see Movie 5.2).

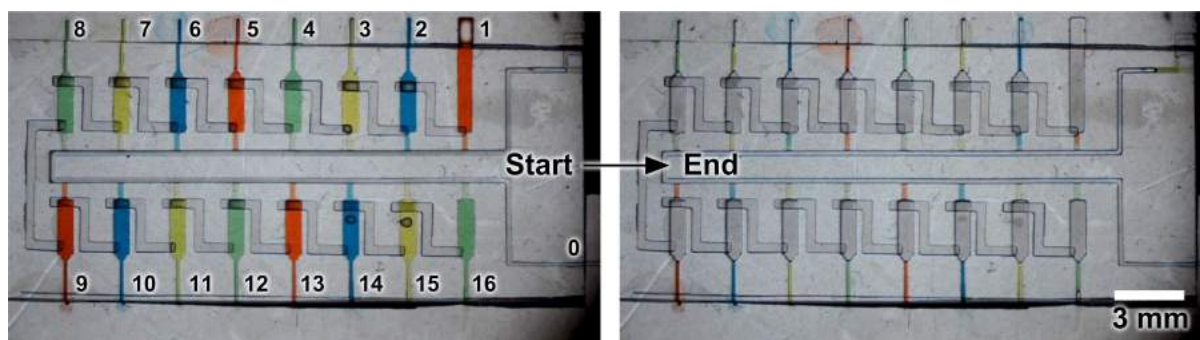


FIGURE 6.4: **Sequential drainage of 16 reservoirs by domino capillary circuit.** To demonstrate the scalability, a DCC with 16 reservoirs – double the number in our previous work with capillary circuits[14] – was made. Sequential drainage of all 16 reservoirs was accomplished in < 1min using identical air conduits, with the only exception being that the conduit between reservoirs 8 and 9 was lengthened to fit the serpentine shape of the device. A video of the 16-reservoir DCC is included in the Electronic Supplementary Information for this thesis (Movie 6.2)

In our previous work with CCs, we were limited to 8 preprogrammed liquid delivery steps based on the resolution and accuracy of the 3D-printer.[14] Here, however, we were able to more than double the number of preprogrammed liquid delivery steps using DCCs. By using air conduits for flow control, we were able to bypass 3D-printer resolution limits since each reservoir does not require a unique RBV in order to drain in the correct order.

### 6.4.5 Domino capillarics for simultaneous liquid delivery

To demonstrate the versatility of DCCs, we designed devices that enable simultaneous delivery of two liquids by connecting a single air conduit across two reservoirs - akin to knocking down two dominos with a single domino. Fig. 6.5A shows timelapse images of the DCC for simultaneous reservoir drainage. The device has 5 branches (#0 – #4) all placed on the same side. As in previous designs, branches #1 - #4 are connected to branch #0 via trigger valves and branch #0 connects all the branches to a single capillary pump. There are two air conduits - one that connects the downstream end of branch #1 to the upstream end of branch #2, and another that connects the downstream end of reservoir #2 to the upstream ends of *both* reservoirs #3 and #4. The connection of a single air conduit across these two reservoirs enables their simultaneous drainage once reservoir #2 is empty.

To validate simultaneous liquid delivery, branches #1 - #4 were preloaded with aqueous food dye solutions and the liquids were held in place by trigger valves (Fig. 6.5A,  $t = 0\text{m } 44\text{s}$ ). Next, the reservoirs were connected to the capillary pump by filling branch #0 (Fig. 6.5A,  $t = 1\text{m } 36\text{s}$ ). As expected, RBV #1 drained first since it has the lowest capillary pressure (Fig. 6.5A,  $t = 2\text{m } 00\text{s}$ ). This opens the air conduit between reservoirs #1 and #2 triggering the domino effect. Thus, reservoir #2 drains next (Fig. 6.5A,  $t = 2\text{m } 12\text{s}$ ) and opens the air conduit connecting reservoir #2 to reservoirs #3 and #4 allowing them to drain simultaneously (Fig. 6.5A,  $t = 2\text{m } 21\text{s}$ ). When reservoirs #1 - #4 have finished draining then RBV #2 at the end of branch #0 bursts and branch #0 empties to end the liquid delivery process. A video of preprogrammed simultaneous drainage using DCCs is available in Movie 6.3.

To demonstrate the usefulness of simultaneous drainage in DCCs we implemented a silver amplification assay. Silver amplification is commonly used for visualization of bioassay results via gold nanoparticle catalyzed reduction of silver salts to form visible dark precipitates on a surface.[12, 16] However, the silver salt and reducing agent solutions must be stored separately, and mixed only immediately before use to

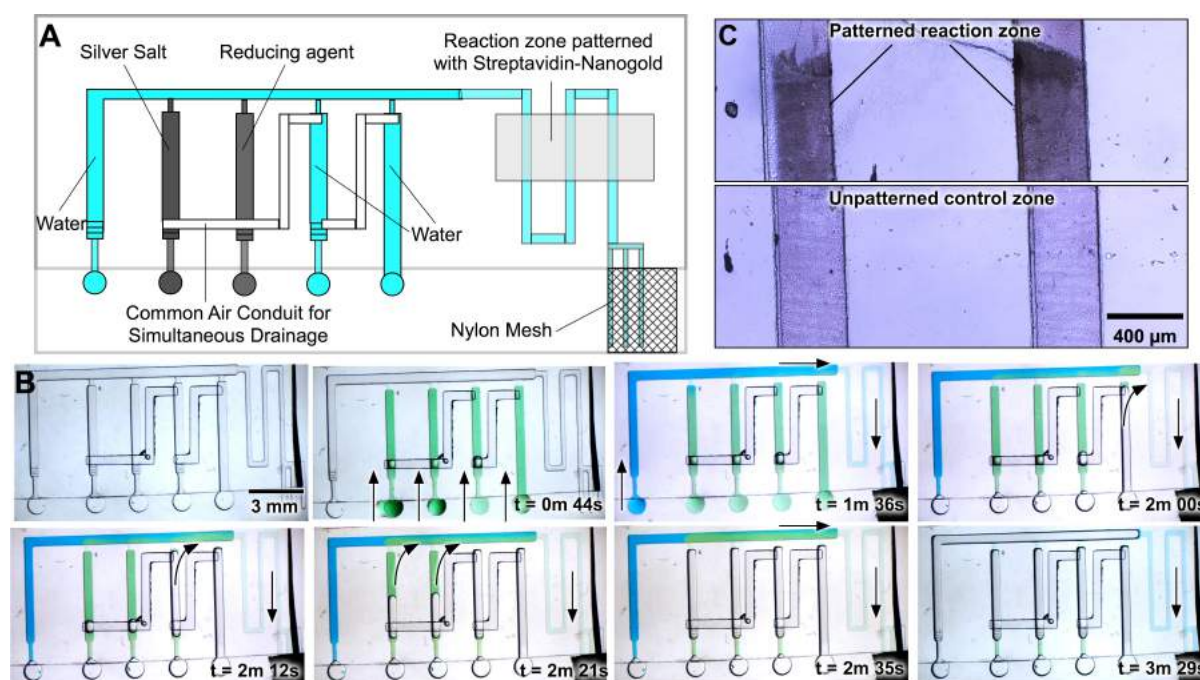


FIGURE 6.5: **Domino capillric circuit with simultaneous reservoir drainage for silver enhancement.** (A) Time-lapse images with aqueous food dye to verify simultaneous drainage of liquid in DCC with air conduit that connects reservoirs #3 and #4. A video of the preprogrammed simultaneous liquid drainage is provided in Movie 5.3. (B) Design of domino chip for simultaneous drainage of two reservoirs using a common air conduit. Reservoirs 3 and 4, connected with a single air conduit, drain simultaneously. The resistance of the central channel was designed to be minimal compared with the resistance of the trigger valve along each flow path. As such, the difference in drainage time between the two connected reservoirs is < 10%. (C) The simultaneous drainage device was used to implement a silver enhancement assay that requires simultaneous delivery of a silver salt and reducing agent. Optical micrographs showing differential colorimetric signal between reaction zone patterned with streptavidin-nanogold and unpatterned control region. Like sequential drainage, simultaneous drainage could simply be scaled up by extending the air conduit over 3 or more channels, which can readily be realized with dominos.

prevent unwanted background silver precipitation and low signal-to-noise ratio.

Fig. 6.5B shows how liquids were loaded into the DCC to implement the silver amplification assay. Branch #3 and #4 that share a common air conduit were filled with silver salt and reducing agent, the liquids that needed to be delivered simultaneously. Meanwhile, all other branches were filled with deionized water that acted as a wash buffer to stop the silver precipitation reaction. The hydrophobic PDMS cover of the DCC was patterned with neutravidin-nanogold (1.4 nm gold nanoparticles) using a PDMS capillary microfluidic chip, as described in our group's past work[17], prior to bonding the two layers of the DCC. The neutravidin-nanogold was adsorbed onto the pneumatic PDMS layer in a region that overlapped with the flow resistor in the hydraulic layer. The neutravidin-nanogold acts as a catalyst that promotes reduction of silver salts to form silver metal precipitates. The PDMS cover was patterned so that the flow resistor region was not entirely patterned with neutravidin-nanogold so that after the silver enhancement assay one could distinguish between the patterned and unpatterned regions. The flow resistor acts as a mixer for the silver salt and reducing agents solutions required for the silver enhancement assay.

Preprogrammed liquid delivery including simultaneous drainage of silver salts and reducing agent were carried out as described in Fig. 6.5A. After completion of liquid delivery, we observed a clear visual difference between the regions of the flow resistor patterned with neutravidin-nanogold and the unpatterned region (Fig. 6.5C). The region patterned with neutravidin-nanogold appeared darker than the unpatterned region. These results provide a proof of principle demonstration of silver amplification in the DCC for simultaneous liquid delivery and could enable sensitive colorimetric immunoassays in DCCs.

#### **6.4.6 Domino capillarics to limit effect of surface tension variations**

In addition, DCCs also have the benefit of being able to provide robustness against variations in the surface tensions of liquids inside reservoirs. Differences between

the surface tensions of liquids in RBVs could lead to wrong drainage sequences and limit the scalability of the number of liquid delivery steps in CCs. The Young-Laplace equation shows that the surface tension of liquid in a microchannel affects the capillary pressure.[4, 5] This could be a practical problem in applications of CCs since surfactants are often added to wash buffers used in immunoassays. The presence of surfactant lowers surface tension of liquid and may lead to wrong drainage sequences in the current design of RBVs that rely on geometric differences between RBVs to encode drainage sequence. The presence of surfactant in an RBV could lead it to drain earlier than expected and prevent proper operation of the CC. This is a greater concern when the capillary pressure difference between successive RBVs is small ( $\approx 40$  Pa) in order to accommodate a greater number of liquid delivery steps in a CC. In such situations, capillary pressure differences due to variations in the surface tension of liquids in RBVs could have a greater effect on the expected liquid drainage sequence and could lead to failed bioassays.

Since DCCs only have two RBV sizes, one RBV that is easily drained and another that never drains, one could make circuits where the surface tension variations due to surfactants do not affect the drainage sequence. Since the flow control is regulated by identical air conduits, one could fill reservoirs with multiple liquids without having to compensate for the difference in surface tension between the liquids.

## 6.5 Conclusion

DCCs enable preprogrammed delivery of multiple liquids using identical control units that consist of reservoirs and air conduits. These control units can be easily stacked the same way multiple dominos can be lined up. This makes it easy to scale up the number of liquid delivery steps in DCCs. Using identical air conduits we demonstrated preprogrammed sequential delivery of 9 liquids using only two RBVs, and 7 identical air conduits in a DCC. This was easily scaled up for preprogrammed delivery of 17 liquids also using only two RBV sizes and 16 identical air conduits. In addition,

the arrangement of air conduits on the hydrophobic cover layer makes DCCs versatile since the same hydraulic layer design can be used to implement either sequential or simultaneous liquid delivery. We demonstrated simultaneous drainage of liquids in DCCs using an air conduit that was connected to two reservoirs and showed that this enabled drainage of silver enhancement reagents that must be delivered at the same time but cannot be mixed prior to their desired drainage time. The rapid prototyping offered by 3D-printing means that functional hydraulic layers for DCCs can be fabricated in < 10 min. The hydrophobic cover layer currently requires a PDMS replication step; however, multiple copies of the hydrophobic layer can be fabricated from a single mold. In future, flexible silicone sheets could be patterned for example using laser cutting or a knife plotter to manufacture the hydrophobic cover layer which typically has large features (> 500  $\mu\text{m}$ ) also within minutes. In addition, as materials for 3D-printing improve, one may also be able to directly 3D-print flexible materials with microchannels to act as covers for the DCCs. DCCs are robust as they are insensitive to surface tension, and can readily be scaled up, and hence may find numerous applications in research, clinic or industry.

## Acknowledgements

We thank NSERC and CIHR for funding. A.O. is grateful for funding from the NSERC CREATE Integrated Sensor Systems Training Program, the CIHR Systems Biology Training Program, and the Quebec Merit Scholarship for Foreign Students (PBEEE). D.J. acknowledges a Canada Research Chair. We are grateful for helpful discussions with Dr. Sebastien Bergeron of Paralex Bioassays.

## Bibliography

- [1] M. Zimmermann, H. Schmid, P. Hunziker, and E. Delamarche, "Capillary pumps for autonomous capillary systems," *Lab Chip*, vol. 7, no. 1, pp. 119–125, 2007.
- [2] P. Man, C. H. Mastrangelo, M. A. Burns, and D. T. Burke, "Microfabricated capillarity-driven stop valve and sample injector," in *Proceedings of the the IEEE MEMS Conference*, Jan. 1998, pp. 45–50.
- [3] J. Melin, N. Roxhed, G. Gimenez, P. Griss, W. van der Wijngaart, and G. Stemme, "A liquid-triggered liquid microvalve for on-chip flow control," *Sensors & Actuators: B. Chemical*, vol. 100, no. 3, pp. 463–468, Jan. 2004.
- [4] D. Juncker, H. Schmid, U. Drechsler, H. Wolf, M. Wolf, B. Michel, N. de Rooij, and E. Delamarche, "Autonomous Microfluidic Capillary System," *Anal. Chem.*, vol. 74, no. 24, pp. 6139–6144, Dec. 2002.
- [5] R. Safavi-eh and D. Juncker, "Capillarics: Pre-programmed, self-powered microfluidic circuits built from capillary elements," *Lab Chip*, vol. 13, no. 21, pp. 4180–4189, Nov. 2013.
- [6] L. Gervais and E. Delamarche, "Toward one-step point-of-care immunodiagnostics using capillary-driven microfluidics and PDMS substrates." *Lab Chip*, vol. 9, no. 23, pp. 3330–3337, Dec. 2009.
- [7] C. Jönsson, M. Aronsson, G. Rundström, C. Pettersson, I. Mendel-Hartvig, J. Bakker, E. Martinsson, B. Liedberg, B. MacCraith, O. Öhman, and J. Melin, "Silane–dextran chemistry on lateral flow polymer chips for immunoassays," *Lab Chip*, vol. 8, no. 7, p. 1191, 2008.

- [8] P. Novo, F. Volpetti, V. Chu, and J. P. Conde, "Control of sequential fluid delivery in a fully autonomous capillary microfluidic device." *Lab Chip*, vol. 13, no. 4, pp. 641–645, Feb. 2013.
- [9] S.-J. Kim, S. Paczesny, S. Takayama, and K. Kurabayashi, "Preprogrammed capillarity to passively control system-level sequential and parallel microfluidic flows." *Lab Chip*, vol. 13, no. 11, pp. 2091–2098, Jun. 2013.
- [10] G. Lenk, "Delay valving in capillary driven devices based on dissolvable thin films," in *Proceedings of microTAS 2014*, Jan. 2014, pp. 216–218.
- [11] E. Fu, T. Liang, P. Spicar-Mihalic, J. Houghtaling, S. Ramachandran, and P. Yager, "Two-Dimensional Paper Network Format That Enables Simple Multistep Assays for Use in Low-Resource Settings in the Context of Malaria Antigen Detection," *Anal. Chem.*, vol. 84, no. 10, pp. 4574–4579, May 2012.
- [12] C. D. Chin, T. Laksanasopin, Y. K. Cheung, D. Steinmiller, V. Linder, H. Parsa, J. Wang, H. Moore, R. Rouse, G. Umvilighozo, E. Karita, L. Mwambarangwe, S. L. Braunstein, J. van de Wijgert, R. Sahabo, J. E. Justman, W. El-Sadr, and S. K. Sia, "Microfluidics-based diagnostics of infectious diseases in the developing world," *Nature Medicine*, vol. 17, no. 8, pp. 1015–1019, Jul. 2011.
- [13] P. Novo, V. Chu, and J. P. Conde, "Integrated optical detection of autonomous capillary microfluidic immunoassays: a hand-held point-of-care prototype," *Biosensors and Bioelectronics*, vol. 57, no. C, pp. 284–291, Jul. 2014.
- [14] A. O. Olanrewaju, A. Robillard, M. Dagher, and D. Juncker, "Autonomous microfluidic capillary circuits replicated from 3D-printed molds." *Lab Chip*, vol. 16, no. 19, pp. 3804–3814, Sep. 2016.
- [15] A. O. Olanrewaju, A. Ng, P. Decorwin-Martin, A. Robillard, and D. Juncker, "Microfluidic Capillary Circuit for Rapid and Facile Bacteria Detection." *Anal. Chem.*, vol. 89, no. 12, pp. 6846–6853, Jun. 2017.

- 
- [16] R. Larochelle and R. Magar, "The Application of Immunogold Silver Staining (IGSS) for the Detection of Transmissible Gastroenteritis Virus in Fixed Tissues," *Journal of Veterinary Diagnostic Investigation*, vol. 5, no. 1, pp. 16–20, Jan. 1993.
- [17] M. Pla-Roca and D. Juncker, "PDMS Microfluidic Capillary Systems for Patterning Proteins on Surfaces and Performing Miniaturized Immunoassays," in *Methods in Molecular Biology*, A. Khademhosseini, K.-Y. Suh, and M. Zourob, Eds. Totowa, NJ: Humana Press, Sep. 2010, pp. 177–194.

## Chapter 7

# Conclusions and Outlook

### 7.1 Summary of scientific contributions

In this dissertation, we developed microfluidic capillary circuits (CCs) manufactured by 3D-printing. Prior to this work, the conventional view was that capillary microfluidic devices required high precision ( $\approx 10 \mu\text{m}$ ) and sub-micron surface roughness provided by cleanroom fabrication to obtain functional capillary valves and circuits. The reliance on cleanroom fabrication increased the time required to develop new design iterations to advance the understanding of capillary valves and circuits, and employ them in clinically-relevant applications. In this thesis, we demonstrated for the first time that reliable capillary valves and circuits can be obtained using 3D-printing. The rapid prototyping and multi-level fabrication available with 3D-printing allowed us to better understand and extend the design of CCs for preprogrammed liquid delivery. We developed analytical and empirical design rules taking into account the entire circuit architecture of CCs, and were able to rapidly design new devices to test our hypotheses.

In addition, we used 3D-printed CCs to develop a proof-of-concept diagnostic for a challenging clinical problem - the rapid detection of bacteria in urine. Detection of bacteria that causes urinary tract infections is a slow process in clinical microbiology labs because bacteria must be grown overnight to get a specific and sensitive count of the pathogens that are present. While there have been multiple microfluidic approaches to providing fast and sensitive bacterial diagnosis, most tests require at least

30 minutes to provide results and typically involve cell lysis and DNA analysis that are challenging to automate. We leveraged the automatic liquid handling capability of CCs to implement a rapid bacterial capture assay in  $< 7$  min, making our test one of the fastest bacterial detection methods reported so far. We developed an automated sandwich immunoassay, with on-the-fly packing of functionalized microbeads and preprogrammed delivery of sample and reagents with fluorescence readout that can be simply interpreted by the user. The assay format allows capture of bacteria from urine samples without need for cumbersome sample preparation steps like lysis or nucleic acid preparation. This assay format may be readily applied to other analytes including proteins and viruses.

Furthermore, we developed a newer, more scalable and versatile approach to the design and fabrication of CCs. Domino capillary circuits, DCCs, reduce the burden and complexity of designing CCs by allowing the user to stack modular control units consisting of identical air conduits (similar to stacking identical dominos), rather than having to design unique control components for each liquid delivery step. In our past work with CCs that used unique burst valves to control liquid delivery we were limited to only 8 sequential liquid delivery steps due to 3D-printer resolution limits. However, we were easily able to implement 17 liquid delivery steps with DCCs using identical air conduits, strategically placed between reservoirs, to control liquid delivery. Consequently, DCCs are conceptually and practically easier to design and the number of liquid delivery steps can readily be scaling up merely by adding additional air conduits and reservoirs, similar to adding more dominos to a line. In addition, DCCs are more versatile since reservoirs can be drained simultaneously by extending an air conduit over two reservoirs - similar to using one domino to knock over 2 dominos. Air conduits could also be extended over 3 or more reservoirs to make increase the number of reservoirs that are drained simultaneously. DCCs can also be designed in a single-level structure that does not require a microstructured cover, so that functional devices can be 3D-printed in  $< 10$  min.

## 7.2 Recommendations for future directions

The presented work extends, applies, and introduces new directions in capillary microfluidics. As a result of the rapid prototyping offered by 3D-printing, for the first time, new microchannel-based capillary valves, pumps, and integrated circuits can be obtained in  $< 10$  min. Nevertheless, further studies could improve upon the presented work in a number of ways and move CCs and DMs closer to use at the point-of-care.

### 7.2.1 Material choice and device storage

Further research is required to investigate the differences in capillary-driven flow of liquid between 3D-printed and cleanroom-fabricated microchannels. Indeed, the roughness and layer-by-layer structure of 3D-printed microchannels is very different from that of cleanroom-fabricated channels (see Fig 4.1). However, in practice we did not observe any major differences between the flow rates in 3D-printed microchannels and cleanroom-fabricated channels. One area where one might expect a difference, might be that corner flow in the rougher 3D-printed microchannels might be a bigger issue than with cleanroom-fabricated channels that have smoother walls. Other researchers have observed intermittent flow and flow stoppage due to pinning on rough surfaces but that was only when 3D-printing was carried out using techniques such as fused deposition modelling that produced surface roughness up to  $20 \mu\text{m}$ .<sup>[1]</sup> Further research with stereolithographic 3D-printed microchannels is required to study capillary-driven flow in 3D-printed microchannels.

The CCs demonstrated in Chapter 4 were replicated in PDMS which was plasma-activated for hydrophilicity. PDMS gradually recovers its hydrophobicity a few hours after plasma treatment,<sup>[2]</sup> so alternate materials will be required to ensure stable long term storage of CCs.

3D-printing is useful as a prototyping technology to quickly test out new ideas

and designs. PDMS molds can be obtained from 3D-printed molds by double replication, and the resulting PDMS molds can be electroplated with nickel and then subsequently used for hot embossing of thousands of copies of devices. 3D-printed molds may also be used as intermediate step to manufacture silicone molds for injection molding.[3, 4] CC mold designs manufactured with 3D-printing are compatible with conventional metal micromachining which can be used to produce durable molds for injection molding. Laser micromachining of molds is a technique that can already be used to manufacture high precision molds once for mass production.[5] As 3D-printing of metals[6, 7] improves, one could envision direct 3D-printing of metal molds for durable high-volume injection molding. CCs can be injection molded into polymers like Cyclic Olefin Copolymer (COC) that can be chemically treated to obtain stable hydrophilic surfaces.[8]

In addition, the ability to use 3D-printing for low- or medium-throughput development of custom diagnostic devices directly in areas of need, such as a doctor's office, is also appealing, especially as the cost of 3D-printers and 3D-printing resin decreases. For example, one could envision a future with on-demand 3D-printing of CCs for diagnostics in areas of need that do not have sufficient demand to justify the cost of a large-scale injection molding manufacturing process. Indeed, research is already moving in this direction with the development of a portable 3D-printer that combines filament extrusion and ink-jet liquid handling to print reaction beds and fill them with bacterial growth medium, bacteria samples, and antibiotics in order to determine antibiotic susceptibility directly at the point of need.[9] CCs could automate liquid handling in such 3D-printed devices and minimize the need for tubing and inkjet liquid handling, thereby reducing the need for peripheral equipment for liquid handling. One technical problem with printing CCs on location is the need for surface treatment of the devices for hydrophilicity. The use of hydrophilic, photocurable, 3D-printer resins such as polyethylene glycol[10] could help to address this concern. However, non-technical concerns such as regulatory approval would need to be considered for on-location 3D-printing of CCs.

### 7.2.2 Making CCs more user-friendly

The CCs developed in Chapter 4 for rapid bacteria detection require four pipetting steps to automate a 5-step process for bacteria detection. The CCs operate in a “walk-away” format where the user can complete the first three pipetting steps (i.e. preloading the sample and reagents) up to 30 min before they are ready to start the assay. This is because trigger valves hold the liquids in place until the user is ready to start the assay by adding the microbead suspension to the central branch (Fig. 5.1). Subsequently the CC controls the sequence of delivery of the sample and reagents without further user intervention. The automated assay in the CC is simpler than what the user would have to do if they were to manually complete the same processes by timing the addition of the sample and reagents in an eppendorf tube or a 96-well plate. And this automation in the CC does not require bulky peripheral pumping equipment.

Nevertheless, the CC for bacteria detection could be made more user-friendly with a few technological improvements. Our goal was to develop a device that could be used by a medical practitioner directly at the point-of-care, so minimizing the number of pipetting steps would be ideal. For example, antibodies and microbeads could be deposited with an inkjet spotter and dried on the chip and later reconstituted by sample addition.[11] Reagent integrators[12] or orthogonal flow mixers[13] could be included along the flow path of the CC for rapid and efficient reagent reconstitution to ensure even distribution and delivery of reagents. A CC with pre-dried reagents and beads could function with the addition of only the sample which could also serve as a wash buffer as is done in lateral flow assays. However, if additional liquid delivery steps - such as a final wash with buffer to improve signal to noise ratio[14] - are desired, liquids could be stored in blisters and integrated onto the CC or its cover. The blisters filled with liquid could easily be dispensed by integrating lancing structures within the CC to pierce the blisters in order to start the assay.

### **Aliquoting/Overflow Structures**

Another fluidic element that could be developed to improve the user-friendliness of the assay is aliquoting/overflow structures for metering the sample volume. Currently, the CC does not require precise pipetting since trigger valves hold liquids in place and excess liquid at inlets can be simply wiped away with a piece of paper as is currently done. Nevertheless integrating on-chip aliquoting structures to accurately meter sample volume would ensure accurate control over the volume of liquid delivered and make device operation more user-friendly. Such aliquoting structures could be implemented by connecting capillary pumps to the liquid inlet and designing the inlet and flow resistance in the direction of the aliquoting structure so that liquid first fills the reservoir before excess liquid reaches the overflow pump which can be a simple piece of paper. The size of the inlet and the microchannels connected to the overflow capillary pump can be designed such that when excess liquid is drained, the microchannel leading to the overflow pump empties completely. This would completely disconnect the overflow pump from the reagent reservoir and prevent interference of the overflow pump with sequential liquid delivery in the CC.

### **7.2.3 Simplifying assay readout**

Although optical detection for CCs for bacteria detection was carried out using fluorescence microscopes, simpler and more inexpensive methods may be used to facilitate use at the point-of-care. For example, low-cost and portable fluorescence microscopes[15, 16] or cell phones with optical adaptors[17] may enable quantitative, yet minimally instrumented detection. Similarly, chemical signal amplification methods such as silver enhancement may be used to provide colorimetric results that are visible to the naked eye.[14, 18, 19] Given that the bacteria assay was developed using biotinylated antibodies, switching to a colorimetric detection scheme could be as simple as substituting fluorescently-tagged streptavidin for nanogold-conjugated streptavidin, and then delivering silver enhancement solutions as demonstrated in chapter 6. Given

that we now have the capability to easily scale up the number of liquid delivery steps using DCCs, we could also include additional wash and blocking steps that are often required to improve the signal to noise ratio when using colorimetric detection techniques.[14] There have also been demonstrations of integration of optical sensing elements like photodiodes within 3D-printed microfluidic devices for integrated optical readout.[20]

#### 7.2.4 Improving sensitivity of CCs for bacteria detection

Our proof of principle demonstration of bacteria detection in synthetic urine had a limit of detection of  $7.1 \times 10^3$  CFU/mL, which is well below the traditional diagnostic requirement for UTI ( $10^5$  CFU/mL). However, recent reviews suggest that LODs as low as  $10^2$  CFU/mL may be required for some symptomatic patients with UTI.[21] To meet these more stringent requirements, the LOD of the CC may be further improved by using smaller microbeads to increase the efficiency of bacteria capture.

3D-printing CCs with smaller feature sizes would allow the use of microbeads with lower diameters which would decrease the gap size between beads. Smaller gaps between microbeads would increase the likelihood of bacteria capture.[22, 23] In chapter 5, bead diameter was limited to sizes  $\geq 50 \mu m$  due to the minimum Z-resolution of the EnvisionTEC Perfactory MicroEDU 3D-printer used.[24] Recently, 3D-printers with minimum Z-feature sizes down to  $10 \mu m$  have become available at a cost of  $\approx$  US\$10,000, which is affordable for many research labs.[25, 26] These 3D-printers with finer resolution would allow trapping of smaller microbeads and could potentially lead to improved bacteria capture.

However, given a constant capillary pressure, there is a trade-off between the size of microbeads and the flow resistance in the CC. As the microbead diameter decreases, the flow resistance increases rapidly and the time required to flow  $100 \mu L$  of sample through the CC would also increase significantly. The CC design in chapter 5 allowed processing of a large sample volume (i.e.  $100 \mu L$ ) in a short time (i.e.  $< 7$  min) with a

capture efficiency of  $\approx 1$  in 100 bacteria. Using numerically derived correlation equations that describe the expected capture profile of bacteria in porous media[23] one could estimate the likely capture efficiency of bacteria and develop design rules for CCs for bacteria detection. Such correlation equations were developed to study passive capture of bacteria in porous media such as sand over larger distances and would need to be modified to account for the specific interactions over much smaller length scales within the CC. Predictions from the equations would be empirically verified with experiments where the microbead size was systematically varied to study its influence on bacteria capture efficiency and flow rate. Thus, for applications that require bacteria detection at much lower concentrations one could rationally design a circuit with appropriate bead diameter and flow resistance based on the acceptable trade-off capture efficiency and sample processing time.

### 7.2.5 Testing clinical urine samples

The CC for bacteria detection developed in chapter 5 was demonstrated to meet a clinically-relevant limit of detection. However, the work was carried out using bacteria spiked into synthetic urine. Although synthetic urine has the same chemical composition as real urine, it does not have the same debris that may be present in real patient urine. For example, clinical urine samples often have materials such as: pus, skin cells, white blood cells, red blood cells, and proteins.[27]

#### Presence of debris in clinical urine samples

The presence of debris could impact the results of fluorescence readout of bioassays. As such, an initial filtration step would be required to remove large debris from the urine samples prior to on-chip testing. Given that *E. coli* cells are expected to be  $\approx 1 \times 2 \mu\text{m}^2$  and white blood cells are typically  $> 10 \mu\text{m}$  in size, a simple syringe filtration step with a filter with pores  $> 5 \mu\text{m}$  could be used to remove debris while leaving bacteria in the sample. Characterization would be required to determine the required

pore size and surface area of the filter to avoid filter clogging and loss of bacteria during the filtration step.

Another potential challenge when working with clinical samples is that bacteria that cause UTI may clump and bind to each other and to epithelial cells, possibly as a virulence factor that helps them evade the host's immune response.[28] Clumping of bacteria with themselves and with other cells might prevent the use of only filtration as a means to separate bacteria from other debris in clinical urine samples. Characterization of the frequency and size range of bacteria clumps present in clinical urine samples would need to be carried out. This can be tested in tube-based experiments and if necessary different declumping strategies such as ultrasonication or the use of chemicals could be explored to break up large bacteria clumps. Also, the presence of bacteria clumps does not necessarily have to deter accurate measurement of the presence of UTI. The bacteria spot counting algorithm can be adjusted to identify large clumps that are specifically labelled with detection antibodies. The bead size could be adjusted to account for the typical size of clumps. Alternately, the formation of bacteria clumps might result in trapping of bacteria at the leading edge of the microbead column and could resemble assays where filtration and specific antibody staining are combined for bacteria detection.[29]

Initial attempts were made to test real clinical samples. One major issue encountered was the presence of autofluorescent materials (crystals, white blood cells, cellular debris) in clinical urine samples. The presence of this heterogeneously-sized autofluorescent debris precluded fluorescence-based detection as was carried in Chapter 5. To address this concern, the bacteria capture assay could be re-designed to use colorimetric detection since the biotinylated detection antibodies readily be detected using streptavidin-conjugated enzymes that process colorimetric substrates. Further research is required to validate and determine the assay sensitivity using colorimetric assays.

### Detecting different bacteria species

Another important consideration when working with clinical urine samples is that the need to detect multiple bacterial species. Our proof of concept test in chapter 5 targeted *E. coli* which is the cause of > 80 % of UTIs[30]. We used *E. coli* O157:H7 as the target bacterium spiked into synthetic urine since it is a well-characterized bacterial pathogen with readily available antibodies that target it. However, there are many different strains of *E. coli* that have been isolated from the urine of patients with UTI. For example, a study investigated the strains of *E. coli* that cause UTI in Montreal, Quebec.[31] The authors found that *E. coli* serotypes O1, O6, O17, and O25 were particularly well-represented in samples collected from 256 consecutive episodes of UTI diagnosed by the Student Health Services at McGill University in Montreal in 2006.[31] To detect the diversity of *E. coli* strains implicated in UTI, polyclonal capture and detection antibodies that target conserved extracellular regions of the *E. coli* cell wall would need to be obtained. Such antibodies are commercially available and have already been purchased and validated in our lab using *E. coli* K12 and O157:H7 strains. Further validation of polyclonal antibodies using clinical urine samples will be required.

Although *E. coli* causes 80 - 85 % of UTI infections among walk-in patients, other bacteria such as *Klebsiella pneumoniae* (6.2 %), *Enterococcus species* (5.3 %), Group B *Streptococcus* (2.8 %), *Proteus mirabilis* (2.0 %), and *Staphylococcus saprophyticus* (1.4 %) are also implicated in UTI. Consequently, CCs functionalized with antibodies that target these common bacterial strains could also be developed. Given that a proof of principle assay format has been demonstrated, assay conditions would need to be tested and optimized for each bacterial uropathogen. Parallel microchips could be set up to test for each of the different strains. In addition, microchip architecture could be designed such that a single sample inlet feeds several CCs with preprogrammed liquid delivery.

### Detecting antibiotic resistance

The CC design detailed in chapter 5 is envisioned as an initial triage tool to rapidly identify the most common bacterial species implicated in UTI. This could help to prevent over-prescription of antibiotics to patients without UTI. Although the sandwich immunoassay for bacteria detection implemented in the CC enables rapid and specific identification of bacterial species, it does not provide information about the antibiotic resistance of bacteria. This is because the assay targets extracellular markers for bacterial identification. There are a few extracellular markers of antibiotic resistance. For example, there are antibodies that target the modified form of the penicillin binding protein that confers resistance to  $\beta$ -lactam antibiotics such as penicillin.[32] However, given the diversity of mechanisms of antibiotic resistance, accurate detection of the antibiotic resistance requires nucleic acid testing.

Future work could incorporate the capability to do combined bacterial detection and antibiotic susceptibility testing. For example, cell lysis reagents could be stored in additional reservoirs in CCs or DMs, and delivered after initial bacteria detection to release DNA. One could combine the CC for bacteria capture with downstream continuous flow polymerase chain reaction (PCR) for DNA amplification and real-time fluorescence detection[33, 34]. Alternatively, one could also design the CC to incorporate a reaction chamber for temperature cycling and DNA amplification[35, 36].

### 7.2.6 Applications of Capillary Circuits

One of the exciting future prospects for the work presented in this thesis is finding applications that showcase the scalability and robustness of the CCs presented in this thesis. In chapter 6, DCCs were used for preprogrammed delivery of multiple liquids and were demonstrated for 9 liquids and 17 liquids thus far. Since the control units are identical reservoirs and air conduits, one can readily envision a DCC for preprogrammed delivery of 96 or 384 liquids.

We are now at the point where the number of preprogrammed liquid delivery operations that can be implemented in capillary systems exceeds the immediate apparatus need. At this point, the question then becomes “which applications require such throughput and capillary-driven flow control?” There are a variety of applications that could benefit from such flexibility. For example, one can envision a DCC with capture antibodies for a 16-protein panel spotted in a reaction chamber in front of the capillary pump. Although antibodies could be mixed in a single chamber, such mixing results in cross-reactivity between antibodies that increases quadratically with the number of targets and often prevents practical implementation of multiplexed assays.[37] Cross-reactivity between antibodies in a multiplexed immunoassay may be minimized by avoiding mixing of different antibodies, and this can be accomplished by spatially separating them.[37] The DCC could be used to implement preprogrammed sequential delivery of a single blood sample followed by detection antibodies (separated into distinct reservoirs) and wash buffer for each of the 16 proteins in the panel. Such a setup would require at least 33 sequential liquid delivery steps and could be readily implemented with DCCs. There are a variety of applications that could benefit from rapid screening of protein panels, for instance, one could use such a disposable device for portable point-of-care testing for breast cancer biomarker signatures in blood that were identified using proteomic techniques.[37] Other bioassays including time-dependent enzymatic assays, immunohistochemistry, or chemical synthesis could also benefit from the scalable and robust liquid delivery offered by DCCs.

Another important consideration in the design of DCCs is how to minimize the number of pipetting steps. Currently, each reservoir requires its own pipetting step. One could design DCCs to have common inlets for all buffer solutions, possibly by taking advantage of 3-dimensional microchannel architectures that can be obtained using 3D-printing.[38]

### 7.2.7 Closing Remarks

At the start of this PhD project, fabrication of new capillary system designs required slow and expensive photomask design and several hours in a cleanroom facility. The work described in this dissertation shows a path to truly rapidly prototyped capillary microfluidics by leveraging 3D-printing technology. Despite the current resolution limits of 3D-printers, we do not sacrifice liquid delivery capabilities in capillary microfluidics. Instead, by developing design rules and new liquid handling paradigms, we exceed previous liquid delivery capabilities in capillary microfluidics and offer accessible technologies that may be applied to a variety of applications in diagnostics, research, or education.

# Bibliography

- [1] R. K. Lade, E. J. Hippchen, C. W. Macosko, and L. F. Francis, "Dynamics of Capillary-Driven Flow in 3D Printed Open Microchannels." *Langmuir*, vol. 33, no. 12, pp. 2949–2964, Mar. 2017.
- [2] D. Bodas and C. Khan-Malek, "Hydrophilization and hydrophobic recovery of PDMS by oxygen plasma and chemical treatment—An SEM investigation," *Sensors & Actuators: B. Chemical*, vol. 123, no. 1, pp. 368–373, Apr. 2007.
- [3] T. Mueller, "Stereolithography-based prototyping: case histories of applications in product development," in *IEEE Technical Applications Conference and Workshops. Northcon/95. Conference Record.* IEEE, 1995, pp. 305–310.
- [4] P. Chung, J. A. Heller, M. Etemadi, P. E. Ottoson, J. A. Liu, L. Rand, and S. Roy, "Rapid and Low-cost Prototyping of Medical Devices Using 3D Printed Molds for Liquid Injection Molding," *JoVE*, no. 88, p. e51745, 2014.
- [5] L. Cerami, E. Mazur, S. Nolte, and C. B. Schaffer, "Femtosecond Laser Micromachining," in *Ultrafast Nonlinear Optics.* Heidelberg: Springer International Publishing, Jan. 2013, pp. 287–321.
- [6] C. Ladd, J. H. So, J. Muth, and M. D. Dickey, "3D printing of free standing liquid metal microstructures," *Adv. Mater.*, vol. 25, no. 36, pp. 5081–5085, 2013.
- [7] D. P. Parekh, C. Ladd, L. Panich, K. Moussa, and M. D. Dickey, "3D printing of liquid metals as fugitive inks for fabrication of 3D microfluidic channels," *Lab Chip*, vol. 16, no. 10, pp. 1812–1820, 2016.

- [8] C. Jönsson, M. Aronsson, G. Rundström, C. Pettersson, I. Mendel-Hartvig, J. Bakker, E. Martinsson, B. Liedberg, B. MacCraith, O. Öhman, and J. Melin, "Silane–dextran chemistry on lateral flow polymer chips for immunoassays," *Lab Chip*, vol. 8, no. 7, p. 1191, 2008.
- [9] S. Glatzel, M. Hezwani, P. J. Kitson, P. S. Gromski, S. Schürer, and L. Cronin, "A Portable 3D Printer System for the Diagnosis and Treatment of Multidrug-Resistant Bacteria," *Chem*, vol. 1, no. 3, pp. 494–504, Sep. 2016.
- [10] H. Gong, A. T. Woolley, and G. P. Nordin, "High density 3D printed microfluidic valves, pumps, and multiplexers." *Lab Chip*, vol. 16, no. 13, pp. 2450–2458, Jul. 2016.
- [11] L. Gervais, M. Hitzbleck, and E. Delamarche, "Capillary-driven multiparametric microfluidic chips for one-step immunoassays." *Biosensors and Bioelectronics*, vol. 27, no. 1, pp. 64–70, Sep. 2011.
- [12] M. Hitzbleck, L. Gervais, and E. Delamarche, "Controlled release of reagents in capillary-driven microfluidics using reagent integrators." *Lab Chip*, vol. 11, no. 16, pp. 2680–2685, Aug. 2011.
- [13] O. Gökçe, "Passive "orthogonal flow mixers" for homogeneous dissolution of reagents in microfluidics," in *Proceedings of microTAS 2016*, Jan. 2016, pp. 9–10.
- [14] C. D. Chin, T. Laksanasopin, Y. K. Cheung, D. Steinmiller, V. Linder, H. Parsa, J. Wang, H. Moore, R. Rouse, G. Umviligihozo, E. Karita, L. Mwambarangwe, S. L. Braunstein, J. van de Wijgert, R. Sahabo, J. E. Justman, W. El-Sadr, and S. K. Sia, "Microfluidics-based diagnostics of infectious diseases in the developing world," *Nature Medicine*, vol. 17, no. 8, pp. 1015–1019, Jul. 2011.
- [15] A. R. Miller, G. L. Davis, Z. M. Oden, M. R. Razavi, A. Fateh, M. Ghazanfari, F. Abdolrahimi, S. Poorazar, F. Sakhaie, R. J. Olsen, A. R. Bahrmand, M. C. Pierce, E. A. Graviss, and R. Richards-Kortum, "Portable, Battery-Operated, Low-Cost,

- Bright Field and Fluorescence Microscope," *PLoS ONE*, vol. 5, no. 8, p. e11890, Aug. 2010.
- [16] M. M. Hasan, M. W. Alam, K. A. Wahid, S. Miah, and K. E. Lukong, "A Low-Cost Digital Microscope with Real-Time Fluorescent Imaging Capability," *PLoS ONE*, vol. 11, no. 12, p. e0167863, Dec. 2016.
- [17] A. Ozcan, "Mobile phones democratize and cultivate next-generation imaging, diagnostics and measurement tools," *Lab Chip*, vol. 14, no. 17, p. 3187, Feb. 2014.
- [18] E. Fu, T. Liang, J. Houghtaling, S. Ramachandran, S. A. Ramsey, B. Lutz, and P. Yager, "Enhanced sensitivity of lateral flow tests using a two-dimensional paper network format." *Anal. Chem.*, vol. 83, no. 20, pp. 7941–7946, Oct. 2011.
- [19] G. Zhou, S. Bergeron, and D. Juncker, "High-performance low-cost antibody microarrays using enzyme-mediated silver amplification," *J. Proteome Res.*, vol. 14, no. 4, pp. 1872–1879, 2015.
- [20] K. C. Bhargava, B. Thompson, and N. Malmstadt, "Discrete elements for 3D microfluidics." *Proceedings of the National Academy of Sciences*, vol. 111, no. 42, pp. 15 013–15 018, Oct. 2014.
- [21] B. Foxman, "The epidemiology of urinary tract infection." *Nature Reviews Urology*, vol. 7, no. 12, pp. 653–660, Dec. 2010.
- [22] J. D. Brewster, "Isolation and concentration of Salmonellae with an immunoaffinity column," *Journal of Microbiological Methods*, vol. 55, no. 1, pp. 287–293, Oct. 2003.
- [23] N. Tufenkji, "Modeling microbial transport in porous media: Traditional approaches and recent developments," *Advances in Water Resources*, vol. 30, no. 6-7, pp. 1455–1469, Jun. 2007.

- [24] A. O. Olanrewaju, A. Robillard, M. Dagher, and D. Juncker, "Autonomous microfluidic capillary circuits replicated from 3D-printed molds." *Lab Chip*, vol. 16, no. 19, pp. 3804–3814, Sep. 2016.
- [25] A. K. Au, W. Huynh, L. F. Horowitz, and A. Folch, "3D-Printed Microfluidics." *Angewandte Chemie. International edition in English*, vol. 55, no. 12, pp. 3862–3881, 2016.
- [26] S. Waheed, J. M. Cabot, N. P. Macdonald, T. Lewis, R. M. Guijt, B. Paull, and M. C. Breadmore, "3D printed microfluidic devices: enablers and barriers," *Lab Chip*, vol. 16, no. 11, pp. 1993–2013, 2016.
- [27] L. Song, W. Li, G. Li, D. Wei, P. Ge, G. Li, F. Zheng, and X. Sun, "Rapid detection of bacteria in urine samples by the "three-plug-injection" method using capillary electrophoresis." *J. Chromatogr. B Analyt. Technol. Biomed. Life Sci.*, vol. 935, pp. 32–35, Sep. 2013.
- [28] G. Reid, J. A. McGroarty, P. A. Gil Domingue, A. W. Chow, A. W. Bruce, A. Eisen, and J. W. Costerton, "Coaggregation of urogenital bacteria in vitro and in vivo," *Current Microbiology*, vol. 20, no. 1, pp. 47–52, Jan. 1990.
- [29] J. Mai, V. V. Abhyankar, M. E. Piccini, J. P. Olano, R. Willson, and A. V. Hatch, "Biosensors and Bioelectronics," *Biosensors and Bioelectronics*, vol. 54, no. C, pp. 435–441, Apr. 2014.
- [30] L. E. Nicolle, "Uncomplicated Urinary Tract Infection in Adults Including Uncomplicated Pyelonephritis," *Urologic Clinics of North America*, vol. 35, no. 1, pp. 1–12, Feb. 2008.
- [31] A. R. Manges, H. Tabor, P. Tellis, C. Vincent, and P.-P. Tellier, "Endemic and Epidemic Lineages of *Escherichia coli* that Cause Urinary Tract Infections," *Emerging Infectious Disease journal*, vol. 14, no. 10, p. 1575, 2008.

- [32] Z. Hussain, L. Stoakes, S. Garrow, S. Longo, V. Fitzgerald, and R. Lannigan, "Rapid detection of *mecA*-positive and *mecA*-negative coagulase-negative staphylococci by an anti-penicillin binding protein 2a slide latex agglutination test." *Journal of Clinical Microbiology*, vol. 38, no. 6, pp. 2051–2054, Jun. 2000.
- [33] H. Tachibana, M. Saito, K. Tsuji, K. Yamanaka, L. Q. Hoa, and E. Tamiya, "Self-propelled continuous-flow PCR in capillary-driven microfluidic device: Microfluidic behavior and DNA amplification," *Sensors & Actuators: B. Chemical*, vol. 206, pp. 303–310, Jan. 2015.
- [34] H. Tachibana, M. Saito, S. Shibuya, K. Tsuji, N. Miyagawa, K. Yamanaka, and E. Tamiya, "On-chip quantitative detection of pathogen genes by autonomous microfluidic PCR platform." *Biosensors and Bioelectronics*, vol. 74, pp. 725–730, Dec. 2015.
- [35] N. Ramalingam, H.-B. Liu, C.-C. Dai, Y. Jiang, H. Wang, Q. Wang, K. M Hui, and H.-Q. Gong, "Real-time PCR array chip with capillary-driven sample loading and reactor sealing for point-of-care applications." *Biomed Microdevices*, vol. 11, no. 5, pp. 1007–1020, Oct. 2009.
- [36] A. Sposito, V. Hoang, and D. L. DeVoe, "Rapid real-time PCR and high resolution melt analysis in a self-filling thermoplastic chip," *Lab Chip*, vol. 16, no. 18, pp. 3524–3531, 2016.
- [37] M. Pla Roca, R. F. Leulmi, S. Tourekhanova, S. Bergeron, V. Laforte, E. Moreau, S. J. C. Gosline, N. Bertos, M. Hallett, M. Park, and D. Juncker, "Antibody Colocalization Microarray: A Scalable Technology for Multiplex Protein Analysis in Complex Samples," *Molecular & Cellular Proteomics*, vol. 11, no. 4, pp. M111.011 460–M111.011 460, Apr. 2012.
- [38] A. I. Shallen, P. Smejkal, M. Corban, R. M. Guijt, and M. C. Breadmore, "Cost-Effective Three-Dimensional Printing of Visibly Transparent Microchips within Minutes," *Anal. Chem.*, vol. 86, no. 6, pp. 3124–3130, Mar. 2014.